TRANSACTIONS
OF THE ASME
Series A

Journal of ENGINEERING FOR POWER

October 1960

Divisions: POWER • GAS TURBINE POWER • NUCLEAR ENGINEERING • FUELS OIL AND GAS POWER • HYDRAULIC • **Research Committees:** FURNACE PERFORMANCE FACTORS • CORROSION AND DEPOSITS FROM COMBUSTION GASES • BOILER FEEDWATER STUDIES • HIGH TEMPERATURE STEAM GENERATION • CONDENSER TUBES • PROPERTIES OF STEAM • **Committees on:** AIR POLLUTION CONTROLS SOLAR ENERGY APPLICATION • **And:** POWER TEST CODES COMMITTEES

Published Quarterly by
THE AMERICAN SOCIETY OF MECHANICAL ENGINEERS

TRANSACTIONS OF THE ASME
Series A

EDITORIAL DEPARTMENT

Editor, J. J. JAKLITSCH, JR.
Consulting Editor, LEO BLODGETT
Production, JEAN NORTH
Art Editor, HENRY BALFOUR

OFFICERS OF THE ASME

President, W. L. CISLER
Secretary, O. B. SCHIER, II
Treasurer, E. J. KATES
Assistant Treasurer, H. J. BAUER

PUBLICATIONS COMMITTEE

Chairman, B. G. A. SKROTZKI
HENDLEY N. BLACKMON
K. D. MINDLIN
MARVIN MOLAND
VITO L. SALERNO
Junior Representatives
A. S. GOLDSTEIN
J. W. FOLLANSBEE

REGIONAL ADVISORY BOARD

Region I, H. M. ROGERS, JR.
Region II, GLENN R. FRYLING
Region III, F. J. HEINZE
Region IV, FRANCIS C. SMITH
Region V, H. M. CATHEY
Region VI, C. R. EARLE
Region VII, M. S. UMBENHAUER
Region VIII, CARL J. ECKHARDT

Published quarterly by The American Society of Mechanical Engineers. Publication office at 20th and Northampton Streets, Easton, Pa. The editorial department is located at the headquarters of the Society, 29 West Thirty-Ninth Street, New York 18, N. Y. Cable address, "Mechanaser," New York. Price $3.00 a copy, $10.00 annually; to members, $1.50 a copy, $5.00 annually. Add 50 cents for postage to all countries outside the United States and Canada. Changes of address must be received at Society headquarters seven weeks before they are to be effective on the mailing list. Please send old as well as new address. . . . By-Law: The Society shall not be responsible for statements or opinions advanced in papers or . . . printed in its publications (B13, Par. 4). . . . Second-class mail privileges authorized at Easton, Penna. . . . This publication is authorized to be mailed at the special rates of postage prescribed by Section 132.122 . . . © Copyright, 1960, by The American Society of Mechanical Engineers. Reprints from this publication may be made on condition that full credit be given the TRANSACTIONS OF THE ASME, Series A—Journal of Engineering for Power, and the author, and that date of publication be stated.

TRANSACTIONS OF THE ASME is indexed by the Engineering Index, Inc.

Journal of
ENGINEERING FOR POWER
VOLUME 82 • SERIES A • NUMBER 4
October 1960

CONTENTS

247 **Throat Tap Nozzles Used for Accurate Flow Measurements** (59—A-174)
K. C. Cotton and J. C. Westcott

264 **Water-Treatment, Corrosion, and Internal-Deposit Studies for Eddystone** (59—A-147)
R. C. Ulmer, H. A. Grabowski, and R. C. Patterson

275 **The Selection of Materials and Fabricating Techniques for the Eddystone Boiler and Sulzer Control Valves** (59—A-318)
E. C. Chapman and R. E. Lorentz, Jr.

286 **Development Associated With the Superpressure Turbine for Eddystone Station Unit No. 1** (59—A-288)
W. E. Trumpler, Jr., A. F. LeBreton, E. A. Fox, and R. B. Williamson

293 **Material Selection and Fabrication, Main Steam Piping for Eddystone No. 1, 1200-F and 5000-Psi Service** (59—A-327)
R. H. Caughey and W. G. Benz, Jr.

315 **Solar Turbo Power-Plant Design** (59—A-74)
D. B. Mackay and E. L. Leventhal

325 **Analysis of Solar-Furnace Performance in Mechanical Testing at Extremely High Temperatures** (59—A-79)
G. S. Leon and M. E. Shank

TRANSACTIONS OF THE ASME Series D

Journal of
BASIC ENGINEERING
Vol. 82 • Series D • No. 3

CONTENTS FOR SEPTEMBER, 1960

505 Theoretical and Experimental Analysis of Hydrostatic Thrust Bearings, by R. C. Elwell and B. Sternlicht. (59—A-152)

513 Precise Measurement of Clothes Insulation During Controlled Operation of the Human, by A. S. Iberall. (59—A-197)

528 Radial Distributions of Temporal-Mean Peripheral Velocity and Pressure for Fully Developed Turbulent Flow in Curved Channels, by A. W. Marris. (59—A-51)

539 Flow Phenomena of Partially Enclosed Rotating Disks, by L. A. Maroti, G. Deak, and F. Kreith. (59—A-49)

553 Roughness Effects on Frictional Resistance of Enclosed Rotating Disks, by R. E. Nece and J. W. Daily. (59—A-55)

563 Rotating Wakes in Vaneless Diffusers, by R. C. Dean, Jr., and Y. Senoo. (59—A-104)

575 Incidence and Deviation-Angle Correlations for Compressor Cascades, by Seymour Lieblein. (59—A-171)

588 A Study of Boundary-Layer Characteristics of Turbomachine Blade Rows and Their Relation to Over-All Blade Loss, by W. L. Stewart, W. J. Whitney, and R. Y. Wong. (59—A-23)

593 Laminar Boundary Layers in Oscillatory Flow, by P. G. Hill and A. H. Stenning. (59—A-265)

609 Experimental Determination of Statistical Properties of Two-Phase Turbulent Motion, by S. L. Soo, H. K. Ihrig, Jr., and A. F. El Kouh. (59—A-59)

622 The Turbulent Boundary Layer at a Plane of Symmetry in a Three-Dimensional Flow, by J. P. Johnston. (59—A-72)

629 Heat-Transfer Characteristics of Hot-Film Sensing Element Used in Flow Measurement, by S. C. Ling. (59—A-172)

635 The Adiabatic Bulk Modulus of Normal Paraffin Hydrocarbons From Hexane to Hexadecane, by R. E. Rolling and C. J. Vogt. (59—A-169)

645 Variable Flow Resistance With Adjustable Multihole Orifice Plates in Series, by J. Sherman, F. A. Grochowski, and J. E. Sharbaugh. (59—A-182)

654 Cycle-Dependent Stress Relaxation of A-286 Alloy, by A. S. Ross and JoDean Morrow. (59—A-116)

661 Low-Cycle Fatigue of Two Nickel-Base Alloys by Thermal-Stress Cycling, by F. J. Mehringer and R. P. Felgar. (59—A-58)

671 The Stability of Metals Under Cyclic Plastic Strain, by L. F. Coffin, Jr. (59—A-100)

683 Roll-Force and Torque Coefficients for Hot-Strip Steel Mill, by B. N. Garudachar and H. A. Peterson. (59—A-153)

689 Steady-State Creep of a Thick-Walled Cylinder Under Combined Axial Load and Internal Pressure, by Iain Finnie. (59—A-57)

695 Burst Strengths and Deformations of Welded Composite Turbine Wheels as Related to Weld Quality and Plasticity Calculations, by A. G. Holms and A. J. Repko. (59—A-28)

710 The Twin Throat Venturi: A New Fluid-Flow Measuring Device, by A. A. Kalinske. (59—A-154)

717 A Study of Viscosity Effect and Its Compensation on Turbine-Type Flowmeters, by W. F. Z. Lee and Henning Karlby. (59—A-105)

729 The Quadrant Edge Orifice—A Fluid Meter for Low Reynolds Numbers, by M. Bogema and P. L. Monkmeyer. (59—A-140)

735 Small-Diameter-Orifice Metering, by T. J. Filban and W. A. Griffin. (59—A-101)

741 Analysis of Axially Loaded Annular Shells With Applications to Welded Bellows, by M. Hetenyi and R. J. Timms. (59—A-175)

756 Cavitation Problems in Cryogenics, by R. B. Jacobs and K. B. Martin.

TRANSACTIONS OF THE ASME Series C

Journal of
HEAT TRANSFER
Vol. 82 • Series C • No. 3

CONTENTS FOR AUGUST, 1960

155 Rocket Heat-Transfer Literature.

170 Unsteady Turbulent Heat Transfer in Tubes, by E. M. Sparrow and R. Siegel. (59—HT-16)

181 Improved Lumped Parameter Method for Transient Heat Conduction Calculations, by H. G. Elrod, Jr. (59—HT-28)

189 Local and Average Heat Transfer and Pressure Drop for Refrigerants Evaporating in Horizontal Tubes, by M. Altman, R. H. Norris, and F. W. Staub. (59—A-278)

199 Heat-Transfer and Flow-Friction Characteristics of Crossed-Rod Matrices, by A. L. London, J. W. Mitchell, and W. A. Sutherland. (59—A-168)

214 Experiments on Heat Transfer From Spheres Including Combined Natural and Forced Convection, by T. Yuge. (59—A-123)

221 Heat Transfer to Freon 12 Near the Critical State in a Natural-Circulation Loop, by J. P. Holman and J. H. Boggs. (59—A-142)

227 Combined Free and Forced-Convection Heat-Generating Laminar Flow Inside Vertical Pipes With Circular Sector Cross Sections, by Pau-Chang Lu. (59—A-145)

233 On Combined Free and Forced Convection in Channels, by L. N. Tao. (59—A-77)

239 The Role of the Skin in Heat Transfer, by A. M. Stoll. (59—A-138)

243 The Prediction of Human Thermal Tolerance When Using a Ventilating Garment With an Anti-exposure Suit, by J. W. Mc Cutchan. (59—A-114)

252 Heat Transfer by Laminar Flow From a Rotating Cone, by C. L. Tien.

253 Apparent Emissivity and Heat Transfer in a Long Cylindrical Hole, by E. M. Sparrow and L. U. Albers.

255 On the Variable-Density Single-Fluid Model for Two-Phase Flow, by Novak Zuber.

258 Nearly Quasi-Steady Free Convection Heat Transfer in Gases, by E. M. Sparrow and J. L Gregg.

260 The Effect of Mass Transfer on Free Convection, by R. Eichhorn.

263 An Interferometric Method of Studying Boundary Layer Oscillations, by J. P. Holman, H. E. Gartrell, and E. E. Soehngen.

TRANSACTIONS OF THE ASME Series E

Journal of
APPLIED MECHANICS
Volume 82 • Series E • No. 3

CONTENTS FOR SEPTEMBER, 1960

TECHNICAL PAPERS

381 On Three and Two-Dimensional Disturbances of Pipe Flow, Kurt Spielberg and Hans Timan. (60—APM–12)

390 On the Indeterminateness of the Boundary Conditions for the Mixing of Two Parallel Streams, K. T. Yen. (59—A-68)

393 Thermal Transfer in Turbulent Gas Streams. Effect of Turbulence on Local Transport From Spheres, W. W. Short, R. A. S. Brown, and B. H. Sage. (60—APM-30)

403 Hydrodynamic Entrance Lengths for Incompressible Laminar Flow in Rectangular Ducts, L. S. Han. (59—A–82)

410 Stability of a Turbine-Generator Rotor Including the Effects of Certain Types of Steam and Bearing Excitations, A. H. Landzberg. (60—APM-9)

417 On Saint Venant's Principle: Elastic Shells and Plates, P. M. Naghdi. (60—APM-11)

423 On the Airy Stress Functions of Plane Dislocation Problems, F. D. Ju. (60—APM-14)

429 The Effect of Pressure on the Bending Characteristics of an Actuator System, Paul Seide. (60—APM-16)

438 The Contact Problem for Viscoelastic Bodies, E. H. Lee and J. R. M. Radok. (59—A-83)

445 Stresses in Curved Beams of Noncircular Center Line, M. M. Abbassi. (60—APM-21)

455 Shear Buckling of Bars, G. Herrmann and A. E. Armenakas. (59—A-91)

458 Buckling of Circular Cones Under Axial Compression, Leslie Lackman and Joseph Penzien. (60—APM-17)

461 The Additional Deflection of a Cantilever Due to the Elasticity of the Support, W. J. O'Donnell. (60—APMW-3)

465 Thermoelastic Stresses in Beams, E. S. Barrekette. (60—APM-28)

474 Elastic Instability of Rectangular Sandwich Panel of Orthotropic Core With Different Face Thicknesses and Materials, C. C. Chang and I. K. Ebcioglu. (60—APM-26)

481 Transient and Residual Thermal Stresses in an Elastic-Plastic Cylinder, H. G. Landau and E. E. Zwicky, Jr. (60—APM-4)

489 On Strain-Hardened Circular Cylindrical Shells, Nicholas Perrone and P. G. Hodge, Jr. (60—APM-20)

496 The Elastoplastic Thick-Walled Sphere Subjected to a Radial Temperature Gradient, G. R. Cowper. (60—APM-22)

501 Rupture Instability of Membranes and Solids, S. F. Borg. (60—APM-1)

505 Expansion of Thick-Walled Cylinders Fabricated From Cold Bent Plates, Irwin Berman. (60—APMW-2)

513 Dispersion of Flexural Waves in an Elastic, Circular Cylinder, Yih-Hsing Pao and R. D Mindlin. (59—A-84)

521 Modeling of Large Transient Elastic and Plastic Deformations of Structures Subjected to Blast Loading, W. E. Baker. (60—APM-18)

528 Shock Spectra of a Nonlinear System, W. T. Thomson. (60—APM-23)

535 Forced Flexural Vibrations of Sandwich Plates in Plane Strain, Yi-Yuan Yu.

541 Extensional Vibrations and Waves in a Circular Disk and a Semi-Infinite Plate, D. C. Gazis and R. D. Mindlin. (60—APM-3)

548 Effect of Small Hub-Radius Change on Bending Frequencies of a Rotating Beam, Hsu Lo, J. E. Goldberg, and J. L. Bogdanoff. (60—APMW-5)

551 Forced Lateral Vibration of a Uniform Cantilever Beam With Internal and External Damping, Ho Chong Lee. (60—APM-15)

557 A Method for Investigating Certain Eigenvalue Problems of the Buckling and Vibration of Plates, H. D. Conway and A. W. Leissa. (60—APM-25)

559 Dynamical Response of an Elastic Half-Space to Tangential Surface Loadings, Chi-Chang Chao. (60—APM-29)

568 On a Special Class of Self-Sustained Oscillations, K. Klotter and E. Kreyszig.

575 Random Excitation of a Loaded Nonlinear String, T. K. Caughey. (60—APMW-1)

579 On the Use of Nonsinusoidal Approximating Functions for Nonlinear Oscillation Problems, K. Klotter and P. R. Cobb.

TRANSACTIONS OF THE ASME Series B

Journal of
ENGINEERING FOR INDUSTRY
Volume 82 • Series B • Number 3

CONTENTS FOR AUGUST, 1960

173 Synthesis of Epicyclic Gear Trains Using the Velocity Ratio Spectrum, by R. C. Brewer. (59—A-22)

179 Helixform Bevel and Hypoid Gears, by G. M. Spear, C. B. King, and M. L. Baxter, Jr. (59—A-90)

191 The Twinworm Drive—A Self-Locking Worm-Gear Transmission of High Efficiency, by B. Popper and D. W. Pessen. (59—A-75)

200 Determination of Cutter Trajectories for Contoured Turbine Buckets, by R. G. DeBiase. (59—A-111)

205 An Analysis of Factors Used for Strength Rating Helical Gears, by E. J. Wellauer. (59—A-121)

213 Bending Strength of Gear Teeth by Cantilever-Plate Theory, by E. J. Wellauer and A. Seireg. (59—A-50)

223 Rocket Motor Gear Tooth Analysis (Hertzian Contact Stresses and Times), by E. K. Gatcombe and R. W. Prowell. (59—A-256)

231 Analysis of Power Spinning of Cones, by B. Avitzur and C. T. Yang. (59—A-173)

246 Some Problems of Press Forging Lead and Aluminum, by A. G. MacDonald, S. Kobayashi, and E. G. Thomsen. (59—A-164)

253 The Deformation Process in Metal-Cutting, by W. J. McDonald and B. F. Murphey. (59—A-165)

259 Influence Coefficients and Pressure Vessel Analysis, by G. D. Galletly. (59—A-163)

270 Tube Metal Temperatures for Structural Design, by E. E. Ungar and L. A. Mekler. (59—A-166)

277 Supersonic-Wind-Tunnel Air-Drying-System Design, by T. W. Macios. (59—A-161)

K. C. COTTON
Supervisor—Turbine Performance
Mem. ASME

J. C. WESTCOTT
Engineer, Large Steam Turbine-Generator Department, General Electric Company, Schenectady, N. Y.

Throat Tap Nozzles Used for Accurate Flow Measurements

The history of the design, manufacture, calibration, and use of 17 nozzles built by the General Electric Company for accurate flow measurements in conducting performance tests on large steam turbine-generator units are presented.

THE MEASUREMENT of physical phenomena must be based on an accepted standard. Unfortunately the measurement of fluid flow has no exact standard of extremely high accuracy such as is possible with temperature, pressure, voltage, and many others. Measurement of fluid flow is dependent on the measurement of weight or volume and time. It is possible to measure accurately time and also density which is the correlation between volume flow and weight flow. However, the accurate measurement of large weight or volume is difficult. It is difficult and expensive to attempt to operate large weigh tanks or volume tanks in other than a laboratory specifically set up for the measurement of flow. For this reason science and industry have devised flow measuring devices which are more readily usable. Much has been done in the past to develop nozzles, venturis, weirs, orifices, and other types of flow measuring devices. Little work has been done since about 1932 to further develop these devices. However, a tremendous amount of information concerning the behavior of these devices has been accumulated. Most of the information concerning orifices and nozzles with the pressure measuring taps in the pipes has been published and various claims as to the desirability of one type over another have been made.

In 1934 B. O. Buckland [1][1] published the results of the calibration of seven nozzles, one of which had four separate throat pressure taps. Since then the authors' company has built and used 16 nozzles with four separate throat pressure taps. Experience with these throat tap nozzles and with other types of flow measuring devices shows that the primary flow measurement for large steam-turbine performance tests can most accurately be obtained by using throat tap nozzles.

This paper presents the history of the design, manufacture, calibration, and use of these nozzles to measure water flow during performance tests. It is important to note that the requirements and procedures established are based on the philosophy of eliminating all known errors that affect the flow measurement by 0.1 per cent or greater. The economic justification for this philosophy is the fact that the performance of very large steam turbine-generator units has been evaluated as high as $700,000 per 1 per cent.

Nozzle and Pipe Section Design

The nozzles have a ratio of throat diameter to pipe diameter of 0.5 or less. Prior to 1949 the nozzles were calibrated in pipes which were available at the place of calibration. In actual use they were installed between flanges in existing station piping. To eliminate the potential error due to the differences in the calibration pipe configuration and that used for the performance test, upstream and downstream pipe sections were made. The flow measuring device from that time on was considered to be the nozzle plus the upstream pipe with flow straightener and the downstream pipe with which it was calibrated. The upstream sections are 20 pipe diameters long and have a tube bundle flow straightener $1^1/_2$ pipe diameters long. The tube bundle straightener divides the pipe into approximately 50 areas. The downstream sections are 10 diameters long. Fig. 1 shows the dimensions of the pipe section and the location of pressure taps and flow straightener. The curves and analysis of nozzle coefficients presented in this paper are based only on calibrations of nozzles using the upstream and downstream pipe sections.

Fig. 2 shows the dimensions of the nozzle as a function of the nozzle diameter. The pressure taps in the nozzle throat are located one half of the nozzle throat diameter downstream from the nozzle elliptical entrance. These dimensions are fundamentally the same as those used by Mr. Buckland.

Nozzle Manufacture

The early nozzles were made from 12 per cent chrome steel. Nozzles made since 1950 have been manufactured from No. 347 or No. 303 stainless.

Our present manufacturing practice is to start with a rough machined forging of No. 303 stainless steel. The forging is x-rayed to make sure there are no imperfections. A cam for machining the quarter elliptical entrance shape is made and is checked on an optical comparator against a ten-times-size layout. The rough forging is machined leaving about 0.050 inch on the bore and elliptical entrance section for finish machining and polishing. The four pressure tap holes are drilled and bored and openings are plugged where necessary. Press fit pins are inserted in the throat taps. The machining and polishing of the bore and entrance section is then completed. A four micro-inch finish is required.

A plastic cast is made of a section parallel to the center line of the elliptical entrance section and the first half inch of the bore. This cast is compared to the same ten-times-size drawing used in checking the cam. The bore of the nozzle is measured at three places along its length. The bore diameter at each of these three places is determined from three measurements 60 deg apart An out-of-roundness of ±0.0002 times nozzle diameter is allowed A convergence of the bore of 0.001 inch per inch is allowed. Any divergence is not acceptable.

After all dimensions are determined to be within the specified tolerances, the pins in the throat pressure taps are removed. The edges of the throat pressure tap may have a very fine burr which can be easily removed by rolling a tapered hard wood rod around the edge of the tap.

The only differences between the nozzles described here and the ASME nozzle shape is that the ASME nozzle shape has an elliptical entrance with a minor axis of $^1/_2$ the nozzle diameter instead of $^1/_3$, and the length of the cylindrical throat section is 0.6 of a nozzle diameter instead of 0.75. These differences should have neg-

[1] Numbers in bracket designate References at end of paper.

Contributed by the Power Test Codes Committee and presented at the Annual Meeting, Atlantic City, N. J., November 29–December 4, 1959, of THE AMERICAN SOCIETY OF MECHANICAL ENGINEERS.

NOTE: Statements and opinions advanced in papers are to be understood as individual expressions of their authors and not those of the Society. Manuscript received at ASME Headquarters, September 4, 1959. Paper No. 59—A-174.

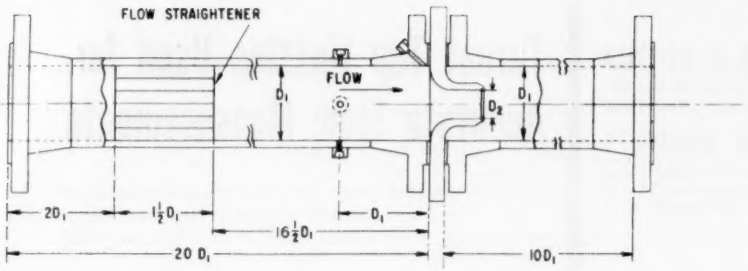

Fig. 1 Flow measuring device

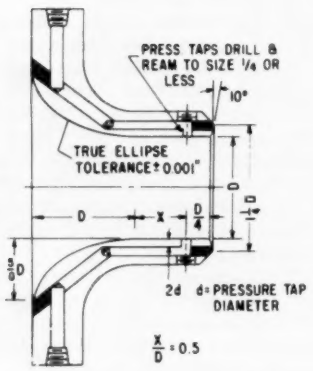

Fig. 2 Throat tap nozzle

ligible effect on the coefficient of discharge comparison of the two different nozzles if throat taps are used.

Nozzle Calibration Facilities

These nozzles have been calibrated in three different university laboratories and recently we have calibrated two nozzles in our own Turbine-Generator Development Laboratory.

The laboratory at Ohio State University is in the Mechanical Engineering Department and comes under the direction of the Engineering Experiment Station. This laboratory measures flow using a single large volume tank. The nozzle and pipe section being calibrated is installed in a horizontal position. The water is pumped directly from the main storage bay through the nozzle and then diverted either into the volume tank or back to the storage bay by the use of an air-operated diverter. The volume tank has been calibrated by weighing water and dumping it into the volume tank. The change in level in the volume tank is then recorded using piezometers which have been accurately calibrated. The measuring time is determined by using a calibrated stop watch. The stop watch is started and stopped by the switching action of the diverter from the storage bay to the volume tank and vice versa.

The pumping of the water directly through the nozzle causes some fluctuation in the flow and subsequently this shows up in the pressure drop measuring instruments. Solenoid-operated valves are used as an aid to obtain better readings by trapping the deflection at a given instant. The maximum Reynolds number that has been obtained during calibration of our nozzles at this laboratory is 2.7 million. At one time an attempt was made to increase the Reynolds number range by heating the water. This proved to be impractical as the heat changed the calibration of the volume tank.

The calibration facility at the University of Pennsylvania is operated by the Civil Engineering Department. In this facility water is pumped from a storage reservoir into a large head tank. This tank has overflow weirs at various levels which allow the tank to maintain a constant head over a large range of flows. The flow of water is from the side of the bottom of the tank and passes through straightening vanes in order to obtain good flow characteristics. The nozzle is calibrated in a horizontal pipe, the discharge of which has one elbow and a gate valve. The gate valve is used as part of the control of the water flow through the nozzle. The flow is measured using two weigh tanks of approximately 15,000-lb capacity. The scales are of course calibrated and are maintained in a very careful manner.

The use of the constant head tank allows very accurate calibrations at low flows. The flow is steady enough so that a hook gage may be used for measuring very low differentials. The highest Reynolds number that has been obtained in this facility during the calibration of our nozzles is 1.5 million. This Reynolds number range could be doubled if the water were heated to a temperature of 140 F.

The Alden Hydraulics Laboratory at Worcester Polytechnic Institute operates a calibration facility which uses a pond as a constant head tank. The range of Reynolds numbers is determined by the time of year of calibration, since during colder weather the colder water results in a lower Reynolds number for the same flow. The maximum Reynolds number which has been obtained at this facility during calibration of our nozzles is 1.4 million. The flow is measured using weigh tanks and a weighing system which is essentially the same as that used at the University of Pennsylvania. The results of calibrations at this laboratory and those at the University of Pennsylvania agree very closely.

The General Electric Company's Turbine-Generator Development Laboratory has a calibration facility for calibrating nozzles in a vertical run of pipe. The flow is measured by two weigh tanks of 50,000-lb capacity. Weighing is done in a manner different from that used at the University of Pennsylvania or the Alden Hydraulics Laboratory. All water is weighed statically; that is, weighing is only done on one tank when water is flowing into the other tank. This is possible because of the use of electronic counters for timing the weighing cycle of each tank. These counters are accurate to ±0.003 sec. For the maximum flow the filling time for one tank is 92 sec.

The pressure differential across the nozzle is measured using manometers which have a bore of 1/2 in. These manometers are equipped with antiparallax readers and a vernier which allows the deflection to be read to 0.01 in. A correction is made for the difference in elevation of the pressure taps. The absolute accuracy of these manometers is 0.03 in.

The weighing and timing of the flow is accomplished automatically by the use of a programming unit for switching from one tank to the other and for opening and closing the weigh tank dump valves. Calibrations have been made at water temperatures as high as 175 F. Calibrations at these high temperatures have been checked by running calibrations at lower water temperatures but

at the same Reynolds number. The repeatability of results is ±0.1 per cent.

For ideal conditions the error in measuring flow with this facility is ±0.1 per cent. This error is composed of the maximum calibration error of the weigh tanks, the weighing error during the calibration of the flow nozzle, and the error in the measurement of the pressure drop across the flow nozzle. The maximum Reynolds number to which we have calibrated to date is 5 million.

Calibration Results

Each of the four sets of pressure taps installed in the nozzle and pipe section is calibrated and the nozzle flow coefficients are plotted versus Reynolds number. The more consistent two sets 180 deg apart are used during the turbine performance test. Unfortunately, the performance test Reynolds number is considerably higher than the maximum value obtainable with the present calibration facilities. Thus the calibration results have to be extrapolated up to values of Reynolds numbers as high as 10,000,000.

The theoretical nozzle flow coefficient curve shown in Fig. 3 was calculated from the experimental and analytical work of A. H. Shapiro and R. D. Smith [2] to serve as a basis for comparison of the nozzle calibration results presented in this paper. The following equation was derived by Messrs. Shapiro and Smith for calculating the nozzle flow coefficient:

$$C_q = \frac{1}{\sqrt{1 + 4\bar{f}_{App}(X/D)}}$$

where C_q = nozzle coefficient of discharge
$\bar{f}_{App}$ = apparent friction factor
X = distance along the nozzle bore to the throat tap
D = nozzle bore diameter

The value of X/D for all 17 nozzles is 1/2. The actual values of friction factors used were measured in the inlet length of smooth, round tubes [2] and are shown in Fig. 4.

The results of the two nozzles calibrated in the Turbine-Generator Development Laboratory are shown in Figs. 5 and 6. The four sets of pressure taps are individually calibrated and plotted as separate curves. Taps 2 and 4 were selected to be used for the performance test. In the region where the nozzle boundary layer flow is turbulent (values of Reynolds number greater than 1,300,000) the calibration results are about 0.25 per cent higher than the theoretical curve for the taps selected. The standard deviation of the individual points from the calibration curve in the turbulent region is ±0.05 per cent. In the transition region between laminar and turbulent flow (800,000 to 1,300,000 Reynolds number) the variation between the calibration results and the theoretical curve is somewhat greater; however, this is to be expected since the transition region is less stable than either the laminar or turbulent region. These calibrations did not extend very far into the laminar region since the nozzles are used only in the turbulent region. The agreement with the theoretical curve in the laminar region is fairly good, though this is of academic interest only.

These same two nozzles were also calibrated at the University of Pennsylvania. The results are shown in Figs. 7 and 8 along with the theoretical curve and the results from the Turbine-Generator Development Laboratory. The extrapolated curve from the University of Pennsylvania calibration is about 0.15 per cent lower than the calibration curve obtained in the Turbine-Generator Development Laboratory. At very low Reynolds numbers the calibration curves have a greater deviation from

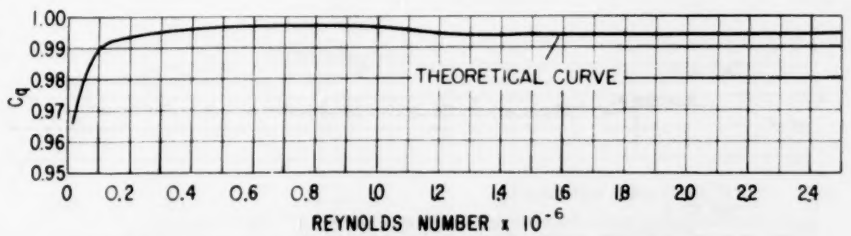

Fig. 3 Theoretical flow coefficient curve for throat tap nozzles with X/D = 0.5

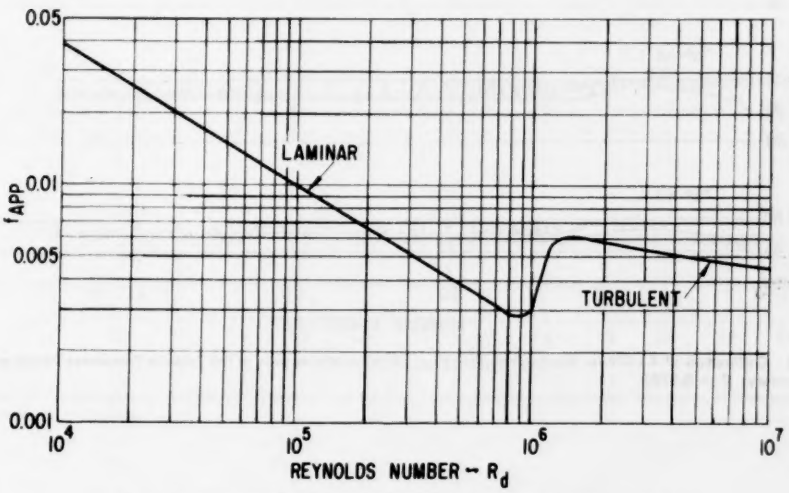

Fig. 4 Apparent friction factors in the entrance of smooth round tubes [2]

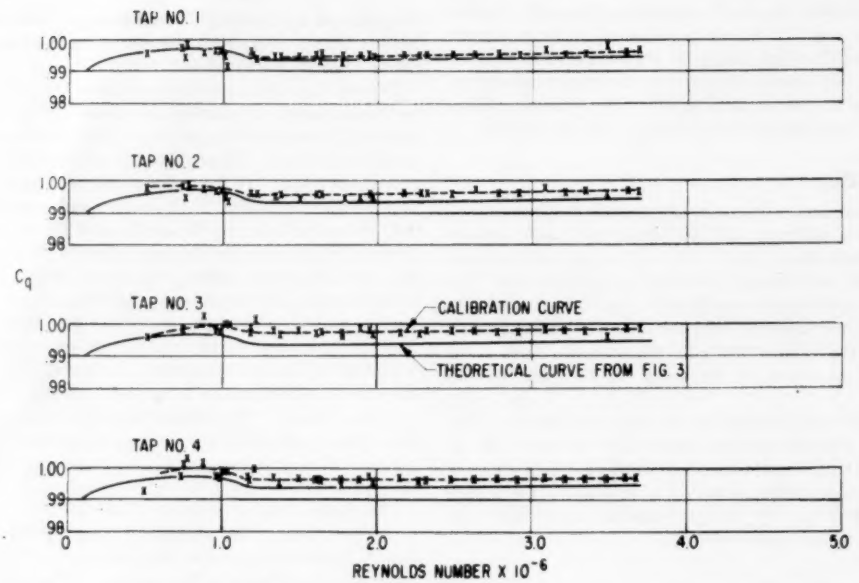

Fig. 5 Calibration of 3.1989-in. diameter nozzle in an 8-in. diameter pipe at the Turbine-Generator Development Laboratory; $\beta = 0.3942$

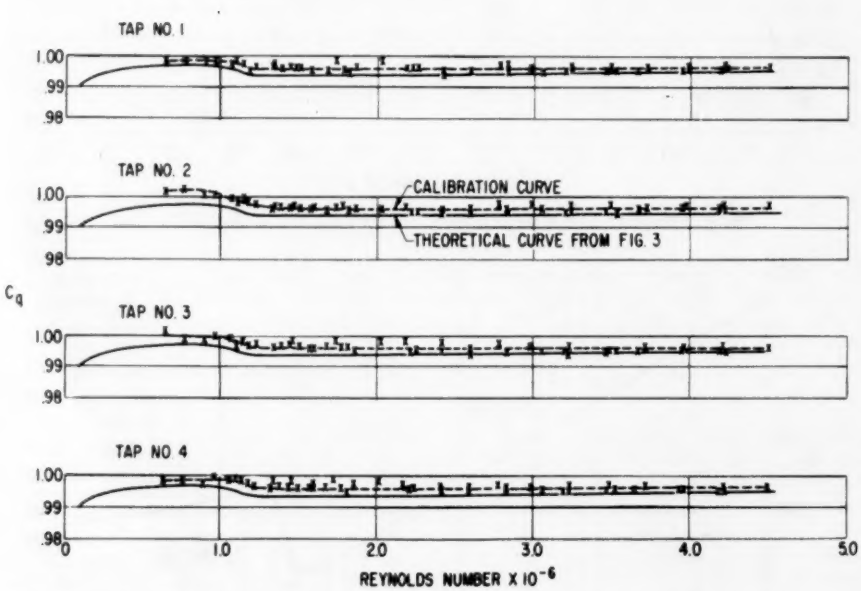

Fig. 6 Calibration of 4.4502-in. diameter nozzle in a 12-in. diameter pipe at the Turbine-Generator Development Laboratory; $\beta = 0.3708$

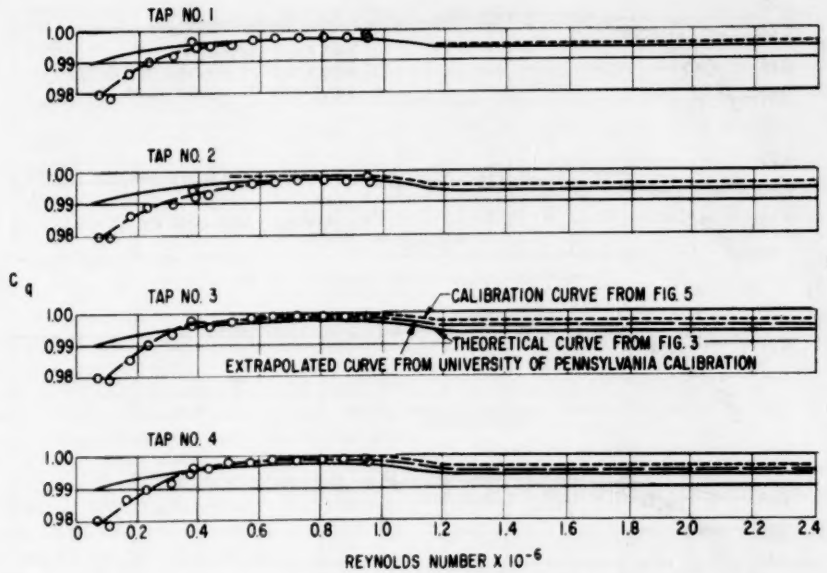

Fig. 7 Calibration of 3.1989-in. diameter nozzle in an 8-in. diameter pipe at the University of Pennsylvania; $\beta = 0.3942$

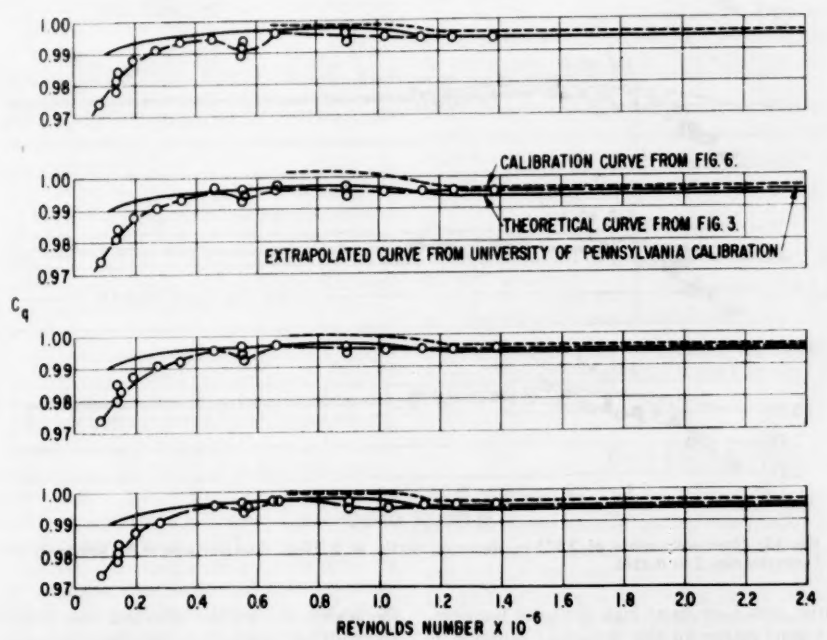

Fig. 8 Calibration of 4.4502-in. diameter nozzle in a 12-in. diameter pipe at the University of Pennsylvania; $\beta = 0.3708$

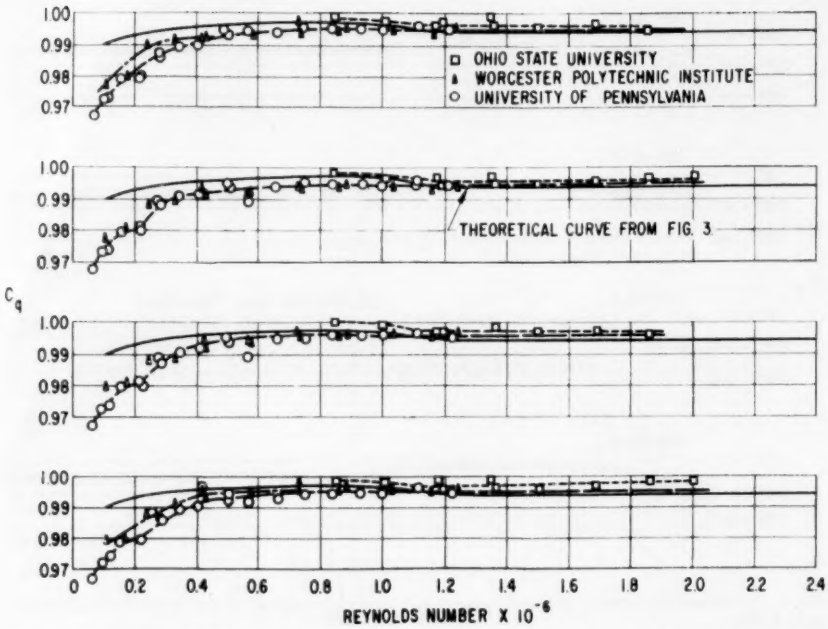

Fig. 9 Calibration of 3.875-in. diameter nozzle in a 10-in. diameter pipe at three different laboratories; $\beta = 0.3875$

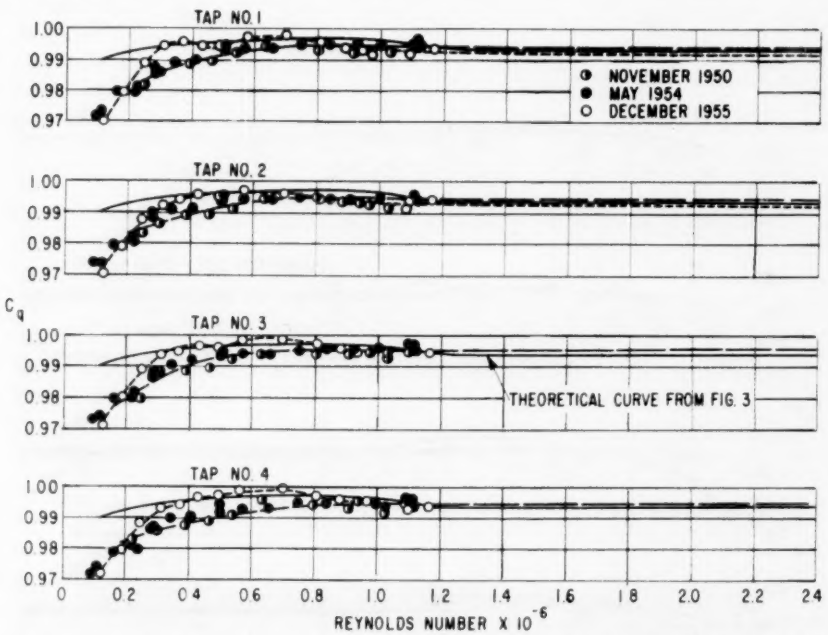

Fig. 10 Three calibrations of 3.875-in. diameter nozzle in a 10-in. diameter pipe at the University of Pennsylvania; $\beta = 0.3875$

the theoretical curve than they do at high Reynolds numbers. We wish we had a good reason for this deviation; however, it is of no practical significance since accurate flow measurements are not attempted in this region.

Fig. 9 shows a comparison of results of one nozzle calibrated at three different laboratories. Taps 1 and 3 were selected to be used for the performance test. Again the agreement with the theoretical curve is very good. The extrapolated curves from two of the laboratories are the same and they differ from the third by about 0.1 per cent for the taps selected.

The repeatability of three calibrations of the same nozzle at the University of Pennsylvania at different times is illustrated in Fig. 10. The extrapolated curves are at the most different from the theoretical curve by 0.2 per cent. In the laminar region there is considerable deviation, but here again this has not been a matter of great concern.

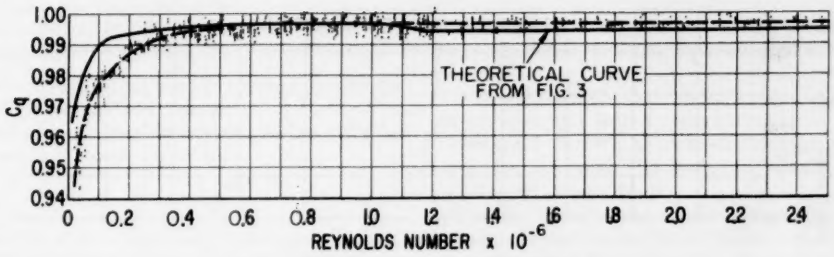

Fig. 11 Composite plot of nozzle calibrations

The foregoing calibrations are representative of the large number of results obtained during the past 10 years. Rather than present these results individually a composite curve shown in Fig. 11 is presented. This composite plot includes results from nozzles ranging in throat diameters from $2^1/_4$ to $5^1/_4$ in., calibrated in 6, 8, 10, and 12-in. pipes with throat diameter to pipe diameter ratios from 0.28 to 0.44 and at four independent laboratories. In the turbulent region the average of all calibrations is about 0.2 per cent higher than the theoretical curve and the standard deviation from the average is 0.13 per cent.

Primary Flow Measurements in Steam Turbine Tests

The results of performance tests using throat tap nozzles for measuring primary flow are used to evaluate the changes in turbine efficiency which result from basic developments made using single-stage or group-stage testing in air and in steam turbine laboratories. The test results are also used as a comparison to guarantee performance for acceptance of steam turbine-generator units. Since we are looking for gains in steam path efficiencies as small as a couple of tenths of one per cent, and we have no testing tolerances applied to results when used as a comparison to guarantee performance, it is necessary that the absolute error of testing be as small as possible. The measurement of flow in the feedwater cycle is, at present, the largest contributor to the over-all inaccuracy of performance testing. An evaluation of these inaccuracies is available in Reference [3].

Manometer accuracy is essential to accurate flow measurement with nozzles. Until 1954, $^3/_{16}$-in. bore, single leg manometers were used to measure the nozzle pressure differential. These were "standard" manometers and at a deflection of 10 in. introduced an error in the flow measurement of 0.5 per cent. The next step was to obtain single leg manometers which had $^1/_2$-in. ID precision bore tubing and were equipped with antiparallax readers. These manometers also have machine-divided scales and a vernier which makes it possible to read to 0.01 in., and were used with zero-displacement, solenoid-operated valves to trap the deflection for reading. At a 10-in. deflection this decreased the error in flow measurement due to manometer and observer error to 0.15 per cent. These manometers have proved to be reasonably satisfactory for flow measurement.

Our next step to decrease manometer and observer error was to obtain manometers with a servo system which would automatically follow the mercury level and would indicate the deflection on a mechanical counter with a smallest division of 0.002 in. These manometers are installed in a temperature controlled case. Their maximum error is less than 0.003 in. or 0.01 per cent of reading, whichever is greater. The counter can be read to the nearest 0.001 in.

During steam turbine tests flow is measured using two sets of pressure taps on a nozzle. The value of flow is calculated for each set of taps and the average used to calculate turbine performance. The use of automatic following manometers improved the standard deviation of the individual flows from the average from 0.1 to 0.02 per cent.

Conclusions

1 Throat tap nozzles manufactured and calibrated in the manner described in this paper should have a flow coefficient in the range of 0.994 to 0.998 at Reynolds numbers higher than 1.3×10^6.

2 Both the theoretical curve and the results of the nozzle calibrations show that the flow coefficient increases very slightly with increasing Reynolds number in the turbulent region.

3 It is difficult to measure flow accurately if the nozzle is used in the laminar region and considerable error can be expected if it is used in the transition region.

4 If the calibration results deviate from the theoretical curve by more than $^1/_4$ per cent the nozzle and flow section should be carefully examined for manufacturing defects and recalibrated. Burrs on the pressure taps are often the cause of peculiar calibration results.

5 Facilities capable of accurate calibration at higher Reynolds numbers are required. At the present time it is necessary to extrapolate these results out to about 10,000,000 Reynolds number.

6 Attention must be given to the method of installing the nozzle and measuring the pressure differential. If this is not done the errors will overshadow the advances made by increased accuracy of calibration.

References

1 B. O. Buckland, "Fluid-Meter Nozzles," TRANS. ASME, vol. 56, 1934, p. 827.

2 A. H. Shapiro and R. D. Smith, "Friction Coefficients in the Inlet Length of Smooth Round Tubes," NACA Technical Note No. 1785.

3 E. M. Kratz and J. C. Westcott, "Procedures for Testing Large Steam Turbine-Generators in Central Stations," TRANS. ASME, vol. 79, 1957, pp. 365–371.

DISCUSSION

N. R. Deming[2]

Improved methods of making flow measurements are of much interest to the manufacturers of steam turbine-generator units and to their industrial and electric utility customers, because of the great influence of flow measurement on the results of acceptance tests. Hence the authors' experience with throat tap flow nozzles is welcomed as a contribution to the common pool of knowledge concerning this important phase of economy testing.

While the authors' paper deals solely with throat tap flow nozzles, it may be of interest to compare and contrast their curves

[2] Supervisory Engineer, Large and Medium Turbine Engineering, Westinghouse Electric Corporation, Lester, Pa. Mem. ASME.

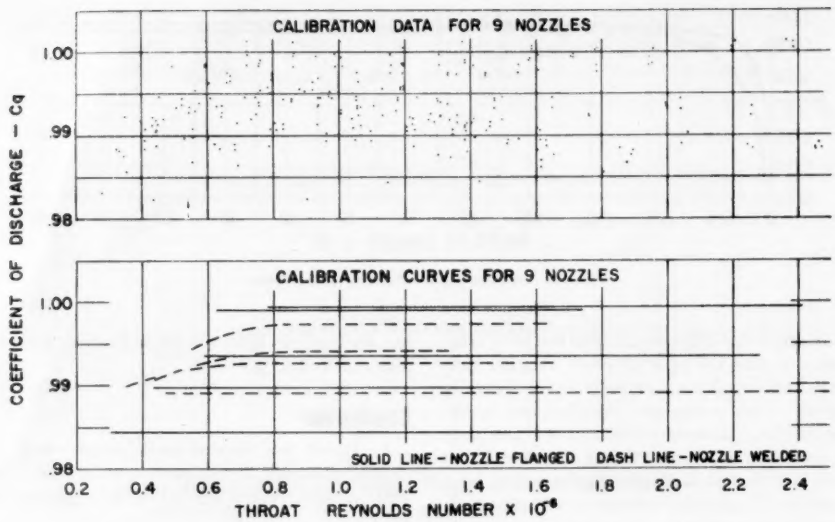
CALIBRATION DATA FOR 9 NOZZLES
1.00
.99
.98
COEFFICIENT OF DISCHARGE – Cq
CALIBRATION CURVES FOR 9 NOZZLES
1.00
.99
.98
SOLID LINE – NOZZLE FLANGED DASH LINE – NOZZLE WELDED
0.2 0.4 0.6 0.8 1.0 1.2 1.4 1.6 1.8 2.0 2.2 2.4
THROAT REYNOLDS NUMBER X 10⁻⁶

Fig. 12

with the calibrations from some flow nozzles using the more familiar pipe-wall pressure taps.

During the past 10 years the writer's company has been a party to numerous field economy tests. For many of these the utility had installed a calibrated flow nozzle for measurement of boiler feedwater flow or as the primary flow measurement in the condensate system. It is to the data in the calibration reports of these flow nozzles that the writer has referred in the preparation of these comments.

The reports available covered calibrations on 27 flow nozzles manufactured by a well-known meter company and calibrated at the Robinson laboratory in Columbus. For the purposes of this discussion only 9 of these are being considered, having met the following specifications:

(1) Beta ratio less than 0.5.

(2) Calibration points at throat Reynolds numbers exceeding 1.3×10^6.

Some more details will help to describe more completely these flow nozzles. Each was installed in its own section of pipe, either between flanges or by a welding procedure. All except one had two sets of pressure taps. Nominal pipe sizes of 6, 8, 10, and 12 in. are represented. Six sections had their own flow straighteners. All received the benefit of the laboratory flow straighteners placed farther upstream.

What did the calibration curves look like?

First of all the line drawn to best represent the individual calibration points was a straight line of constant coefficient value, except for the left-hand end of some which curved downward in the familiar fashion. Individual points off the curve by as much as 0.25 per cent were not infrequent. The value of the constant coefficient of discharge for the 9 curves varied between 0.9845 and 0.9995, a spread of 1.6 per cent, see Fig. 12. The straight numerical average was 0.9933.

If we plot each calibration point on a common curve sheet (see Fig. 12) and examine the portion between a throat Reynolds number of 1.3×10^6 and 2.5×10^6 we find that the 102 individual points are spread between $C = 0.984$ and $C = 1.001$ with substantial proportions of the total occurring between 0.988 and 1.000. There is no heavy concentration around an average value. In fact, there is almost a complete absence of points at $C = 0.995$ to 0.996.

When we turn our attention to the left-hand end of the "flat" portion of the calibration included between Reynolds numbers of 0.7×10^6 and 1.3×10^6 we find 104 individual points scattered between $C = 0.982$ and $C = 1.001$ or almost the same range as for the higher Reynolds numbers.

An examination of the individual calibration curve plots shows that on only two nozzles was there any suggestion of a "hump" in the curve (such as shown by the authors' theoretical curve) followed by lower values of C at higher Reynolds numbers. This occurred in only one of the two sets of taps for each of these two cases.

In summary, we found that the variation between calibration curves is about 4 times as great as the authors say should be found with throat tap flow nozzles, properly manufactured and calibrated.

How much of the reason for this difference is related to the design of the pressure taps (throat taps versus wall taps) is not known to the writer. There may be other factors to be considered. For instance, it is known that in many cases the area of the vent hole through the nozzle was included in arriving at an equivalent nozzle throat diameter which was subsequently used in the computation of the coefficient of discharge. This may tend to slightly decrease the coefficient because of the smaller coefficient applicable to the flow which passes through the vent hole. A second factor is the condition of the pressure taps themselves which is considered to be quite important. In the absence of any inspection reports, it must be assumed that the taps in the 9 flow sections included in this discussion were in good condition and in accordance with the specifications at the time of calibration.

In conclusion, according to the authors the throat tap flow nozzle when manufactured and calibrated in the prescribed manner should have a coefficient of discharge in the range of 0.994 to 0.998 at Reynolds numbers greater than 1.3×10^6. This is important for at least 2 reasons.

1 Those people not electing to calibrate their flow nozzle can be more certain of a flow measurement when suitable manometers are used than experience shows to be possible at present when using flow nozzles equipped with pipe-wall taps.

2 When a nozzle is calibrated and the resulting coefficient falls within the predicted range, a greater sense of security is justified in the belief that the coefficient will be stable and not

change to another value under different flow conditions having the same Reynolds number.

If further experience with throat tap flow nozzles substantiates the data presented by the authors, then another step has been taken in the process of improving the accuracy of flow measurement and consequently of economy testing.

A. H. Gibeling[3]

It is evident that the authors have done a great deal of precise experimental work in developing the flow characteristics of a specific type of a differential head flowmeter. Undoubtedly, these exacting studies have added much needed information to this difficult field of fluid flow measurement. I believe that the close correlation they have been able to show between the theoretical coefficient of discharge and their test results is just cause for firm confidence in the reliability and repeatability of this type meter.

It is noted that construction details of the flow nozzles described call for a very smooth finish of four microinches. Professor Jorissen reported several years ago that there is evidence to indicate that a very smooth surface may be subject to a more rapid change in value of flow coefficient due to deposits than is a less highly polished nozzle.[4] In this regard, it would be interesting to know if the authors have any experimental results showing the effect of surface finish on flow coefficient, or the effect of surface finish on the susceptability of flow coefficient to change with deposits of the type that may occur in turbine testing.

C. B. Haughton, Jr.[5]

The writer is familiar with the authors' perennial concern for accuracy of flow measurement in steam turbine performance testing, and shares their eagerness for examining all known errors that might affect the flow measurement by 0.1 per cent or greater.

It is particularly interesting and useful to have test data from ASME flow nozzles used in a "round robin" of calibrations at several different hydraulic laboratories around the country. The writer feels sure that the laboratories themselves will benefit substantially from the presentation of these calibration results, leading them perhaps to make little improvements which they had been wanting to make in the past, but for which they heretofore may not have had quite the right incentive. It is hoped, therefore, that detailed examination of the point scatter herein reported will be made by all concerned, especially where data at the same Reynolds number differ among several laboratories by one half per cent or more.

A person faced with the necessity of determining a nozzle coefficient of discharge by hydraulic means often wonders about the "absolute value" of the coefficient, or its agreement with the *true* value. In spite of sincere and sometimes elaborate efforts on the part of the hydraulic laboratory to justify its statement of precision of volume or weight measurement, precision of time measurement, and so on, the fact remains that few such laboratories are able to make any exact statements of *absolute* accuracy of the coefficient without checking every measurement by really independent means on the premises, or by sending a given calibrated meter to several other similar laboratories for independent checking. The authors are to be congratulated for having indirectly performed this service, not only for the laboratories mentioned, but also for their past and prospective customers.

In connection with the foregoing it might be helpful to mention the existence of a British paper having to do considerably with this subject.[6] It would be useful to compare the detailed practice outlined in this paper with that of the several laboratories mentioned in the authors' paper.

It is also gratifying to see the authors demonstrate the advantages of comparing nozzle coefficient tests with theory. Until the publication of Reference [3] of the paper, supplemented by a paper by Rivas and Shapiro,[7] there did not seem to be many attempts, if any, to calculate the discharge coefficient of a nozzle and then to run tests to justify or check the original assumptions. It is believed that, had more investigators done this, a greater insight into the meaning of a discharge coefficient would have resulted, and might have led to the optimum refinement of nozzle and venturi geometries on a less empirical basis than seems to have been actually used. On the other hand, it must be recognized, too, that the subject of fluid and gas dynamics itself has matured only during the last twenty years, and that this will partially account somewhat for the prior lack of theoretical treatment of nozzle discharge coefficients using the computation techniques now available.

The following suggestion is made in the Rivas and Shapiro paper, page 496 of the Reference, pertaining to the diameter of the pressure hole of the throat taps: ". . . . . it is important to keep in mind that the static tap is in a region where the boundary-layer thickness may be smaller than the diameter of the pressure hole. In order to avoid large errors in the static pressure reading, therefore, the pressure hole must be meticulously constructed." Would the authors comment on their experience with throat tap hole size, especially as a function of the throat diameter, as well as location upstream of the nozzle exit face? It would certainly seem that the data point scatter throughout the Reynolds number transition region on the curves of the paper could well be attributed somewhat to improper hole geometries, although a definition of just what is "proper" for every case may be very elusive.

The comments just mentioned in the Rivas and Shapiro paper are seconded in another way by Redding, a British investigator of metering nozzles. He states[8] in the second part of his paper (page 43) in a footnote, that ". . . . . it appears that direct determinations of the flow coefficient using '1 *D*-nozzle exit' taps are subject to large probable error. This, it is believed, is due to the difficulty of establishing reproducible conditions at a tapping point which connects with a zone of very high velocity, as is often apparent when the downstream tapping is made directly into the wall of the throat itself." (The "1 *D*-nozzle exit" refers to the taps in the throat.)

Thus it appears that the authors have done an excellent job in keeping flow errors due to tap location and construction to a minimum, and it is believed that they will agree wholeheartedly with the cautions of Redding, Rivas, and Shapiro, regarding the extreme care one must use in making throat tap nozzles for very accurate flow measurements.

---

[3] Supervisory Engineer, Steam Turbine Department, Allis-Chalmers Manufacturing Company, Milwaukee, Wis. Mem. ASME.

[4] Andre L. Jorissen, "International Standardization of the Measurement of Flow," presented at the ASME Annual Meeting, 1955.

[5] Staff Engineering Specialist, Flight Propulsion Laboratory Department, General Electric Company, Lynn, Mass. Mem. ASME.

[6] E. A. Spencer and A. T. J. Hayward, "The Accurate Calibration of Flowmeters With Water," *Trans. The Society of Instrument Technology*," vol. 9, no. 1, 1957, page 1.

[7] M. A. Rivas, Jr., and A. H. Shapiro, "On the Theory of Discharge Coefficients for Rounded-Entrance Flowmeters and Venturis," TRANS. ASME, vol. 78, 1956.

[8] T. H. Redding, "Minor Losses in Metering Nozzles," *The Engineer (London)*, vol. 204, no. 5293, p. 4; no. 5294, p. 41; and no. 5295, p. 76, July 5, 12, and 19, 1957, respectively.

James W. Murdock[9,10]

The experimental data presented in this paper make a substantial contribution to the literature on the use of nozzles employing throat taps. The authors' general conclusions that there is need for more such data at high Reynolds numbers certainly cannot be argued with.

The theoretical aspects of this paper are of major concern since the danger exists that the authors' theoretical curve might be used to extrapolate data without an appreciation of the basis of this curve.

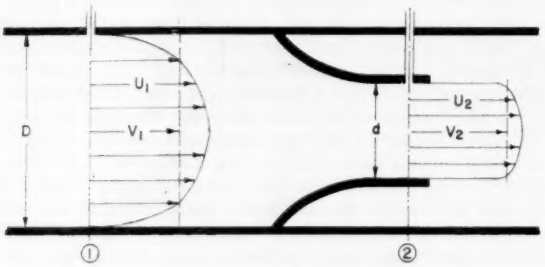

ACTUAL

$$\frac{p_1}{\gamma} + \frac{\alpha_1 V_1^2}{2g} = \frac{p_2}{\gamma} + \frac{\alpha_2 V_2^2}{2g} + H_{1L_2} \qquad [1]$$

IDEAL

$$\frac{p_1}{\gamma} + \frac{V_1^2}{2g} = \frac{p_2}{\gamma} + \frac{V_2^2}{2g} \qquad [2]$$

Fig. 13 Nozzle energy equations

The coefficient of discharge of a flow nozzle is defined as the ratio of the actual to the ideal flow rate. Fig. 13 shows the flow of a fluid through a throat tap nozzle indicating the velocity profile of the local velocity U with the average velocity V at the inlet and throat tap locations. Equation (1) takes into account energy relationships of an incompressible fluid with nonuniform velocity distribution and fluid friction. Equation (2) shows the energy relationships of an ideal incompressible fluid having a uniform velocity distribution.

Fig. 14 defines the individual components that make up the frictional losses in a flow nozzle. If Equation (3) be substituted for the head loss term of Equation (1) and the principle of continuity be employed, together with the definition of coefficient of discharge, the expression for coefficient of discharge of Equation (4) may be obtained. The steps of such development are omitted to conserve space but techniques for accomplishing this may be found in any elementary fluid mechanics text.

The Shapiro and Smith nozzle equation is based on flow from an infinite reservoir, or in terms of the pipe flow nozzle, the pipe diameter approaches infinity and the ratio of throat to pipe diameter (beta) becomes zero. For such a condition Equation (4) reduces to Equation (5). If the velocity distribution at the throat tap is assumed to be uniform, then alpha 2 becomes unity and if the bellmouth loss is translated into equivalent length of throat, Equation (5) may be written in the form of Equation (6), which is essentially the Shapiro and Smith relationship.

Cotton and Westcott state in their paper that a value of one half is to be used for X/D when applying their equation asserted to be the Shapiro and Smith equation. In the nozzles described in the paper the distance from the bellmouth exit to the center line of the throat tap is one half throat diameter. This can only mean that no allowance is made for bellmouth losses. This is difficult to understand since Shapiro and Smith suggest that this value is approximately 0.4 of the throat diameter. In a more sophisticated theoretical treatment of bellmouth losses Rivas and Shapiro[11] suggest values ranging from 0.25 throat diameters at Reynolds number of 1000 to 0.56 at 1,000,000. The effective X/D would of the flow nozzle thus range from 0.75 to 1.06.

Fig. 4 is stated to be taken from the work of Shapiro and Smith to determine the value of $4f_{App}$ to be used in their equation. Careful reading of the source material reveals no curve or curves equivalent to Fig. 4. Instead there is only the result of some water tests on smooth tubes. These data have been reproduced as discussion Fig. 16 with the Cotton and Westcott curve superimposed. It is clear that there is not a definite demarcation of transition from laminar to turbulent flow but rather a widespread zone and considerable data scatter.

From this discussion it is evident that the "theoretical" nozzle curve should be used only with the understanding that:

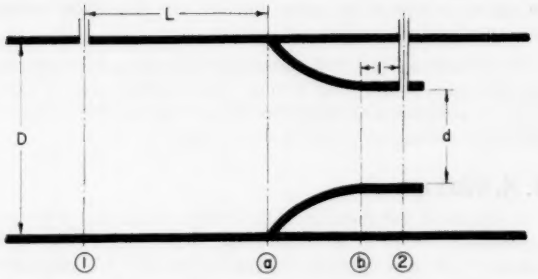

HEADLOSS = PIPE FRICTION + BELLMOUTH + THROAT

$$H_1L_2 = H_1L_a + H_aL_b + H_bL_2$$

$$H_1L_2 = \left(\frac{fL}{D}\right)\frac{V_1^2}{2g} + K_b\frac{V_2^2}{2g} + \left(\frac{\bar{f}l}{d}\right)\frac{V_2^2}{2g} \qquad [3]$$

Fig. 14 Nozzle losses

$$Cd = \left[\frac{1-\beta^4}{(\alpha_2 + K_b + (\frac{\bar{f}l}{d}) - (\alpha_1 + \frac{fL}{D})\beta^4}\right]^{\frac{1}{2}} \qquad [4]$$

$$\beta = \frac{d}{D} \qquad \text{IF} \quad D \to \infty \quad \beta \to 0$$

$$Cd = \left[\frac{1}{\alpha_2 + K_b + \frac{\bar{f}l}{d}}\right]^{\frac{1}{2}} \qquad [5]$$

$$\text{IF} \quad \alpha_2 = 1, \quad K_b + \frac{\bar{f}l}{d} = \frac{\bar{f}l_{eq}}{d} + \frac{\bar{f}l}{d} = \frac{\bar{f}l'}{d}$$

$$Cd = \left[\frac{1}{1 + \frac{\bar{f}l'}{d}}\right]^{\frac{1}{2}} \qquad [6]$$

Fig. 15 Coefficient equations

[9] The opinions and assertions in this discussion are the private ones of the discusser, and are not to be construed as official or reflecting the views of the Navy Department or the Naval Service at large.

[10] Head, Applied Physics Division, U. S. Naval Boiler and Turbine Laboratory, U. S. Naval Base, Philadelphia, Pa. Mem. ASME.

[11] M. A. Rivas, Jr., and A. H. Shapiro, "On the Theory of Discharge Coefficients for Rounded-Entrance Flow Meters and Venturis," TRANS. ASME, vol. 78, 1956.

It is not a truly theoretical curve, but is based on experimental data that apply only to one of the losses of a flow nozzle.

2 The experimental data to substantiate this curve are subject to some scatter and an uncertain zone of transition from laminar to turbulent flow.

3 No allowance has been made for bellmouth loss and hence the curve inflection points might well occur at half the values shown.

4 No allowance has been made for the effects of the approach pipe velocity profile or losses from inlet tap to bellmouth entrance.

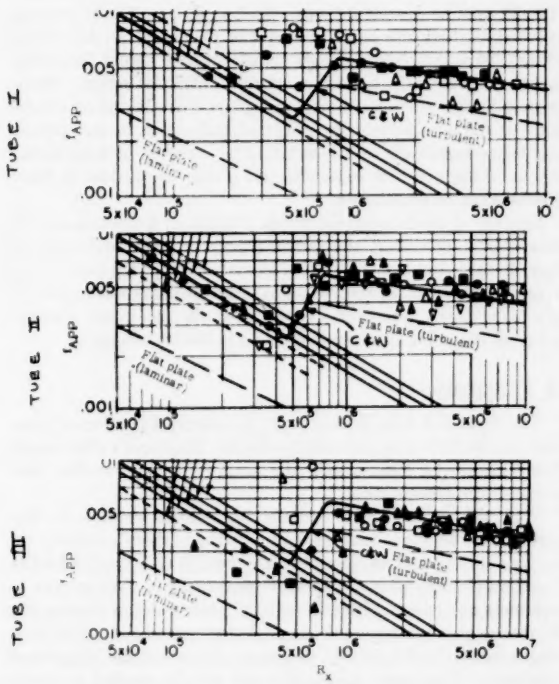

Fig. 16 Source data for Cotton and Westcott Fig. 4

Fig. 17 shows the various theoretical nozzle curves now available in the literature. The work of Hall[12] is so recent that it could not have been available to the authors at the time of their preparation of this paper. All are based on flow from an infinite reservoir. The Rivas and Shapiro curve is based on boundary layer theory and experimental data. The Hall work is based on boundary layer theory using the concept of displacement thickness.

Examination of Fig. 17 indicates a wide range of Reynolds numbers possible for transition from laminar to turbulent flow. Even with calibration it is possible to have an uncertainty of 0.1 per cent or greater in the Reynolds number range from 100,000 to 1,500,000.

It is believed that extrapolation of data on the basis of the Cotton and Westcott theoretical curve as was done in Fig. 7 is not justified. In the present state of the art only calibration of Reynolds numbers over 1,500,000 should be used to determine the coefficient.

Lawrence C. Neale[13]

The authors have presented a most interesting study of the necessary preparation and effort required to secure accurate flow measurements. The paper also affords an opportunity to compare the work in three university laboratories operating in the calibration field in the U. S. A. This comparison indicates that all three laboratories are doing very consistent work.

In reviewing the descriptive matter on the laboratories, one or

[12] G. W. Hall, "Application of Boundary Layer Theory to Explain Same Nozzle and Venturi Flow Peculiarities," The Institution of Mechanical Engineers, London, England, Advanced Copy dated 10/59.

[13] Associate Professor, Alden Hydraulic Laboratory, Worcester Polytechnic Institute, Worcester, Mass. Mem. ASME.

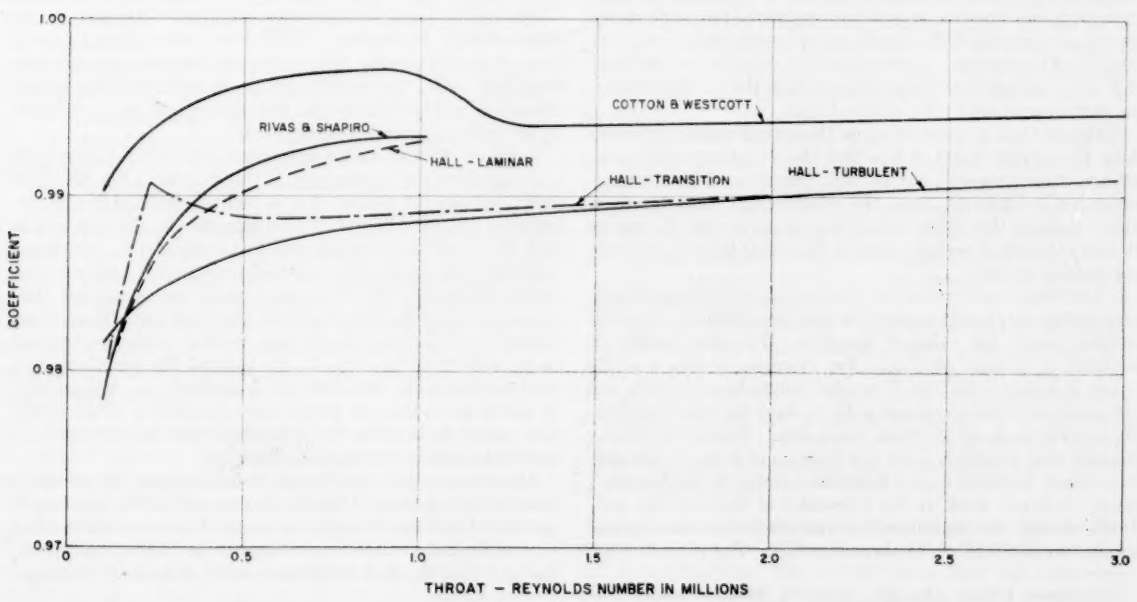

Fig. 17 Theoretical nozzle coefficients

two items could be stated more clearly. At the Alden Hydraulic Laboratory the flow was measured using a single 50,000 pound capacity weighing tank. The weight is measured statically for each run since the water is switched in and out of the tank at the beginning and end of each flow determination, with no flow entering the tank during either the initial or final weight determination.

The time is measured using a Standard Electric timer which is actuated automatically with the flow switching device at the tank.

Therefore it is not understood how the Alden Hydraulic Laboratory system differs in character from the G. E. Turbine-Generator Development Laboratory.

In reviewing paragraph four of the conclusions, it would seem that proper treatment of piezometer taps before test would eliminate this possibility of trouble. Although an absolutely square corner with no burrs is the ideal, it has been found that a radius on the tap hole of $^1/_4$ the tap diameter can be more easily machined, is less sensitive to damage or change, and gives the same pressure reading. For more details refer to the paper entitled, "Piezometer Investigations," by C. M. Allen and L. J. Hooper, TRANS. ASME, 1932.

R. E. Smith, Jr.[14]

The authors of this paper have done a major service in bringing together, for direct comparison, calibration data from several of the outstanding hydraulic laboratories in this country. Since the design concepts and operating techniques of these laboratories are different, a comparison of these data yields an insight into the absolute accuracy of the "total" calibration techniques at each laboratory.

It is gratifying to see a real attempt made to utilize long existing theoretical techniques in conjunction with good experimental data. Too often the complete acceptance of experimental results without regard for theoretical results leads to erroneous conclusions.

The selection of nozzle throat taps as the downstream sensing station really establishes a major portion of the job to be done by the authors. The location of sensing taps in the region of maximum dynamic pressure or velocity maximizes the error of the taps due to manufacturing flaws and to foreign objects accumulated during operation. Agreement of the data from several taps (e.g., Fig. 7 of paper) indicates the success of the tap manufacturing technique in producing identical taps.

Although there is no net effect on the experimental calibration data, the authors might deduce that the throat taps read a significant "overpressure" due to their diameter. This overpressurization is apparent since the experimental data for C_q is higher than the theoretical values (Figs. 5 and 6) even though the theoretical method neglects some of the nozzle losses (e.g., loss in contraction section).

It is extremely unfortunate that the maximum calibration Reynolds number only barely exceeds the apparent transition Reynolds number, since the value of transition Reynolds number is sensitive to several variables. For example, in Fig. 9 of the paper, it is shown that the Worcester Polytechnic Institute and University of Pennsylvania data do not have the same transition characteristics as do the Ohio State data. Present techniques consider that transition point is a function of surface roughness, free stream turbulence, and Reynolds number in the boundary layer; however, work at the University of Berlin in the early 1940's showed that transition was also affected in some manner by the "wettability" of the channel surface. Therefore, it might be expected that the transition point will vary from lab to lab, depending upon the nozzle cleaning techniques used (type of solvent, method of solvent application, amount of handling during and after cleaning, etc.) and type of water (treated feedwater, pond water, etc). As a result the agreement of transition region in the Turbine Generator Development Laboratory data (Fig. 5) and Ohio State data (Fig. 9) with the values from work of Shapiro (Fig. 3) must be considered somewhat fortuitous. The Worcester Polytechnic Institute and University of Pennsylvania data (Fig. 9) may be interpreted to show transition at a throat Reynolds number significantly less than 800,000–1,300,000 range. Since the free-stream turbulence level also plays a role in the establishment of the boundary layer transition, differences in turbulence, and hence transition, would certainly be expected in lines downstream of such devices as mechanical pumps as opposed to lines downstream of standpipes.

Because of the importance of the position of transition on the flow coefficient values, the use of a very smooth nozzle surface may be undesirable. The use of boundary layer trippers in the contraction section of the nozzle to insure that turbulent boundary layer flow exists in the nozzle over the maximum possible range of Reynolds numbers might be a useful technique.

R. E. Sprenkle[15]

The technical data in this paper are especially welcome since they are the first to be published since Mr. Buckland's 1932 paper. We accordingly congratulate the authors in this excellent and worth-while presentation.

With the accuracy of the throat tap nozzles we have no dispute, since they have long been used by the authors' company for turbine testing and are generally accepted in this specific field as excellent primary elements for flow measurement. We are also in complete agreement with the authors' philosophy of eliminating in their turbine test procedures all known errors that affect flow measurement by 0.1 per cent or greater, in view of the high stakes involved. This same philosophy can also be applied to many other areas such as continuous performance monitoring which also requires the maximum in accuracy and reliability of flow measurement.

We wish to point out, however, that equal precision can be obtained with the standard ASME flow nozzle, using pipe wall taps, or by a concentric orifice, provided the same specifications were met as to the precision of its manufacture, the careful laboratory calibration, and the installation and use, as outlined by the authors for the throat tap nozzle.

Evidence of what can be expected of the ASME nozzle using pipe taps is shown, for example, in this discusser's Fig. 18. This 10-in. pipe size, 44 per cent β ratio precision-finished flow nozzle, together with its adjacent 30 pipe diameters on the inlet and 10 pipe diameters on the outlet, was first calibrated at Ohio State, using the tube bundle type of straightening vanes similar to that shown and described in this paper. Nearly two years later, after we had replaced the tube bundle in this assembly with our more modern multiplate flow straightener, the flow nozzle assembly was again calibrated, this time in the General Electric Company's Turbine-Generator Development Laboratory in Schenectady. It will be noted that the scatter and repeatability of the ASME flow nozzle tests using the multiplate flow straightener were within the desired ± 0.1 per cent tolerance.

About a year and a half ago a 10-in. pipe size, 40 per cent β ratio throat tap General Electric nozzle, and a 10-in. pipe size, 60 per cent β ratio ASME pipe tap nozzle, both precision-finished, were calibrated at Ohio State University in identical piping setups and using the flow straightener on the inlet side. Results of

[14] Assistant Branch Manager, Turbojet Branch, Engine Test Facility, ARO, Inc., Arnold Air Force Station, Tenn. Assoc. Mem. ASME.

[15] Director of Education, Bailey Meter Company, Cleveland, Ohio. Mem. ASME.

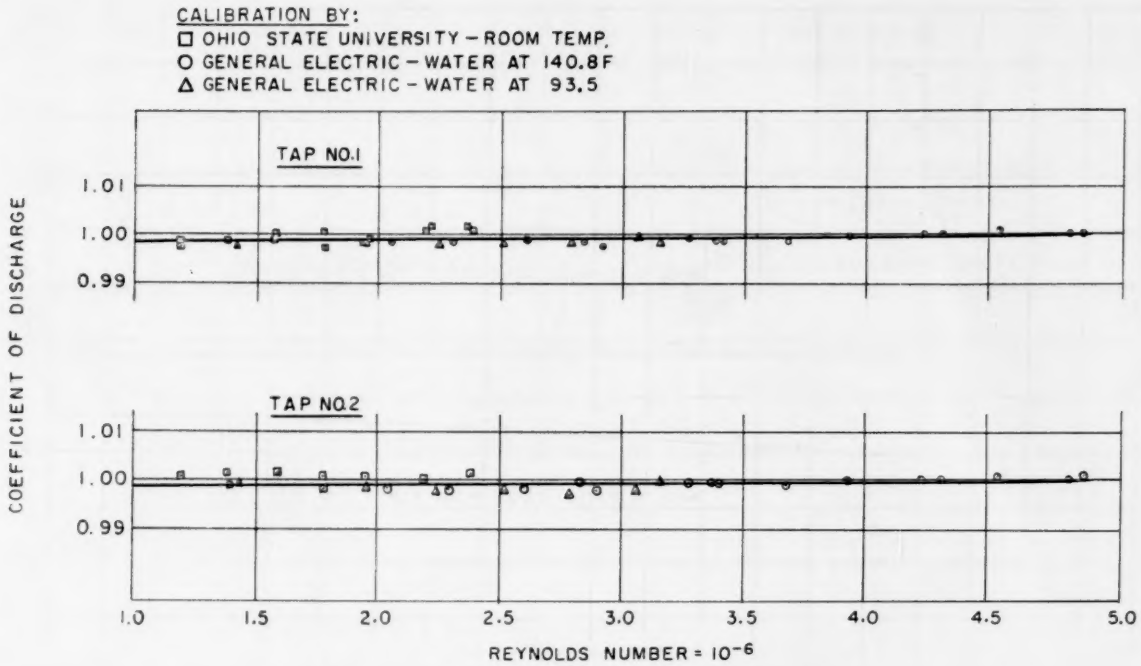

Fig. 18 Coefficient of discharge, 4.472-in. throat diameter flow nozzle

these tests are shown in Fig. 19 from which it will be noted that the scatter and reproducibility of the tests for both types of nozzles was about the same, and again within ±0.1 per cent. As would be expected from the data published in the ASME 1959 Fluid Meter Report, fifth edition, the coefficient curve of the ASME nozzle started to drop slightly as Reynolds numbers progressively decreased below 2,000,000, but agreed perfectly with ASME data above that value. Again, this drop in coefficient is of no practical significance, since this is below the Reynolds number range normally used in maximum accuracy flow measurements.

In connection with these same tests at Ohio State University, a standard 74 per cent β ratio concentric orifice was also calibrated using vena contracta connections. As illustrated in Fig. 20, no single test point in this calibration deviated from the average curve more than ±0.1 per cent.

From the foregoing examples, which are typical of many others, it can be seen that there is no perceptible difference in accuracy between the throat tap nozzle and the ASME pipe tap nozzle, when both are carefully built and calibrated with their adjacent piping and the flow straightener. The precision-made concentric orifice, likewise, is just as accurate and consistent as any other form of primary element, within its capacity range, when similarly individually calibrated. The choice of which to use then is dependent upon considerations other than maximum accuracy. Some of these are as follows:

1 The accumulation of dirt and other substances foreign to the metered fluid is of little or no importance in short turbine and similar testing, but it is a major factor in the continuous monitoring of the performance of a boiler or turbine unit or of a process. In cases where extraneous material does exist, the orifice is best within its capacity range, because dirt will not adhere to its sharp inlet edge, and thus the orifice stays cleaner longer. Further, it can be more easily removed for inspection and cleaning when necessary. The ASME nozzle extends the capacity range of the orifice and has the further advantage that the outlet pipe tap, being back of the nozzle throat, does not tend to become fouled with dirt, as do the throat taps.

2 It is quite difficult to so machine the throat tap openings into the nozzle throat that each tap will produce the same pressure measurement as the others. The authors' Fig. 5, for example, shows that the coefficient curve for Tap 1 is not quite the same as for Tap 3; this cannot help but lead to uncertainty as to which tap is correct. The ASME nozzle has no connections into the throat where the velocity is highest, but places this tap in the pipe wall back of the nozzle throat and out of the pathway of the flowing fluid, so that it is not difficult even when 2 taps are made to have them both agree as indicated by the results shown in Fig. 18.

3 The extreme care which must be used in machining the throat taps, plus the additional wall thickness required to accommodate these throat tap passageways, results in a high cost of fabrication and consequently a high sales price. While this higher cost is of no great consequence to the turbine manufacturer who furnishes the equipment to prove his guarantees are being met, it is of considerable importance to the customer who buys flow nozzles for his own permanent use.

4 Because the ASME flow nozzle can be used up to 70 per cent β ratio, it has a considerable capacity advantage over the throat tap nozzle whose upper limit is 50 per cent β ratio. For example, an ASME flow was chosen for a pending research project partially because the maximum differential to be measured was 60 inches of Hg, whereas to have used a 50 per cent β ratio throat tap nozzle, the resultant differential would have been at least 120 inches of Hg.

It is our feeling, therefore, that while the throat tap nozzle is quite satisfactory for turbine tests it should be limited to that type of application. The ASME nozzle and the concentric orifice, on the other hand, are more versatile and, when installed and calibrated with the flow straightener as indicated in Fig. 21,

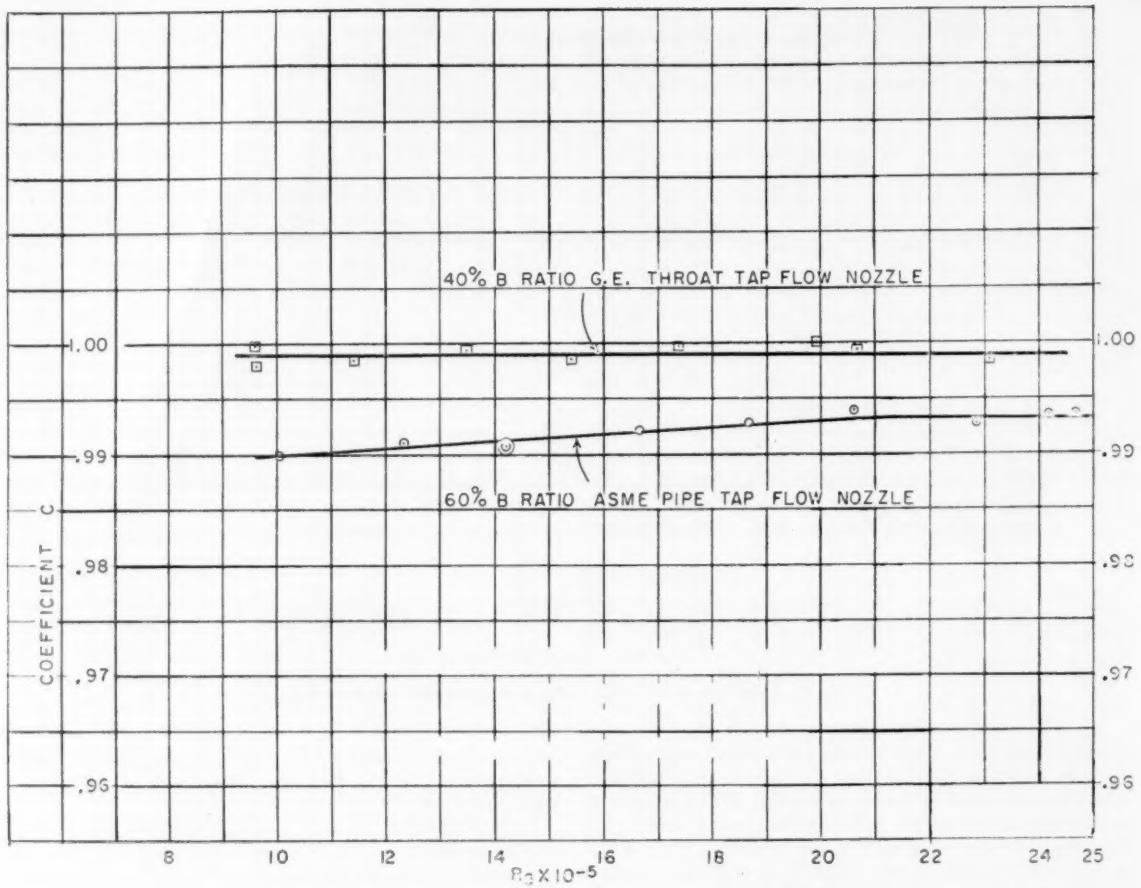

Fig. 19 Comparison tests of two 10-in. pipe size flow nozzles at Ohio State University

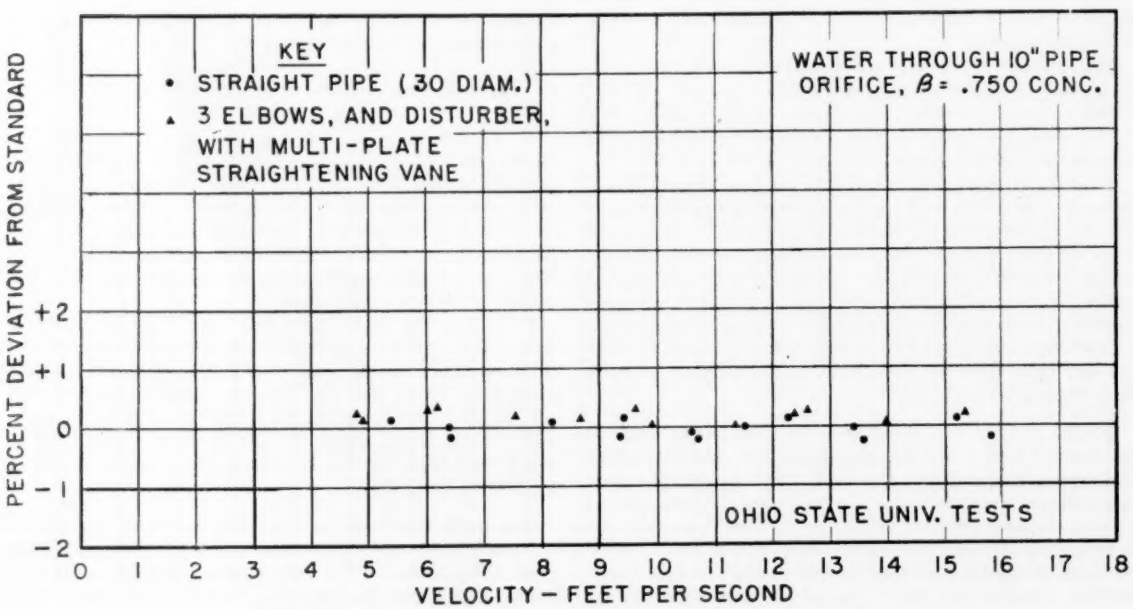
KEY
• STRAIGHT PIPE (30 DIAM.)
▲ 3 ELBOWS, AND DISTURBER, WITH MULTI-PLATE STRAIGHTENING VANE
WATER THROUGH 10" PIPE ORIFICE, β = .750 CONC.
OHIO STATE UNIV. TESTS
PERCENT DEVIATION FROM STANDARD
+2
+1
0
−1
−2
0 1 2 3 4 5 6 7 8 9 10 11 12 13 14 15 16 17 18
VELOCITY — FEET PER SECOND

Fig. 20 Coefficient of discharge of 74 per cent β ratio concentric orifice

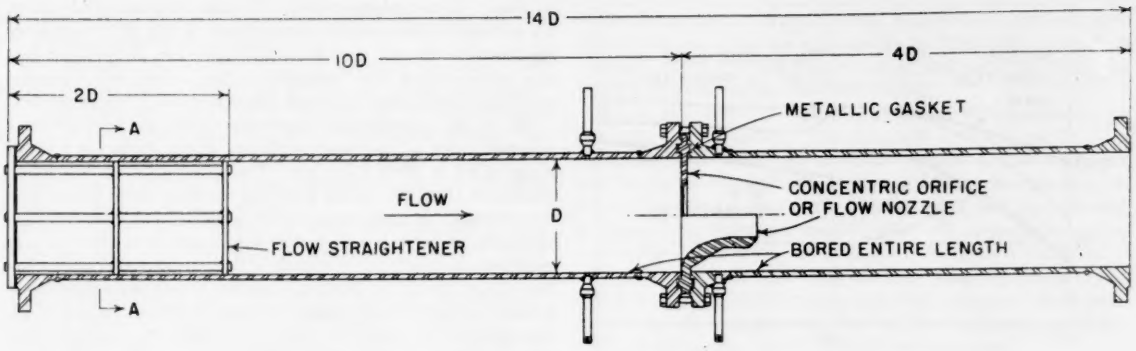

NOTE :- NO PROJECTIONS SUCH AS THERMOMETER WELLS, BACKING RINGS, ETC, INSIDE OF PIPE.

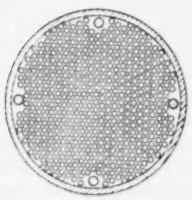

SECTION A-A

Fig. 21 Flow tube assembly

can be used not only for accurate precision testing, but also for day-by-day performance monitoring where consistency and reliability through long periods of time are of paramount importance.

Authors' Closure

We are indebted to the discussers for their very pertinent comments, in particular, those on the theoretical discharge coefficient curve. As a result of the interest shown in this curve and the information made available to us since the paper was written, we have calculated a new theoretical curve based on the total friction loss in the nozzle boundary layer and the increase in boundary layer thickness as the flow passes through the nozzle. Essentially, we extended the work of Rivas and Shapiro[11] beyond the laminar region. The following is a description of the method used:

1 The turbulent boundary layer characteristics, θ and δ^*, were calculated by numerical integration of the following three boundary layer equations. Step by step corrections were applied to account for three-dimensional flow.

$$a \quad \frac{\tau_0}{\rho u_1^2} = \frac{1}{u_1}\frac{du_1}{ds}(H+2)\theta + \frac{d\theta}{ds} \quad \text{(Momentum Integral)}$$

$$b \quad \frac{\rho u_1^2}{\tau_0} = [2.557 \ln (4.075\, R_\theta)]^2 \quad \text{(Squire-Young Formula)}$$

$$c \quad \theta\frac{dH}{ds} = [e^{4.69(H-2.975)}]\left[-\frac{\theta}{q_1}\frac{dq_1}{ds}\frac{2q_1}{\tau_0} - 2.635(H-1.294)\right] \quad \text{(Shape Factor Equation)}$$

where

$$q_1 = \frac{\rho u_1^2}{2}$$

τ_0 = shear stress at solid boundary

ρ = mass density

u_1 = free stream velocity

s = surface distance along solid boundary

θ = boundary layer momentum thickness

δ^* = boundary layer displacement thickness

$H = \delta^*/\theta$

This method of turbulent boundary layer calculation was worked out by Von Doenhoff and Tetervin (NACA 772).

2 From equations (5) and (13) of Rivas and Shapiro's paper, the theoretical flow coefficient can be expressed as:

$$C_q = 1 - 4\frac{\delta^*}{D} + 4\left(\frac{\delta}{D}\right)^2 \int_0^1 \left(1 - 2\frac{y}{\delta}\frac{u}{u_1}\right) d\left(\frac{y}{\delta}\right)$$

where

u = boundary layer velocity at points y

δ = boundary layer thickness

and we used:

$$\frac{u}{u_1} = \left(\frac{y}{\delta}\right)^{1/7} \quad \text{(for turbulent flow)}$$

$$\delta^* = \int_0^\delta \left(1 - \frac{u}{u_1}\right) dy$$

3 The turbulent calculations were started at the point of transition from laminar to turbulent boundary layer flow which was determined by calculating the criterion for transition, R_{θ_c}. The value, 470, used for this critical Reynolds number was calculated from Fig. 4 of this paper and Fig. 8 of Rivas and Shapiro.[11]

4 The laminar boundary layer characteristics and the free stream velocity distribution were taken from Rivas and Shapiro.[11]

The results of these calculations, plus Rivas and Shapiro's results, are shown in Fig. 22.

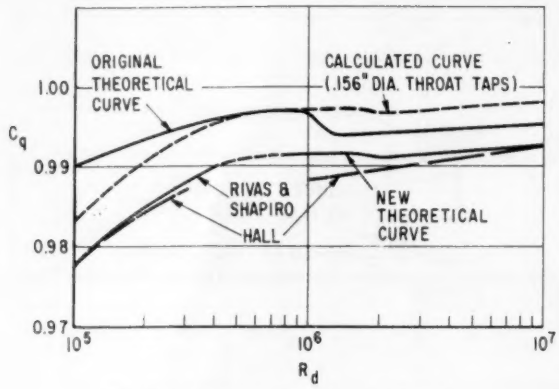

Fig. 22 Calculated nozzle flow coefficients

An investigation of the effect of static pressure tap size on the pressure readings confirmed the results published by R. E. Rayle, ASME Paper No. 59—A-234. Using these results and the new theoretical curve, we calculated the discharge coefficient curve, Fig. 22, for 43 per cent β ratio throat tap nozzles with 0.156-in. diameter taps. Also plotted in Fig. 22 are the results calculated by Hall[12] for a straight piece of pipe one diameter in length.

It is interesting to note that the slopes of the new theoretical curve and the calculated curve are very close to the slope of the original theoretical curve in the turbulent region.

The calculated curve agrees better than the original theoretical curve with the test results as can be seen by comparing Figs. 23 and 11.

The calculated curves neglect the approach velocity profile upstream of the nozzle since the effect on discharge coefficient is very small for β ratios less than 50 per cent. Assuming the distribution of velocity obeys the $^1/_7$-power law, the error is 0.015 per cent.

We agree with Mr. J. W. Murdock that extrapolation of calibration curves is subject to error; however, until facilities are available for calibrating at test Reynolds numbers or a better method of extrapolation is derived, we recommend that the calculated curve shown in Fig. 22 be used as a guide to extrapolate discharge coefficients for throat tap nozzles similar in design to the nozzles described in this paper.

We also agree with Mr. J. W. Murdock that there is no definite demarcation or transition from laminar to turbulent flow. This is the reason we state in our paper, "It is difficult to measure flow accurately if the nozzle is used in the laminar region and considerable error can be expected if it is used in the transition region."

We do not agree that the scatter in Smith and Shapiro's experimental data introduced significant errors in our original analysis. In the turbulent region, the test points are within about 0.1 per cent of the average values shown in Fig. 3. Much more significant is the fact that we used local values of apparent friction factors rather than integrated values. Since we abandoned our original analytical approach this correction is not presented.

Mr. N. R. Deming's pipe tap nozzle calibration curves have a constant value of discharge coefficient in the Reynolds number range of 0.8×10^6 to 2.4×10^6. The variation of the theoretical coefficient (Fig. 22) in this Reynolds number range is less than 0.1 per cent. If these nozzles were calibrated at higher Reynolds numbers, we expected that they would also show the discharge coefficient increasing very slightly with increasing Reynolds number. Only two of Mr. Deming's nozzles showed any suggestion of a *hump* as shown in our original theoretical curve. In view of our new analysis, we agree that this *hump* is very much smaller than indicated by our original theoretical curve. The variation of discharge coefficient in the neighborhood of the *hump* is about 0.05 per cent rather than the 0.3 per cent as shown in the paper. Had we used integrated values of apparent friction factor instead of local values, the magnitude of the *hump* would have been reduced considerably.

Mr. Deming noted the absence of calibration points at $C = 0.995$ to 0.996 in his data. In light of our recent analysis, we would not expect pipe tap nozzle discharge coefficients to be the same as throat tap nozzle coefficients. To obtain the expected pipe tap nozzle discharge coefficient it would be necessary to determine the pressure gradient from the nozzle exit to the pipe tap location.

We agree with Mr. A. H. Gibeling that nozzles with a very smooth surface may be subject to a more rapid change in discharge coefficient due to deposits than a less highly polished nozzle. We use a very smooth surface because it is easier to reproduce than a given roughness. We have not carried out a complete experimental investigation to determine the effect of surface finish on nozzle discharge coefficient. In general, the deposit collected during a two to three week test only amounts to a slight film. However, on one occasion the deposit was about a mil thick and the nozzle was recalibrated in this condition. The change in discharge coefficient was less than 0.1 per cent. Perhaps more work should be done in this area.

As a result of Messrs. C. B. Haughton and R. E. Smith's comments on static pressure measurements, we drilled two 0.020-in. and two 0.060-in. diameter taps in a 4.14-in. throat diameter nozzle in the same plane as the 0.156-in. diameter throat taps. This nozzle was installed in a 12-in. diameter flow section and calibrated in our turbine-generator development laboratory. Measurements taken from these three sets of taps confirmed the results obtained by R. E. Rayle in a 1-in. pipe. It appears that Rayle's results are not a function of throat diameter and thus are applicable to any size of throat tap nozzle.

We have no experimental data on the effect of the distance from the throat taps to the nozzle exit face. However, from theoretical

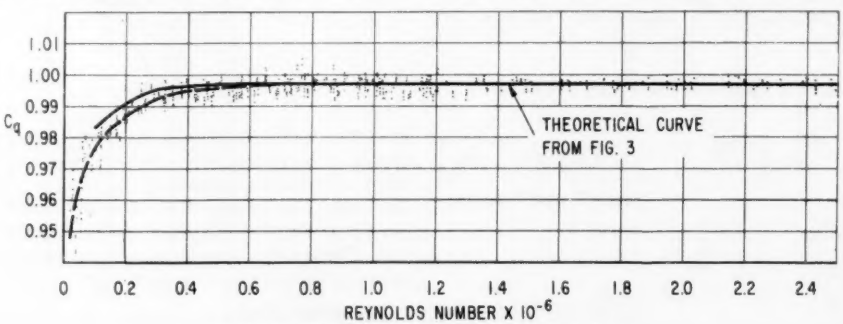

Fig. 23 Composite plot of nozzle calibrations

considerations, it does not appear that this is a significant effect. "It's what's up front that counts!"

We were very interested in Mr. R. E. Sprenkle's comment that equal precision can be obtained with pipe tap nozzles and orifices. The data submitted by Mr. N. R. Deming do not seem to substantiate this claim for pipe tap nozzles. Similar information has been presented in ASME Paper No. 57—A-206 which shows variations of 1.5 per cent in orifice calibrations made at the same laboratory on four different occasions.

Mr. Sprenkle's Figs. 19 and 20 show two pipe tap nozzles whose discharge coefficient differ by about $^3/_4$ per cent. These nozzles have different β ratios. However, according to the data published in ASME P.T.C. 19.5: 4-1959, this only accounts for about 0.1 per cent of the difference in discharge coefficients.

Both throat tap nozzles and pipe tap nozzles can be made for the same capacity. The throat tap nozzle does not suffer any greater loss of accuracy when used at large β ratios than does the pipe tap nozzle. The reasons we prefer throat taps are:

1 They measure the static pressure at the theoretically correct point, that is, at the point where the area is measured.

2 Throat taps are located in the well guided portion of the nozzle which makes them less sensitive to down-stream disturbances than pipe taps.

3 They are part of the precision device which receives special care in handling.

4 We have experienced very little deposit in the throat of the nozzle and have found very rough deposits at the downstream pipe tap location.

5 Throat tap nozzle discharge coefficients fall quite close to 0.996 at Reynolds numbers higher than 1.3×10^6.

Throat taps are more expensive to machine than pipe taps; however, the cost of this operation is only about 10 per cent of the cost of the flow measuring device. This cost is insignificant compared to the cost of incorrect heat rate test data. Total cost is of prime importance to the turbine manufacturer.

Mr. Sprenkle pointed out that Fig. 5 shows the coefficient curve for tap 1 is not quite the same as tap 3. This difference is 0.18 per cent. Taps 1, 2, and 4 agree within 0.06 per cent; therefore, taps 2 and 4 are used for heat rate testing.

We do not feel that orifices can be used with confidence for accurate precision testing. The authors of ASME Paper No. 57—A-206 felt that their 1.5 per cent variation in flow coefficient may be due to deposits on the pipe walls of the flow section. If this is true, an inspection of the orifice plate alone is not sufficient to insure accurate measurements. Nor will cleaning the orifice only restore the flow measuring device to its original condition.

Recently we calibrated two carefully made precision orifice flow measuring devices for a power station operator. Both were made from the same drawing, yet the flow coefficients were different by 0.6 per cent as nearly as we could measure.

The following are the reasons we prefer a nozzle rather than an orifice for accurate flow measurements:

1 We feel more confident in the extrapolated values of nozzle discharge coefficients than in extrapolated values of orifice flow coefficients.

2 The flow is well guided in a nozzle, whereas the vena contracta area of an orifice may be affected by such things as vortexes and downstream disturbances.

3 We have had less trouble due to damage and distortion with nozzles than we have had with orifices.

4 The change in discharge coefficient of a nozzle is much less than an orifice for variations in physical dimensions such as β.

Our experience has led us to believe that the most accurate flow measurement can be obtained with throat tap nozzles designed and manufactured as described in this paper.

The authors gratefully acknowledge the discussers' comments which led to the calculation of the new theoretical curve; to Professor Shapiro for his consultation; and to our colleague S. Chesmejef for his numerical integration of the turbulent boundary layer equations.

Water-Treatment, Corrosion, and Internal-Deposit Studies for Eddystone

R. C. ULMER
Manager, Research Department
Mem. ASME

H. A. GRABOWSKI
Chief Chemist, Mem. ASME

R. C. PATTERSON
Manager, Kreisinger Laboratory,
Combustion Engineering, Inc.,
New York, N. Y. Mem. ASME

Since water conditions could well decide whether the 5000-psi 1200-F Eddystone unit could be operated satisfactorily, every condition which might lead to a problem was given careful consideration. Tests at supercritical pressure indicated that a considerable amount of "soluble salts" deposited in the 850 to 950-F range when initially present at 2.0 ppm. Less deposition occurred with potassium salts than with sodium, but it was sufficient to make careful control of solids in the whole system imperative. This will be accomplished by demineralization of the make-up and by bypass demineralization of condensate as required.

When present in the amount anticipated for Eddystone, even at 1200 F there was no measurable decomposition or deposition of salts.

As to corrosion, proper control of dissolved oxygen and maintaining 10-ppb hydrazine and sufficient ammonia to give an 8.5 to 9.5 pH range, insured low metal pickup. Thus, deposition of metallic oxides in the boiler and turbine does not appear to be a problem. Corrosion tests and metallographic examination of the various alloys used indicate no harmful loss of metal or change in structure, hence no service-life problems are expected.

THE ENGINEERING ASPECTS of the Eddystone Plant were covered in three papers presented at the 1956 Annual Meeting [1, 2, 3].[1] Briefly No. 1 Steam Generating Unit is designed to deliver 2,000,000 lb per hr of steam at 5000 psi and 1200 F. There are two stages of reheat both at 1050 F. These steam conditions make this the most advanced thermal cycle in operation.

From the start, it was realized that water conditions could well decide whether the unit could be operated satisfactorily. Therefore, careful consideration was given to every anticipated condition which might lead to a problem. As was pointed out in the paper by Powell [2], the chief investigation along these lines involved two test boilers. The first, Fig. 1, is in the Laboratory of Sulzer Brothers in Winterthur, Switzerland, which operated initially at 4260 psi and 977 F, and was later modified for 1200 F. The second, Fig. 2, is in the Kreisinger Laboratory at Chattanooga, Tenn., and is operated as a joint project with Philadelphia Electric Company. It operates at 5000 psi and 1200 F and is a scaled model of the Eddystone unit.

The remainder of the paper presents a description of the two test units and results obtained to date.

Tests at Winterthur

The Sulzer test monotube unit, Fig. 1, was designed with four chief objectives in mind: (*a*) To study salt deposition in the tube system, (*b*) to determine whether any deposits that would form could be removed readily, (*c*) stability of water-treating chemicals that might be used in an operating unit, (*d*) pickup or corrosion of metals by supercritical steam.

In studying salt deposition in the tube system, it was desired to actually determine the amount of material depositing at a given location. This is in contrast to methods of other investigators who depend on measurement of temperature as an indication of the presence of deposits [4]. The amount of salt in a given section was determined by rinsing through sampling connections located at 20 to 30-foot intervals along the length of the tube. Nitrogen pressure was applied at each end of the tube at a greater pressure than existed in the system. This enabled any individual section to be rinsed and the wash liquid to be analyzed thoroughly. When using soluble salts, a chemical balance showed that all of the salt that deposited could be accounted for by rinsing the various sections of the tube. Also in one case, after a run with 2.0 ppm of salt, the unit was shut down "hot" and sections of the tube removed for examination. It was found that the heaviest deposit was present where "washing data" indicated it would be.

Data obtained for various sodium salts are shown in Fig. 3. In all cases the feedwater contained 2.0 ppm of the salt or mixture. First, referring to the scale on the right, it will be noted that 50 per cent of the sodium sulfate deposited. Lesser amounts of the other salts and the mixture deposited. It will be noted that in general most of the deposition occurs in the 850 to 950-F range with 900 F showing the maximum. Note that the mixture deposited over a wider temperature range and showed lower "peaks."

Although not shown in Fig. 3, some sodium hydroxide and sodium chloride deposited in the 400 to 520-F range. This corresponds roughly to the temperature at which hide out has been encountered in subcritical-pressure boilers.

Results with the corresponding potassium salts were similar except that less deposit formed. Caustic potash also deposited over a wide range of temperature, 150 F to 950 F. Potassium chloride deposited over three ranges of temperature, 390 to 540 F, 625 to 750 F, and 790 to 890 F.

The 2.0 ppm solids used in the tests should not be construed as the amount advocated or condoned for operating units. Also, it cannot be predicted whether the data apply to lower concentrations of solids. In this respect it is generally thought that a threshold value exists for each salt, below which no appreciable deposition will occur. This value may be as low as 100 ppb (0.1 ppm) as will be brought out later. For the records, the value of 2.0 ppm was selected so that sufficient material would deposit for test evaluation.

[1] Numbers in brackets designate References at end of paper.

Contributed by the Power Division and presented at the Annual Meeting, Atlantic City, N. J., November 29–December 4, 1959, of THE AMERICAN SOCIETY OF MECHANICAL ENGINEERS.

NOTE: Statements and opinions advanced in papers are to be understood as individual expressions of their authors and not those of the Society. Manuscript received at ASME Headquarters, September 1, 1959. Paper No. 59—A-147.

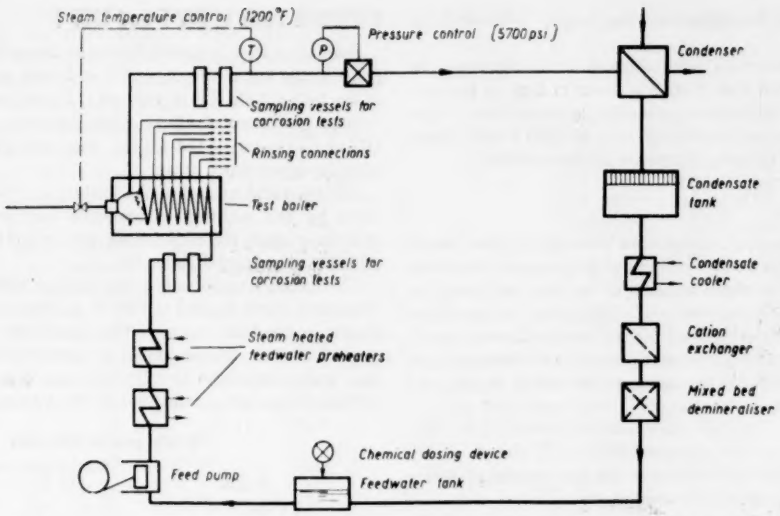

Fig. 1 Diagram of CE-Sulzer test monotube steam generating plant for supercritical pressure

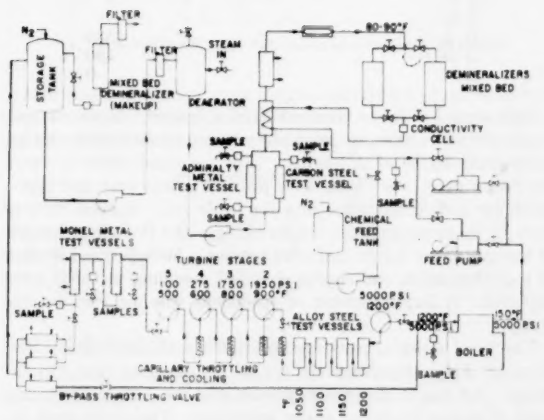

Fig. 2 Kreisinger Laboratory supercritical pilot plant flow diagram (simplified)

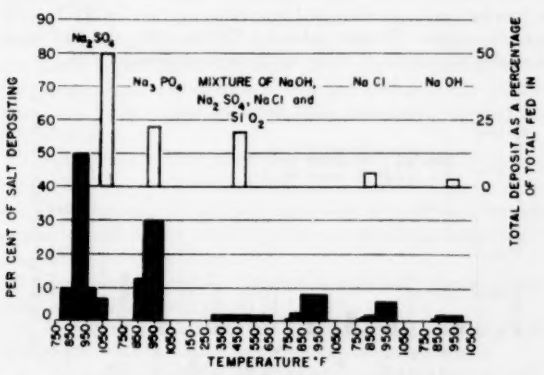

Fig. 3 Accumulation of sodium salts in CE-Sulzer supercritical pressure boiler

A prime concern in the investigation was the evaluation of the procedure for removal of deposits in the test unit. Water washing of the individual test sections proved to be a satisfactory means of removing the salts introduced into the system as a contaminating source. The salts referred to, with the exception of silica, are normally water soluble and did not revert to an insoluble phase. As metallic oxides may be present or constitute the whole deposit, data for these materials was desirable, and the program at Chattanooga contains work on this subject.

Stability of Treating Chemicals

Using the arrangement shown in Fig. 1, one-week tests were run with the treating chemicals given in the following table. Samples of condensate and feedwater were analyzed for their content of the chemical tested and the amount of decomposition was calculated from these results.

Chemical	Formula	Pressure, psi	Temp, deg F	Quantity decomposed in per cent of quantity in feedwater
Ammonia	NH_3	4270	1202	0
Cyclohexylamine	$C_6H_{11}NH_2$	4270	1202	88
Morpholine	$O(C_2H_4)_2NH$	4270	1202	100
Hydrazine	N_2H_4	4270	1202	100

Morpholine was investigated at other pressures and temperatures as shown in the following table.

Temp, deg F	Pressure, psi	Decomposition, per cent
932	(2940 (2205 (1470	0
1022	(2940 (2205	13
1112	(2675 (2940 (2205	60
1202	4410	100

It was found that decomposition was largely controlled by temperature.

These data are in line with those followed in this country. In general, it is considered that 1000 F is about as high as the materials can be used without appreciable decomposition. Ammonia, of course, does not decompose even at 1200 F and, therefore, generally is used for temperatures at or above 1000 F.

Corrosion Studies

The corrosion of metals in feedwater and supercritical steam has been determined in a series of tests with equipment shown in Fig. 1. These tests involved samples of (*a*) iron and nickel in the condensate and feedwater sections of the cycle, in pure water and in pH-adjusted water; (*b*) ferritic and austenitic-steel specimens in test vessels at supercritical pressure and temperatures of 842 F and 1202 F; and (*c*) metals used for tubing, piping, and valve-component parts in test vessels at 842 F and 4550 psi, and 1202 F and 4410 psi. Part (*c*) was conducted to extend the data of corrosion of chrome and chrome-nickel steels and to clarify differences of corrosion rates noted in the test results at Sulzer and Combustion Engineering Laboratories.

The oxygen content of the feedwater in parts (*a*) and (*b*) in the Sulzer tests was between 20 to 40 ppb. The cycle was a closed system and only the make-up water was deaerated in operation. A small fraction of the steam was used to deaerate make-up water. Thus, in this system, hydrogen formed in the reaction of supercritical steam and steel would accumulate in the recirculated water. In the Kreisinger Laboratory tests, all the water supplied to the boiler was deaerated and the hydrogen content in the feedwater was reduced to zero. Reviewing the preliminary corrosion data at the two laboratories, it was reasonable to assume that the lower corrosion data at Sulzer could have been due to the increased hydrogen content in the supercritical steam in contact with steel surfaces. The apparatus at Sulzer was modified in the last series of tests to deaerate all the feedwater and to introduce a fixed quantity of hydrogen into the water delivered to the boiler.

Pickup of Metals in Supercritical-Pressure Steam

The first tests were performed to establish the pickup of iron and nickel from the boiler. Corrosion data were obtained in pure water and when an amine was used to raise the pH value to between 8 and 9. The oxygen content of the feedwater was about 43 ppb. In this cycle, the contact time of water and steel was about 60 seconds and a significant pickup of metal would not be expected. The soluble iron and nickel found is summarized in the following table.

Iron pickup—Sulzer test boiler, 4270 psi, 1202 F

Feedwater		Fe, ppb[a]	
pH	O_2, ppb	Feedwater	Condensate
Without treatment			
6.9	43	3.5	4
With amine treatment			
8 to 9	43	4.4	4.4

[a] Average of 12 determinations.

In no case was more than 5 ppb of nickel found in the condensate or feedwater samples.

These tests show no measurable pickup of iron in the system. For the short contact time for one cycle, it was apparent that pH would not affect the pickup of iron. The condensate and feedwater piping, condensate storage tank, deaerator, and auxiliary apparatus were of 18-8 stainless material and would not contribute to the iron solubility in the cycle. Copper was not used in the system.

Corrosion Tests at 842 F and 1202 F

Specimens were installed in vessels located at an intermediate point in the boiler circuit, 842 F and 4550 psi, and at the outlet of the boiler, 1202 F and 4400 psi. In the second group of tests, tubular specimens of alloys, approximately 1.5 in. long with an OD of $^3/_4$ in. and ID of 1.2 in., were used to establish corrosion rates in supercritical steam.

The chemical control of the feedwater consisted of pH adjustment by the addition of ammonia and brief introduction of hydrazine upon start-up for oxygen reduction. Ammonia was added to keep the pH above 7.0.

The metals studied were those used for tubing and valve parts. Austenitic steels studied at 1202 F and ferritic steels at 842 F are shown in the table below. The specimens were machined and ground to size. Measurement of corrosion was based on weight gain and is expressed as milligrams per square decimeter. The corrosion data are summarized in the following table.

Weight gain in 500 hours

Steel	Weight gain, mg/sq decimeter 842 F	1202 F
TP-347		12
TP-316		15
17-14 Cu Mo		23
TP-321		32
T-11	72	
T-22	71	
H 46		580
G 18 B		190
G 32		0

This second series of tests involved a limited number of materials and there was a question of hydrogen accumulation and an inadequate degree of deaeration. For the third series of tests, the Sulzer cycle was changed to provide a deaerator and apparatus for adding hydrogen into the feedwater. Special devices were set up to measure the weight changes and thickness changes of the specimens before and after testing. Metallurgical studies of scale formation and special chemical descaling methods were included. A larger number of specimens was included in this study.

The third series of tests was conducted with specimens in the form of disks approximately $^3/_4$ in. in diameter and $^1/_{12}$ in. thick. All disk surfaces were ground and the surface finish and scale thickness could be easily measured. The disks were inserted in four test vessels in the supercritical boiler.

Fig. 4 indicates the gain in weight in supercritical steam at 842 F and 1202 F of various steels considered for high-temperature tubing and valve-component parts. The gain in weight per unit surface area and the calculated penetration in mils for 500 hr is of low magnitude. Weight gains for TP-316, 321, and 347 were of similar magnitude to those for the second series of tests.

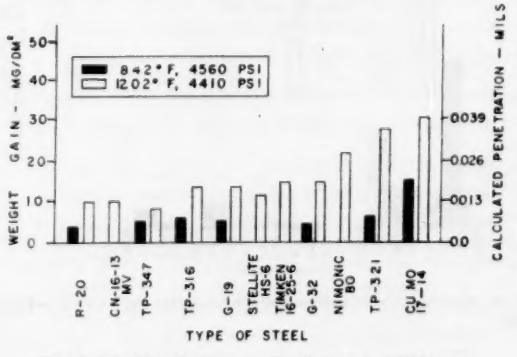

Fig. 4 Weight gain in supercritical steam in 500 hours

Hydrogen formed in the corrosion process was removed by the deaerator installed in the third series of tests. The effect of hydrogen addition on the iron-steam reaction was checked by the introduction of about 340 ppb of hydrogen into the boiler feedwater. Comparison of the gain in weight data for 500 hr, with and without addition of hydrogen, indicated that, for the quantity of hydrogen added, there was no apparent increase or decrease in general corrosion rate. Photomicrographs disclosed a slightly deeper local penetration of oxide into the base metal when hydrogen was added.

Some unmachined specimens were included in this series of tests. The corrosion rate increased markedly and the data for TP-321, 347, and 316 are shown in Fig. 5.

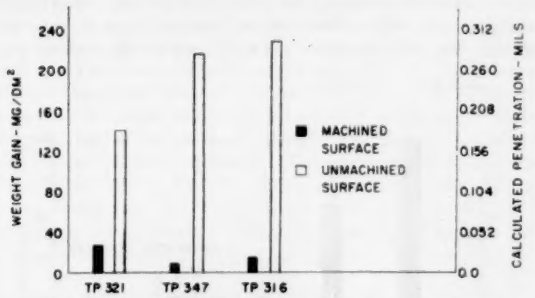

Fig. 5 Weight gain after 500 hours at 4400 psi and 1202 F

Acid washing did not have a significant effect upon the corrosion-rate data for ferritic and austenitic steel in supercritical steam. This is illustrated in the following table.

Weight-gain data in 500 hr

Steel	Temp, deg F	Weight gain, mg/dm² Normal	Acid washed
T-11	842	50	50
T-22	842	48	48
TP-347	1202	8	12

Tests at Kreisinger Laboratory

As mentioned, the second test boiler, at the Kreisinger Laboratory in Chattanooga, is essentially a model of the Eddystone No. 1 installation, and it operates in a simulated version of the Eddystone No. 1 water cycle. It comprises full-flow and make-up demineralizers, a deaerator, chemical feed equipment, boiler feed pumps, simulated turbine stages, a condenser, and storage tank as shown in Fig. 2. Incorporated into the water cycle at various points are several "test vessels," which are pressure chambers containing either metal shavings or weighed metal specimens. Installation and removal of test vessels has varied the system diagram from time to time but that shown is typical. More than 15,000 boiler operating hours have been logged at the time of writing.

This Laboratory pilot plant was designed with the following objectives:

1 To determine the solubility effects of 5000-psi water on the various metals in the circuit in their expected-use temperature ranges.

2 To study deposition of materials, principally metal oxides, in the simulated turbine stages.

3 To determine corrosion rates of system metals and alloys in 5000-psi water in their expected-use temperature ranges.

4 To evaluate the effect of proposed system water-treatment methods on the foregoing.

5 To study any unusual metallurgical effects which might develop in system metals during operation.

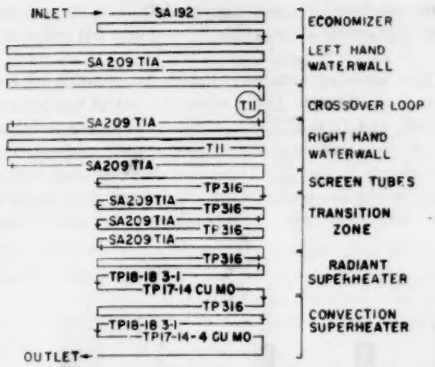

Fig. 6 Boiler circuit arrangement at Kreisinger Laboratory

6 To evaluate proposed methods of acid cleaning the internal surfaces of the entire system.

The preliminary feedwater control limits established for Eddystone No. 1 have been used in the tests when chemicals were added to the water.

The general water conditions were: (*a*) Complete demineralization of make-up water plus full-flow demineralization of boiler feedwater to ensure that all boiler feed is demineralized to 0.1 mmho conductance or better, (*b*) continuous deaeration of all boiler feedwater to 5 ppb O_2 or better.

The only chemical treatments proposed for the system have been addition of hydrazine to the feedwater for O_2 scavenging and ammonia for pH control as required. Numerous sampling connections and sample coolers are installed in the system to check such items as iron, copper, H_2, O_2, ammonia, hydrazine, and pH. Chemical feed, when used, is injected after the full-flow demineralizers but ahead of the boiler feed pump.

All system surfaces in contact with water are type 316 stainless steel except demineralizer housings which are plastic, test vessels and their contents (identified in Fig. 2), and the boiler tubing which duplicates the distribution of various types of steel and alloy tubing used in the Eddystone economizer, transition, superheat, and reheat zones. Several experimental superalloys of possible future use in high-temperature superheaters have been included in the model boiler and in the test vessels for evaluation purposes. A typical arrangement of tube metals in the test unit is shown in Fig. 6.

Reaction of Steel in Supercritical Steam

A principal objective in the study of the reaction of various steels in supercritical steam was to determine the suitability of various steels at elevated temperatures and to evaluate the deposition of metallic oxides when the steam was expanded through various turbine stages. The degree of reaction was measured by the analysis of iron and hydrogen in the steam leaving the boiler and test vessels and later by weight gain of specimens in the test vessels.

Three series of tests were conducted to evaluate the reaction of various steels at supercritical pressures in which the temperature and water treatment was varied. These studies involved the determination of: (*a*) The reaction of boiler steels with steam when the outlet temperature was 1000, 1100, and 1200 F with and without chemical treatment; (*b*) reaction of TP-316 in steam at 1000, 1100, and 1200 F with and without chemical treatment; (*c*) the reaction of TP-316, 347, 321, and 17-14 Cu Mo at 1200 F in steam without chemical treatment.

Solubility tests of steel in supercritical steam were conducted with a feedwater which was deaerated and passed through a polishing mixed-bed demineralizer. Chemical treatment of the

feedwater consisted of a continuous addition of 10 ppb of hydrazine and a quantity of ammonia to obtain a pH value of 9.0 to 9.2.

The first series of tests established the quantity of iron and hydrogen formed in the boiler when the outlet temperature was 1000, 1100, and 1200 F. Solubility of the boiler steels in pure water and when ammonia and hydrazine were added to the feedwater is shown in Fig. 7. These data indicate that evolution of hydrogen in the reaction of steel and supercritical steam is temperature dependent and is not affected by water treatment.

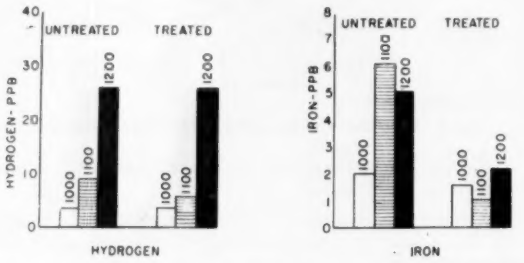

Fig. 7 Hydrogen and iron in supercritical steam at boiler outlet

The hydrogen content in the steam increased from 3 ppb at 1000 F, to 23 ppb at 1200 F. An increase in pH from 6.8 to 9.2 reduced the iron content in the steam leaving the boiler to about 2 ppb.

The solubility of TP-316 in steam at 5000 psi and 1200 F was determined in the second series of tests. A test vessel was filled with machined shavings of TP-316 to assure a high specific surface of stainless steel in contact with the steam. The reaction values would approach equilibrium since the specific surface was high and the velocity of the steam through the test vessel was low. Test results with and without chemical treatment are shown in Fig. 8.

The hydrogen content of the steam increased from 15 ppb to over 180 ppb when the feedwater was not treated with ammonia and hydrazine. With treatment the hydrogen content of the steam was reduced to 130 ppb. The iron dissolved into the steam was reduced from about 20 ppb to 2 ppb by chemical treatment.

Supercritical steam leaving the test vessels was passed through the simulated turbine during the first two series of tests. Examination of the turbine blades indicated no significant or measurable deposition of oxides. The only deposit observed was the thin layer of "blue-blush" oxide formed on the surface of the blades.

In the third series of tests, steam at 5000 psi and 1200 F was passed through four test vessels located in parallel. Each vessel was filled with an alloy steel so that the steam would be in contact with a high specific surface of the material. TP-316, 347, 321, and 17-14 Cu Mo were tested in this manner.

Fig. 9 summarizes the reaction data when the feedwater was not treated. As in the previous study, the hydrogen content in the steam from each reaction vessel was high, above the measuring limit of the recording analyzer, 180 ppb. The total iron analyzed at the outlets of the test vessels was below 5 ppb.

The results shown in Figs. 8 and 9 indicate that the solubility of the ferritic and austenitic steels in supercritical steam is of a low magnitude. There was no apparent relationship between the iron dissolved and the hydrogen measurements in the steam leaving the test vessels. It was evident that the dissolved-iron content did not provide a satisfactory index of corrosion at high temperatures and the testing procedure was altered to obtain a correlation of the hydrogen formed and the reaction rate of steels and supercritical steam.

Corrosion Rates

The testing procedure was altered to substitute weighed specimens of the alloy under test in lieu of a high specific surface in the form of metal turnings. The corrosion rate, as measured by gain in weight of the specimens, was in good correlation with the hydrogen evolved in the reaction. It was apparent that the reaction was proceeding according to the equation:

$$3\ Fe + 4\ H_2O = Fe_3O_4 + 4\ H_2$$

Practically all of the Fe_3O_4 remained on the specimens and was measured as weight gain. Owing to this condition tests for iron in the water are not an indication of corrosion rate.

The samples used for the corrosion-rate tests consisted of tubular specimens procured for service in the boiler. Sections of tubing were cleaned and weighed prior to installation into the test vessels. Fig. 10 indicates the weight gain for the various ma-

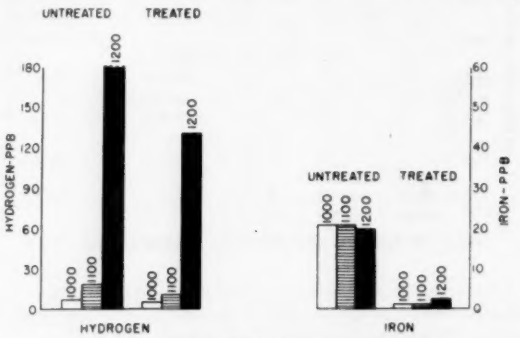

Fig. 8 Reaction of TP-316 in supercritical steam

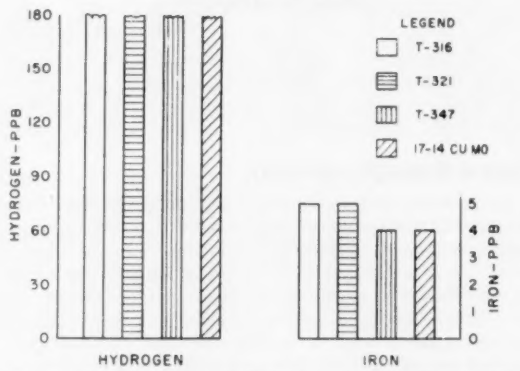

Fig. 9 Reaction of stainless steels in steam at 5000 psi and 1200 F

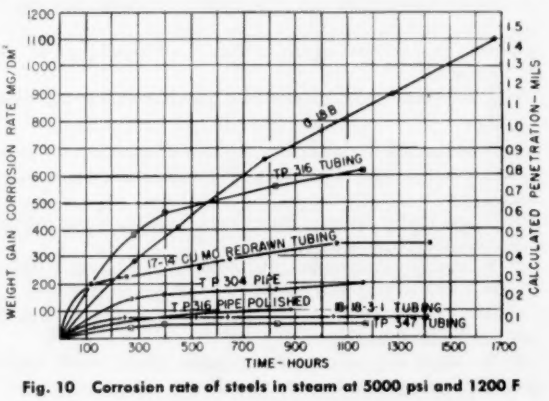

Fig. 10 Corrosion rate of steels in steam at 5000 psi and 1200 F

terials. The values noted were nearly 60 times greater than those reported by Sulzer in their preliminary corrosion tests as shown in Fig. 4.

These results were also in excess of those reported by Battelle in autoclave tests [5]. Though of higher relative magnitude, the corrosion rate leveled off at about 1100 hr and the calculated penetration was less than 0.8 mils for all materials tested with the exception of a valve material G 18 B. TP-316, 304, 347, Timken 18-18-3-1, and 17-14 Cu Mo tubing were tested in the first series of corrosion-rate tests.

The tube specimens were alternately heat-treated, acid washed, and polished to establish whether surface impurities contributed to the increased corrosion rate. None of these procedures altered the high rate of corrosion to any significant degree.

Following a metallurgical check of the mill scale, the tube samples were machined lightly to remove 2 to 3 mils of tube surface. The machined surfaces were installed into the test vessels and the results obtained are shown in Fig. 11. A significant reduction in weight gain was in evidence immediately. The corrosion rate of the machined surfaces was in close agreement with the data reported by Sulzer. The magnitude or reduction is clearly illustrated in Fig. 12. Thus, in machining the surface, the corrosion rate of TP-316 decreased from about 650 to 9 milligrams per sq decimeter after an exposure of nearly 1100 hr in supercritical steam at 1200 F.

Chemical Cleaning and Metallurgical Analysis

At the end of 7300 hr of operation, the supercritical boiler at Kreisinger Laboratory was removed from service for the purpose of checking the condition of the tube surfaces. Representative

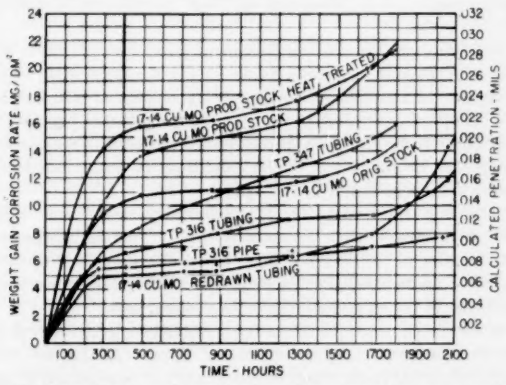
WEIGHT GAIN CORROSION RATE MG/DM²
CALCULATED PENETRATION - MILS
TIME - HOURS
17-14 CU MO PROD STOCK HEAT TREATED
17-14 CU MO PROD STOCK
TP 347 TUBING
17-14 CU MO ORIG STOCK
TP 316 TUBING
TP 316 PIPE
17-14 CU MO REDRAWN TUBING

Fig. 11 Corrosion rate of machined steel specimens in steam at 5000 psi and 1200 F

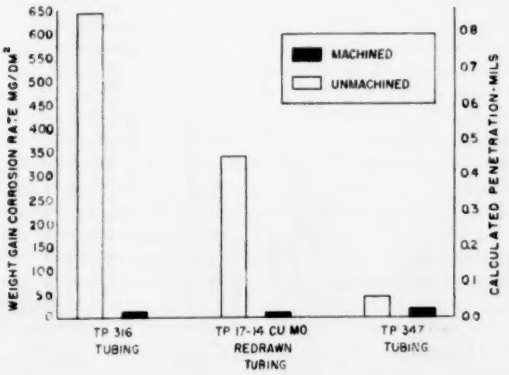

Fig. 12 Weight gain after 1700 hours in steam at 5000 psi and 1200 F

sections of tubing were taken from the economizer (SA-192), water wall (SA-209 and T-11), transition zone (SA-209 and TP-316), radiant and convection superheaters (TP-316) for metallurgical analysis. Samples of 17-14 Cu Mo, 18-18-3-1, 304, and 321 were installed in the boiler following this shutdown.

Fig. 13 illustrates the measured thickness of oxide on the steam-contacted surfaces of the tubing. The oxide formed is not considered objectionable for the service application of the various steels. The small amount present confirms the data obtained with specimens in the test vessels.

Physical tests and microscopic examination after service indicated no embrittlement as a result of sigma-phase formation in TP-316 during service. A normal carbide migration and agglomeration was in evidence in the ferritic steels removed for examination.

Photomicrographs of two specimens are shown in Fig. 14. This figure indicates the scale layer of a SA-209Tla specimen taken at the outlet of the transition area and a section of TP-316 taken from the convection superheater. The SA-209Tla had an estimated inside scale thickness of 0.006 in. The metallographic structure showed a normal ferrite structure with partly dissolved carbides. The TP-316 had an inside scale of 0.004 in. There was a slight evidence of intergranular oxidation in local areas of TP-316. Comparison of unused TP-316 tubing, taken from the same batch of tubing, revealed that the oxidation did not occur in service but during the annealing process prior to service. The intergranular oxidation is a "catastrophic oxidation" and results from the sublimation of molybdenum oxide at annealing temperatures.

The boiler had been acid cleaned prior to initial operation. Cleaning with formic acid at 200 F did not remove surface scale or impurities. The unit was cleaned subsequently with hydrochloric acid. No evidence of sensitization of TP-316 or stress-corrosion cracking was noted as a result of this cleaning procedure.

At the end of 13,000 hr of service, the boiler was sectioned and the individual areas were acid washed with citric acid and later with hydrochloric acid for an estimation of deposit formation in service. Fig. 15 summarizes the location and relative percentage of deposits removed from the various boiler sections. It is evident that the principal amount of oxide deposit formed in the economizer, transition zone, and radiant superheater. The insoluble deposits occurred primarily in the temperature range 850 to 1050 F.

The citric-acid wash only removed part of the deposits. Hydrochloric acid was effective in removing the remainder. The use of hydrochloric acid caused no damage to the unit, which could be flushed thoroughly. Its use in actual units is not recommended unless thorough flushing is possible.

STEEL	APPROXIMATE TEMPERATURE °F	OXIDE THICKNESS INSIDE DIAMETER-INCHES
WATER WALL		
SA 209 Tla	300	0.005
SA 209 Tla	315	NO SCALE
SA 213 Tll	735	0.006
SA 213 Tll	750	0.001
SCREEN TUBE		
TP 316	775	0.001
TRANSITION ZONE		
SA 209 Tla	800	0.002
SA 209 Tla	850	0.004
SA 209 Tla	900	0.004
RADIANT SUPERHEATER		
TP 316	1000	0.004
TP 316	1015	NO SCALE
CONVECTION SUPERHEATER		
TP 316	1050	0.004
TP 316	1075	0.006

Fig. 13 Thickness of oxide scale on inside diameter after 7300 hours

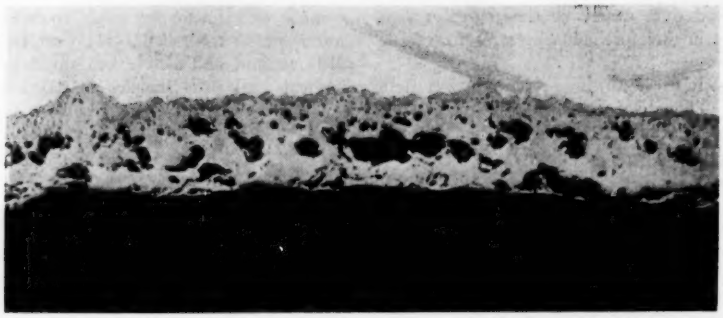

(a) SA-209T1a from outlet of transition zone (100X, unetched)

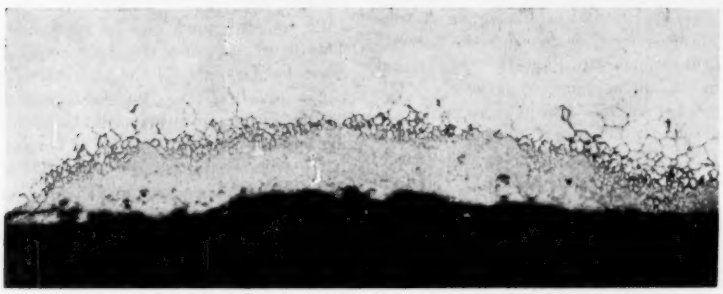

(b) SA-213 TP-316 from inlet of convection superheater (100X, unetched)

Fig. 14 Scale formation in 7300 hours in supercritical steam

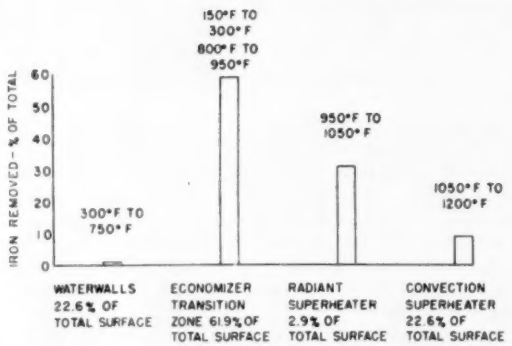

Fig. 15 Results of acid washing boiler at 13,000 hours

Copper

Recent experience and papers [6, 7, 8] on high-pressure boiler operation has centered attention on copper. There is concern regarding its effect on failures of boiler tubes as well as the possibility of forming deposits on heat-transfer surfaces and in the turbine. There especially was concern as to what might be expected in connection with the Eddystone unit. With this in mind test vessels containing copper-bearing specimens were installed in the system.

To obtain information regarding what might be expected in low-temperature heaters, a TP-316 alloy vessel containing lengths of Admiralty tubing was installed after the deaerator. The water temperature was 225 F. To determine what might be expected in high-temperature heaters, two 316 alloy vessels containing monel tubing were installed after the turbine stages. The first of these referred to as "dry Monel vessel" has steam at 100 psi and 500 F flowing through it. This simulates the dry portion of the heat-transfer surface. This steam then flows through the second vessel with sufficient cooling to cause some condensation. This simulates the "wet" portions of heaters and the drip systems.

To determine the effect of treatment, especially pH, tests were run with 10-ppb hydrazine alone at pH 6.5, and with 10-ppb hydrazine and sufficient ammonia to give pHs of 8.0, 9.0, and 9.5. Typical average data for the tests are given in Fig. 16.

It is interesting to note that excessive amounts of copper were not picked up under any of the conditions of test. The copper values were quite low even at 9.5 pH.

Referring specifically to the Admiralty vessel the copper pickup decreased with increase in pH. This is in line with field studies [9, 10]. There is no trend in values for the monel vessels. As mentioned previously, the values are quite low and of the order of the reproducibility of the copper test.

It should be mentioned that the dissolved oxygen was very low in all of the tests, being of the order of 3 ppb. At this low value, variation of pH in the range tested would not be expected to have much effect on the copper pickup. Assuming the same low value

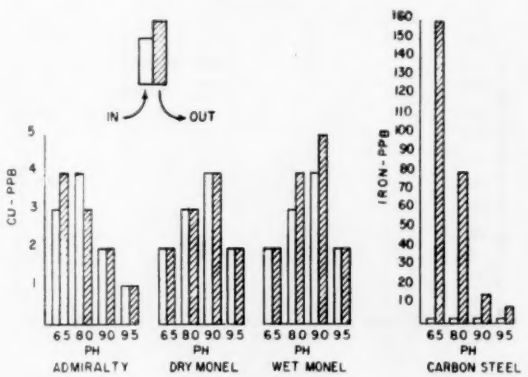

Fig. 16 Copper and iron dissolved from test vessels

for dissolved oxygen in the Eddystone plant, these data indicate that a pH value of 9.0 or even 9.5 is satisfactory for operation. A high pH, of course, is considered desirable to insure a low iron concentration in the system.

Discussion of Results

The incentive to carry out corrosion and deposition studies in supercritical steam was influenced by the work of Morey [11] who illustrated increased solubility of iron in water at very high pressures. Partridge [12] discussed the latter work which stated that at 15,000 psi and 932 F "pure water passing over mineral hematite, which is crystalline ferric oxide, picked up 90 ppm of Fe_2O_3." He speculated as to problems that might occur at 5000 psi and 1200 F.

The work at Kreisinger Laboratory and at Sulzer has clearly demonstrated that the solubility of iron in service at supercritical pressures is of a low magnitude. The major portion of the reaction product remains in situ on the tube surface. Also, the over-all corrosion rate of steel in water is relatively low even at supercritical pressures and temperature of 1200 F.

The investigation at Kreisinger Laboratory was developed to determine corrosion data in the boiler and the deposition characteristics of the corrosion products in a simulated turbine. This has been realized and the indications to date point to a low corrosion and deposition rate when the feedwater was treated as tentatively outlined for Eddystone.

One item which has proved to be troublesome is the interpretation of the corrosion rates of machined and unmachined surfaces. The effect of mill scale on the initial corrosion rate has been confirmed by Sulzer. Data obtained at both laboratories have pinpointed the mill surface finish as the prime cause for the increased corrosion rate at 1200 F.

A metallurgical examination of the unmachined surfaces prior to testing has disclosed a large quantity of finely distributed metallic inclusions in the mill-scale layer. The surface area of the inclusions was considerably greater than the area of the specimen. Exposure of the specimen in steam resulted in the oxidation of the impurities in the scale layer. It is believed that the oxidation of these particles contributed to the large gain in weight of the specimen and it assisted in the formation of a nonstable oxide film. This would account for the difference in the corrosion rate of machined and unmachined surfaces. Examination of scale layers of unmachined surfaces after exposure confirmed this observation in that the evidence of metallic inclusions was removed in the oxidation process. While the relative gain in weight appeared to be high at 1200 F for machined surfaces, the over-all penetration of the metal was of a low magnitude being between 0.15 to 0.30 mils for 500-hr exposure of TP-321, 316, and 347 in steam. Consequently no corrosion troubles are expected in the use of the materials.

The hydrogen corrosion rate for steel at Kreisinger Laboratory appeared to confirm the reaction of iron and steam to form magnetic iron oxide and hydrogen. Technically, this reaction should be reduced by the addition of hydrogen to the system as investigated by Sulzer. No significant reduction was apparent in their tests. It should be noted that the amount of hydrogen added, 340 ppb, is much lower than that generally added for corrosion control. A minimum of 4500 ppb generally is recommended. Also its use generally is confined to liquid-phase operation. In the tests under consideration most of the test vessels were in "vapor."

The local deeper penetration of the base metal, with the addition of hydrogen, suggests an increased activity along the grain boundaries of the metal.

The tendency of an ammonia-hydrazine treatment to reduce the corrosion rate at high pressures and temperatures cannot be explained satisfactorily. Normally, ammonia separates from the liquid phase and passes off as a gas. Our present concept of the action may not be totally correct. Recent tests of the monotube unit at Dayton indicated an appreciable quantity of ammonia in the water removed from the separator. It is possible that ammonia, at elevated pressures, may remain in the homogenous mixture passing through the unit without a complete separation from the dense medium.

As indicated, operation of the simulated boiler and turbine units has supplied much useful information. Especially it confirms design, selections of materials, and planned water treatment and control.

In addition the acid wash of the Kreisinger boiler for the removal of insoluble deposits, and the water-wash procedure of Sulzer for the removal of soluble deposits have assisted in locating areas where deposits can form and can be of potential use to the designer in locating and proportioning the heat-transfer areas.

Acknowledgment

Grateful appreciation is expressed to the Philadelphia Electric Company for their participation in the project, especially in planning the work and in interpreting the results.

References

1 J. H. Harlow, "Engineering the Eddystone Plant for 5000-Lb, 1200-Deg Steam," TRANS. ASME, vol. 79, 1957, p. 1410.

2 E. M. Powell, "Engineering the Eddystone Steam Generator for 5000-Psig, 1200-F Steam," TRANS. ASME, vol. 79, 1957, p. 1447.

3 C. B. Campbell, C. C. Frank, Sr., and J. C. Spahr, "The Eddystone Superpressure Unit," TRANS. ASME, vol. 79, 1957, p. 1431.

4 N. L. Dickinson, W. A. Keilbaugh, and F. J. Pocock, "Some Physico-Chemical Phenomena in Supercritical Water," ASME Paper No. 58—A-267.

5 H. A. Pray and W. K. Boyd, "Corrosion of Stainless Steels in Supercritical Water," Battelle Memorial Institute, Report No. 901.

6 E. S. Johnson and H. Kehmna, "Some Relations Between Deposition and Corrosion Contamination in Low-Make-Up Systems for Steam Power Plants," *Corrosion*, vol. 14, 1958, pp. 429T–433T.

7 T. T. Frankberg, A. G. Loyd, and E. B. Morris, "The Second Year of Operating Experience With the Philo Supercritical-Pressure Unit," American Power Conference Paper, April, 1959.

8 Von H. Weyrauch, "Über die Bedeutung des Kupfers bei Kesselkorosionen," *Mitteilungen der Gross-Kessel-Besitzer*, vol. 25, September, 1953.

9 F. G. Straub, "Comparison of Ammonia, Amines, and Hydrazine in Reducing Metal Pickup in the Condensate and Feedwater Systems of Closed-Cycle Power Plants," Proceedings of the Fourteenth Annual Water Conference, October, 1953, p. 90.

10 H. A. Grabowski, H. D. Ongman, and W. B. Willsey, "Field Studies of Pre-Boiler Corrosion in Higher Pressure Steam Plants," Proceedings of the American Power Conference, March, 1956, vol. 18, pp. 591–600.

11 G. W. Morey and J. M. Hesselgesser, "The Solubility of Some Minerals in Superheated Steam at High Pressures," *Journal of Economic Geology*, vol. 46, 1951, pp. 821–835.

12 E. P. Partridge, "Water Problems in Power Generation at Supercritical Pressures," *Mechanical Engineering*, vol. 77, 1955, pp. 883–903.

DISCUSSION

V. J. Calise[2]

Make-up water as well as condensate and feedwater of ultrapurity and prescribed dependable analysis are the raw materials of high pressure and supercritical pressure plant operation just as much as mechanical design, metallurgy, fuel technology, automatic control, and other factors. In this paper, as well as in other papers presented at this session, the importance of water and its absolute purity, ultrapure water of 10 to 20 ppb total solids,

[2] General Sales Manager, Graver Water Conditioning Company, New York, N. Y.

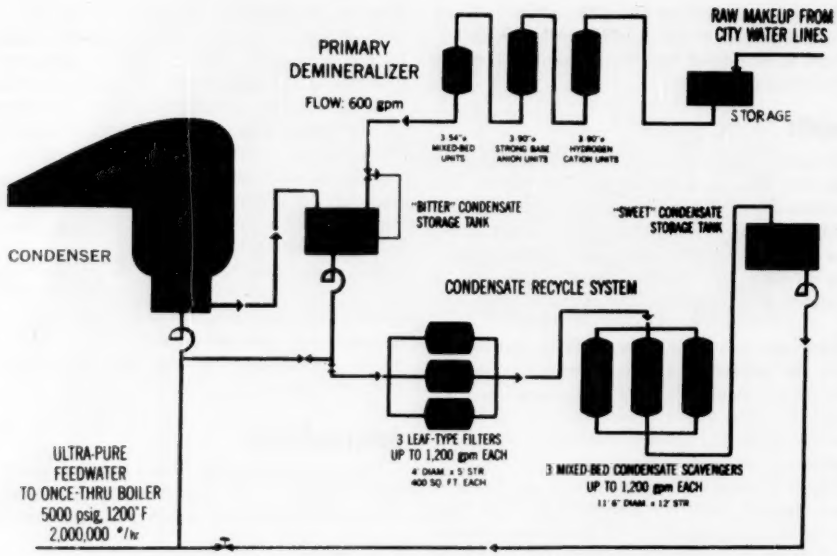
RAW MAKEUP FROM CITY WATER LINES
PRIMARY DEMINERALIZER
FLOW: 600 gpm
STORAGE
"BITTER" CONDENSATE STORAGE TANK
"SWEET" CONDENSATE STORAGE TANK
CONDENSER
CONDENSATE RECYCLE SYSTEM
3 LEAF-TYPE FILTERS UP TO 1,200 gpm EACH
3 MIXED-BED CONDENSATE SCAVENGERS UP TO 1,200 gpm EACH
ULTRA-PURE FEEDWATER TO ONCE-THRU BOILER 5000 psig, 1200°F 2,000,000 #/hr

Fig. 17 Eddystone Station—units 1 and 2 Philadelphia Electric Company

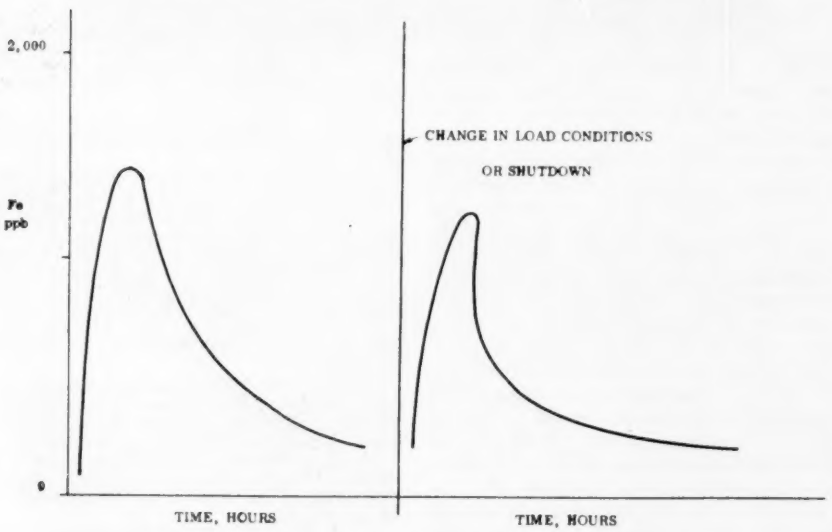

Fig. 18 Iron in condensate during start-up, Eddystone Station

is properly highlighted in good pressure and supercritical station design and operation.

The authors have presented an excellent paper showing the results of a rather thorough investigation of the effects of each of the various impurities entering into the Eddystone supercritical cycle. This work was done at Chattanooga and in Europe on two small experimental setups duplicating the metallurgy and components of the actual Eddystone cycle. These results were obtained mainly under equilibrium conditions and are of great value in determining the data pertinent to metallurgy, temperature, pressure, and water-treatment of both make-up and condensate.

Fig. 17 shows a flow diagram of the actual components of the make-up and condensate scavenging plant design mainly as a result of these studies. This flow diagram showing the components of three 4-ft $\phi \times$ 115-in. leaf filters and three 11-ft 6-in. ϕ mixed-bed demineralizers for full flow condensate scavenging will be discussed in more detail later in this session. However, it may be of interest to discuss briefly some factors involved in actual start-up of Eddystone supercritical that were not clearly indicated in this work and other preliminary, experimental work. Many of these factors were duplicated at Philo Station and in other once-through and drum-type boiler plants. First, and most important, was the factor of high iron concentration found in the range of 1000–2000 ppb during start-up for short periods of time as compared to less than 20 ppb expected on equilibrium after start-up.

Although the Graver-Davis leaf filters, using cellulose precoat ahead of the mixed-bed units at Eddystone are designed for a conservative 2 gpm/sq ft flow rate and normal runs of 8 to 16 days with equilibrium conditions, actual experience with the very high iron concentration found in the condensate on start-up reduces service time to 4 to 8 hours, during this start-up period.

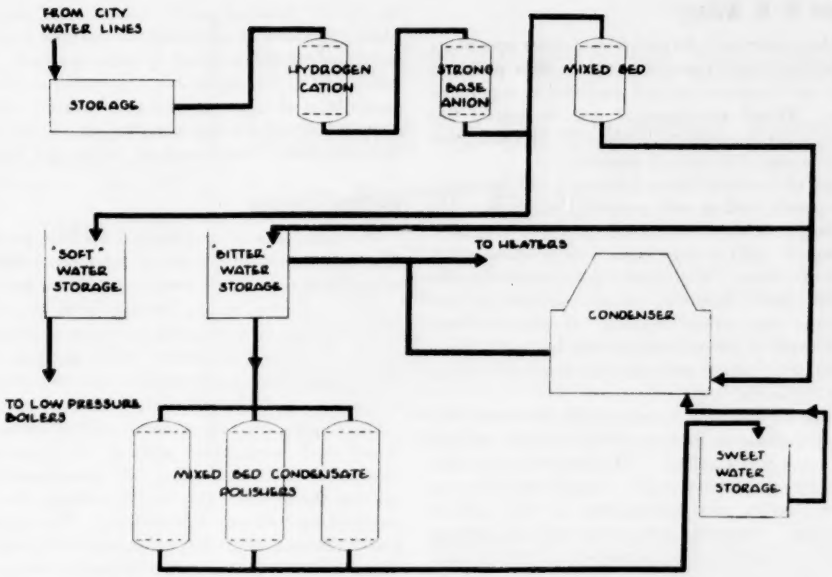

Fig. 19 Simplified flow diagram of water-treating system at Eddystone Station

Secondly, during the start-up period any change in load, pressure, or temperature or shutdown followed by start-up produced a "cloud effect" of very high iron in the 1000–2000 ppb range followed by gradual leveling off at some low value in the 100–200 ppb range. This is shown graphically in Fig. 18. We might point out the steepness of the leveling off curve is made possible by the rapid cleanup of all of the condensate going into the supercritical pressure boiler by means of the filters mainly ahead of the mixed-bed units. If filters and demineralizers of proper design and size were not provided, large amounts of blowdown would be required to eliminate these iron corrosion products. If only mixed-bed demineralizers were provided without filters, appreciable fouling or significant reduction in performance characteristics of these mixed-bed units could be expected.

The design of both make-up water and condensate scavenging plants at Eddystone is based on some rather simple rules established as a result of the work presented by the authors and our own experience with condensate problems in many other high pressure cycles. One of the cardinal rules is to avoid introduction of insoluble impurities into ion exchange units whenever possible. Another rule is the higher the flow passing through an ion exchanger, the clearer must be the water being treated to avoid unduly high and unpredictable pressure losses.

Both rules clearly indicate the need for high purity filters of the cellulose type to precede mixed-bed demineralizers on condensate scavenging service if continuous service, utter dependibility, and low cost operation are to be maintained.

In the work presented by the authors on the Chattanooga pilot plant, a cartridge filter and mixed-bed cell were used to treat all of the condensate entering the cycle. The results of the analyses of the filter and mixed-bed resin[3] showed clearly the presence of high iron mainly by the filter and other constituents, Fig. 19.

Although a value of 2000 ppb or 2.0 ppm was used as dissolved solids introduced into the system in this work, normally and on start-up, dissolved solids anticipated in condensate and feedwater average less than 500 ppb, as anticipated in this condensate scavenging plant design. Excellent results in dissolved solids removal down to less than 20 ppb TDS including silica, sodium, and other salts are found in actual practice.

The work in this paper, plus the work of Philadelphia Electric Company and their engineering and chemical personnel, and the other suppliers as well, in pinpointing problems that could arise in advance is the "warp and woof" of a plant design that presents the least number of start-up problems and provides lowest cost operation and high thermal advantage for this pioneering pressure, temperature, and size of supercritical power plant.

[3] J. A. Levendusky and V. J. Calise, "Research Problems Relating to Production and Quality Control of Ultrapure Feedwater for Eddystone Station," ASME Paper No. 59—A-240.

C. L. Clark[4]

The authors are to be congratulated on the excellent manner in which they conducted this investigation. From a tube producer's standpoint, one of their most outstanding discoveries is the apparent difference in the corrosion rate of the machined surface as compared to the surface of the original tube. It is unfortunate that the authors did not include microstructures of the scaled surface for these two surface conditions as these might have provided a clue as to the difference in behavior. Ordinarily, it would be expected that the cleaner, machined surface would be more readily attacked. Is it possible that the corrosion products were more easily removed from the machined surface and thus the gain in weight was not the proper criterion for the evaluation of corrosion rate? This could be checked by descaling and determining loss in weight.

In general austenitic tubes are supplied in the pickled, scale-free condition. It is surprising therefore that the authors report "large quantities of finely distributed metallic inclusions in the mill-scale layer." A question is raised as to whether this applies to the as-received tubes, or after further processing or heat-treatment. A microstructure illustrating this condition would be of value.

Often in corrosion work too great emphasis is placed on the magnitude of the differences observed. If one has one cent and the other ten cents, one is ten times richer than the other but both are still poor. This is in agreement with the author's conclusion that "consequently no corrosion troubles are expected in the use of the material."

[4] Staff Metallurgical Engineer, Steel and Tube Division, The Timken Roller Bearing Company, Canton, Ohio. Mem. ASME.

H. C. Farmer[5] and W. B. Willsey[6]

The authors of this paper are to be complimented for presenting this very comprehensive paper concerning the various problems and reactions that can be expected and predicted in supercritical boiler systems. Their's was no small task to extract this inclusive and informative paper from the reams of data and years of work that were necessary to make it possible.

To be sure, much of the information presented will be useful, not only to those people dealing with supercritical systems, but also to many dealing with conventional high pressure systems.

This paper brings to light a very important problem which needs emphasis at this time. The authors pointed out that citric acid was not suitable for removing oxide scales formed during operation of the supercritical system. However, it was shown that the removal of these deposits was successful when using hydrochloric acid, which was not recommended unless thorough flushing is possible.

It should be noted at this time, however, that citric acid was used for the initial cleaning of Eddystone No. 1 boiler and the quality of the cleaning was excellent. The effectiveness of the cleaning was judged by two main criteria. Inspection of cleaned surfaces wherever possible and examination of test sections welded into the system. These test sections were field cut sections of tubings, actually used in the boiler, representing all the various materials in the boiler. All post cleaning examinations were indicative of an excellent cleaning job in the boiler.

It is apparent then, that we can clean our mill scale and rust with citric acid, but feel a definite need for additional information on how we can clean operational deposits, formed in a supercritical system, without using hydrochloric acid, and have some assurance of a job well done.

Edwin P. Nye[6]

The authors are to be commended for the fine quality of both the research work itself and the lucid presentation of the results thereof. As frequently happens, the investigations made by the authors thus far have pointed up other factors which appear worthy of further study. I am especially interested by the marked reduction in corrosion rates produced by the so-called machining operation. This could be of great importance at still higher temperatures where the corrosion rate of unmachined surfaces would become intolerable.

Further research appears necessary to determine the precise mechanism which is involved. Is actual surface-metal removal necessary or would shot-peening or swaging produce a comparable effect? Internal metal removal itself would likely be completely impractical on tubing but perhaps a comparable surface condition can be produced by other methods. Acid washing is mentioned in the paper, but the results are inconclusive. The possibilities of a simple surface treatment which would retard corrosive attack are very tempting, and I trust that further work on this problem is contemplated in the near future.

[5] Philadelphia Electric Company, Philadelphia, Pa.

[6] Professor of Engineering, Trinity College, Hartford, Conn. Mem. ASME.

Authors' Closure

We wish to thank the discussers for their interesting comments. The Eddystone unit has accumulated some 1000 hours of service so operating data can be compared with the Laboratory data.

First, referring to the comments by Mr. V. J. Calise, the demineralizers have supplied very pure make-up, of the order of 50 ppb or lower total solids. Silica has been 20 ppb or lower. The bypass demineralizers have been very effective in removing soluble and insoluble materials during start-up and during service.

Dr. Clark's comments about relative corrosion rates of machined and unmachined surfaces are quite apropos. Heat-treatments could well cause the impurities that appear to accelerate the attack. Our results indicate that these cannot be removed by ordinary acid cleaning. Perhaps more severe acid treatment such as pickling would remove them. We did not try this as we did not want to incorporate any steps or processes that would not be used in the actual unit.

We plan to further investigate this phenomenon.

As to the comments of Messrs. Farmer and Willsey they too are to be complimented for their co-operation in the work as they were active in the planning and interpretation of the work.

We agree that more work must be done on chemical cleaning especially of a unit after it has been in service. As hydrochloric acid has limitations perhaps phosphoric or nitric should be considered.

As to cleaning new units versus units that have been in operation, it is quite possible that the difference in chemical composition of the material to be removed is controlling. Considerable copper, chromium, and nickel are present after service and these are difficult to remove. It will be interesting to observe results of acid cleaning of the unit when and if it requires acid cleaning during service.

Finally, we agree with Mr. Nye that more attention should be given the corrosion mechanism of machined versus unmachined surfaces. It is hoped that the tubing manufacturers will become interested in this aspect of the problem.

Again we wish to thank the discussers who submitted written discussions and those that presented oral ones when the paper was given.

The Selection of Materials and Fabricating Techniques for the Eddystone Boiler and Sulzer Control Valves

E. C. CHAPMAN
Director of Material, Research and Development. Mem. ASME

R. E. LORENTZ, JR.
Supervisor, Metallurgical Development.
Combustion Engineering, Inc.
Chattanooga, Tenn.

The Eddystone supercritical boiler, designed to operate at a maximum pressure of 5000 psig and 1200-F temperature, required the use of new high-temperature materials in tubes and stop valves in order to avoid excessive wall thicknesses. None of the materials approved by the ASME Boiler and Pressure Vessel Code for superheater service had the required properties. The present paper describes the high-temperature tests carried out and the welding development which led to the selection of the new materials. The properties of these new materials are discussed. Design features and fabricating procedures for the tubes and valves are presented.

All available information on some 130 alloys and superalloys was reviewed in selecting materials for Eddystone. The highest expected tube-metal temperature was 1300–1350 F which would require a prohibitive wall thickness for the strongest ASME approved material. Most recent research in developing new materials has been aimed at gas-turbine and jet-engine service, but the requirements for superheater tubes are quite different and in many respects more restrictive. A superheater-tube material must lend itself to tube-making operations and the finished product must possess properties suitable for fabrication, including good weldability. The long-time service requirements call for long-time creep and rupture testing for checking stability. The size and geometry of the elements impose restrictions on final condition as affected by working and final heat-treatment. If heat-treatment of welds is required the material must lend itself to this operation in the field. Acceptable welding processes must be available for joining the material to itself and to the dissimilar material preceding it in the circuit. The costs of new superheater-tube materials must not greatly exceed those of the conventional austenitic steels used in the past.

ASME-Code-approved materials were selected for use up to the maximum temperature for which each was suitable. These included Types 321 and 316, the maximum temperature for each being dictated by the maximum practical wall thickness as determined by the pressure drop and other design considerations. Type 316, an old alloy on which there was no long-time steam service experience, was chosen because it had the highest Code-allowable working stress above 1150 F. High-temperature tests were conducted on this alloy to augment published data and establish fabricating procedures including the optimum heat-treatment. In spite of the extensive use of Type 321 in steam service, many gaps existed in the data available on this material and tests to extend the metallurgical knowledge of this alloy were included.

For temperatures above the maximum for Type 316, the investigation led to the selection of 17-14 CuMo steel, an alloy developed by the Armco Steel Company during World War II and sometimes termed "the poor man's superalloy." Tentative selection of this alloy was made after reviewing the considerable data and test results available and final choice was made when the results of the test program indicated that it was the most suitable alloy available at the time for this application.

The control valves to be furnished by Sulzer Brothers Ltd. of Switzerland presented another material problem and an extensive development program was carried out by Sulzer with the cooperation of Combustion Engineering. If made of Type 316 to match the piping material, excessive wall thickness of the valve bodies would result, hence another non-ASME-Code material with higher strength than any ASME-Code material was essential. G-18B, an alloy developed by the William Jessop Company of England, was selected for investigation. Sulzer had had prior experience with this alloy in other types of service and it had been used extensively in Europe for gas-turbine rotors and for other high-temperature applications. Many data were available on its properties and there had been considerable experience with welding it.

This choice was fortunate as the results of the tests bring out and this alloy was eventually chosen for the valves. The development work included high-temperature tests on both the base material and the deposited weld metal used for joining the heavy G-18B sections and for making the required dissimilar metal joint between G-18B and Type 316. Development of welding procedures for these valve joints involved many months of extensive investigation.

The Eddystone boiler represents the first "break through" in the utilization of new materials for steam-generation service. It is predicted that this will be the beginning of a trend.

Table 1 Composition of tube and valve materials deposited-metal analysis

TUBES & FORGINGS		C	Mn	P	S	Si	Cr	Ni	Mo	Cb & Ta	Cu	Other Elements
TP 316 Forgings	Max.	.079	1.89	.023	.026	.38	17.47	13.26	2.45			
	Min.	.048	1.65	.012	.012	.21	16.63	12.57	2.30			
17-14 CuMo Tubes	Max.	.125	.90	.026	.020	.82	16.29	14.65	2.40	.63	3.50	Ti .35
	Min.	.099	.80	.016	.010	.37	15.26	14.00	2.10	.48	3.01	.19
G-18B Forgings	Max.	.43	.86	.024	.014	1.25	13.60	13.10	1.96	3.10		Co W 10.10 2.85
	Min.	.36	.71	.010	.010	.75	12.70	12.60	1.61	2.75		9.21 2.30
DEPOSITED METAL												
17-14 CuMo	Max.	.156	1.34	.012	.010	.63	16.15	14.51	2.76	.92	3.61	
	Min.	.116	1.15	.006	.007	.34	16.01	14.24	2.32	.49	2.89	
TP 316	Max.	.078	1.92	.021	.019	.41	19.72	13.29	2.28			Ferrite 1.5 to 3.0
	Min.	.056	1.41	.011	.007	.25	19.29	12.46	2.09			
FOX CN 16/13 Co		.10	1.70	.023	.005	.27	14.40	12.00	.22	1.00		Co (?)

Contributed by the Power Division and presented at the Annual Meeting, Atlantic City, N. J., November 29–December 4, 1959, of The American Society of Mechanical Engineers.

Note: Statements and opinions advanced in papers are to be understood as individual expressions of their authors and not those of the Society. Manuscript received at ASME Headquarters, October 27, 1959. Paper No. 59—A-318.

Tube-Material Properties

The chief deterrent to the development and utilization of new materials for high-temperature service is the time required for the necessary long-time creep and rupture tests. Costly alloys of the austenitic-steel variety must give many years of service to make their use economical for service in steam generation. In contrast with aircraft-engine service requirements, for which materials can be tested for the full life of a unit, the life of parts under creep in boilers must be predicted by extrapolating data derived from tests extending over only a fraction of the required life. The minimum time for the testing, the number and type of tests to be made before a material should be approved for use have only been established to a limited degree and evaluation is still largely a matter of judgment, based on experience. Many ASME-Code-approved materials were not so extensively tested before approval as 17-14 CuMo had been before selection for Eddystone. Stress-rupture tests of over 10,000-hr duration had been conducted, tubes had been produced experimentally and had been under tests in service for over 5000 hr. Additional tests and development of fabricating procedures were considered essential, although more information on this alloy was available than for any other material having comparable strength and reasonable cost.

The curves for the stress-rupture tests, both strip and tubular, are plotted from Table 2 in Fig. 1. Available data indicated that annealing at 2050 and 2250 F resulted in lower strength but greater ductility to rupture when treated at the lower temperature and that the ductility after an anneal at 2250 F was on the low side. Tests were conducted at 1350 F on material annealed at several temperatures to establish the one to give the optimum combination of strength and ductility, Fig. 1. The increase in strength from raising the annealing temperature will be observed. The stability of the material indicated by the excellent very-long-time test results was most encouraging. Although the ductility to rupture was not as high as is usually shown by the approved austenitic types, the very high creep strength was considered as offsetting this deficiency. Fig. 2 compares the creep strength of Type 321 at 1200 F with that of 17-14 CuMo at 1350 F at the same stress level. The very high creep strength of the 17-14 CuMo alloy is noteworthy.

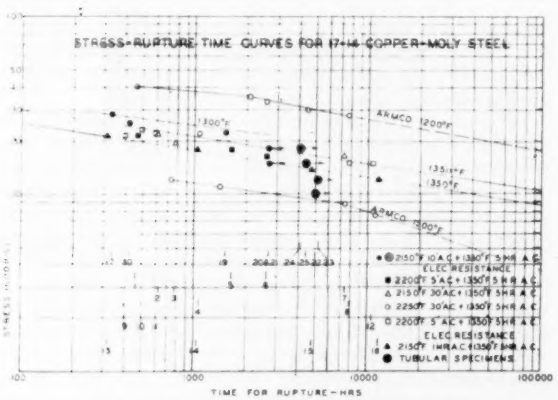

Fig. 1 Stress-rupture curves for 17-14 CuMo steel

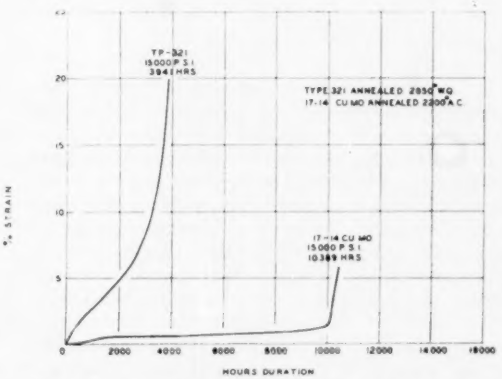

Fig. 2 Strain-time curves Type 321 and 17-14 CuMo steel. Resistance to creep comparison.

Table 2 17-14 CuMo stress rupture tests. All samples aged at 1350 F for 5 hr after heat-treatment; 1 1/2 in. OD by 0.313 in. wall. See Fig. 1 for curves.

No.	Heat Treatment	Longitudinal Strips Grain Size	psi Stress	Rupture Life (Hrs.)	% El.	% R.A.	Test Temp.
1	2200°F. 5 Min. A. C.	3/5(6)	21,500	167	13.6	34.3	1350°F.
5	"	"	18,000	1615	7.8	23.4	"
6	"	"	16,500	2601	7.5	21.9	"
2	2150°F. 30 Min. A. C.	"	22,000	616	21.3	32.8	"
3	"	"	19,500	759	12.5	31.3	"
7	"	"	16,500	7275	3.5	10.9	"
4	2250°F. 30 Min. A. C.	"	22,000	1087	4.9	25.0	"
8	"	"	15,000	7761	4.6	10.9	"
9	2200°F. 5 Min. A. C.	"	21,500	402	6.0	38.0	"
	Elec. Resist.						
10	"	"	23,000	500	4.0	25.4	"
11	"	"	22,000	611	4.6	36.9	"
12	"	"	15,000	10389	5.3	6.3	"
13	2150°F. 1 Hr. A. C.	3/5	21,500	309	4.0	15.6	"
14	"	"	18,000	1038	4.4	11.3	"
15	"	"	16,000	4761	3.9	9.1	"
16	"	"	12,000	11103	2.4	6.3	"
17	2150°F. 10 Min. A. C.	"	28,000	328	9.0	16.0	1300°F.
18	"	"	25,000	421	4.6	28.0	"
19	"	"	20,000	1600	8.0	20.0	"
20	"	"	18,000	2728 I.P.			"
21	"	"	16,000	9728 I.P.			"

Straight Tubular Rupture Tests
All Samples Heat Treated 2150°F. 10 Min. A.C. and Aged
All Samples Tested at 1300°F.

No.	Grain Size	Stress psi	Rupture Life (Hrs.)	Pressure psi	Dia.	Min. Wall
22	3/5	20,000	5021 I.P.	6400	1.506"	.315"
23	"	19,000	5192 I.P.	7700	1.505"	.316"
24	"	18,000	4104 I.P.	11100	1.505"	.313"
26	"	18,000	4475 I.P.	9600	1.506"	.317"

Long-time tubular rupture tests at 1300 F were included in the investigation and are still in progress as shown in Fig. 1. These tests were started at some time after the strip tests and 1300 F was chosen in lieu of 1350 F because it more accurately represented the maximum metal temperature in operation as determined by final design calculations. Special attention is called to the low stresses used in two of these tests with an extrapolated life of 100,000 hr indicated for the specimen at 10,000-psi stress.

Examination of the microstructure after treatment at 2050 to 2250 F, Fig. 3, indicated an excellent resistance to grain growth at all temperatures. This was believed to be an important property when considering this alloy for production heat-treatment. Very little difference in grain size is shown regardless of the heat-treating temperatures.

General fine-carbide precipitation was found throughout the matrix and at grain boundaries after long time at temperature, Fig. 3(*d*). No evidence of sigma formation was found.

Both strip and tubular tests were included in the stress-rupture investigation of Type-316 tubes, Figs. 4 and 5, Tables 3 and 4. The directional-property strip tests, Fig. 4, made on longitudinal and circumferential specimens showed lower strength in the circumferential direction. The difference was not considered significant. The tubular-test results compared very closely with the circumferential-strip-test results. Very high ductility to rupture was shown for Type 316, with relatively low creep strength associated with this high ductility.

Rupture tests on strip specimens removed from bends to determine the effect of cold work, Fig. 5, showed that the strength was enhanced by cold work to the degree of bending tested and the

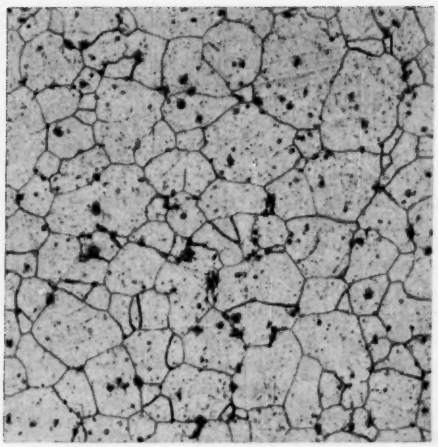

(a) HT 2150 F 15 min AC; aged 1350 F 5 hr; 100×; etched 60 per cent nitric + 10 NKOH; GS 4/6 (3)

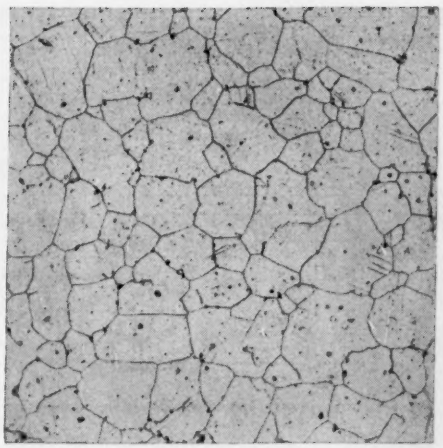

(b) HT 2200 F 5 min AC; aged 1350 F 5 hr; 100×; etched 60 per cent nitric + 10 NKOH; GS 4/6 (3)

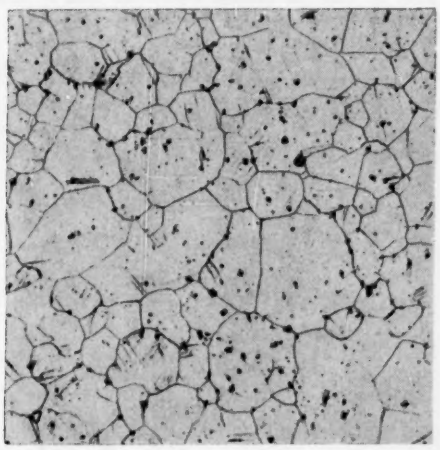

(c) HT 2250 F AC; aged 1350 F 5 hr; 100×; etched 60 per cent nitric + 10 NKOH; GS 3/6

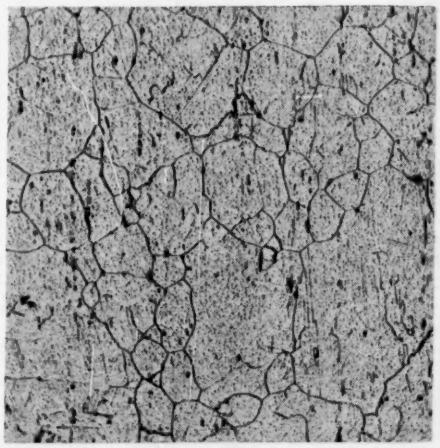

(d) HT 2300 F 5 min AC; aged 1350 F 5 hr; stressed 15,000 psi, 10,389 hr at 1350 F; 100×; etched 60 per cent HNO_3 + 10 NKOH; GS 3/6 (2)

Fig. 3 Microstructure study 17-14 CuMo steel

ductility to rupture remained adequate. As a result of these tests heat-treatment of production bends was omitted. The possibility of improving the high-temperature strength of Type 316 by moderate cold work without sacrifice of essential ductility was a by-product of these tests and is under investigation.

The data from tests to determine the effect of different heat-treating temperatures, Fig. 5 and Table 4, show that within the range 1900 to 2100 F rupture strength was not appreciably affected, but creep strength was improved by higher temperatures although ductility to rupture was reduced. This apparently was a result of progressively larger grain size resulting from the higher temperature. The effect of annealing temperature on the grain size is shown in Fig. 6.

Microscopic examination before and after long-time exposure at temperature indicated that sigma phase had developed but this is reflected in the rupture-test results. Tubular rupture tests made on bends—one specimen shown in Fig. 7 failed in the straight section—substantiated the conclusion that heat-treatment of the production bends was not required and was deemed inadvisable. Fig. 6 shows the Type-316 microstructure after annealing at the several temperatures. The difference in grain size is not marked, indicating that this alloy is not as sensitive to temperature as some other steels including Types 321 and 347. Carbides go into solution below 1850 F so the only benefit from heating above this temperature is slightly improved creep strength, attributed to the somewhat coarser grain. The long-time rupture-test data indicated consistent performance and that any instability due to sigma formation was reflected in both the long-time and short-time test results.

Rupture tests were made on specimens taken from the compression side and tension side of Type 321 bends made cold, Fig. 8 and Table 5. These data show that when cold-working is sufficient to reduce the elongation to rupture below approximately 3.5 per cent a reduction in rupture life can be expected. They also indicate that the compression side of the bend suffers the greatest loss in ductility. Tubular rupture tests on bends in fine-grain tubing annealed at 1750 and 2050 F indicated low strength after the low-temperature treatment and very good strength after the higher temperature treatment. For example, a bend in 2 in. OD × 0.250-in. wall tubing failed in 46 hr when in the fine-grain condition and 240 hr after the 2050 F treatment. The samples were stressed at 27,000 psi as calculated by ASME

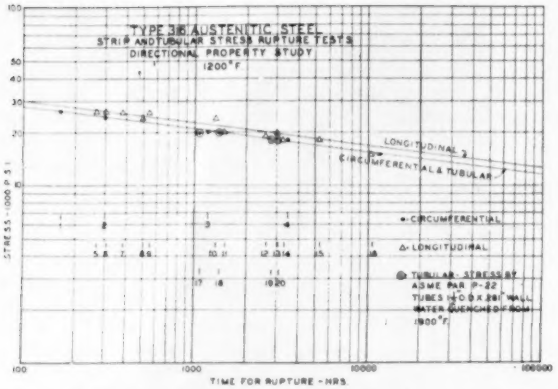

Fig. 4 Stress-rupture curves Type 316. Directional property study at 1200 F.

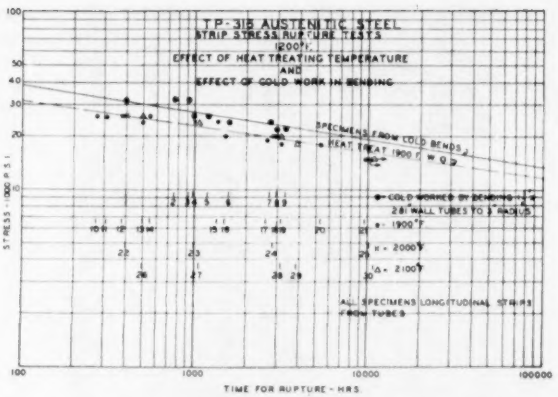

Fig. 5 Stress rupture curves Type 316. Effect of heat-treating temperature and cold work in bending on properties at 1200 F.

Table 3 SA-213-type 316 material. Effect of cold work and heat-treatment on stress rupture properties at 1200 F. See Fig. 5 for curves.

No.	Heat Treatment	Grain Size	Stress psi-	Rupture Life (Hrs.)	Elong. %	R. A. %
1	Cold Work[2] T[3]	4/6(7)	32,000	397	12.6	48.0
2	" C	"	"	761	7.0	28.0
3	" T	"	"	923	13.4	37.5
4	" C	"	26,000	982	31.2	62.5
5	" T	"	"	1181	31.0	52.0
6	" C	"	24,000	1582	32.0	39.1
7	" T	"	"	2735	12.5	24.0
8	" C	"	22,000	2990	21.6	32.0
9	" T	"	"	3352	17.0	36.0
	Annealed					
10	1900°F. W. Q.	3/6	26,000	273	53.1	62.5
11	"	4/6(7)	"	307	34.9	56.0
12	"	4/6(3)	"	384	30.2	56.0
13	"	3/6	24,000	498	39.0	48.0
14	"	4/6(3)	26,000	551	29.8	56.0
15	"		24,000	345	41.8	48.4
16	"	3/6	20,000	1476	33.0	48.0
17	"	"	19,000	2590	35.0	45.8
18	"	4/6(7)	20,000	3026	32.4	13.7
19	"	3/6	18,000	3175	45.0	44.0
20	"	4/6(7)	"	5235	20.4	28.6
21	"	4/6	15,000	9990	18.7	20.3
	Annealed					
22	2000°F. W. Q.	4/6(3)	26,000	393	29.5	52.0
23	"	"	24,000	1004	33.3	42.2
24	"	"	20,000	2922	23.1	32.8
25	"	"	15,000	10200 I.P.		
	Annealed					
26	2100°F. W. Q.	3/5/(2)	26,000	498	24.6	7.8
27	"	"	24,000	1007	25.7	39.1
28	"	"	20,000	3067	18.8	26.5
29	"	"	18,000	3871	18.2	25.0
30	"	"	15,000	10200 I.P.		

[1] All tests of longitudinal strips taken from 1-1/2" OD x 0.281" wall tubing

[2] Tubing as received (annealed at 1900°F, water quench) then cold bent to 3" radius

[3] T = Tension side C = Compression side of bend

Table 4 SA-213-type 316 stress rupture tests. All samples $1^1/_2$ in. OD × 0.281 in. wall; all samples heat-treated 1900 F; W.Q.; all samples tested at 1200 F. See Fig. 4 for curves.

Longitudinal and Circumferential Strips

No.	Type	Grain Size	Stress psi	Rupture Life-Hrs.	Elong. %	R. A. %
1	Circum.	4/6/(3)	26,000	167	48.7	42.0
2	"	"	24,000	303	49.6	60.0
3	"	"	20,000	1209	59.2	52.0
4	"	"	18,000	3468	31.0	41.7
5	Long.	3/6	26,000	273	53.1	62.5
6	"	4/6(7)	26,000	307	34.9	56.0
7	"	4/6(3)	26,000	384	30.2	56.0
8	"	3/6	24,000	498	39.0	48.0
9	"	4/6(7)	26,000	551	29.8	56.0
10	"	"	24,000	1345	41.8	48.4
11	"	3/6	20,000	1476	33.0	48.0
12	"	"	19,000	2590	35.0	45.8
13	"	4/6(7)	20,000	3026	32.4	13.7
14	"	3/6	18,000	3175	45.0	44.0
15	"	4/6(7)	18,000	5235	20.4	28.6
16	"	"	15,000	9990	18.7	20.3

Straight Tubular Rupture Tests

No.	Grain Size	Stress psi	Rupture Life-Hrs.	Pressure psi	Min. Wall	Ave. Dia.	Stress Formula
17	3/5	20,000	1095	10,500	.274	1.497	P-22
18	4/6(7)	20,000	1105	10,600	.277	1.498	"
19	4/6	18,000	2788	9,200	.271	1.501	"
20	3/5	18,000	3132	9,400	.273	1.498	"

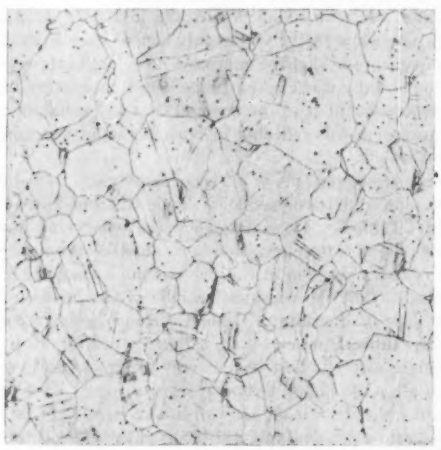

(a) HT 1900 F 15 min WQ; 100×; 60 per cent HNO_3, GS 7/4 (3)

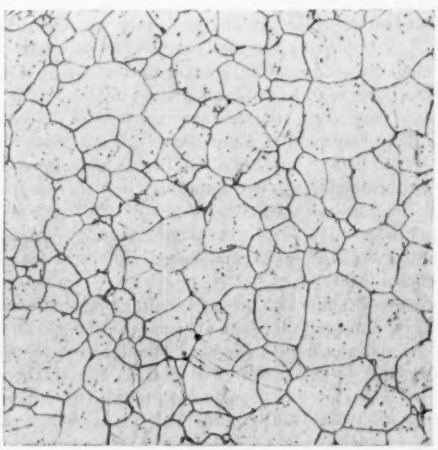

(b) HT 2000 F 15 min WQ; 100×; 60 per cent HNO_3, GS 7/4

formula P-22. The data show that tubular-test results using straight-tube specimens checked very closely with the strip-test results.

Valve-Material Properties

Rupture testing of G-18B by Sulzer at 1202 F indicated rupture and creep strengths superior to the ASME-approved types and very close to the properties shown by 17-14 CuMo steel, Fig. 9. However, much greater ductility to rupture was realized in the G-18B tests. Rupture tests on notched bars gave strengths equal to or greater than the results from the unnotched bar tests. The properties of this material appeared suitable for tubing and Jessop is investigating the possibility of its use in this form. This alloy showed excellent stability in the long-time tests, with no evidence of such conversion products as sigma phase. Studies of the microstructure are shown in Fig. 14.

In Sulzer's stress-rupture tests on Fox CN 16/13 Co weld metal, Fig. 10, strengths equal or superior to the G-18B base material were obtained on both smooth and notched specimens. This weld metal also showed excellent ductility to rupture. The deposited metal was found to be completely austenitic with no

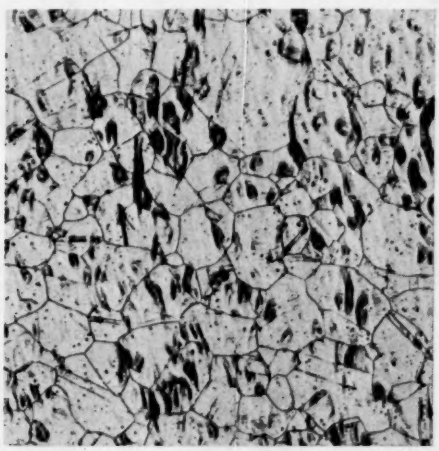

(c) HT 2100 F 5 min WQ; 100×; 60 per cent HNO_3 + 10 NKOH, GS 6/3

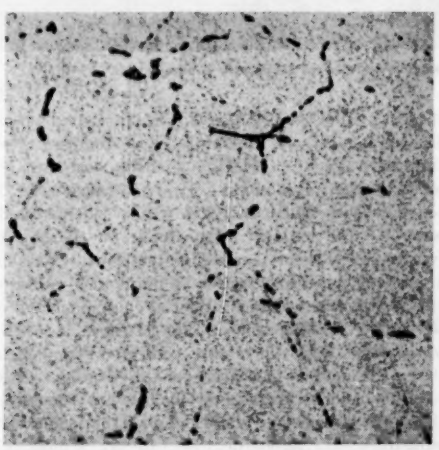

(d) HT 1900 F 15 min WQ; 9990 hr at 1200 F and 15000 psi stress; 500×; 10 NKOH, GS 7/4

Fig. 6 Microstructure study Type 316 showing effect of heat-treating temperature and 9940 hr at 1200 F on structure

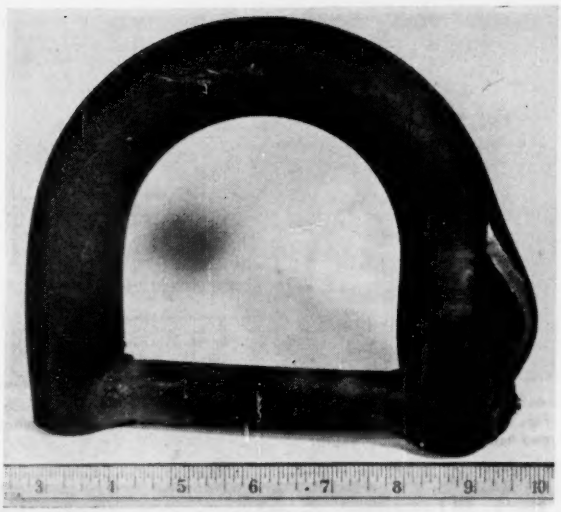

Fig. 7 Bend tubular rupture test specimens. Type-316 tube 1 1/2 in. × 0.281 wall bent to 3 in. R.

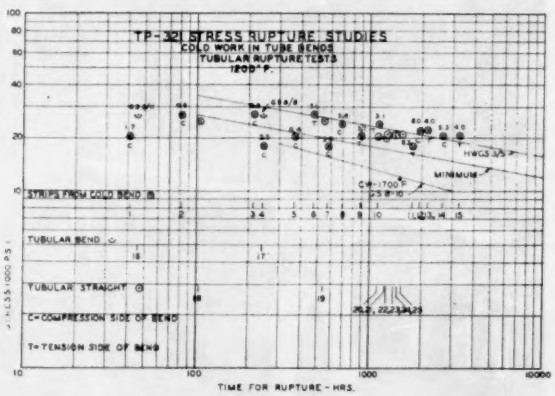

Fig. 8 Stress rupture curves Type-321 strip and tubular tests. Shows effect of cold work on properties.

Table 5 SA-213-type 321 stress rupture tests. All samples tested at 1200 F. See Fig. 8 for curves.

Longitudinal Strips - All Heat Treated Before Bending - 2050°F. W.Q.

No.	Grain Size	Stress psi	Rupture Life-Hrs.	Elong. %	R. A. %	Location	Size O.D. Wall	Bend
1	1/6	30,500	41	1.7	1.6	C	2-1/8" x .281"	4-5/8"R
2	3/5	27,000	82	0.9	6.3	C	2-1/8" x .281"	4-5/8"R
3	1/6	27,000	216	9.3	23.8	C	3" x .410"	12"R
4	"	13,000	246	2.0	3.1	C	2-1/8" x .281"	4-5/8"R
5	3/5	20,500	371	0.4	2.0	C	2-1/8" x .281"	9"R
6	1/6	27,000	479	7.1	9.7	T	3" x .410"	18"R
7	3/5	15,000	579	3.5	1.6	C	2-1/8" x .281"	8"R
8	1/6	24,000	638	5.8	12.5	C	3" x .410"	13"R
9	"	20,500	991	25.7	3.2	T	2-1/8" x .281"	4-5/8"R
10	"	24,000	1135	3.1	7.9	T	3" x .410"	18"R
11	3/5	18,000	1793	8.3	1.5	T	2-1/8" x .281"	8"R
12	1/6	22,000	1936	8.0	14.3	C	3" x .410"	18"R
13	"	22,000	2159	4.0	7.8	T	3" x .410"	18"R
14	"	20,500	2645	5.3	9.4	C	3" x .410"	18"R
15	"	20,500	3290	4.0	1.6	T	3" x .410"	18"R

Tubular Straight and Bend
Heat Treated as Straight Lengths and as Bends after Bending

No.	Type	Heat Treatment	Grain Size	Stress psi	Rupture Life-Hrs.	Pressure psi	Stress Formula	Min. Wall	Ave. Dia.
16	5"R	1750°F. W.Q.	9/11	27,000	46	8050	P-22	0.257"	2.003"
17	"	2050°F. W.Q.	6/8	27,000	280	8500	"	0.266"	1.997"
18	Str.	"	7/9	25,000	105	13100	"	0.281"	1.503"
19	"	1900°F. A.C.	4/8	25,000	548	4305	Barlow	0.130"	1.510"
20	"	2050°F. W.Q.	4/6	20,500	1119	5200	P-22	0.265"	2.127"
21	"	2050°F. A.C.	5/7	20,000	1223	2222	Barlow	0.139"	2.730"
22	"	2050°F. W.Q.	5/6	21,000	1277	8000	P-22	0.249"	1.503"
23	"	"	"	21,000	1416	9100	"	0.277"	1.503"
24	"	"	"	21,000	1447	8500	"	0.271"	1.503"
25	"	"	"	22,000	1527	6100	"	0.198"	1.503"

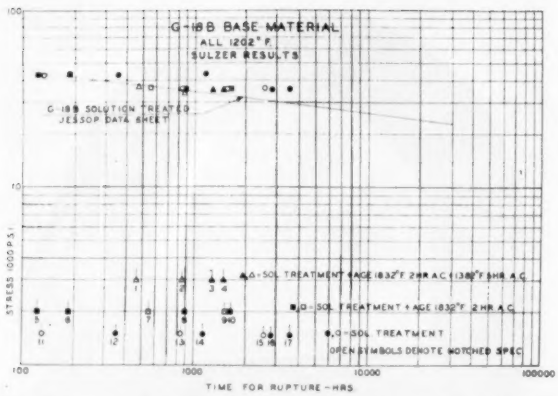

Fig. 9 Stress rupture curves for G-18B alloy. Shows effect of notches and heat-treatment on strength.

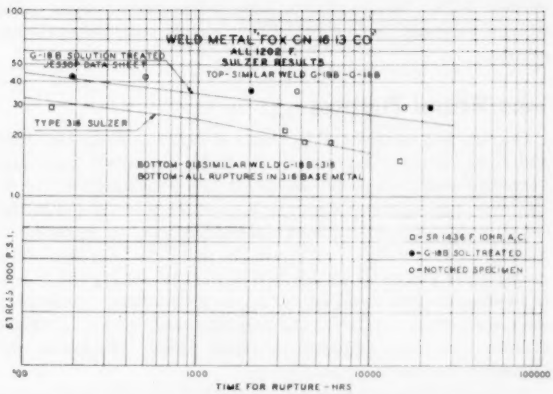

Fig. 10 Stress rupture curves Fox CN 16/13 Co weld metal. Shows effect of notches and heat-treatment on strength.

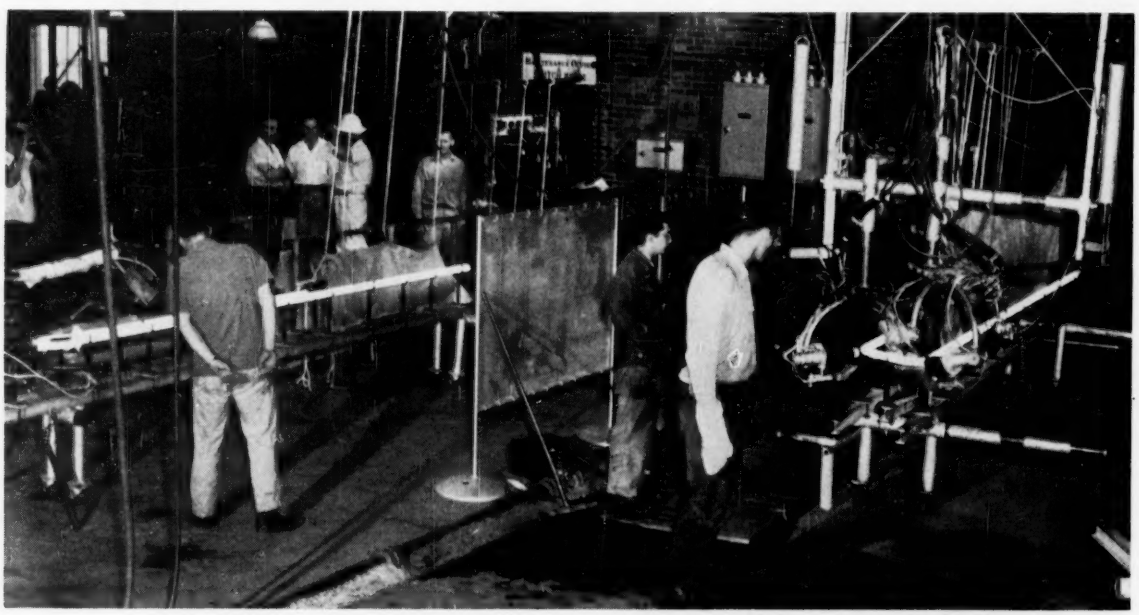

Fig. 11 Production heat-treatment of 17-14 CuMo tubes by electrical resistance method

ferrite required to prevent microfissures, Figs. 14(*c* and *d*). Some tendency toward microfissuring was eliminated by increasing the carbon content to about 0.18 per cent.

Fabrication Procedures

All shop tube welds were made by the induction-pressure-welding process eliminating the necessity for a deposited weld metal. All field tube welds were made using the inert-gas, tungsten-arc method for the first pass and were completed by the metal-arc method using coated electrodes. The deposited-metal analysis for the 17-14 CuMo manual welds is shown in Table 1. Research carried out by Armco had shown considerable improvement in weld-metal quality of this analysis through reduction in the phosphorus and sulfur contents. The analysis shows that these elements were held to unusually low percentages. No backing rings were used in any heat-absorbing joints. Fig. 12 shows a tubular rupture-test specimen containing both an induction pressure weld and a manual weld. The failure in the tube material is obvious.

Heat-treatment of the 17-14 CuMo steel presented a problem as will other superalloys in the future, since temperatures above those normally used for ASME austenitic steels are required, in order to realize full strength. Heat-treatment after bending with negligible subsequent cold work was considered essential for this material. Furthermore, close control of the heat-treating temperature was necessary as the high-temperature data indicate. Heat-treatment in a furnace appeared impractical so the electric-resistance method was chosen. Special equipment and controls were developed for this purpose. Fig. 11 shows how this operation was carried out. Very close control of temperature was possible by this method of heating for tube straight sections but concentration of current toward the inside of bends made auxiliary heating of the outside and air cooling of the inside necessary. This adjustment was automatically controlled by means of radiation pyrometers visible in the photograph. Very little distortion resulted and the over-all results were very satisfactory. Very accurate control of time at temperature was possible. This time was reduced from 30 to 10 min after rupture testing proved that

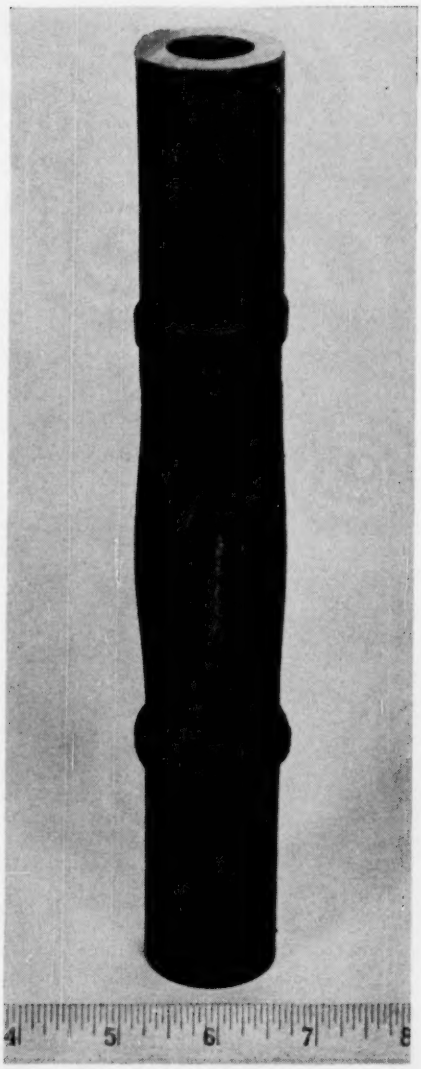

Fig. 12 Tubular rupture test specimen including induction pressure weld and manual weld

5 min were sufficient. This short holding time, possible since heat is generated in the metal, minimizes oxidation and limits time as a factor in grain growth. No unforeseen fabricating problems whatsoever were encountered with the 17-14 CuMo tubing. This tubing had been ultrasonically tested with no rejections. No failures resulted from bending. Great care was used in design to avoid attachment welds. Water-cooled tube loops were employed for controlling the spacing at the lower end of the elements. Short longitudinal fillet welds for support were unavoidable at the upper end of the elements. These were the only welds made on the outside of the tubes.

A typical radiant-superheater panel composed of both Types-316 and 321 tubes, Fig. 13, has studs welded to the back side of the tubes for supporting the panels in service. Trouble from stress concentration around these welds was not feared because the back side of the tubes would be cooler than the furnace side in service. No unusual problems worthy of reporting were encountered in the fabrication of these elements. All tubes were

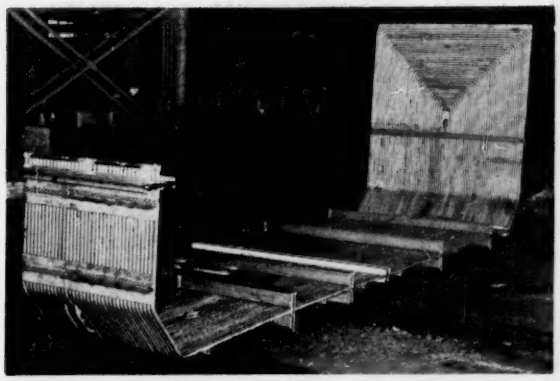

Fig. 13 Radiant superheater panel Eddystone supercritical unit. Panel made of Type-316 and 321 tubes.

given final heat-treatment at the mill. Bends in the Type-321 tubes were locally stress relieved and the bends in Type-316 tubing received no final heat-treatment for reasons explained previously.

Joining the G-18B valves together and welding the Type-316 extensions to them called for a major welding development program by Sulzer. Several weld-metal compositions were tried before the modified Fox CN 16/13 Co electrode was developed. Compositions having the required strength were completely austenitic and, as American experience has shown, had a tendency to give microfissures in the deposited weld metal. Elimination of ferrite was most desirable but the presence of microfissures in such heavy welds was highly objectionable. The Fox CN 16/13 Co electrode, produced by the Bohler Company of Germany, seemed to give fewer microfissures than any other electrode investigated, when completely austenitic. One heat which was found to be free of these defects was reserved for the valves unless general improvements could be made. Increasing the carbon was suggested to Bohler and this produced a marked improvement, resulting in the apparent elimination of microfissures. There was a close similarity in composition to the G-18B analysis, each containing cobalt—10 per cent in G-18B and 6 per cent in the weld metal. For welding the dissimilar-metal joints involving Type 316 welded to G-18B, weld metal with strength equal only to Type 316 was required. Tests using Type 316 and 16-8-2 electrode resulted in extensive cracking in the weld metal along the G-18B fusion line. These tests preceded the development work with the Fox electrode and a serious obstacle was indicated until this electrode was also found satisfactory for these joints. The valves and extensions to them therefore were welded using only this one electrode.

Heat-treatment of the valve welds presented a problem. Local heating was mandatory since final machining could not be done after the valves were joined. A stress relief as high as 1850 F was believed desirable to guard against a stress-rupture failure in service which might result from high residual welding stresses. However, the temperature possible was limited by the maximum temperature of 1382 F that the G-18B valve bodies could reach without suffering loss in strength. The short connections between valves could make it impossible to hold the desired temperature gradient. Furthermore, the valves required preheating to a high temperature to avoid the possibility of distortion. In spite of these complications Sulzer has reported that the stress relieving was successfully carried out at the desired temperature. Some minor cracking was experienced in one weld but a successful repair was made. The welds were nondestructively tested by all known methods including the gamma-ray, ultrasonic, and penetrant-oil-powder methods. Fortunately, the

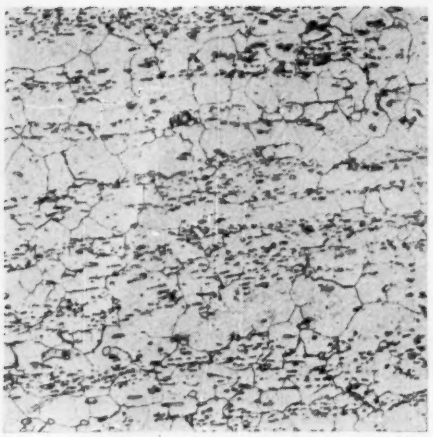

(a) G-18B base material, ht. 2350 F WQ; 100×; 90 per cent HNO_3, GS 7/5

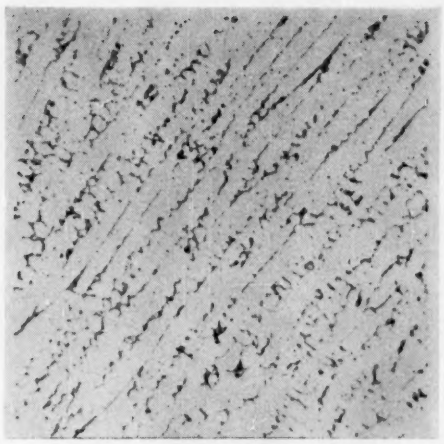

(b) Fox CN 16/13 Co deposited metal, stress relieved 1436 F, 10 hr AC

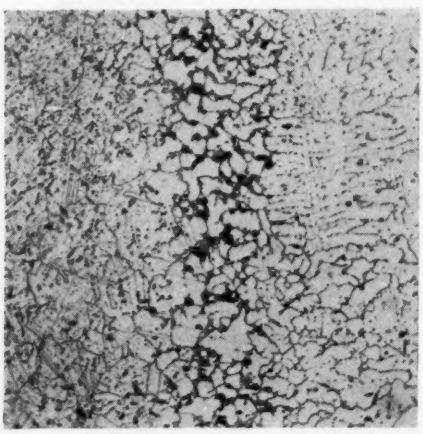

(c) Fusion zone G-18B base material and Fox CN 16/13 Co weld metal after 500 hr at 1382 F, 250×

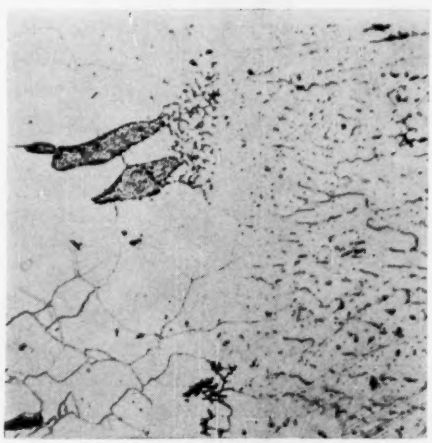

(d) Fusion zone Type 316 and Fox CN 16/13 Co weld metal, stress relieved 1430 F, ht. 1850 F AC, 250×

Fig. 14 Microstructure study G-18B valve base material and Fox CN 16/13 Co weld metal

welds were accessible for close inspection both inside and outside. Fig. 15 shows the valve assembly while being welded.

Reference is made to Fig. 14 for a review of the microstructure. The Fox CN 16/13 Co weld metal shows an austenitic-ledeburitic structure free from ferrite with interdendritic embedment of carbide eutectic. After long-time heating at 1202 F the microstructure shows no appreciable change. The authors are confident that these joints will prove serviceable under operation at 1200 F temperature.

Conclusions

1 17-14 CuMo steel has high-temperature strength superior to the strength of ASME-approved austenitic steels, and tubes of this analysis can be made using conventional steel-mill procedures. Tubes of this alloy can be fabricated without difficulty provided close control of heat-treatment is exercised.

2 Type 316 is a very satisfactory alloy for fabricating and has high-temperature properties which seem to justify present Code stress values.

3 Jessop G-18B alloy is an excellent material for many applications and deserves consideration as a material for use at the

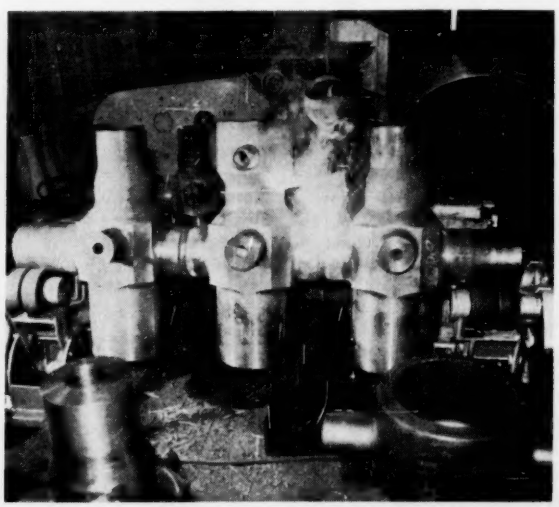

Fig. 15 Welding joint between G-18B control valves

higher temperatures not only for valves but possibly for tubes and other parts.

4 The Fox CN-16/13 Co electrode appears to possess characteristics and provide high-temperature properties in deposited metal superior to any known American welding electrode. Satisfactory welds, completely austenitic, are possible and this is an important and unusual achievement.

Bibliography

1 F. Eberle, F. G. Ely, and J. A. Dillon, "Experimental Superheater for Steam at 2000 Psi and 1250 F—Progress Report After 12,000 Hours of Operation," TRANS ASME, vol. 76, 1954, pp. 665–677.

2 H. S. Blumberg, "Metallurgical Considerations of Main Steam Piping for High-Temperature, High-Pressure Service," TRANS. ASME, vol. 79, 1957, pp. 1377–1397.

3 C. B. Campbell, C. C. Franck, Sr., and J. C. Spahr, "The Eddystone Superpressure Unit," TRANS. ASME, vol. 79, 1957, pp. 1431–1446.

4 J. H. Harlow "Engineering the Eddystone Plant for 5000-Lb 1200-Deg Steam," TRANS. ASME, vol. 79, 1957, pp. 1410–1430.

5 E. M. Powell, "Engineering the Eddystone Plant for 5000-Psig, 1200-F Steam," TRANS. ASME, vol. 79, 1957, pp. 1447–1457.

6 R. M. Curran and A. W. Rankin, "Austenitic Steels in High-Temperature Steam Piping," TRANS. ASME, vol. 79, 1957, pp. 1398–1409.

7 F. P. Fairchild, "Eight Years of Experience With Austenitic Steel Piping Materials at Elevated Steam Conditions," TRANS. ASME, vol. 79, 1957, pp. 1371–1376.

8 J. H. Hoke and F. Eberle, "Experimental Superheater for Steam at 2000 Psi and 1250 F—Report After 14,281 Hours of Operation," TRANS. ASME, vol. 79, 1957, pp. 307–317.

9 R. A. Lula, A. J. Lena, and H. M. Johnson, "Effect of Cold Work on Elevated-Temperature Properties of Types 301, 305, and 310 Stainless Steels," TRANS. ASME, vol. 79, 1957, pp. 921–926.

DISCUSSION

C. L. Clark[1]

The authors are to be congratulated for the additional high temperature data they have presented under temperature and stress conditions where information of this type is meager. As the suppliers of the 17-14 CuMo tubes used in the Eddystone boiler, we were also interested in the high-temperature properties of this alloy and consequently conducted a large number of long-

[1] Staff Metallurgical Engineer, Steel and Tube Division, The Timken Roller Bearing Company, Canton, Ohio.

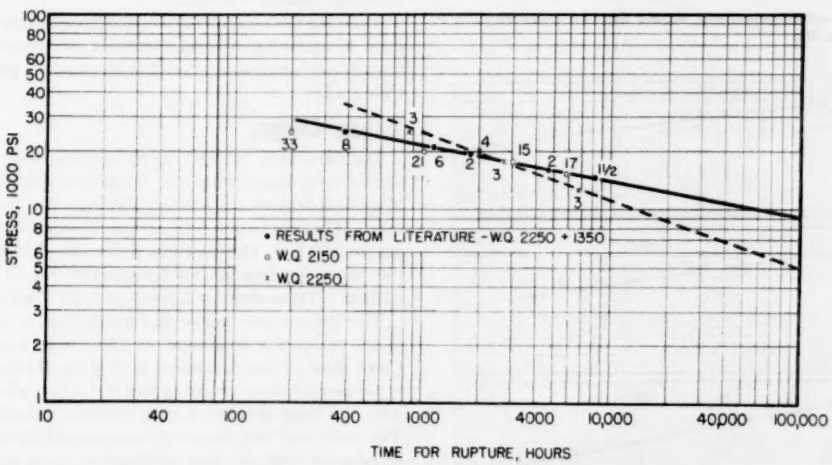

Fig. 16 Stress rupture characteristics of 17-14 Cu + Mo at 1350 F; heat 02706, specimens from pierced tube

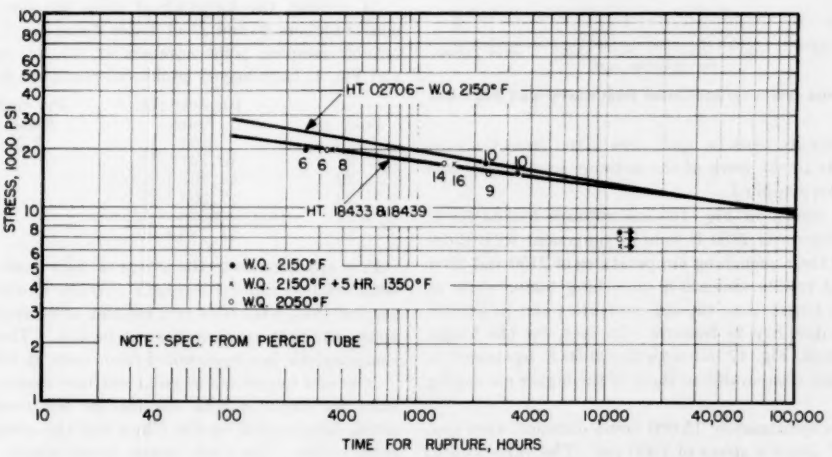
STRESS, 1000 PSI
TIME FOR RUPTURE, HOURS
HT. 02706 - W.Q. 2150° F
HT. 18433 & 18439
• W.Q. 2150°F
× W.Q. 2150°F +5 HR. 1350°F
○ W.Q. 2050°F
NOTE: SPEC. FROM PIERCED TUBE

Fig. 17 Effect of heat-treatment on rupture strength at 1350 F of 17-14 CuMo; ht 18433 and 18439

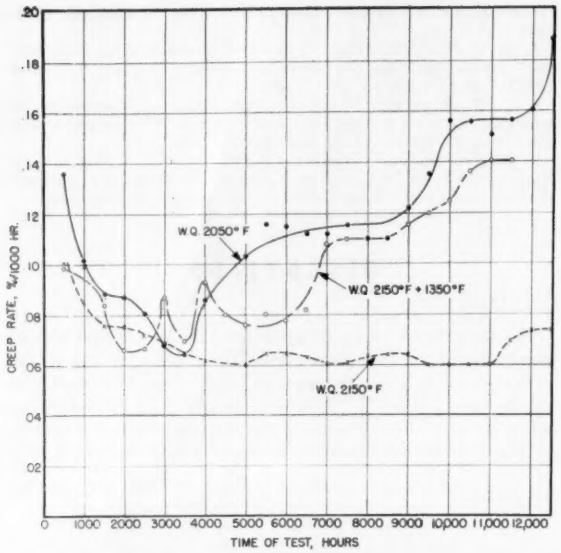

Fig. 18 Effect of heat-treatment and testing time on creep at 1350 F, 7000 psi of 17-14 Cu-Mo

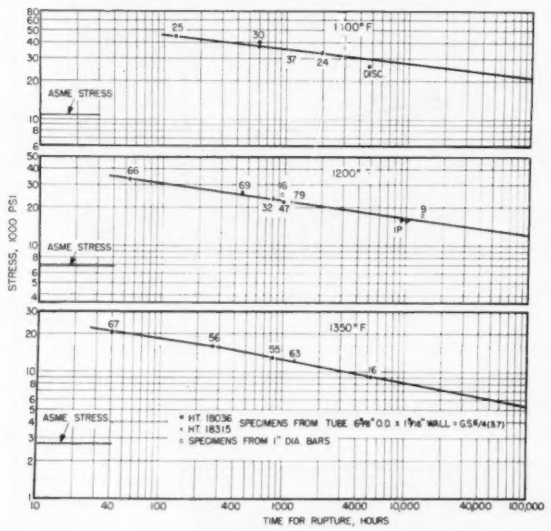

Fig. 19 Stress rupture curves for specimens from heavy wall 316 tubes

time creep and rupture tests on specimens taken from the production tubes. As in the work of the authors, several different heat-treatments were applied.

In general, as shown in Fig. 16, our rupture results for a quenching temperature of 2150 F were in agreement with those of the authors for their quenching temperatures of 2150 and 2200 F. However, our results indicate a quenching temperature of 2250 to lower the longer time rupture properties and to greatly decrease the hot ductility to fracture. In fact, for the longer rupture time periods, Fig. 17 indicates the 2050 F treatment to yield rupture results comparable to those of the higher quenching temperatures.

Creep tests of approximately 15,000 hours duration were conducted at 1350 F under a stress of 7000 psi. The variations in creep rate with time, Fig. 18, show the 2150 F treatment to be superior to the 2050 F treatment and that the aging treatment at 1350 F increases the creep rate, that is, decreases the creep resistance.

With reference to Fig. 17 of the authors' paper, it can not always be assumed that a higher creep resistance necessarily insures a longer life. Specimens of 17-14 CuMo, one quenched from 2150 and the other from 2250 F, were creep-tested at 1350 F under a stress of 17,000 psi. The sample quenched from the higher temperature showed a creep rate of 0.02 per cent/1000 hours and the one quenched from 2150 F, 0.20 per cent, or 10 times as great. Yet both specimens fractured in approximately 3000 hours. However, their respective elongation to fracture was 3.5 and 15.5 per cent.

As in the case of the authors, we found the structure of 17-14 CuMo to be stable under the prolonged test periods with no evidence of sigma formation. However, the examination of the tube of this analysis, removed from the ASME High Temperature Steam Generation test unit at the Phil Sporn Station, has shown a decrease in the room temperature impact resistance after exposure for six months at 1200, 1350, and 1500 F.

Likewise, as shown in Fig. 19, our results from prolonged tests on Type 316 are in close agreement with those of the authors even though the specimens for our tests were taken from larger diameter, heavier wall tubes.

Applying the present rules of the Boiler Code for the establishment of maximum allowable stresses, we would be interested in the authors' suggested allowable stresses at 1350 F for this 17-14 CuMo alloy.

Authors' Closure

The discussion by Dr. Clark includes test results on 17-14 CuMo steel heat-treated at several temperatures but none of these heat-treatments exactly duplicate the one used in fabrication. The fabrication heat-treatment consisted of rapidly heating to 2200 F by the electrical resistance method, as described in the paper, holding at this temperature for 10 minutes, and air cooling. Tempering for 5 hours at 1350 F was then carried out.

The authors are unable to furnish data to confirm the effect of the tempering treatment on creep rate as presented by Dr. Clark since all test specimens were given this treatment. Armco recommended the tempering treatment and all of their data likewise had been developed from material treated in this manner. The results of long-time rupture tests and the status of those still in progress indicate very satisfactory creep strength as well as rupture strength. Since many more hours have been logged since the paper was written, the following results are reported.

At present the longitudinal strip samples of 17-14 CuMo point numbers 20 and 21 of Table 2 and Fig. 1, and the straight tubular samples, point numbers 22, 23, 24, and 25 of Table 2 and Fig. 1, have logged additional results as follows:

Point no.	Rupture life, hours	Per cent elong.	Per cent R.A.
20	3394	4.5	18.0
21	10,721 I.P.		
22	12,787 I.P.		
23	12,268 I.P.		
24	6016		
25	11,745 I.P.		

It is apparent from the status of these tests that the extrapolated 100,000 rupture strength at 1300 F will be above 10,500 psi and that, with tests still running after approximately 13,000 hours, the rupture curve has not broken. This same significant characteristic has been noted from tests at 1350 F.

It is also important to point out how closely the strip test results are checking with the tubular test results. The rupture strengths obtained by Dr. Clark and the authors at 1350 F are comparable. The Code stress values would, of course, be obtained by following the Code basis.

The elongations obtained in the longest time tests have been very satisfactory when compared with those from the medium time tests, indicating that where some loss occurred in the first thousand hours, probably due to precipitation, the material is stable from then on. Long time tubular rupture tests have shown good creep strength as determined by the amount of swelling and also shown good ductility, in fact, better than was expected.

The authors cannot explain why a tempering treatment at 1350 F should be beneficial when the operating temperature is the same, especially in view of Dr. Clark's data which indicate that the creep rate during the first several thousand hours is unaffected by this treatment. Although precipitation, which may result from tempering, could explain why it is desirable to temper in the unstressed condition before service, it appears that operations at the same temperature would accomplish the same result, and in a shorter time if the stress has any effect at all.

The authors suggest that the close control possible with the Electrical Resistance method permits reducing the time at the annealing temperature in order to produce the same metallurgical effect and, hence, grain growth at temperatures as high as 2200 F is minimized.

Replying to Dr. Clark's request for a recommended allowable stress for 17-14 CuMo steel at 1350 F, a review of the data, which is now considerable, shows that 5500 psi is a conservative value and that 6000 psi may be permitted, depending on how conservatively the curves are drawn. These values are based on applying the same heat-treatment as that used in fabrication and utilizing the same methods to give the same complete thermal cycle.

W. E. TRUMPLER, JR.
Manager, Mechanical Design Section
Mem. ASME

A. F. LeBRETON
Mechanical Design Section

E. A. FOX
Manager, Metallurgical Section

R. B. WILLIAMSON
Apparatus Section, Assoc. Mem. ASME
Large Turbine Engineering Department,
Westinghouse Electric Corporation,
Steam Division, Lester, Pa.

Development Associated With the Superpressure Turbine for Eddystone Station Unit No. 1

Design, material selection, and testing of the Eddystone 1200-F superpressure turbine elements are described. This unit features a radially disposed labyrinth seal not heretofore employed in electric utility turbines in this country.

THE 325-mw Eddystone steam-turbine generator unit No. 1 is interesting from several viewpoints. However, its most significant innovations are those related to the use of exceptionally high initial steam pressure and temperature. This paper supplements a 1956 report on the general design aspects of the No. 1 unit whose basic characteristics were adhered to in construction[1] but limits its scope to some of the unique features of the superpressure element only.

This single element, Fig. 1, will be recognized by the relatively few stages of blading as a comparatively small component of the whole machine. Yet by receiving steam at 5000 psi, 1200 F, and expanding it to 2500 psi at its exhaust, it develops approximately 1/8 of the entire rated output of the cross-compound, double-reheat, turbine-generator set. Thus the superpressure element presented unique problems with regard to the selection and procurement of alloys suitable for the high service temperatures, as well as the development of efficient shaft end seals which have to operate against unusually large pressure differentials while occupying relatively little space.

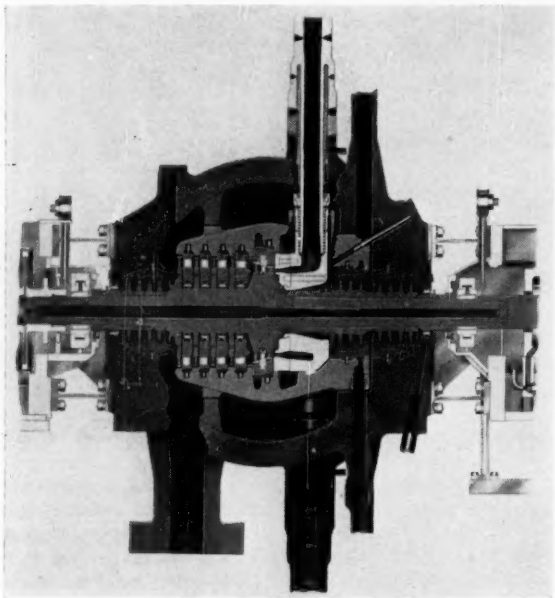

Fig. 1 Superpressure turbine

Shaft Seals

At rated output the superpressure-element exhaust pressure was set at 2500 psi rather than, as conventionally, at the first reheat pressure, 1125 psi. The resulting smaller physical size of unit permitted continuation with established general principles of turbine-casing design. Of greater importance, it afforded wider latitude in the selection of higher temperature alloys, some of which are subject to rather rigid size or weight limitations. These advantages could have been offset to some degree had it been necessary to employ conventional labyrinth-type sealing to limit shaft-gland leakage to acceptable values, in spite of the unusually high exhaust steam pressure involved.

The seals actually used, however, reduce the axial space requirement for sealing by a factor of four when compared to previous radial-seal labyrinth designs for the same leakage level. This has been accomplished by radially compounding the throttlings as shown in Fig. 2, requiring the steam to follow a tortuous leakage path outward and inward radially as it moves axially along the shaft. There has been successful experience elsewhere with this general type of construction. Studies and experimentation leading to the adoption of this design for the Eddystone turbine have been very encouraging. It is recognized that such a radially compounded seal requires increased diametral space, has increased circumferential leakage length, complicates the axial-thrust analysis, and presents an unusual assembly and inspection problem.

The logic of the use of radial, nested-type seals is obvious from a comparison of the shaft length required versus that to do an equivalent job with conventional seals. The bearing span of this particular superpressure-turbine rotor has been reduced approximately 3 1/2 ft by such change in construction alone. The correspondingly stiffer rotor is, of course, less sensitive to minor unbalanced forces and there is substantially less liability to vibration at an amplitude such as to contact and rub radial seals, with resulting increase in steam-leakage losses, Fig. 3.

Nested-type seals are used in this installation to perform two sealing functions. Three rotating disks with their meshing stationary disks provide a seal between the forward end of the inner casing and the rotor. They operate at rated output under a pressure differential of 1270 psi and a temperature near 1120 F. The shaft end seals, at the points where the rotor emerges from the outer casing, are formed by four rotating disks with their corresponding stationary disks, with an over-all pressure differential of 2500 psi at rated output.

[1] C. B. Campbell, C. C. Franck, J. C. Spahr, "The Eddystone Superpressure Unit," TRANS. ASME, vol. 79, 1957, pp. 1431–1446.

Contributed by the Power Division and presented at the Annual Meeting, Atlantic City, N. J., November 29–December 4, 1959, of THE AMERICAN SOCIETY OF MECHANICAL ENGINEERS.

NOTE: Statements and opinions advanced in manuscripts are to be understood as individual expressions of their authors and not those of the Society. Manuscript received at ASME Headquarters, October 6, 1959. Paper No. 59—A-288.

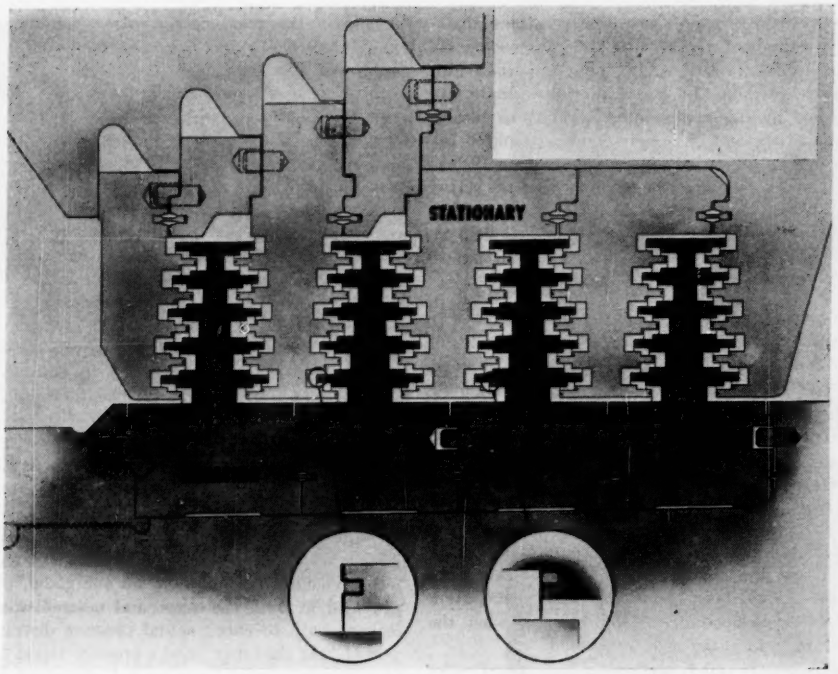

Fig. 2 Radially compounded labyrinth seal

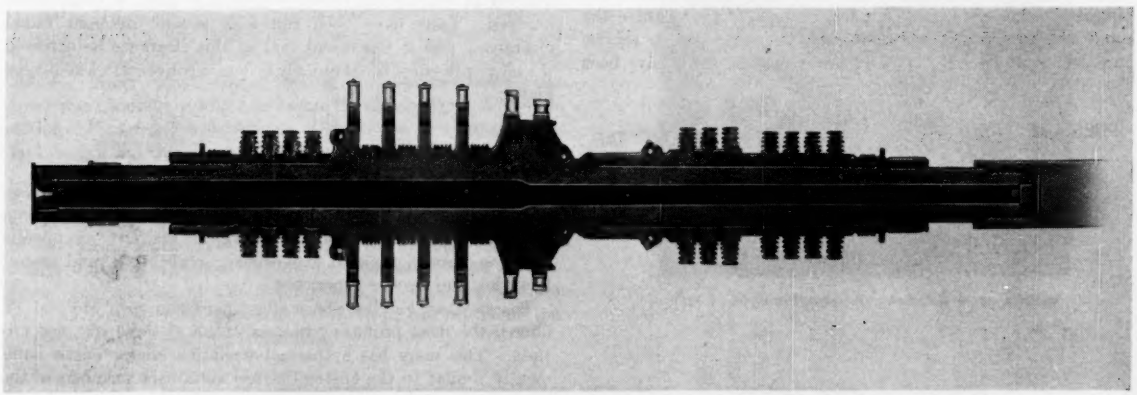

Fig. 3 Superpressure integral rotor

Each of the rotating disks is shrunk onto the rotor with 1-mil-per-in. of diameter interference fit. The stationary disks are continuous rings between which the rotating disks are located. Assembly is accomplished by alternately placing a stationary disk in its proper axial location on the shaft and shrinking on the next rotating disk. The complete gland must therefore be assembled prior to placing the rotor in the casing. This construction is such that once the disks are assembled on the rotor it is impossible to inspect the sealing details visually, or to measure axial location or axial or radial-seal clearances directly.

Since a complete disassembly is required for an inspection of the seals, a fast and easy method for removal and replacement of the shrunk-on rotating disks is provided by incorporating an oil-injection system developed by SKF Industries. The oil is injected between the shrunk-on member and the rotor with sufficient pressure to stretch the ring elastically a slight amount, and thus form a film of oil between the two members. The shrunk-on ring may then be moved axially along the shaft. A tapered fit also facilitates disk positioning. The optimum angle for taper was determined experimentally. Hydraulic pressures of the order of 40,000 psi from a pump of 0.3-gpm capacity are required in the task of assembling or removing these seal disks.

High accuracy of machining is required. The meshing "branches" of each ring must be heavy enough to contain the separate seal strips and their calked retainers. At the same time they must provide the largest practical margin against interference of relatively moving heavy parts under the axial displacement of the rotor with respect to stationary members which is inherent in turbine operation. The assembly of sealing strips in ribbon form into their locating grooves, and the calking of their wire retainers, is an operation requiring considerable care and finesse.

Discaloy[2] was chosen as the seal-disk material in order to match

[2] Westinghouse trade name.

thermal-expansion coefficients with those of the turbine shaft and also to obtain high-temperature strength, since some of these disks must operate at 1150 F. AISI Type 316 Ni-Cr-Mo stainless steel was selected as the seal-strip ribbon material. This steel is processed by cold-rolling and annealing to obtain sufficient ductility to withstand the severe bending required by this design. The calking wire is of 12 per cent chrome 12 per cent nickel steel annealed to produce maximum softness. The calking-strip cross section is basically a rectangle of 0.018 by 0.030 in. with 0.008 in. radius at each corner. The seal strip as purchased is 0.008 in. thick by 0.281 in. wide. A watch manufacturer was the source of supply for these materials.

Thrust

The seals at the end of the inner casing between the first-stage pressure and the exhaust pressure are made slightly larger in diameter than those at the two ends of the outer casing. Therefore they form a piston to balance axial thrust resulting from the flow of steam through working stages of the superpressure element. The pressure drop across one rotating ring from the smallest to the largest diameter and back to the smallest diameter is not a linear function of the radial travel; therefore the effective thrust pressure acting on the ring annulus is not the average pressure between inlet and outlet. To solve this problem, analytical studies have been made of pressure distribution and factors have been developed for calculating thrust when the pressure ratio and the radii of the seals are known.

A rotating test of the actual Eddystone governor end outer glands was conducted at high temperatures and pressure as part of the development program for the superpressure unit. The purpose of this test was to duplicate as closely as possible the conditions to which the gland would be subjected in service and thus bring to light any problems which may not have been foreseen in the gland design. As a result of this test it was found necessary to provide circumferential keys between the shrunk-on disks and the shaft. This was done to insure proper axial location of the disks on the shaft and also to maintain positive clearance between disk hubs to prevent shaft bowing by uneven circumferential temperature distribution. By intentionally creating heavy radial and axial rubs it was found that this type of construction did not produce shaft bowing, always a possibility with conventional seals.

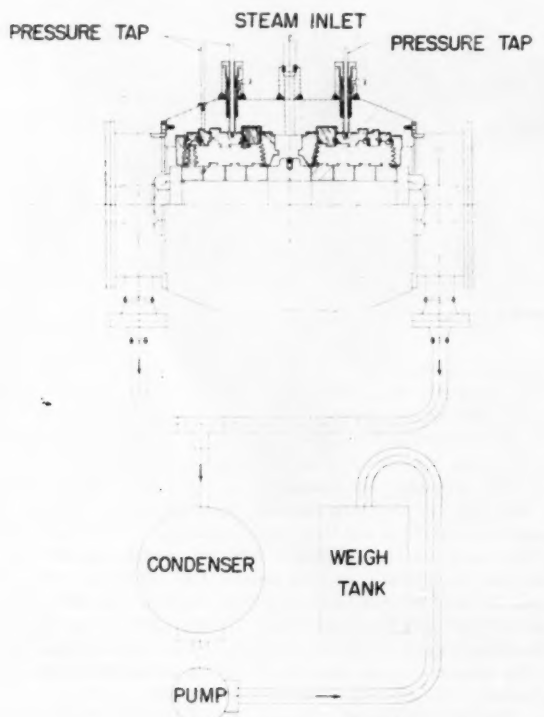

Fig. 4 Seal test

A number of leakage tests with steam conditions comparable to those which will be experienced, conducted with the apparatus shown in Fig. 4, have confirmed calculations. The shaft on which the rotating disks are mounted was driven at 3600 rpm by a steam turbine. Steam was admitted to the casing with glands at each end throttling the pressure down to approximately atmospheric. Steam pressure and temperature at the inlet to the test machine were measured. Four exhaust lines from each gland were combined into one line in which there was an orifice and a thermocouple. These two lines were then combined into one line leading to a condenser where, with hot-well level maintained constant, the condensate was pumped into tanks and weighed. Thus the expected leakage based on inlet steam conditions and exhaust pressure could be compared with weighed value of leakage which, in turn, could be segregated to the two glands with the orifice measurements. In addition, on one gland, pressure taps were provided at both the outer and inner diameter of each disk-leakage path to check actual pressure distribution against expected. At the other gland a pressure tap at the outer diameter of each rotating disk provided a double check on these zones.

The pressure distribution obtained in the tests verified the method of calculating pressure gradients used in axial-thrust analysis. Tests have been run with several different radial clearances, and it was found that as this clearance is increased the labyrinth effect is not quickly lost as in conventional step-type glands.

The Superpressure Integral-Disk Rotor

The principal factors considered in the selection of an alloy for the superpressure rotor shown in Fig. 3 were strength at room temperature, strength and metallurgical stability at operating temperature, thermal expansivity, availability, and manufacturing and service experience.

Discaloy, an Fe-Ni-Cr-base alloy, hardened with Mo and Ti, offered the most promising balance to all of these specified criteria. This alloy has a thermal-expansion characteristic sufficiently similar to the austenitic-steel stationary members of the superpressure unit to permit clearances to be maintained with changes in temperature. The room-temperature strength and operating-temperature creep resistance are sufficient to give reasonable latitude in mechanical design. Metallurgical stability in reasonably long-time service in industrial gas turbines has been demonstrated with this alloy, while only short-life information in jet engines, and so on, was available for many other "high-temperature alloys" screened in preliminary considerations. Adequate laboratory test information was available so that the material composition and heat-treatment could be balanced to give maximum long-time metallurgical stability commensurate with the strength level required by the superpressure design. Finally, previous manufacturing experiences with gas-turbine disk forgings indicated probable success in obtaining sufficiently large superpressure rotor forgings of Discaloy material.

The Bethlehem Steel Company manufactured the forging for the integral-disk rotor. This forging represents a noteworthy metallurgical accomplishment since it required as large an ingot of electric-arc-furnace-melted Discaloy as had been previously produced. Most heats of alloys of this type have been induction-

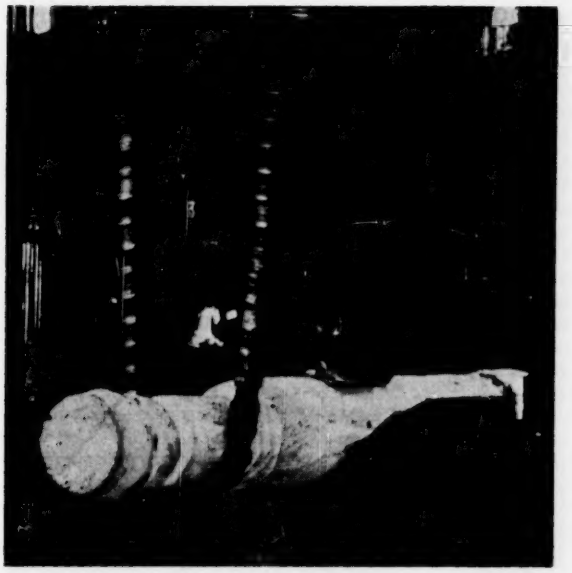

Fig. 5 Forging the superpressure rotor

melted and greater experience has been acquired in the control of composition and quality with this melting method. However, Bethlehem did succeed in producing an ingot of approximately 15,500 lb and forged it to the required rotor shape. All stages of forging reduction and subsequent heat-treatment were designed to control metallurgical structure at optimum for long-time service. After completion of forging and heat-treatment, the rotor was thoroughly tested to assure its suitability to the application. Figs. 5 and 6 show some of the stages of forging manufacture and the type of equipment used in producing the forging.

Creep-rupture tests and short-time tensile tests were conducted on material cut from between the disks on this forging so that a rather complete knowledge was obtained of the quality of the metal immediately adjacent to the regions where the blades would be fastened. Additional test metal was available from prolongations of the forging ends. Creep-rupture tests were obtainable from specimens taken from the center of the forging under the body by trepanning.

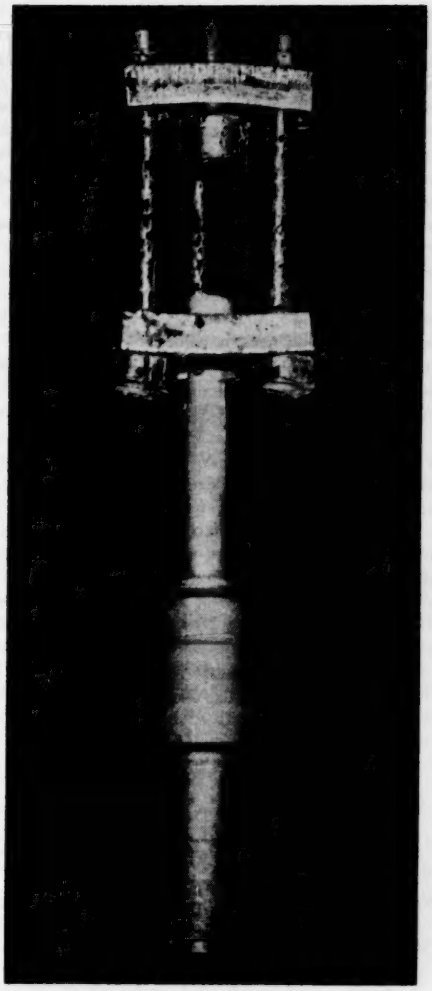

Fig. 6 Superpressure rotor entering water quench

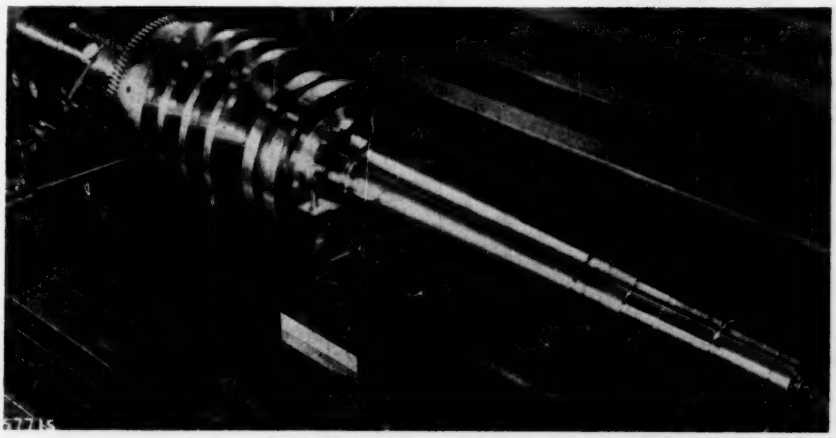

Fig. 7 Superpressure rotor being broached for blade fastenings

Since dimensional stability at operating conditions is a prime requirement of the superpressure rotor, tests to assure thermal stability were made at various stages of manufacture. The rough-turned forging was first given our standard slow-roll thermal stability or "heat-indication" test at the manufacturer's plant. Next, the forging was machined to form blade-carrying disks, provisions having been made to leave surplus metal on the periphery of these disks to simulate the centrifugal-force loading of the blades. In this condition, as shown in Fig. 7, the forging was operated at temperatures and speeds exceeding design operating conditions for a period of more than 250 hr. The rotor was then machined and bladed and given the standard manufacturing procedure run at service temperature and speed. After assembly of the radial seal disks, the rotor was given an overspeed test in its own casing before shipment.

As insurance against delay in turbine operation if serious difficulty were encountered in the manufacture of the Discaloy forging, three "back-up" integral-disk rotor forgings were made. These rotors were made from AISI Type 422 stainless steel, Jessop G-18-B, and a Cr-Mo-V alloy steel all of which were commercially available in the size required. Figs. 8, 9, and 10 compare the rupture strength, creep strength, and cold strength of the Discaloy, 422, and Cr-Mo-V rotors. From these curves it is obvious that the three back-ups do not exhibit the required strength characteristics and would be useful only for limited operation. Although the creep and rupture strength of the G-18-B rotor is comparable to Discaloy, its lower room-temperature yield strength would necessitate limiting the load which could be carried by the element. Since the integral Discaloy rotor has successfully passed all shop tests, the manufacture of the G-18-B and 422 material rotors has been discontinued and the Cr-Mo-V rotor has been disposed of.

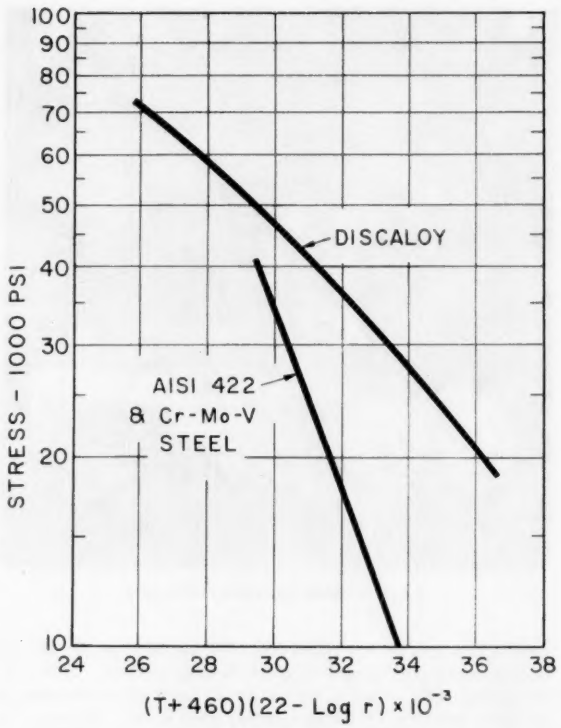

Fig. 9 Creep-rate master curve

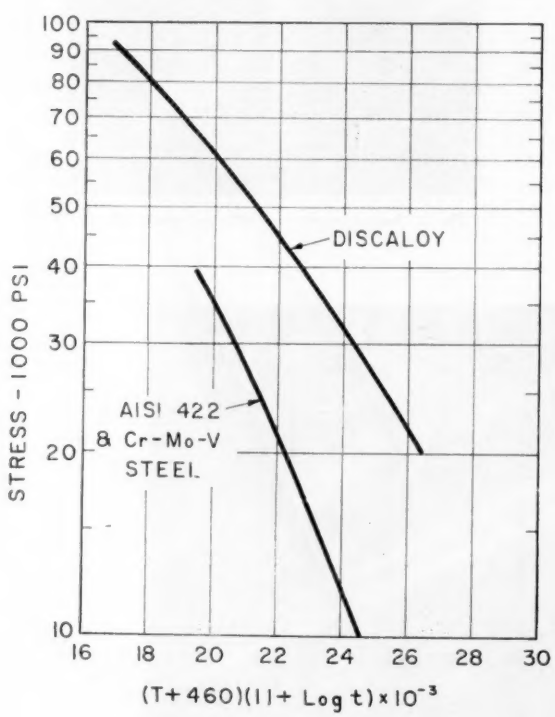

Fig. 8 Rupture-strength master curve

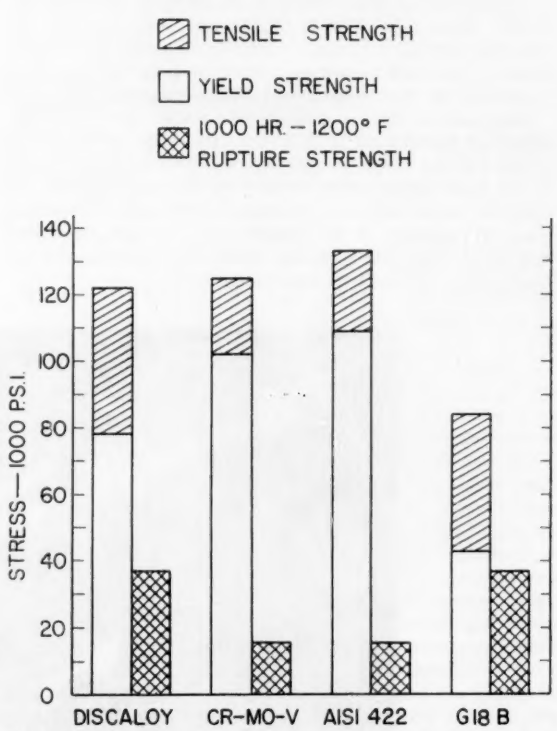

Fig. 10 Room-temperature tensile strength and 1200 F rupture-strength comparison

Separate Disk Rotor

An alternate design of rotor for the superpressure unit has been manufactured. This rotor differs from those previously described in that the turbine blades are carried by disks which are shrunk on a shaft. Such construction results in forgings which are considerably smaller than the one required for the integral-disk rotor. Discaloy material was again selected for both the shaft and the disks. This type rotor was produced not only as a back-up for the integral-disk rotor, but also to gain experience with this type construction. Once the design has been proved entirely satisfactory it would be possible to construct larger high-temperature rotors with any given forging weight limitation. This would also permit a design which could confine the use of superalloys to only the portion of the rotor where they are required.

The separate disk-type superpressure rotor, Fig. 11, has six disks independently shrunk on the shaft, which are axially asymmetrical in longitudinal section. The hub extends one way only from the plane of the disk so that, during operation, an axial centrifugal-stress gradient along the hub creates a moment which tends to conicalize the bore of the hub. Thus the hub will maintain a grip on the shaft at the hub end axial'y disposed from the disk mass center. The mechanics of such an L-section disk can be evaluated and a disk of this type has been tested at high speed and temperature to prove the design. The combination of stress, temperature, and time will ultimately plastically deform even the strongest of materials. In this design the creep in the disk section can proceed without any resultant vibration since the disk will retain its centering on the shaft at the toe end of the hub. The stresses on a symmetric and asymmetric disk design are shown in Fig. 12. The reduced stresses at point B are very beneficial in maintaining the fit at that point. The correspondingly higher stress at the other end of the hub, point A, is still well within the strength of this material.

Under certain very severe transient conditions, temperature difference between disks and shaft may become such as to loosen the disk from the shaft. An arrangement of radial pins is used so that these pins not only act as keys between disk and shaft, but will also maintain a centering of parts if the transient loosening occurs.

This "built-up" rotor is now held in reserve although satisfactory test performance of the integral Discaloy rotor gives every reason for confidence in its successful behavior.

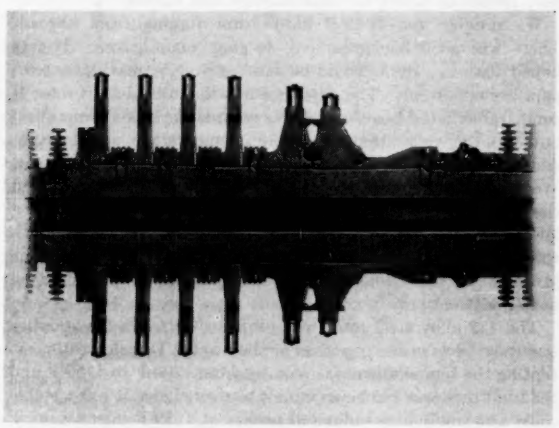

Fig. 11 Separate disk-type superpressure rotor

Blading

Blade port sections for this turbine are conventional in type for impulse stages. The first four rotation rows are of the company's high-temperature alloy, K-42-B.[3] This material has been used successfully for over 4 years in blading electric-utility-turbine service at approximately 125 F lower temperature than will be encountered here. Properties of this alloy are such that the temperature increase causes no critical drop in strength. K-42-B has been used also for blading gas turbines at comparable or even higher temperatures. Because this turbine operates with complete peripheral admission at all loads, vibration stresses even in the control stage are held to a minimum.

The blading in the fifth and sixth row at the lower temperature end of the turbine is of a modified AISI 422 stainless steel. All rotating blade rows are attached by side-entry fir-tree-type serrated fastenings, which achieve the most efficient utilization of material both in the blade and rotor.

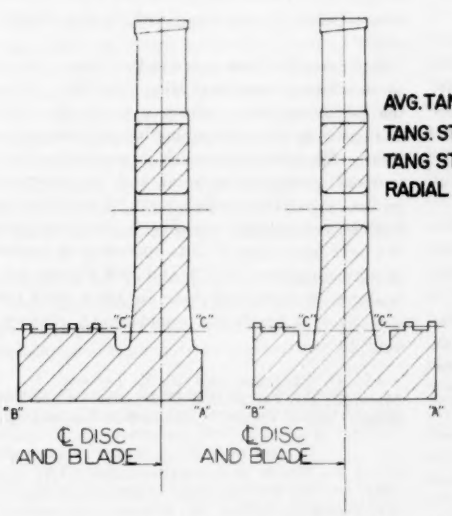

DISC. STRESSES
WITH FREE BORE

	UNSYMMETRIC	SYMMETRIC
AVG. TANG. STRESS	8350	8350
TANG. STRESS AT "A"	13630	10960
TANG STRESS AT "B"	6740	10960
RADIAL STRESS AT "C-C"	3810	4060

Fig. 12 Symmetric and eccentric rotor disk construction

The development of a new turbine-blade material for 1200 F had been accelerated during the past years resulting in an alloy called Nivco.[2] High-temperature strength plus damping capacity were designed into this material. The turbine design was finalized too early to incorporate this development. At the present time several rows of blades made from Nivco are installed and operating satisfactorily in machines of much more moderate steam conditions. Various types of aging treatment have been found to have marked beneficial effects. Studies of such effects are continuing. Because of the critical nature of blading when applied to such extreme conditions, an enormous amount of data must be accumulated and checked before a designer may use it.

The future of high-temperature blading will benefit considerably from the research involving this new material.

Other High-Temperature Parts

Stop and control valves are exposed to steam temperatures exceeding those ever experienced in electric utility service. For long and satisfactory service, these parts must exhibit excellent creep resistance and strength at elevated temperature. Therefore the valve bodies and bonnets were made of a modified Type-316 stainless steel as are the permanent strainers mounted in the valves. The same modified Type-316 austenitic steel resulted in excellent inner cylinder castings. A modified Discaloy was used for the valve stem; the valve-stem bushings and the valve itself are Discaloy.

Conclusions

Some of the materials and many detail design features of the Eddystone superpressure machine described here have not previously been used commercially under the severe operating conditions to be encountered. However, extrapolations from other successful service have been confirmed by extensive laboratory and shop tests on components, and long-time successful operation of Philadelphia Electric Company's Eddystone No. 1 superpressure turbine is looked to optimistically.

DISCUSSION

N. L. Mochel[3]

This is the second time that I have departed from a self-imposed rule of never discussing a Westinghouse-authored paper.

For good and perhaps obvious reasons, my associates have seen fit to compress a tremendous amount of development effort into a short paper of but seven pages, with twelve illustrations. Without prejudice and with no criticism implied in either direction, had they written even in the same degree of restricted detail presentation as some of the other papers in these two Eddystone sessions, it would have been, probably, the most voluminous of the day.

In the matter of the back-up rotor forgings, I feel that some clarification is in order, since the rather condensed form of the paper may leave some impressions not entirely correct, and in one case, a little unfair.

Comparison of the properties of the several rotor forgings has been made only at room temperature and at 1200 F. I can hear, already, some of my metallurgical friends asking the obvious question—were you so foolish as to think that the 422 alloy steel or the Cr-Mo-V steel would have ample properties at 1200 F? And of course the answer is no.

No provisions have been made at Eddystone No. 1 to operate independent of the superpressure turbine. All the steam must pass through that portion of the unit. Were we to have been so unfortunate as to be unable to procure the desired Discaloy rotor, or were we to have lost it for any reason, the delay in realizing the output of this large unit would have been a most serious matter and, naturally, we wanted to guard against such a situation. The provision of back-up rotors was a logical step.

Metal temperatures in the rotor proper are not 1200 F, but somewhat lower. Further, the unit is to be first operated with inlet steam of 1100 F, later moving upward to 1150 F, and later on to 1200 F. Thus, operation could be maintained at 1100 F or at 1150 F with rotors of materials of better procurability background, and adequate for these lower temperatures, during any period necessary to procure a rotor for the maximum temperature, should such need arise for any reason.

There were conditions of procuring and manufacture of the Discaloy rotor that made back-ups desirable. There were uneasy moments during the manufacture and testing.

We ordered the G-18-B alloy rotor forging from abroad. There was good background of forging manufacture. It was hoped that this rotor would be satisfactory for maximum temperature operation. The paper records that the G-18-B rotor is comparable to the Discaloy rotor as regards the 1200 F properties, but its lower yield strength at room temperature would necessitate limiting the load which could be carried by this element. We must, in all fairness, record that when the forging was ordered the output of the superpressure turbine was planned to be at a lower kw level, and no requirement as to a higher yield strength was passed on to the supplier. The G-18-B alloy is by nature one in which the desired higher yield strength cannot be realized by heat-treatment only.

The 422 alloy steel rotor was subjected to the same stability test referred to in the paper, as applied to the Discaloy rotor, excepting the temperature was reduced from 1200 F to 1150 F and the total time was 145 hours, and it was concluded it was a stable rotor and would give unlimited service at 1150 F inlet steam.

The rotor forging ordered of the usual Cr-Mo-V steel analysis, for possible operation at 1100 F, or short interim operation at higher temperature, was actually a composite forging which could be applied to either Eddystone No. 1 or to an order for an 1100 F unit. Before it was completed, it was transferred to the other order.

Reference has been made in this paper, and in this discussion, to the Jessop-developed alloy, G-18-B. In another paper[4] in the Eddystone story, reference was made to the important control valves in the plant piping having been made of this same material. We have been much interested in this alloy as a high-temperature piping material, and the experiences at Eddystone on this material will be followed with much interest. Incidentally, it is not a completely new alloy in our experiences in this country. We have used it for all nuts operating on austenitic steel bolting at temperatures of 1050 F and 1100 F; also for valve stem guide bushings, in a nitrided state, for these same temperatures. The experience is excellent, in some eight turbines, and going back over 10 years.

[3] Manager, Metallurgical Engineering, Westinghouse Electric Corporation, Steam Division, Lester, Pa. Mem. ASME.

[4] E. C. Chapman and R. E. Lorentz, Jr., "The Selection of Materials and Fabricating Techniques for the Eddystone Boiler and Sulzer Control Valves," published in this issue, pp. 275–284.

Material Selection and Fabrication, Main Steam Piping for Eddystone No. 1, 1200-F and 5000-Psi Service

R. H. CAUGHEY
Chief Metallurgist

W. G. BENZ, JR.
Senior Welding Engineer,
The M. W. Kellogg Company,
Manufacturing Department,
Jersey City, N. J.

The results of a metallurgical investigation which led to and supported the selection of Type-316 stainless steel (17 Cr-13 Ni-2.5 Mo) piping and a welding electrode of 16Cr-8 Ni-2 Mo composition for fabricating the main steam system of Eddystone No. 1 are presented.

The investigation revealed the comparative properties of welds in several combinations of columbium and molybdenum-bearing austenitic stainless steels.

A brief description of the major steps required to fabricate the heavy-wall stainless-steel piping is presented.

Among the more difficult problems encountered in the design of the Eddystone plant were those of selecting materials capable of withstanding continuous operation at the extremely high temperatures and pressures which the Philadelphia Electric Company engineers had established. Since Eddystone steam conditions would be more severe than those in any existing utility, there were no previous long-time data on materials or a ready-made guide.

The main-steam-piping system, the subject of this paper, carries the dense steam at 1200 F and 5000 psi at flow rates between 600,000 and 2,000,000 lb per hr from the superheater header to the turbine throttle. It required an exhaustive study of many high-alloy and superstrength steels to select the one most suitable for this supercritical service.

A comprehensive study by the authors' company of various stainless-steels and superstrength-alloy compositions [1][1] covered not only the available mechanical and physical properties of each, but also their equally relevant manufacturing, fabrication, and service histories. This led to the selection of the Type 316 for the Eddystone main steam piping. The electrode selected for welding this alloy was a nominally 16 Cr-8 Ni-2 Mo steel composition, "16-8-2," [2].

Actually the selection was made from two stainless alloy steels, the Type 316 and the chromium, nickel, columbium-bearing Type 347, in lieu of the superstrength alloys surveyed. The principal item in this decision was the fact that there was an established background of information not only on the properties but on the manufacture, fabrication, welding, heat-treatment, and service histories of the two former materials as compared with the superstrength alloys. That these factors were recognized by the ASME Boiler Code, and allowable design stresses of long standing were already established, also had an important bearing on this decision.

Basic in the selection of the Type-316 composition was both a reassessment of facts concerning the Type-347 service history in high-temperature, high-pressure steam piping and a supporting, comparative metallurgical laboratory evaluation of both materials which was designed to study the weldability, heat-treatment, and high-temperature stability of each in component sizes comparable to the dimensions required by Eddystone. Heretofore, the thickest Type-347 piping was $1^5/_8$ in., whereas Eddystone pipe thickness would necessarily range from $2^1/_2$ to almost 3 in.

Preliminary data on the supporting metallurgical evaluation program of the Type-316 and Type-347 compositions have been cited [1]. The data on these materials which have accumulated since will be included here. The final selection of Type 316 was made before much of the laboratory data were available. One aim of the program was to ferret out unexpected material or fabrication problems sufficiently in advance which would either warrant a reconsideration of the selected material or the need of extraordinary fabrication procedures to insure the high degree of requisite quality. Suffice it to say at this point that the data have proved that Type 316 was a highly satisfactory choice.

On the subject of the reassessment of the Type 347 (in relation to Type 316) in the past 11 years a number of important utilities have used Type-347 material for main-steam-pipe service, however, at temperatures which have not exceeded 1100 F [1]. For the most part, the behavior of this material has been satisfactory [3]. However, there have been important and often almost discouraging deviations from this due to sporadic cracking which has been localized wholly at a considerable number of welded joints both during fabrication and early in service [4]. Although a search has been underway to discover the responsible phenomenon, and much has been learned concerning piping design, welding materials, and heat-treatment that permits serious cracking now to be held to a comfortable minimum, the fundamental problem has not been totally resolved.

By the use of a new "hot-ductility" test [5] it has been discovered that the high-temperature ductility of the austenitic stainless steels may be markedly affected by the exposure to temperature levels attendant to welding. This takes place to such a degree that the weld heat-affected zone is left in a "hot short" or brittle condition whereby, it is believed, cracking may result at relatively low orders of stress either during welding and/or heat-treatment or, if not, then in service. This type of test has found wide use in the evaluation of materials with particular reference to the austenitic stainless steels, and many comparisons are available [6]. Relative to the Type-347 composition, it has been shown that it produces the widest variation in this property [7]. What is equally as significant is the fact that a separation of "good" and "bad," in relation to the service history of this ma-

[1] Numbers in brackets designate References at end of paper.

Contributed by the Power Division and presented at the Annual Meeting, Atlantic City, N. J., November 29–December 4, 1959, of The American Society of Mechanical Engineers.

Note: Statements and opinions advanced in papers are to be understood as individual expressions of their authors and not those of the Society. Manuscript received at ASME Headquarters October 30, 1959. Paper No. 59—A-327.

terial, has been possible with this type of test procedure. Type-316 material, subjected to the same procedure, has not shown the same order of variability, and the ductility values have been generally at a higher level. The Type-316 material was thus expected to be, by far, less sensitive to the cracking phenomenon.

A second purpose of this paper is to describe the high lights in the manufacture of the large main-steam-pipe system with particular reference to the steel production, pipe production, hot bending, welding, heat-treatment, and the allied quality-control procedures which were deemed necessary in light of the critical service. In this regard, a few of the statistics relative to the magnitude of the job should be of interest:

Altogether, a total of 2400 ft of pipe in sizes of 4 and 5 in. ID with wall thickness ranging between 2.345 in. (160 lb per ft) and 2.860 in. (239 lb per ft) was required with OD's between 8.690 and 10.658 in. A total of 600 tons of steel ingots was produced by the Sharon Steel Company; the pipe product manufactured by the Pennsylvania Forge Company was 185 tons. In addition to the seamless pipe, the system includes a large junction or "mixing header," weighing close to 15 tons, produced by Midvale Heppenstal Company, into which the steam is carried by eight leads from the superheater header and out of which four leads carry the steam to the four turbine throttle valves. The header, which averages out any inequalities in steam temperature, was also produced from Type 316 and represents a large block forging which was bored and contoured by machine turning and shaping. Integral forged nozzles matched the piping connections.

The shop fabrication of 56 separate welded assemblies, some of which were 50 ft long and weighed from 4 to 5 tons each, was required. Altogether, 61 hot bends were required. The shop fabrication required the production of 92 full-thickness pipe butt welds and the field erection required an additional 76.

In all these respects, the Eddystone main-steam-piping system represents the largest installation of austenitic stainless steel for a single turbine unit in the world today.

Metallurgical Evaluation Program

With only a few exceptions, there was a dearth of information on the weldability and weld-joint properties of the austenitic stainless steels which might be relied upon to reflect the possible effect of mass or thickness contemplated in the piping design, or nearly 3 in. The effects due to thickness which might be related to the forging and thermal history in both steel production and pipe manufacturing and, in welding fabrication, the high degree of restraint, which it is known increases in severity with increased thickness of the weld joint, were appropriately questioned. Therefore, the materials-evaluation program was designed to feature the welding and testing of weld joints completed in full-thickness pipe sections comparable to the Eddystone pipe dimensions.

Two pipe-material compositions, Type 347 and Type 316, which had been produced as "forged-and-bored" pipe specimens, and each of which was furnished in the solution heat-treated condition, were selected for this program; chemical compositions are shown in Table 1.

Table 1 Pipe material—chemical composition

Element	Type 347, per cent	Type 316, per cent (1)	(2)[a]
Carbon	0.067	0.034	0.044
Manganese	1.39	1.74	1.57
Phosphorus	0.021	0.022	0.016
Sulfur	0.015	0.016	0.015
Silicon	0.50	0.39	0.31
Nickel	11.07	13.53	12.26
Chromium	18.57	17.04	17.62
Molybdenum	...	2.23	2.35
Columbium	0.61	...	...
Tantalum	0.12	...	...

[a] Production pipe specimen.

The Type-347 and Type-316 pipe sizes obtained were 11½-in. OD, 5½-in. ID, 3 in. wall thickness. A second pipe specimen of Type 316 was included which represented a production length, or a specimen of the actual pipe used in the Eddystone system. This was substituted for the initial material when, in the course of the long-time thermal-aging treatments, a laboratory-furnace failure resulted in the loss of certain test specimens. It afforded, however, a study of actual piping material.

The program was designed to be completed in two phases. Phase A consisted of a comparison of the weld-joint properties of the Type 316 and Type 347. Phase B consists of a comprehensive test program completed on the Type-316 pipe product manufactured for the main-steam-pipe system.

Phase A—Comparison of Weld-Joint Properties. The weldability of Type 316 and Type 347, and the effect of time at temperature on the stability of the weld-joint properties of each, were the objectives of this phase.

Weldability. Weldability was studied in the course of completing full-thickness butt welds which joined two, 1-ft-long, pipe sections of each composition. To insure sufficient material for subsequent testing, three welded assemblies were completed in the Type-347 composition and five in the Type 316. One of the three Type-347 assemblies was made using a typical Type-347, low-ferrite, electrode composition; the other two were made using the 16-8-2 electrode analysis. Of the five Type-316 assemblies completed, two were made using a matching Type-316 electrode, and three made using the 16-8-2 composition. The typical chemical analysis of each weld metal is shown in Table 2:

Table 2 Weld metal—chemical composition

Element	Type 347, per cent	Type 316, per cent	B & W 16-8-2, per cent
Carbon	0.09	0.049	0.08
Manganese	2.43	1.92	2.02
Silicon	0.26	0.48	0.30
Sulfur	0.004	0.015	0.018
Phosphorus	0.020	0.027	0.015
Chromium	19.78	19.35	16.10
Nickel	9.87	13.42	8.21
Molybdenum	...	2.48	1.80
Columbium	0.91	...	...

Basically, the welding procedure, except for filler material, was the same for all eight assemblies. The details of the joint design and the actual welding technique are the same as used in production, shown in Fig. 24 and described in more detail in a following section.

For the development program, each weld layer, in each joint, was inspected by the dye-penetrant method for evidence of cracks. In addition to this, at weld thicknesses of ⅝, 1½, 2½ in., and full, the weld joint was ground and radiographed. This also was done after any post heat-treatment which was applied to a particular weld joint. Searched for, but not found, was evidence of either weld deposit or base-metal cracking. Slag inclusions were encountered in some cases which were removed by grinding and satisfactory repairs always were possible. A typical cross section of one of the welds is shown in the macro-etched condition in Fig. 1.

Stability. The mechanical and structural stability of each of the separate compositions and weld deposits were studied by comparisons of changes induced in their "as-welded" hardness, notched toughness, bending ability, metallic structure, and high-temperature load-carrying ability, resulting from combinations of thermal treatments which included 1950-F solution heat-treatment and aging at 1300 F for periods of 1000 and 10,000 hr.

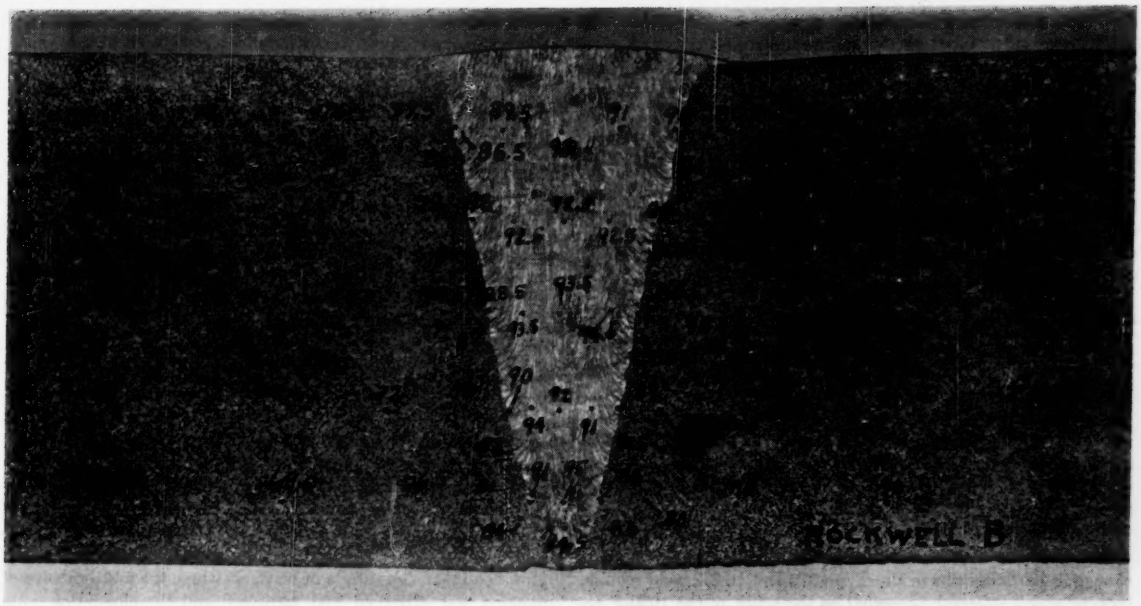

Fig. 1 Cross section through a typical weld joint, acid (macro) etched; numbers are Rockwell hardness values

Table 3 Hardness survey showing effect of thermal aging on each weld joint in each condition of heat-treatment (Rockwell hardness B scale)

Weld Joint		Aging	As Welded			1950 F, Air Cool		
Base Metal	Weld Metal	Time at 1300 F	Weld Metal	H.A.Z.	Base Metal	Weld Metal	H.A.Z.	Base Metal
347	347	None	-	-	-	93	82	80
347	16-8-2	"	100	88	80	83	81	77
316	316	"	92	87	71	81	69	68
316	16-8-2	"	98	91	74	82	67	68
316	16-8-2	"	95	89	76	81	67	71
347	347	1000 hrs.	-	-	-	93	83	80
347	16-8-2	"	96	91	82	85	83	79
316	316	"	89	86	79	83	71	72
316	16-8-2	"	92	82	72	85	68	69
316	16-8-2	"	-	-	-	84	70	72
347	347	10,000 hrs.	-	-	-	97	87	81
347	16-8-2	"	94	87	82	-	-	-
316	316	"	90	82	74	-	-	-
316	16-8-2	"	94	88	78	-	-	-
316	16-8-2	"	-	-	-	85	73	77

Table 4 Summary of hardness values comparing effect of thermal aging on as-welded and solution heat-treated component materials (Rockwell hardness B scale)

Aging Time at 1300 F (Hours)	As Welded						1950 F - Air Cool						
	Base Metal		Weld Metal		H. A. Z.		Base Metal		Weld Metal			H. A. Z.	
	347	316	316	16-8-2	347	316	347	316	347	316	16-8-2	347	316
None	80	74	92	97	88	89	79	69	93	81	82	82	68
1,000	82	75	89	94	91	84	79	70	89	83	84	83	69
10,000	82	76	90	94	87	85	81	77	97	-	85	87	73

The combination of Type-347 base material and Type-347 weld deposit was only tested in the solution-heat-treated condition, whereas the others were also tested in the as-welded condition. This was done because most of the prior laboratory data accumulated by the authors were for this material in the 1950-F solution-heat-treated condition. Therefore, this weld joint served as a basis of comparison for all other combinations.

The 1300 F used in the aging treatments, in lieu of the maximum Eddystone temperature, 1200 F, was used to accelerate aging effects since it is estimated that 1000 and 10,000 hr at 1300 F would roughly be equivalent to 15,000 and 150,000 hr, respectively, at the 1200-F level.

Results Obtained and Discussion.

Hardness Values. A suitably ground and lightly acid-etched, full-thickness cross section of each weld joint was explored by the Rockwell-B hardness method. Values for the base material, weld deposit, and heat-affected zone in each case were recorded. The average of the values for each location in each weld joint in each condition are shown in Table 3. A summary of these values with respect to the separate component materials is shown in Table 4.

Generally, the hardness levels are within the expected range for the individual material compositions. The only noticeable change in hardness was in the Type-316 and 16-8-2 weld metals, both of which softened somewhat as the result of the 1950-F solution heat-treatment. Aging, up to 10,000 hr at 1300 F, did not produce any marked change in the relative hardness of any weld-joint components.

Notch Toughness. Tables 5 and 6 show the results of Charpy keyhole-notched impact tests which were completed on specimens of each weld joint from each of three representative locations; namely, the base material, heat-affected zone, and weld deposit. The individual values in Table 5 are the averages of three or more specimens in each condition. Table 6 is a summary with respect to each component material.

The 1950-F solution heat-treatment and the added long-time aging treatment produced notable changes in the notched toughness of certain of the component materials. Both the Type-316 and 16-8-2 weld metals developed increased toughness as the result of the solution heat-treatment following welding. (The hardness level of these same materials, it should be noted, were reduced by this treatment compared to the others.) The effect of the subsequent aging treatments, however, is the most significant in that most of the gain from the prior solution-treatment is not retained. It is important to note, however, from this standpoint that the 16-8-2 weld metal shows the lesser tendency toward embrittlement than either the Type-316 or 347 weld metals. The Type-347 composition is the worst in this respect.

Bend Tests. Bend tests were completed at room temperature on $^1/_8$-in-thick full pipe cross-sectional specimens of each weld joint in each condition. Each was bent with the weld cross section positioned at the center of the beam or at the point of maximum bending. The angle of bend, at which the first evidence of cracking was observed and recorded, and the elongation were measured across the weld deposit, Table 7.

The bend test is primarily a test of the weld deposit. On this basis, the Type-347 and Type-316 weld compositions showed the

Table 5 Notch toughness survey showing effect of thermal aging on each weld joint in each condition of heat-treatment (ft-lb, Charpy keyhole specimens)

Weld Joint		Aging Time at 1300 F	As Welded			1950 F, Air Cool		
Base Metal	Weld Metal		Weld Metal	H.A.Z.	Base Metal	Weld Metal	H.A.Z.	Base Metal
347	347	None	–	–	–	23	42	52
347	16-8-2	"	33	40	52	56	48	53
316	316	"	27	60	83	42	83	83
316	16-8-2	"	34	61	88	57	86	89
316	16-8-2	"	33	67	81	49	83	87
347	347	1000 hrs.	–	–	–	9	38	43
347	16-8-2	"	25	31	43	31	39	45
316	316	"	21	41	55	23	46	49
316	16-8-2	"	28	41	56	45	64	65
316	16-8-2	"	–	–	–	32	43	45
347	347	10,000 hrs.	–	–	–	4	36	42
347	16-8-2	"	20	30	36	–	–	–
316	316	"	4	25	32	–	–	–
316	16-8-2	"	22	33	41	–	–	–
316	16-8-2	"	–	–	–	25	27	26

Table 6 Summary of notch toughness values comparing effect of thermal aging on as-welded and solution heat-treated component materials (ft-lb, Charpy keyhole specimens)

Aging Time at 1300 F (Hours)	As Welded						1950 F - Air Cool						
	Base Metal		Weld Metal		H. A. Z.		Base Metal		Weld Metal			H. A. Z.	
	347	316	316	16-8-2	347	316	347	316	347	316	16-8-2	347	316
None	52	84	27	33	40	63	53	86	23	42	51	45	84
1,000	43	55	21	27	31	41	44	53	9	23	36	38	51
10,000	36	36	4	21	30	29	42	26	4	–	26	36	27

Table 7 Bend test results showing the effect of thermal aging on each weld joint in each condition of heat-treatment

Weld Joint		Aging	As Welded			1950 F Air Cool		
Base Metal	Weld Metal	Time at 1300 F	Bend Angle	Elong. %	Remarks	Bend Angle	Elong. %	Remarks
347	347	None	-	-	-	180	17-26	O.S.*
347	16-8-2		180	21-29	O.S.	180	26-44	O.S.
316	316		180	12-22	O.S.	180	25-28	O.S.
316	16-8-2		180	21-41	O.S.	180	26-37	O.S.
316	16-8-2		180	24-29	O.S.	180	31-47	O.S.
347	347	1,000	-	-	-	120	14-15	Cracked
347	16-8-2		180	20-24	O.S.	180	24-42	O.S.
316	316		180	17-20	O.S.	180	19-22	O.S.
316	16-8-2		180	20-24	O.S.	180	16-32	O.S.
316	16-8-2		-	-	-	180	22-24	O.S.
347	347	10,000	-	-	-	180	9-12	O.S.
347	16-8-2		180	18-20	O.S.	-	-	-
316	316		40-180	4-8	Cracked	-	-	-
316	16-8-2		180	16-22	O.S.	-	-	-
316	16-8-2		-	-	-	180	22-29	O.S.

*O.S. = opened slightly

Table 8 Summary of rupture test results (featuring 100,000-hr rupture stress)

Weld joint				Aging	100,000 hr rupt. str.			Long time test		Predominant
Code	Base metal	Weld metal	Post H.T.	time at 1300 F	1100 F	1150 F	1200 F	hours	per cent elong.	break location
ASME allowable stress 12,500, 8,000, 5,000										
A	347	347	1950 F	none	22,000	18,500	14,700	1,894	6.8	Base metal
B	347	347	1950 F	1,000	19,500	16,000	12,500	4,943	9.0	Base metal
D	347	16-8-2	none	none	22,000	17,500	14,000	6,030	1.4	Weld-base
E	347	16-8-2	none	1,000	21,500	17,000	13,500	4,490	...	Weld-base
G	347	16-8-2	1950 F	none	21,000	16,500	12,700	6,821	7.7	Weld metal
H	347	16-8-2	1950 F	1,000	20,500	17,000	13,300	9,680	19.6	Weld-base
ASME allowable stress 10,400, 8,500, 6,800										
K	316	316	none	none	18,000	14,000	11,000	3,858	4.1	Weld metal
L	316	316	none	1,000	17,000	13,500	10,300	3,664	4.5	Weld metal
N	316	316	1950 F	none	18,500	15,000	11,700	5,338	10.1	Weld metal
O	316	316	1950 F	1,000	18,000	14,500	11,000	9,114	10.5	Weld metal
R	316	16-8-2	none	none	20,500	16,500	12,500	10,536	12.0	Base metal
S	316	16-8-2	none	1,000	20,000	16,000	12,500	11,808	13.9	Base metal
U	316	16-8-2	1950 F	none	20,000	15,500	11,700	2,595	[a]20.8	Base metal
V	316	16-8-2	1950 F	1,000	19,000	15,300	12,000	4,829	17.3	Weld-base

[a] 1250 F test.

greatest tendency to cracking; the 16-8-2 composition, the least. The greatest effect was brought about by the aging temperature and time. The Type-347 and 316 ductility were significantly reduced and cracking more pronounced. The 16-8-2 deposits, however, were not seriously affected.

Stress-Rupture Tests. The authors are greatly indebted to the General Electric Company [8] for the performance and interpretation of the stress-rupture tests. Five specimens were machined from each weld-joint combination. Because it was necessary to machine the specimens from various levels through the thickness, the width of the weld in the rupture-test specimen varied. Therefore, to provide more uniform test conditions and test all areas of the weld joint, the test bars were machined with a 3-in-long reduced section instead of the usual 2 in. The weld was located in the center of the test section. The bar diameter was 0.357 in.

Four short-time parameter rupture tests and one long-time rupture test at 1200 F were conducted for each weld-joint combination. The results of all tests completed to date (through the 1000-hr-aging combination) are shown in Figs. 2 through 15, which include graphs of the data in accordance with the Larsen-Miller parameter method. The 10,000 hr-aging tests are not yet available. These are being performed through the courtesy of the Westinghouse Electric Corporation.

In order to make certain comparisons, it was elected to further summarize the data on the basis of the 100,000-hr rupture strength derived from the parameter curves at 1100, 1150, and 1200 F, Table 8. Also shown are the specific data for each of the long-time tests completed at 1200 F which include the rupture life, elongation at fracture, and the predominant fracture location.

Although the spread in results among the 14 weld joints studied is small, certain comparisons are possible. Considering only the fracture locations shown for the 1200-F tests, the relative strengths of each of the five component materials studied, from strongest to the weakest, would be 347 weld metal, 347 base metal, 16-8-2 weld metal, 316 base metal, and 316 weld metal. In this respect, however, and with particular reference to relative strength levels of the 347 and 316 base metals, the fact (Table 1) that the carbon content of the 347 material is the higher of the two, 0.067 compared to 0.034, probably explains the differences observed.

Considering the separate effects of the several variables studied on the 100,000 hr rupture strength, the following trends are notable:

1 Pipe Material. Weld joints completed in the Type-347 base material on the average produced higher strength levels than those made in the Type 316.

M-T (C + log t) x 10^{-3}
C = 20

Time Hours	900F	1000F	1100F	1200F	1300F	1400F
1	27.2	29.2	31.2	33.2	35.2	37.2
10	28.6	30.7	32.8	34.9	37.0	39.0
100	29.9	32.1	34.3	36.5	38.7	40.9
1000	31.3	33.6	35.9	38.2	40.6	42.8
10,000	32.6	35.0	37.4	39.8	42.4	44.6
100,000	34.0	36.5	39.0	41.5	44.0	46.5

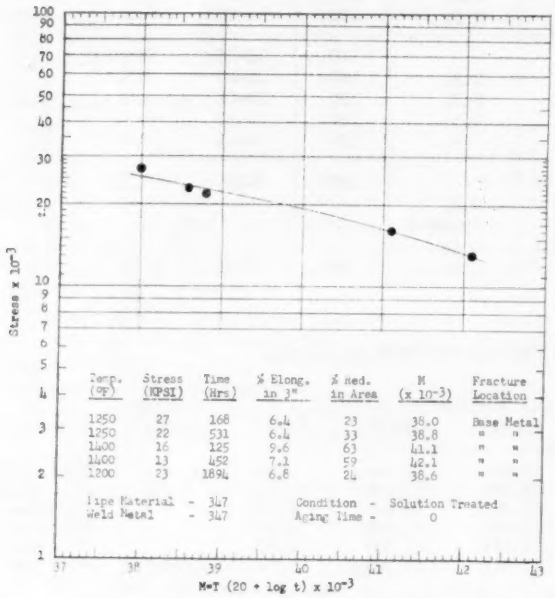
Stress x 10^{-3}
M-T (20 + log t) x 10^{-3}
Temp. (°F) | Stress (KPSI) | Time (Hrs) | % Elong. in 3" | % Red. in Area | M (x 10^{-3}) | Fracture Location
1250 | 27 | 168 | 6.4 | 23 | 38.0 | Base Metal
1250 | 22 | 531 | 6.4 | 33 | 38.8 | " "
1400 | 16 | 125 | 9.6 | 63 | 41.1 | " "
1400 | 13 | 452 | 7.1 | 59 | 42.1 | " "
1200 | 23 | 1894 | 6.8 | 24 | 38.6 | " "
Pipe Material - 347
Weld Metal - 347
Condition - Solution Treated
Aging Time - 0

Fig. 2 Rupture test results, Type-347 pipe, Type-347 weld, 1950 F air cool, no aging

M-T (C + log t) x 10^{-3}
C = 20

Time Hours	900F	1000F	1100F	1200F	1300F	1400F
1	27.2	29.2	31.2	33.2	35.2	37.2
10	28.6	30.7	32.8	34.9	37.0	39.0
100	29.9	32.1	34.3	36.5	38.7	40.9
1000	31.3	33.6	35.9	38.2	40.6	42.8
10,000	32.6	35.0	37.4	39.8	42.4	44.6
100,000	34.0	36.5	39.0	41.5	44.0	46.5

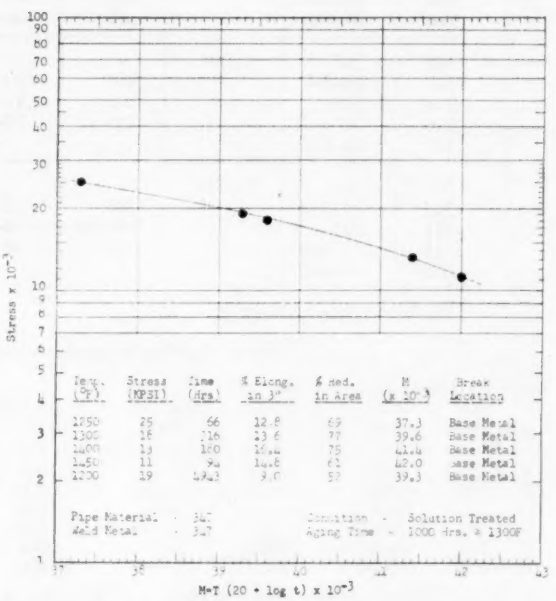
Stress x 10^{-3}
M-T (20 + log t) x 10^{-3}
Temp. (°F) | Stress (KPSI) | Time (Hrs) | % Elong. in 3" | % Red. in Area | M (x 10^{-3}) | Break Location
1250 | 25 | 66 | 12.8 | 69 | 37.3 | Base Metal
1300 | 16 | 216 | 23.6 | 77 | 39.6 | Base Metal
1400 | 13 | 160 | 16.4 | 75 | 41.4 | Base Metal
1450 | 11 | 94 | 14.8 | 61 | 42.0 | Base Metal
1200 | 29 | 494 | 9.0 | 52 | 39.3 | Base Metal
Pipe Material - 347
Weld Metal - 347
Condition - Solution Treated
Aging Time - 1000 Hrs. @ 1300F

Fig. 3 Rupture test results, Type-347 pipe, Type-347 weld, 1950 F air cool, aged 1000 hr at 1300 F

2 Welding Electrodes. Those weld joints containing the Type 16-8-2 deposits developed higher average strength levels than those containing Type-316 deposits; they were equal to those containing Type-347 weld metal.

3 Post weld Solution-Heat-Treatment. There was a slight lowering of the strength in the 16-8-2 weld joints and a slight increase in the Type 316 as the result of the solution heat-treatment.

4 Aging at 1300 F. Aging up to 1000 hr at 1300 F failed to disclose any marked change in the strength levels of any of the weld-joint compositions studied.

The trends just cited considered only the rupture strengths of the various materials studied. In the evaluation of weld joints for elevated temperature service, an equally important property which should be compared is the rupture ductility although this is a far more difficult property to compare than rupture strength, since the significance of any single test is influenced both by temperature and the life of the test. Christoffel of the General Electric Company attempted a comparison on a parameter basis in a similar manner used for the rupture strength, but there was unsatisfactory agreement with certain of the observed data and the trials were discontinued. Accordingly, only relative comparisons are possible and for this purpose the results obtained only in the long-time tests at 1200 F, Table 8, were studied. The following observations with respect to material and thermal treatment are possible:

1 Pipe Material. The weld joints completed in the Type-316 material generally developed higher ductility than those made in the Type-347 composition.

2 Weld Metal. Weld joints which contained the 16-8-2 deposits were markedly more ductile than those which contained either the Type-347 or Type-316 weld metal.

3 Post Solution-Heat-Treatment. A significant increase in ductility was observed in those materials which had been given the 1950-F air-cool treatment over those which were not so treated.

4 Aging at 1300 F. Aging up to 1000 hr at 1300 F did not result in any significant lowering of the ductility in any of the weld joints tested.

5 One other factor was checked in this investigation and that was how typical these results were. The results obtained were compared with those of other tests conducted in the General Electric Company Laboratory [8] as well as published data in the ASTM Special Technical Publications 124 [9] and 226 [10]. In general, the results of this investigation agreed quite well with the other published data. However, the weld joints containing 316 weld metal generally fell in the lower portion or somewhat below the scatterbands for the Type-316 base material.

Metallic Structure. The metallic structures of each material in each condition were studied by microscopic means. The objective was to determine and compare the phases present in each with the view toward explaining certain developed differences in their mechanical properties resulting from the long-time aging treatments.

Aging of the base materials at 1300 F did not produce any phase uncommon either to the Type-347 or Type-316 composition. Both showed evidence of intergranular carbide precipitation. The Type 316 showed the usual evidence of a "shower" type of

M-T (C + log t) x 10^{-3}
C = 20

Time Hours	900F	1000F	1100F	1200F	1300F	1400F
1	27.2	29.2	31.2	33.2	35.2	37.2
10	28.6	30.7	32.8	34.9	37.0	39.0
100	29.9	32.1	34.3	36.5	38.7	40.9
1000	31.3	33.6	35.9	38.2	40.6	42.8
10,000	32.6	35.0	37.4	39.8	42.4	44.6
100,000	34.0	36.5	39.0	41.5	44.0	46.5

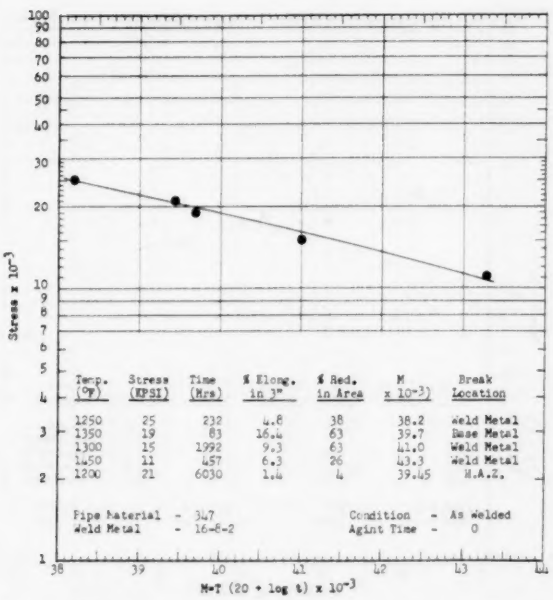
Stress x 10^{-3}
M-T (20 + log t) x 10^{-3}
Temp. (°F) | Stress (KPSI) | Time (Hrs) | % Elong. in 3" | % Red. in Area | M x 10^{-3} | Break Location
1250 | 25 | 232 | 4.8 | 38 | 38.2 | Weld Metal
1350 | 19 | 83 | 16.4 | 63 | 39.7 | Base Metal
1300 | 15 | 1992 | 9.3 | 63 | 41.0 | Weld Metal
1450 | 11 | 457 | 6.3 | 26 | 43.3 | Weld Metal
1200 | 21 | 6030 | 1.4 | 4 | 39.45 | N.A.Z.
Pipe Material - 347
Weld Metal - 16-8-2
Condition - As Welded
Aging Time - 0

Fig. 4 Rupture test results, Type-347 pipe, B & W 16-8-2 weld, as-welded, not aged

M-T (C + log t) x 10^{-3}
C = 20

Time Hours	900F	1000F	1100F	1200F	1300F	1400F
1	27.2	29.2	31.2	33.2	35.2	37.2
10	28.6	30.7	32.8	34.9	37.0	39.0
100	29.9	32.1	34.3	36.5	38.7	40.9
1000	31.3	33.6	35.9	38.2	40.6	42.8
10,000	32.6	35.0	37.4	39.8	42.4	44.6
100,000	34.0	36.5	39.0	41.5	44.0	46.5

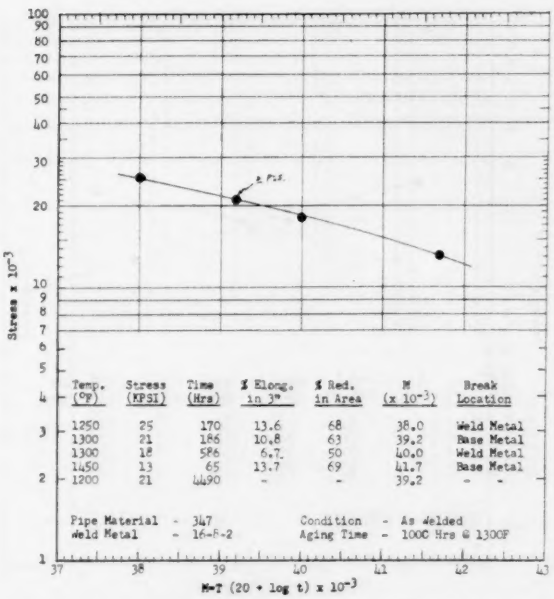
Stress x 10^{-3}
M-T (20 + log t) x 10^{-3}
Temp. (°F) | Stress (KPSI) | Time (Hrs) | % Elong. in 3" | % Red. in Area | M (x 10^{-3}) | Break Location
1250 | 25 | 170 | 13.6 | 68 | 38.0 | Weld Metal
1300 | 21 | 186 | 10.8 | 63 | 39.2 | Base Metal
1300 | 18 | 586 | 6.7 | 50 | 40.0 | Weld Metal
1450 | 13 | 65 | 13.7 | 69 | 41.7 | Base Metal
1200 | 21 | 4490 | - | - | 39.2 | - -
Pipe Material - 347
Weld Metal - 16-8-2
Condition - As Welded
Aging Time - 1000 Hrs @ 1300F

Fig. 5 Rupture test results, Type-347 pipe, B & W 16-8-2 weld, as-welded, aged 1000 hr at 1300 F

precipitate throughout the austenite matrix which is not uncommon in the molybdenum-bearing compositions. Sigma phase was not discernible in either composition. The presence of these phases probably accounts for the tendency toward lower notch toughness with aging.

Aging of the three separate weld deposits, namely, Type 347, 316, and 16-8-2, at 1300 F did not produce any phase uncommon to any of the compositions. Initially, all of the weld deposits in the as-welded condition contained the ferrite phase. The Type 347 showed the higher content, or roughly about 6 per cent, the Type 316 about 2 per cent, and the 16-8-2 about 1 per cent as determined by magna gage. Long-time aging resulted in conversion of most of the ferrite to the sigma phase. The 1950-F prior solution heat-treatment of the three weld deposits dissolved the ferrite content completely in the Type 316 and 16-8-2. Not all of the ferrite was dissolved in the Type-347 weld deposit by this treatment. Accordingly, after aging, this weld deposit still showed certain evidence of the sigma phase. In the molybdenum-bearing weld deposits, the same "shower" type of precipitate in the austenitic matrix was observed as in the base-metal compositions, although it was more pronounced in the weld metal. This was in addition to the intergranular carbide precipitation. A similar type of precipitate was not observed in the Type-347 weld metal.

Photomicrographs showing the microstructures developed in each case as the result of the aging treatments are shown in Figs. 16–19, inclusive.

Since the photomicrographs were prepared from the completed 1200-F stress-rupture specimens tested in each condition, the phases resulting from the combination of both thermal aging and stress are represented in the microstructures. Essentially, the metallic phases shown are the same as those which were observed in the study of only the thermally aged materials, except that the added stress factor was observed to have accelerated their formation.

Summary and Conclusions. For the purpose of evaluating and selecting the most suitable materials for use in the main steam piping of the first supercritical steam power plant to operate at 1200 F and 5000 psi, the mechanical and physical properties of production-made weld joints combining two pipe compositions (Type 347 and Type 316) and three weld-metal compositions (Type 347, Type 316, and B & W 16-8-2) have been compared. The weld-joint combinations were: Type-347 base metal—Type-347 weld metal; Type-347 base metal—B & W 16-8-2 weld metal; Type-316 base metal—Type-316 weld metal; and Type-316 base metal—B & W 16-8-2 weld metal.

The relative weldability of each, including the influence and behavior of each welding electrode, was determined by the actual performance and careful inspections of pipe-weld joints completed in 3-in-thick, 11$^1/_2$-in-diam pipe. The metallurgical stability of each and their component materials were studied by a comparison of their hardness, notch toughness, crack sensitivity in bending, high-temperature stress-to-rupture life, and microstructure, in both the as-welded and solution-heat-treated condition, as affected by long-time thermal-aging treatment at 1300 F for as long as 10,000 hr.

From the viewpoint of hardness, notch toughness, crack sensitivity in bending, and microstructure, both the Type-347 and

$M = T\ (C + \log t) \times 10^{-3}$

$C = 20$

Time Hours	900F	1000F	1100F	1200F	1300F	1400F
1	27.2	29.2	31.2	33.2	35.2	37.2
10	28.6	30.7	32.8	34.9	37.0	39.0
100	29.9	32.1	34.3	36.5	38.7	40.9
1000	31.3	33.6	35.9	38.2	40.6	42.8
10,000	32.6	35.0	37.4	39.8	42.4	44.6
100,000	34.0	36.5	39.0	41.5	44.0	46.5

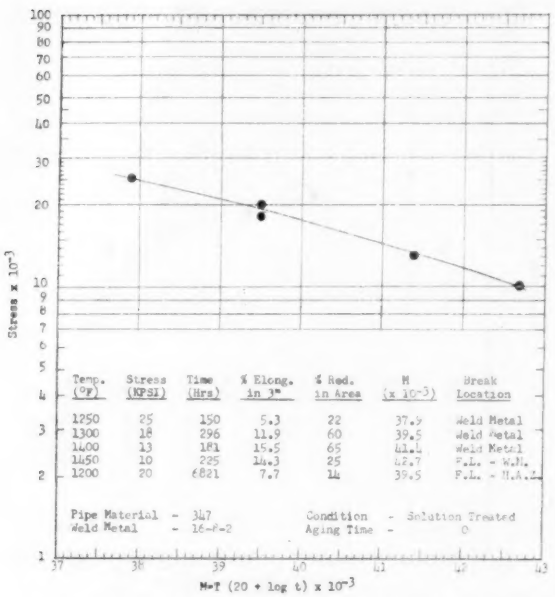
Stress x 10^-3
M=T (20 + log t) x 10^-3
Temp. (°F) | Stress (KPSI) | Time (Hrs) | % Elong. in 3" | % Red. in Area | M (x 10^-3) | Break Location
1250 | 25 | 150 | 5.3 | 22 | 37.9 | Weld Metal
1300 | 18 | 296 | 11.9 | 60 | 39.5 | Weld Metal
1400 | 13 | 181 | 15.5 | 65 | 41.4 | Weld Metal
1450 | 10 | 225 | 14.3 | 25 | 42.7 | F.L. - W.M.
1200 | 20 | 6821 | 7.7 | 14 | 39.5 | F.L. - H.A.Z.
Pipe Material - 347
Weld Metal - 16-8-2
Condition - Solution Treated
Aging Time - 0

Fig. 6 Rupture test results, Type-347 pipe, B & W 16-8-2 weld, 1950 F air cool, not aged

$M = T\ (C + \log t) \times 10^{-3}$

$C = 20$

Time Hours	900F	1000F	1100F	1200F	1300F	1400F
1	27.2	29.2	31.2	33.2	35.2	37.2
10	28.6	30.7	32.8	34.9	37.0	39.0
100	29.9	32.1	34.3	36.5	38.7	40.9
1000	31.3	33.6	35.9	38.2	40.6	42.8
10,000	32.6	35.0	37.4	39.8	42.4	44.6
100,000	34.0	36.5	39.0	41.5	44.0	46.5

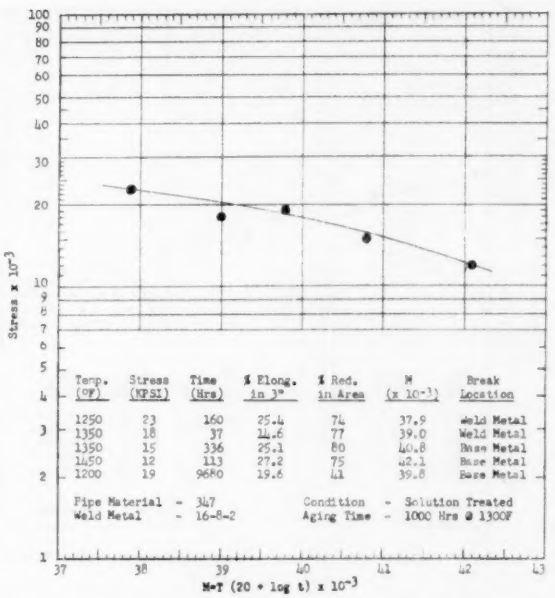
Stress x 10^-3
M=T (20 + log t) x 10^-3
Temp. (°F) | Stress (KPSI) | Time (Hrs) | % Elong. in 3" | % Red. in Area | M (x 10^-3) | Break Location
1250 | 23 | 160 | 25.4 | 74 | 37.9 | Weld Metal
1350 | 18 | 37 | 14.6 | 77 | 39.0 | Weld Metal
1350 | 15 | 336 | 25.1 | 80 | 40.8 | Base Metal
1450 | 12 | 113 | 27.2 | 75 | 42.1 | Base Metal
1200 | 19 | 9680 | 19.6 | 41 | 39.8 | Base Metal
Pipe Material - 347
Weld Metal - 16-8-2
Condition - Solution Treated
Aging Time - 1000 Hrs @ 1300F

Fig. 7 Rupture test results, Type-347 pipe, B & W 16-8-2 weld, 1950 F air cool, aged 1000 hr at 1300 F

Type-316 base metal and the B & W 16-8-2 weld metal are shown to possess what is considered to be adequate toughness and ductility in all conditions tested. The Type-347 and Type-316 weld metal, on the other hand, have shown a definite trend toward marked embrittlement as the result of long-time thermal aging. Certain improvement in the properties of all of the materials resulted from the application of the 1950-F solution-heat-treatment following welding; with subsequent thermal aging, however, the gain was not retained.

The analysis of the elevated stress-rupture data for each of the combinations of weld joints and conditions of thermal treatment has indicated that the best balance between strength and ductility was achieved in those which contained Type-316 pipe material welded with the 16-8-2 electrode. The results were good with this combination both with and without a post solution-heat-treatment. The results on weld joints in the Type-347 pipe also welded with the 16-8-2 electrode, but in the solution-heat-treated condition, however, were equally as good. In respect to each of these materials, the indications are that the controlling factor in producing good over-all properties was the use of the 16-8-2 weld metal. The Type-316 weld metal produced a significantly weaker weld joint as well as one with lower ductility than the 16-8-2 composition. The Type-347 weld metal produced the stronger weld joints, but with much lower ductility; however, the strength advantage was lost after only 1000-hr aging at 1300 F.

On the subject of conclusions, it has been stated that the choice of the Type-316 pipe composition and the 16-8-2 weld-metal composition was made between the Type-347 and Type-316 pipe and weld materials. It also was made on the basis of very preliminary but encouraging data which became available at the beginning of the laboratory evaluation even though there was an abundance of laboratory data and industry experience on the Type-347 material. In the experience with the Type-347 composition there had been certain evidence of cracking at welded joints during both fabrication and in steam-piping service, the reason for which had not yet been explained metallurgically. Considering this fact, and in addition certain collective experience and knowledge possessed by the industry on Type 316, which failed to disclose any similar evidence of cracking, the Type 316 was selected for the main-steam-piping system.

An early decision on the material had to be made to facilitate scheduling. Accordingly, the metallurgical test program was designed to ferret out unexpected material or fabrication problems sufficiently in advance which would either warrant a reconsideration of the selected materials or the need of extraordinary fabrication procedures to insure the high degree of requisite quality.

In view of these objectives and an over-all review of the data, the following conclusions, relative to the use of the Type-316 pipe composition and the 16-8-2 weld metal, are warranted:

1 The best balance between strength and ductility has been achieved by the use of the Type-316 pipe composition and the 16-8-2 weld-metal composition.

2 Sufficient enhancement in the weld-joint properties has been attained to justify the application of the 1950-F solution heat-treatment.

3 The high degree of physical quality obtained in the Type-

$M = T\,(C + \log t) \times 10^{-3}$

$C = 20$

Time Hours	900F	1000F	1100F	1200F	1300F	1400F
1	27.2	29.2	31.2	33.2	35.2	37.2
10	28.6	30.7	32.8	34.9	37.0	39.0
100	29.9	32.1	34.3	36.5	38.7	40.9
1000	31.3	33.6	35.9	38.2	40.6	42.8
10,000	32.6	35.0	37.4	39.8	42.4	44.6
100,000	34.0	36.5	39.0	41.5	44.0	46.5

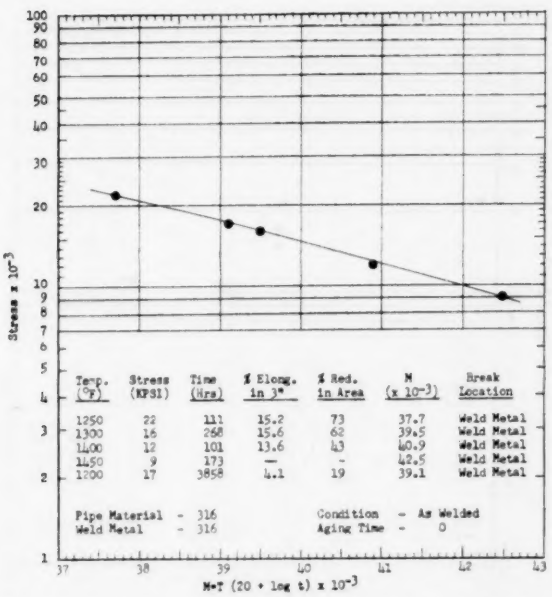
Stress x 10^-3
M=T (20 + log t) x 10^-3
Temp. (°F) | Stress (KPSI) | Time (Hrs) | % Elong. in 3" | % Red. in Area | M (x 10^-3) | Break Location
1250 | 22 | 111 | 15.2 | 73 | 37.7 | Weld Metal
1300 | 16 | 268 | 15.6 | 62 | 39.5 | Weld Metal
1400 | 12 | 101 | 13.6 | 43 | 40.9 | Weld Metal
1450 | 9 | 173 | — | - | 42.5 | Weld Metal
1200 | 17 | 3858 | 4.1 | 19 | 39.1 | Weld Metal
Pipe Material - 316
Weld Metal - 316
Condition - As Welded
Aging Time - 0

Fig. 8 Rupture test results, Type-316 pipe, Type-316 weld, as-welded, not aged

$M = T\,(C + \log t) \times 10^{-3}$

$C = 20$

Time Hours	900F	1000F	1100F	1200F	1300F	1400F
1	27.2	29.2	31.2	33.2	35.2	37.2
10	28.6	30.7	32.8	34.9	37.0	39.0
100	29.9	32.1	34.3	36.5	38.7	40.9
1000	31.3	33.6	35.9	38.2	40.6	42.8
10,000	32.6	35.0	37.4	39.8	42.4	44.6
100,000	34.0	36.5	39.0	41.5	44.0	46.5

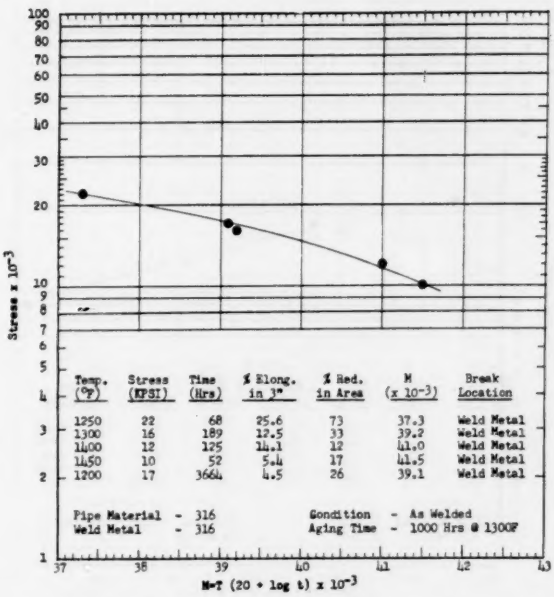
Stress x 10^-3
M=T (20 + log t) x 10^-3
Temp. (°F) | Stress (KPSI) | Time (Hrs) | % Elong. in 3" | % Red. in Area | M (x 10^-3) | Break Location
1250 | 22 | 68 | 25.6 | 73 | 37.3 | Weld Metal
1300 | 16 | 189 | 12.5 | 33 | 39.2 | Weld Metal
1400 | 12 | 125 | 14.1 | 12 | 41.0 | Weld Metal
1450 | 10 | 52 | 5.4 | 17 | 41.5 | Weld Metal
1200 | 17 | 3664 | 4.5 | 26 | 39.1 | Weld Metal
Pipe Material - 316
Weld Metal - 316
Condition - As Welded
Aging Time - 1000 Hrs @ 1300F

Fig. 9 Rupture test results, Type-316 pipe, Type-316 weld, as-welded aged 1000 hr at 1300 F

316, 16-8-2 weld joints indicated that no unusual welding difficulties would be experienced in fabrication which would necessitate the need of unusual or special welding procedures to gain the quality level required.

4 That the Type-316, 16-8-2 weld-joint combination will not be subject to embrittling effects after long-time service to the same degree which has been experienced in the use of Type-347 stainless-steel combination of base metal and weld metal in steam-pipe service.

Phase B—Steel and Pipe Manufacturing. The Eddystone main-steam-piping system required the manufacture of 2500 ft of Type 316 in the following sizes:

4.000 in. ID × 2.400 in. min wall; 8.80 in. OD, 165 lb per ft
4.000 in. ID × 2.525 in. min wall; 9.05 in. OD, 176 lb per ft
4.000 in. ID × 2.345 in. min wall; 8.69 in. OD, 160 lb per ft
4.938 in. ID × 2.860 in. min wall; 10.658 in. OD, 285 lb per ft

In light of the critical service, all effort was extended in both the manufacture and fabrication of the piping which would insure the attainment of exceptionally clean, sound metal, free of injurious defects, having the desired chemical, physical, mechanical properties. In this aim, very enthusiastic co-operation was secured both from the steel and pipe manufacturers.

All aspects of the manufacturing and quality control were clearly defined in advance through mutual discussions with all concerned which led finally to the preparation of suitable material specifications.

Essentially, the pipe was produced in accordance with the applicable requirements, including supplementary testing, of ASTM Specification A376 and A369 which cover piping for high-temperature central-station service. However, it was deemed necessary to modify and add to these basic requirements. Accordingly, a complete purchase specification was prepared which, in addition to the normal requirements for chemical and mechanical tests, featured:

1 A record of the melting, ingot, forging, and conditioning practice of each heat of steel.

2 The identification of heat and ingots and subsequently the identification of each pipe length or multiple thereof by cut number or its orientation and location relative to the original ingot.

3 Hot ductility tests of the RPI type completed on specimens in the as-cast condition; and subsequently for comparison purposes on specimens of pipe in the as-forged and finished heat-treated condition. For the as-cast tests, the steel melter cast a suitable small ingot from which the specimens were obtained. The pipe producer submitted pipe rings which represented, in pipe, the top of the first and bottom of the last ingot in each heat of steel.

4 The requirements that the steel source was to hot-roll the stripped and resoaked ingots directly to suitable size blooms for shipment to and reforging by the pipe vendor. The total cross-sectional reduction by forging from the ingot was not to be less than 4 to 1. It is notable in this respect that often past practices for forged and bored pipe had consisted of the pipe vendor purchasing large cast ingots which had to be reheated for forging

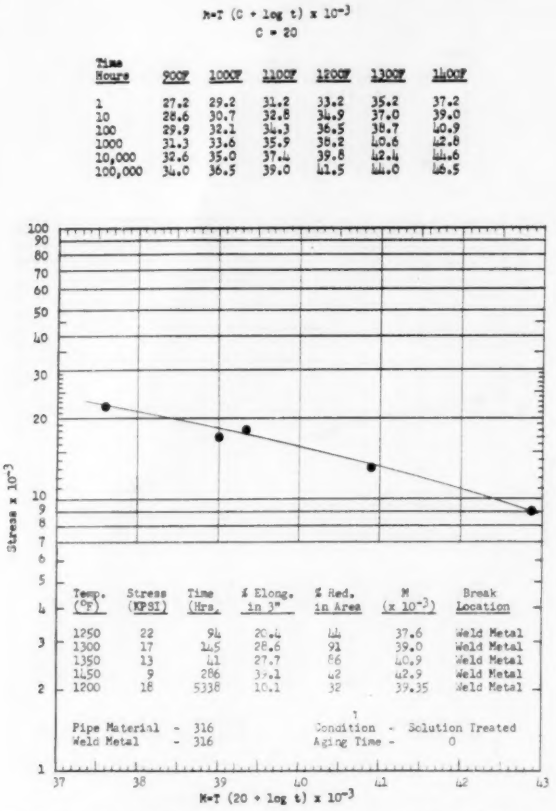

Fig. 10 Rupture test results, Type-316 pipe, Type-316 weld, 1950 F air cool, not aged

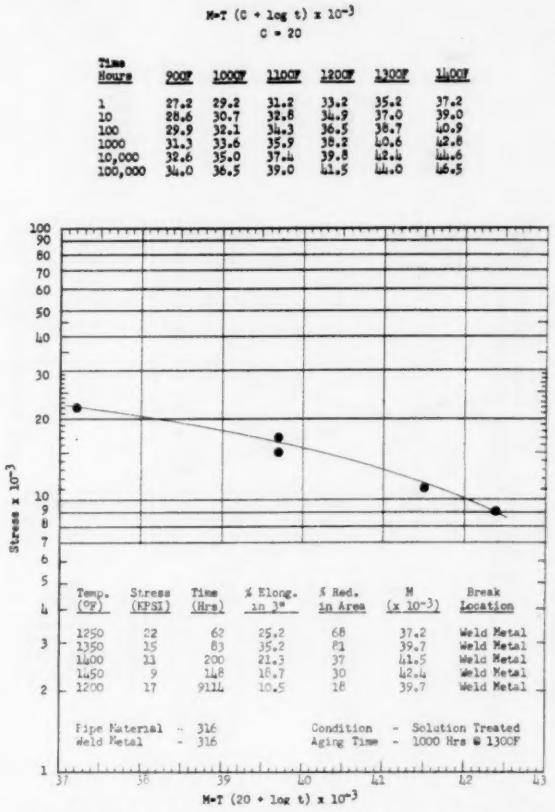

Fig. 11 Rupture test results, Type-316 pipe, Type-316 weld, 1950 F air cool, aged 1000 hr at 1300 F

into pipe rounds. Cognizant of the critical thermal stresses attendant to the reheating of large austenitic-stainless-steel ingots, it was mutually agreed that the practice specified in this instance would better insure the desired product quality. Requirements for heating rates and temperature control throughout forging also were made a part of the specification with specific emphasis directed toward grain-size control in the final pipe product.

5 Final forging was to be completed using V-dies to insure the greatest uniformity in grain structure.

6 Finished machined pipe, after heat-treatment, was required to have a 125 to 250 maximum RMS finish. All pipe was heat-treated at 1950–2000 F for 1 hr followed by water quenching.

7 Dye-penetrant examination of 100 per cent of the outside surface of each pipe length, and the reporting and subsequent removal of all indicated defects which exceeded $^1/_8$ in. in length.

8 A 100 per cent ultrasonic inspection by an approved shear-wave technique to locate injurious defects—defined as any which encroached on the specified minimum wall thickness or otherwise exceeded 3 per cent of the wall thickness.

9 Chemical analysis of two pipe lengths from each heat representing the top of the first and bottom of the last ingot.

10 Transverse tension tests made on specimens machined from pipe rings taken from one end of each pipe length. The specimens were alternated to represent the top and bottom ends of the pipe with respect to the original ingot location.

11 Acid-etch tests completed on full pipe-ring cross sections from one end of each pipe length.

12 Specimens for microstructural studies and grain-size determination from one end of each pipe length.

Results of Quality-Control Tests on Pipe Product. It is not possible to describe quantitatively the results obtained for each of the specific quality-control requirements listed. The results of the more salient features follow. It is believed these demonstrate, from the viewpoint of chemical, physical, and mechanical properties obtained, that a high-quality pipe product was secured.

Chemical Composition. A summary of the chemical composition of the pipe received is shown in Table 9, which also includes a comparison with the initial ladle analyses.

The uniformity of the results obtained within the specified limits is notable. Also noteworthy are the ranges of carbon and silicon contents obtained; the silicon being purposefully specified at 0.50 per cent maximum in lieu of the usual 1.00 per cent maximum. This was done with the objective of improving weldability in light of the authors' and others' [11] past experience which has indicated that crack sensitivity of austenitic weld joints often is associated with high silicon-to-carbon ratios.

Tension Properties. The fact that the specification minimum of 75,000-psi tensile strength in the pipe product was not always obtained will be noted in Table 10. This was found to be the result of the combination of average low carbon content and required heavy wall thickness and not otherwise a reflection of defective pipe material. Permission to use the pipe product for the service intended was granted by the Pennsylvania Department of Labor and Industry.

Acid-Etch Tests. The purpose in these tests was to ascertain pipe soundness. Evidence of gross ingot segregation, "piping," and

M-T (C + log t) x 10^{-3}
C = 20

Time Hours	900F	1000F	1100F	1200F	1300F	1400F
1	27.2	29.2	31.2	33.2	35.2	37.2
10	28.6	30.7	32.8	34.9	37.0	39.0
100	29.9	32.1	34.3	36.5	38.7	40.9
1000	31.3	33.6	35.9	38.2	40.6	42.8
10,000	32.6	35.0	37.4	39.8	42.4	44.6
100,000	34.0	36.5	39.0	41.5	44.0	46.5

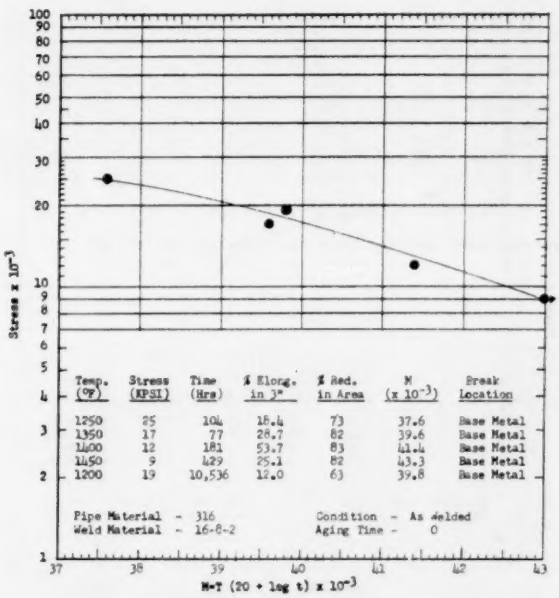
Stress x 10^{-3}
M-T (20 + log t) x 10^{-3}
Temp. (°F) | Stress (KPSI) | Time (Hrs) | % Elong. in 3" | % Red. in Area | M (x 10^{-3}) | Break Location
1250 | 25 | 104 | 16.4 | 73 | 37.6 | Base Metal
1350 | 17 | 77 | 28.7 | 82 | 39.6 | Base Metal
1400 | 12 | 181 | 53.7 | 83 | 41.4 | Base Metal
1450 | 9 | 429 | 25.1 | 82 | 43.3 | Base Metal
1200 | 19 | 10,536 | 12.0 | 63 | 39.8 | Base Metal
Pipe Material - 316
Weld Material - 16-8-2
Condition - As Welded
Aging Time - 0

Fig. 12 Rupture test results, Type-316 pipe, B & W 16-8-2 weld, as-welded, not aged

M-T (C + log t) x 10^{-3}
C = 20

Time Hours	900F	1000F	1100F	1200F	1300F	1400F
1	27.2	29.2	31.2	33.2	35.2	37.2
10	28.6	30.7	32.8	34.9	37.0	39.0
100	29.9	32.1	34.3	36.5	38.7	40.9
1000	31.3	33.6	35.9	38.2	40.6	42.8
10,000	32.6	35.0	37.4	39.8	42.4	44.6
100,000	34.0	36.5	39.0	41.5	44.0	46.5

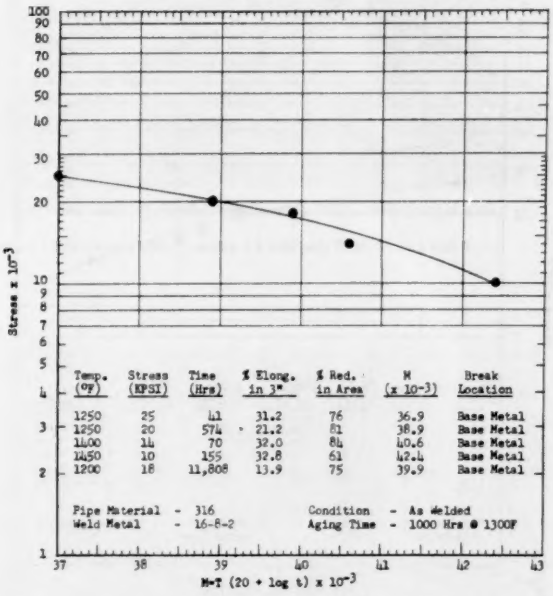
Stress x 10^{-3}
M-T (20 + log t) x 10^{-3}
Temp. (°F) | Stress (KPSI) | Time (Hrs) | % Elong. in 3" | % Red. in Area | M (x 10^{-3}) | Break Location
1250 | 25 | 41 | 31.2 | 76 | 36.9 | Base Metal
1250 | 20 | 574 | 21.2 | 81 | 38.9 | Base Metal
1400 | 14 | 70 | 32.0 | 84 | 40.6 | Base Metal
1450 | 10 | 155 | 32.8 | 61 | 42.4 | Base Metal
1200 | 18 | 11,808 | 13.9 | 75 | 39.9 | Base Metal
Pipe Material - 316
Weld Metal - 16-8-2
Condition - As Welded
Aging Time - 1000 Hrs @ 1300F

Fig. 13 Rupture test results, Type-316 pipe, B & W 16-8-2 weld, as-welded, aged 1000 hr at 1300 F

Table 9 Chemical composition comparisons, ladle analyses and pipe analyses, Type-316 stainless steel forged and bored pipe

		Ladle analyses (19 heats)		Pipe analyses (Top of first ingot)		Pipe analyses (Bot. of last ingot)	
Element	Specified	Ave.	Range	Ave.	Range	Ave.	Range
Carbon	0.08 max	0.046	0.036–0.060	0.048	0.036–0.066	0.048	0.032–0.071
Manganese	1.25–2.00	1.73	1.62–1.89	1.70	1.64–1.83	1.68	1.34–1.86
Silicon	0.50 max	0.37	0.22–0.45	0.34	0.21–0.42	0.33	0.21–0.47
Chromium	16.00–18.00	17.10	16.33–17.61	17.01	16.22–17.55	17.05	16.39–17.69
Nickel	11.00–14.00	12.58	12.26–13.09	12.69	12.24–13.03	12.69	12.17–13.14
Molybdenum	2.00–3.00	2.28	2.11–2.47	2.26	2.13–2.50	2.27	2.08–2.45

Table 10 Tension test results forged and bored pipe product, annealed 1950 F, air cool, Type-316 stainless steel

		Tensile properties (158 coupons)	
Property	Specification	Average	Range
Yield str. (psi)	30,000 min	38,460	34,000–45,000
Ult. str. (psi)	75,000 min	75,450	[a]72,500–80,000
Elong. (per cent in 2 in.)	45.0 per cent min	54.5%	45.6–60.2%
Red. in area, per cent	50.0 per cent min	68.0%	52.8–72.8%

[a] 70,000 psi minimum ultimate str. approved by Pennsylvania Department of Labor and Industry.

cracking was searched for, but not found in any single pipe specimen.

Microstructure. Microscopic inspection showed that the forging practice had effectively reduced the as-cast structure and, in combination with the thermal control and final solution heat-treatment, had produced a typical and satisfactory austenitic structure with the very minimum of carbide precipitation. The grain size ranged from ASTM number 2 to 6.

Dye-Penetrant and Ultrasonic Inspection. It was stated that each pipe length was inspected 100 per cent by these two methods. Of all of the inspections made, these revealed the only physical defects in the pipe quality which required certain added investigation before proper disposition could be made.

Ultrasonic examination of a total of 124 pipe lengths disclosed that nine lengths of pipe were questionable on the basis of subsurface indications, which ranged in size from 2 to 5 per cent of

$M=T\ (C + \log t) \times 10^{-3}$

$C = 20$

Time Hours	900F	1000F	1100F	1200F	1300F	1400F
1	27.2	29.2	31.2	33.2	35.2	37.2
10	28.6	30.7	32.8	34.9	37.0	39.0
100	29.9	32.1	34.3	36.5	38.7	40.9
1000	31.3	33.6	35.9	38.2	40.6	42.8
10,000	32.6	35.0	37.4	39.8	42.4	44.6
100,000	34.0	36.5	39.0	41.5	44.0	46.5

$M=T\ (C + \log t) \times 10^{-3}$

$C = 20$

Time Hours	900F	1000F	1100F	1200F	1300F	1400F
1	27.2	29.2	31.2	33.2	35.2	37.2
10	28.6	30.7	32.8	34.9	37.0	39.0
100	29.9	32.1	34.3	36.5	38.7	40.9
1000	31.3	33.6	35.9	38.2	40.6	42.8
10,000	32.6	35.0	37.4	39.8	42.4	44.6
100,000	34.0	36.5	39.0	41.5	44.0	46.5

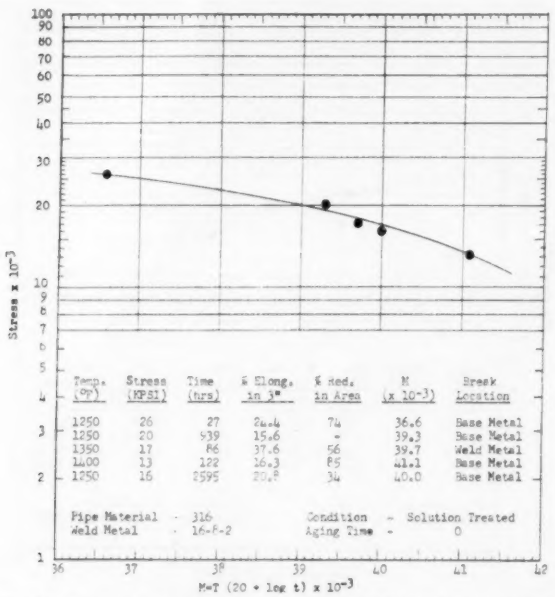
Stress x 10^{-3}
$M=T\ (20 + \log t) \times 10^{-3}$
Temp. (°F) | Stress (KPSI) | Time (hrs) | % Elong. in 3" | % Red. in Area | M (x 10^{-3}) | Break Location
1250 | 26 | 27 | 24.4 | 74 | 36.6 | Base Metal
1250 | 20 | 939 | 15.6 | - | 39.3 | Base Metal
1350 | 17 | 86 | 37.6 | 56 | 39.7 | Weld Metal
1400 | 13 | 122 | 16.3 | 85 | 41.1 | Base Metal
1250 | 16 | 2595 | 20.8 | 34 | 40.0 | Base Metal
Pipe Material - 316
Weld Metal - 16-8-2
Condition - Solution Treated
Aging Time - 0

Fig. 14 Rupture test results, Type-316 pipe, B & W 16-8-2 weld, 1950 F air cool, not aged

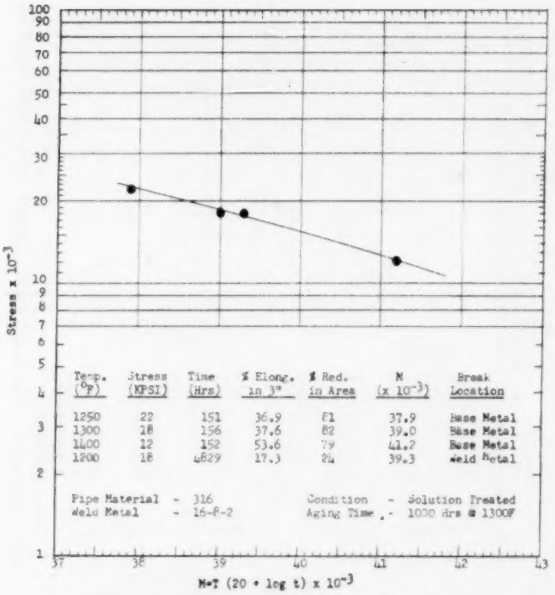
Stress x 10^{-3}
$M=T\ (20 + \log t) \times 10^{-3}$
Temp. (°F) | Stress (KPSI) | Time (Hrs) | % Elong. in 3" | % Red. in Area | M (x 10^{-3}) | Break Location
1250 | 22 | 151 | 36.9 | 81 | 37.9 | Base Metal
1300 | 18 | 156 | 37.6 | 82 | 39.0 | Base Metal
1400 | 12 | 152 | 53.6 | 79 | 41.2 | Base Metal
1200 | 18 | 4829 | 17.3 | 24 | 39.3 | Weld Metal
Pipe Material - 316
Weld Metal - 16-8-2
Condition - Solution Treated
Aging Time - 1000 hrs @ 1300F

Fig. 15 Rupture test results, Type-316 pipe, B & W 16-8-2 weld, 1950 F air cool, aged 1000 hr at 1300 F

(a) Type-347 pipe metal, 100X, aqua regia etch

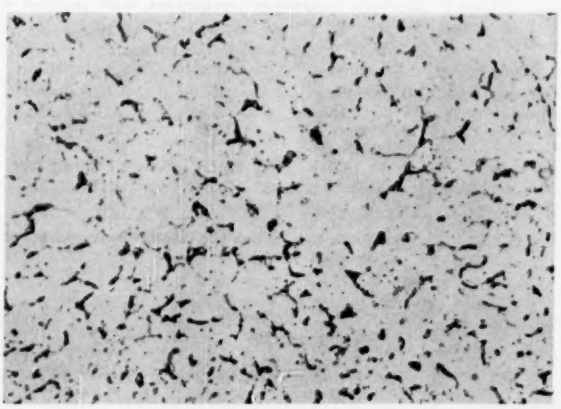

(b) Type-347 weld metal, 500X, chromic acid etch

Fig. 16 Microstructure, rupture test specimen 1950 F air cool, aged 1000 hr at 1300 F; tested 19,000 psi, 4943 hr at 1200 F

the pipe thickness and from 1 to 41 in. long. Each was disposed of by cutting out and discarding that section of the pipe in which each defect was located. Accordingly, all pipe lengths accepted were free of ultrasonic indications.

Dye-penetrant inspection of 100 per cent of the outside pipe surfaces of all lengths revealed that many of the pipes contained numerous, scattered defects which exceeded the permissible $^1/_8$-in. maximum dimension. Many of these were explored for both length and depth, the latter by grinding and re-dye checking. The maximum length obtained was $1^1/_2$ in., the maximum depth did not exceed $^1/_{16}$ in. It is noteworthy that the ultrasonic inspection did not at any time disclose evidence of these particular surface indications.

In addition to this examination of the defects and in order to

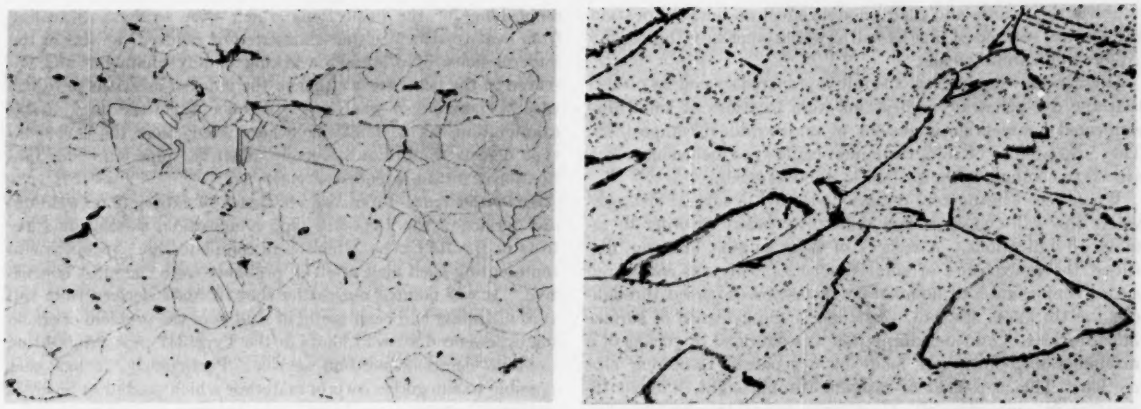

(a) Type-347 pipe metal, 100X, aqua regia etch

(b) B & W 16-8-2 weld metal, 500X, chromic acid etch

Fig. 17 Microstructure, rupture test specimen, 1950 F air cool, aged 1000 hr at 1300 F; tested 19,000 psi, 9680 hr at 1200 F

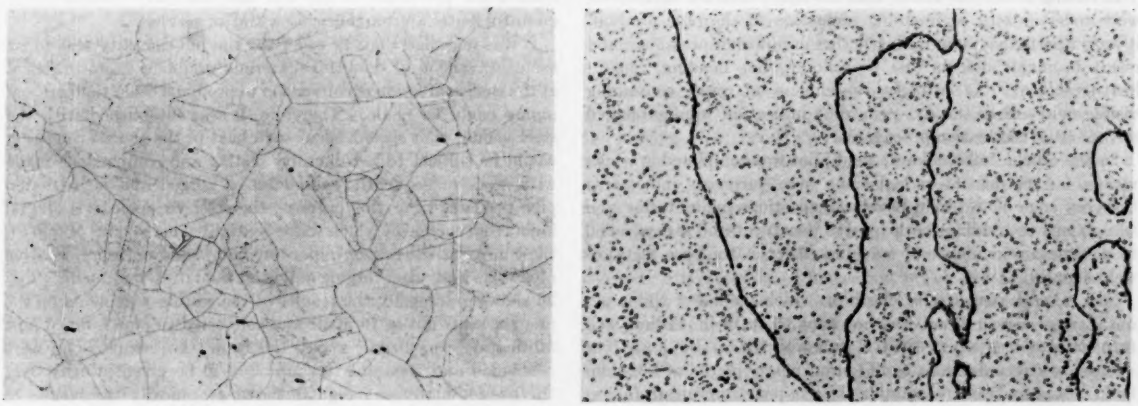

(a) Type-316 pipe metal, 100X, aqua regia etch

(b) Type-316 weld metal, 500X, chromic acid etch

Fig. 18 Microstructure, rupture test specimen, 1950 F air cool, aged 1000 hr at 1300 F; tested 17,000 psi, 9114 hours at 1200 F

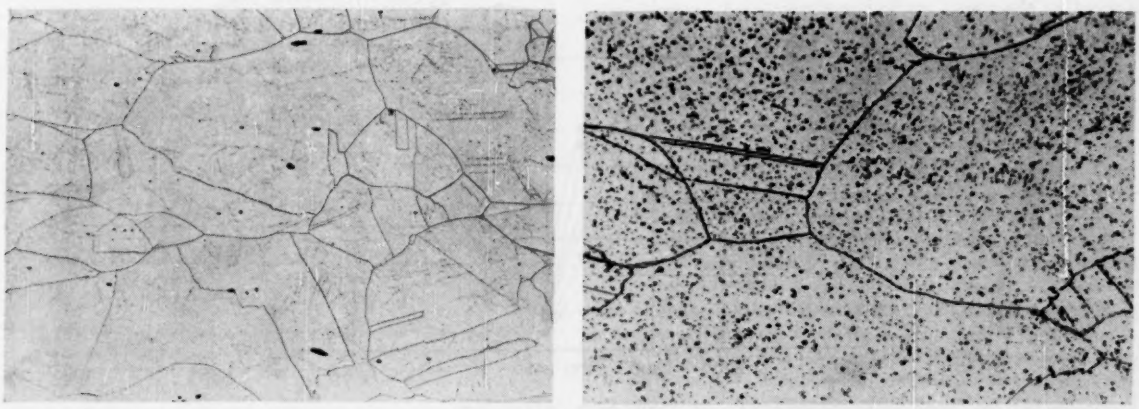

(a) Type-316 pipe metal, 100X, aqua regia etch

(b) B & W 16-8-2 weld metal, 500X, chromic acid etch

Fig. 19 Microstructure, rupture test specimen, 1950 F air cool, aged 1000 hour at 1300 F; tested 18,000 psi, 4829 hours at 1200 F

establish their cause and their possible effect on both fabrication and service, sections of pipe as well as whole pipes were thoroughly explored by various means.

Microscopic examination of suitably prepared specimens proved that the dye-penetrant indications were locations of small disconnected nonmetallic inclusions of undetermined composition. They appeared to be iron, chromium-oxide-type inclusions which are not uncommon in the austenitic stainless steels.

Whole pipe lengths were remachine-turned in several instances where the wall thickness was sufficiently heavy in order to remove all indications. A recheck of these lengths, however, disclosed the re-exposure of similar defects. This was considered added confirmation of nonmetallic inclusions dispersed throughout the thickness and not, therefore, single evidence of surface imperfections. Added confirmation was obtained by means of a machined step-down test made on a separate 12-in-long pipe section. This consisted of machine-turning eight different diameters in approximately $^1/_8$-in. increments thereby exposing successive depths below the surface at each step and, thence, dye-checking the exposed surfaces. Similar dye-penetrant indications were exposed at each location. In spite of these observations, during fabrication the machined weld bevels were dye-penetrant inspected and in no case were these defects found.

It having been determined that the dye-penetrant indications were reflections of nonmetallic inclusions in the pipe product, it was important to determine whether or not their presence could result in major defects due to welding, hot bending, and/or heat-treatment. Accordingly, specimens of pipe containing visible evidence of the dye-penetrant indication were subjected to the actual fabrication procedures.

In one case, a full-thickness weld joint was completed in which visible surface defects or inclusions were purposely indexed at the very edge of the weld bevel. Inspections made during and subsequent to welding, both by dye penetrant and x-ray, failed to disclose any evidence of cracking either in the base metal or weld deposit.

In a second case, a pipe length on which several of the larger indications were indexed was hot bent (5 ft 10 in. radius) and furnace heat-treated at 1950 F, followed by air cooling. The dye-penetrant indications had been purposely placed at the outer bend radius, and were re-examined by dye-penetrant means following both bending and heat-treatment. Certain of the defects which were present initially were not finally present. Those which finally existed were smaller. It was clear that necessary repolishing for the inspections which were made, and scaling from heat-treatment either eliminated or reduced the size of the imperfections. No surface cracking of any character was observed in the bend areas either in the indexed locations or otherwise. Therefore, it was proper to conclude on the basis of this examination, as well as the others cited, that the inclusion-type defects would not adversely affect the pipe either for fabrication or for the intended service.

Hot-Ductility Tests. From the viewpoint of fabrication (welding) and service of the Type-316 pipe composition, the hot-ductility tests of the RPI type, which were completed on pipe specimens representing each melt of steel, probably were the most instructive. It was pointed out earlier that the data derived from this type of testing had been useful in studies of the problem of cracking experienced at weld joints in the Type-347 pipe composition used in electric-generation service. Particularly, it has been possible to categorize certain materials which proved to be crack sensitive either in welding, heat-treatment, and/or service, notwithstanding that the research to date has not resolved the metallurgical phenomenon involved which would explain this behavior.

Objectively, therefore, the RPI hot-ductility tests were employed in the evaluation of the Eddystone piping with the view toward the perfection of the test and the early elimination of doubtful material from fabrication and/or service.

It was reasoned that, in order for the hot-ductility test to be useful, diversion of doubtful materials would be more practical at the steel source where conversion to products other than critical piping could be made. Therefore, it was established with the steel vendor that specimens of each heat in the as-cast condition would be subject to hot-ductility testing and comparisons made with tests subsequently completed on forged and heat-treated pipe product. For this purpose, the steel vendor cast a special ingot from each heat which was essentially 6 in. × 6 in. × 200 lb; the comparative tests on pipe were completed on representative pipe rings both after forging and after final heat-treatment. Fig. 20 shows graphically the results of the testing completed on the first six heats out of 19 made and converted to pipe. Since pipe fabrication was begun about this time the comparisons were concluded and tests only on pipe had to be given priority over the as-cast material. Fig. 21 shows graphically the results of all of the tests completed on the entire pipe product.

The graphs of the data are typically those which result in the RPI type of hot-ductility testing of austenitic stainless steels

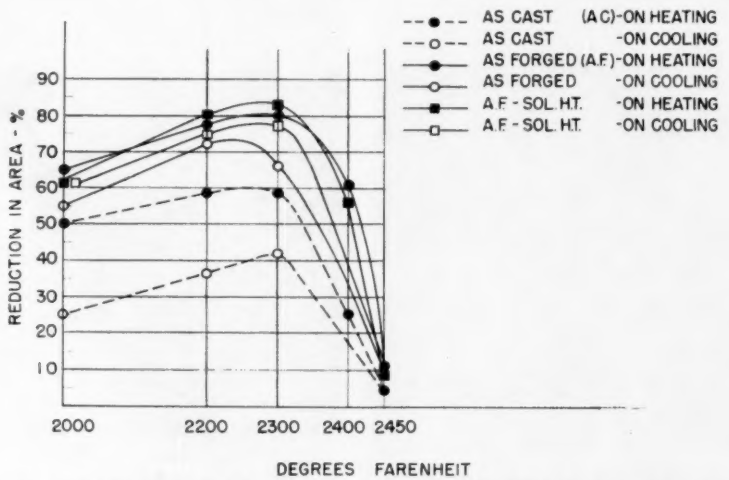

Fig. 20 Hot-ductility test results. A comparison of cast-ingot product with forged and heat-treated pipe product, Type-316 stainless steel.

The test essentially is a tension-testing procedure wherein the specimens can be heated to a temperature level and cooled therefrom under electrically controlled conditions and at rates in each case simulating the thermal history of the base-metal heat-affected zone in a weld joint. The specimens can be broken in tension at any level or combination of desired temperatures. Customarily, specimens of any one material are broken at various temperature levels on heating and compared with data at equal levels on cooling after having been heated to a predetermined terminal temperature. For the tests described, the terminal temperature was 2450 F; temperature levels on heating and cooling were as shown, 1800, 2000, 2200, 2300. Observed data include ultimate strength, per cent elongation, and per cent reduction in cross-sectional areas. The latter, or per cent reduction in area, has proved to be the critical variable in the evaluation of materials.

The assessment is based on the recovery in ductility evidenced by the comparison of the values observed in tests broken on heating and cooling, only the latter of which has been prior exposed to the terminal temperature. It is reasoned that a material unaffected by the high terminal temperature should show complete or nearly complete recovery in ductility on cooling. If it is otherwise, it is considered evidence that the material is subject to embrittlement and, therefore, may prove to be crack sensitive and a liability in welding. Accordingly, the range of the differences observed in the on-heating and on-cooling data is the criteria—in particular, the data for the 2300 and 2200-F levels.

On the basis of the data in Fig. 20, which show the comparison of as-cast data with the pipe product, all conditions show evidence of what is considered to be better than average recovery and no evidence of embrittlement. The significant factor in this comparison is the notable improvement wrought by the forging and, to a certain extent, the final heat-treatment, over the as-cast properties. It seems clear from this that it may, indeed, be possible with further study to perfect this or a similar test for use on as-cast materials preliminary to further conversion into a forged product and, thereby, cull out materials which might prove to be a fabrication or service liability. An equally important factor displayed by these particular tests is the marked evidence of improvement in this property as the result of forging and heat-treatment. This suggests that the thermal history of a product as the result of forging and heat-treatment may have a profound effect on certain of the physical properties of these materials—in particular on its response to the effects of welding. In this regard, an activity with which the authors are connected, namely, the ASME Steam Power Panel, currently has this problem under study at the University of Michigan. The research is directed toward resolving the question of cracking experienced in the Type-347 composition.

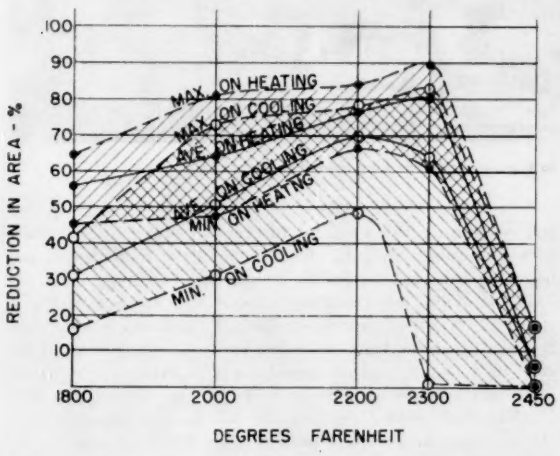

Fig. 21 Hot-ductility test results. Summary of tests completed on pipe product Type-316 stainless steel.

Relative to the hot-ductility tests on the forged and heat-treated pipe product used in Eddystone, Fig. 21, with the single exception of the influence of one heat, or the low value shown for the on-cooling curve at 2300 F, all pipe material was considered highly satisfactory. Indeed, all shop and field welds were completed without any single evidence of cracking either in the base metal, weld heat-affected zone, or in the weld deposit. The pipe product from the one heat about which there might have been some question, based on the hot-ductility data, also was welded without any evidence of crack defects. It should be emphasized that the test results do not necessarily portend failure in those certain cases where low values are experienced. Conversely, they may serve as a guide to the performance of high-quality welds—the circumstance in this case.

Fabrication of Main Steam Piping

As indicated in the foregoing sections, the piping material selected for the main steam system was Type-316 stainless steel (17 Cr-13 Ni-2.5 Mo) and the welding filler wire and electrode was The Babcock & Wilcox 16-8-2 composition (16 Cr-8 Ni-2 Mo).

For this system, 56 assemblies were fabricated in the shop and shipped to the job site for erection. The assemblies required the making of 61 bends and offsets, 92 butt welds of which 61 were postweld-heat-treated by the induction-heating method and 31 were heat-treated in furnaces. In addition, 76 welds were made and induction heat-treated during erection at the job site.

In the fabrication of main steam systems, the principal operations are pipe bending, welding, postweld heat-treating, and nondestructive testing or inspecting. The procedures used for fabricating other stainless-steel main steam systems and which were basically used for this system have been previously described in detail. Diehl and his co-workers [12] have presented the details of welding with the inert-gas tungsten-arc process in conjunction with pressure-controlled inert-gas backup for producing root beads having controlled internal contour. Benz and Caughey [13] have described procedures for bending, welding, heat-treating, and inspecting new main steam systems. Hence only the special techniques which have been developed in the shop to fabricate this special heavy-wall stainless-steel pipe to the highest practicable quality will be described.

Pipe Bending. All 61 bends and offsets were made by heating the section of pipe to be bent to 1900–2000 F and by bending on a table while the pipe was cooling within the range of 2000–1400 F. Ordinarily, to prevent buckling or ovalling, the pipe is packed with sand. In this case, the relation of pipe diameter to wall thickness was such that sand filling was not required. While all of the piping which was to be hot bent was ordered with approximately $^1/_8$ extra thickness on the wall to allow for thinning due to deformation and scaling, the thinning due to the latter was minimized by maintaining an inert-atmosphere inside the pipe during the heating and cooling of the bending cycle. Specifically, the ends of each length of pipe were sealed with plates, one of which contained an inlet for argon gas, Fig. 22, and the other holes for venting. During the time the pipe was heating, air was purged from the inside by an argon flow of 20 to 30 cu ft per hr. After the pipe was purged, the flow was reduced to 5–10 cu ft per hr. In this manner, the inside of each pipe was kept scale-free. (The less expensive nitrogen gas was considered for this operation; however, consideration of the remotest possibility of nitriding or the absorbing of nitrogen by the stainless piping ruled this out.)

Fig. 22 Pipe assembly on bending table showing end plate containing argon inlet

Fig. 23 Pipe assembly being lifted from heat furnace to bending table showing heated portion to be bent

Fig. 23 shows a length of pipe with the section to be bent furnace heated to 1900–2000 F and being lifted from the furnace to the bending table.

Upon completion of the bending operation and after the pipe had cooled, the entire bend area was sand-blasted to remove scale. The bend area was liquid-penetrant and ultrasonically inspected. In no case was a defective pipe section found.

Welding of Main Steam Piping. All butt joints were made with the K-weld process for the root pass (weld bead 1 in Figs. 24 and 25), inert-gas tungsten-arc process for the "undercut-preventing" beads, and the manual metal-arc process for the remainder of the welding and using the special 16 Cr-8 Ni-2 Mo filler wire and covered electrode which had been developed by The Babcock & Wilcox Company. Fig. 26 shows the K-weld root pass between header and three of the stub ends.

The K-weld process mentioned above and described by Diehl, et al. [12], was used to facilitate the making of complete-penetration root welds having a controlled internal contour without the need for backing rings or special inserts. Briefly, K-welds are made in U-grooves with the land of each level abutting. With the joint tack-welded together, the first pass is deposited with the inert-gas tungsten-arc process using a bare $^1/_{16}$ or $^3/_{32}$-in-diam filler wire, in this case, of 16-8-2 composition. Prior to and during welding, a section of the bore of the pipe with the butt-

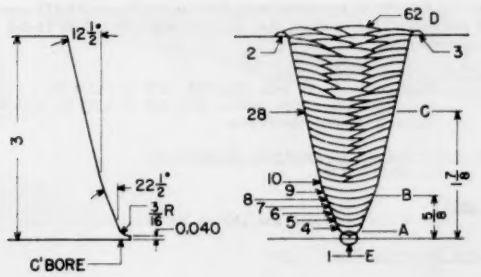

FIXED-HORIZONTAL

BEAD NO.	WELDING PROCESS	FILLET WIRE OR ELECTRODE		CURRENT AMPERES	ARC VOLTS
		TYPE	DIA. IN.		
1, 2, 3	TIG	16-8-2	1/16	85	–
4, 5	METAL-ARC	B&W 16-8-2	3/32	60-70	22-23
6-10	"	"	1/8	85-90	"
11-28	"	"	5/32	110-130	"
29-62	"	"	3/16	130-150	"

NOTE: A VISUALLY INSPECT ROOT PASS OUTSIDE AND WHERE PRACTICAL INSIDE.

B,C,D RADIOGRAPH AND LIQUID PENETRANT INSPECT AT THESE LEVELS.

E ROOT PASS DEPOSITED WITH INERT-GAS BACK UP (K-WELD).

Fig. 24 End preparation, welding technique, and inspection sequence for Type-316 (17 Cr, 13 Ni, 2.5 Mo) piping

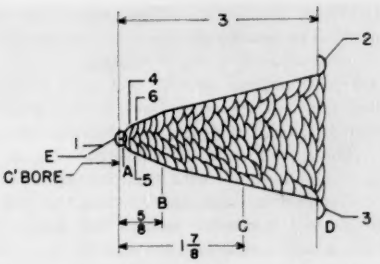

FIXED-VERTICAL

BEAD NO. OR WELD DEPTH	WELDING PROCESS	FILLET WIRE OR ELECTRODE		CURRENT AMPERES	ARC VOLTS
		TYPE	DIA. IN.		
1, 2, 3	TIG	16-8-2	1/16	85	-
4, 5, 6	METAL-ARC	B&W 16-8-2	3/32	60-70	22-23
7-5/8 WELD	"	"	1/8	80-90	"
5/8-1 7/8	"	"	5/32	110-130	"
1 7/8-3	"	"	3/16	130-140	"
COVER LAYER	"	"	5/32	110-130	"

NOTE: A VISUALLY INSPECT ROOT PASS OUTSIDE AND WHERE PRACTICAL INSIDE.

B,C,D RADIOGRAPH AND LIQUID PENETRANT INSPECT AT THESE LEVELS.

E ROOT PASS DEPOSITED WITH INERT GAS BACK UP (K-WELD).

Fig. 25 Welding technique and inspection sequence for fixed-vertical welding of Type-316 (17 Cr, 13 Ni, 2.5 Mo) piping

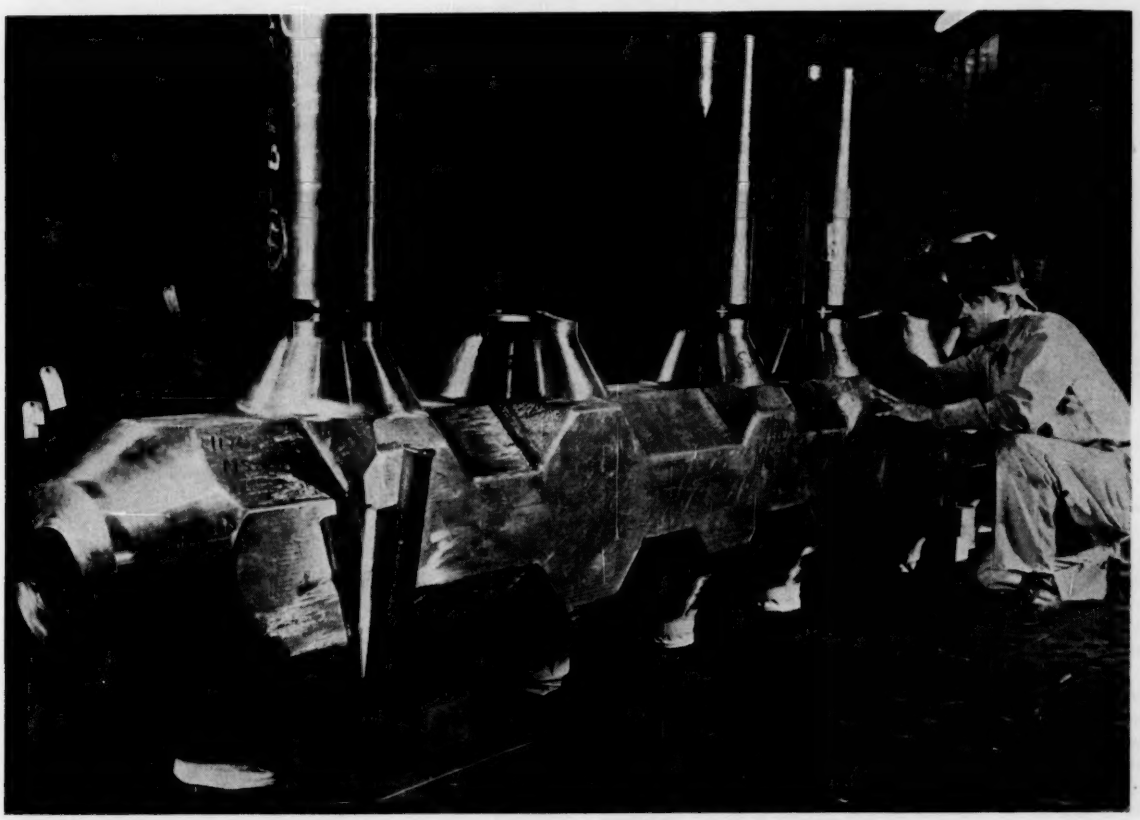

Fig. 26 K-weld root pass between header and three stub ends

joint in the middle is filled with inert-gas (argon), the pressure of which is controlled to contour the inner side of the root pass and to protect the molten metal during deposition.

The "undercut-preventing" beads (at 2 and 3 in Figs. 24 and 25) are deposited with the inert-gas tungsten-arc process on the outside surface of the pipe adjacent to the machined edge of the weld bevel. These two beads are deposited using the inert-gas tungsten-arc process because, with this process, a narrow weld bead can be deposited without undercutting the surface of the pipe. Since covered electrodes used in the manual metal-arc process have a greater propensity for undercutting, particularly during deposition of the cover layer, welding into either bead 2 or 3 which has already been deposited provides a place for the undercutting to take place above the surface of the pipe. Later, on dressing the weld by grinding and polishing for liquid-penetrant and radiographic inspections, the undercut which occurs can be removed by grinding away part of beads 2 and 3 without grinding into the pipe surface, *per se*. (Hence, the undercut-preventing name.)

The remainder of the butt weld was completed by the manual metal-arc process using $^{3}/_{32}$ to $^{5}/_{32}$-in-diam covered electrode.

The fixed-horizontal and fixed-vertical welding procedures shown in Figs. 24 and 25 have been qualified in accordance with the requirements of Section IX of The American Society of Mechanical Engineers, Boiler and Pressure Vessel Code, 1956 Edition. The range of chemical composition of weld metal deposited in a pad from the B & W 16-8-2 electrode is:

Chemical composition range, per cent

C	Mn	Si	Ni
0.07–0.09	1.87–2.16	0.21–0.44	8.06–8.37
	Cr	Mo	
	15.91–16.28	1.73–1.90	

The results of tests conducted for procedure qualification are shown in Table 11. The welding procedures have been qualified both with and without postwelding heat-treat because, at the time of qualification, decision had not been made to heat-treat field welds.

Table 11 Results of procedure qualification for Type-316 (17 per cent Cr-13 per cent Ni-2.5 per cent Mo) pipe welded with B & W 16-8-2 filler wire and electrode

Material:
Eight-inch x 1.5" wall Type 316 (17% Cr - 13% Ni - 2.5% Mo) stainless steel pipe welded with 16% Cr - 8% Ni - 2% Mo filler wire and electrodes.

Radiography and Liquid Penetrant Inspections:
All satisfactory.

Preheat:
60° F for K-welding and 150° F for metal arc welding.

Maximum Interpass Temperature:
300° F

Mechanical Test Results:

Welder	Welder Symbol	Welding Position	Side Bend Tests	Transverse Tensile Tests X 1000 psi
		No Postweld Heat Treat		
Kessner	BS	2G	4-OK	85.0 84.9
Kessner	BS	5G	4-OK	84.2 83.5
		1900-1950 F Postweld Heat Treat		
Kessner	BS	2G	4-OK	81.4 81.5
Kessner	BS	5G	4-OK	82.0 80.7

During the course of welding, the inspections listed in the note in Figs. 24 and 25 were made. After completion of the root pass, it was visually examined for uniformity of weld contour and liquid-penetrant-inspected for cracks. Upon completion of the first $^{5}/_{8}$ in. of weld, the surface was ground and liquid-

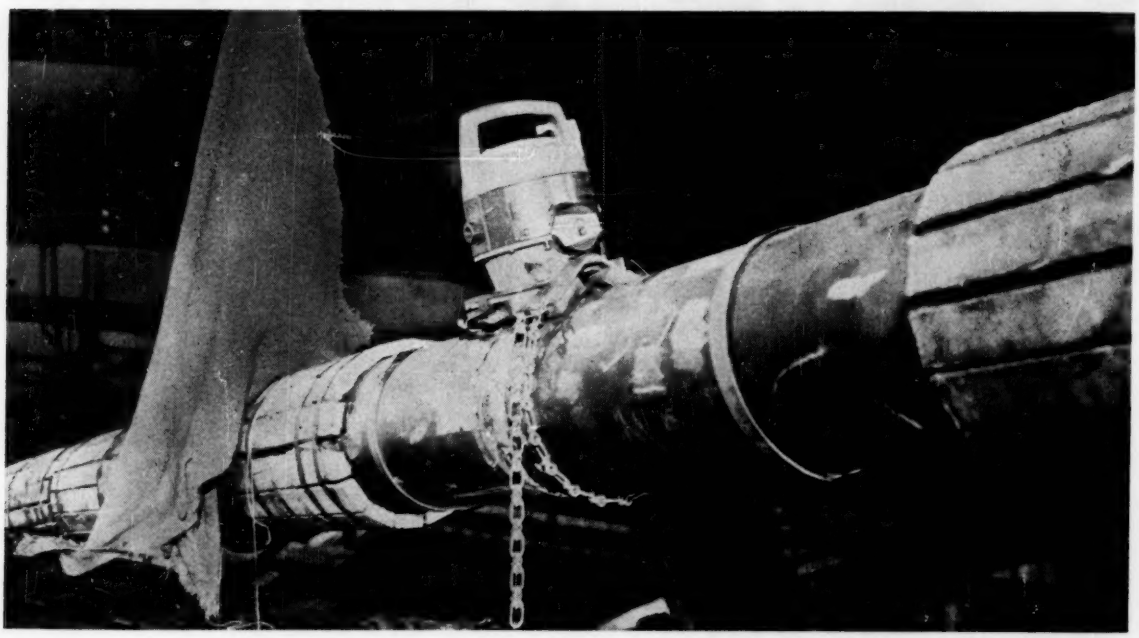

Fig. 27 Iridium-isotope camera in place for radiographing root portion of field weld

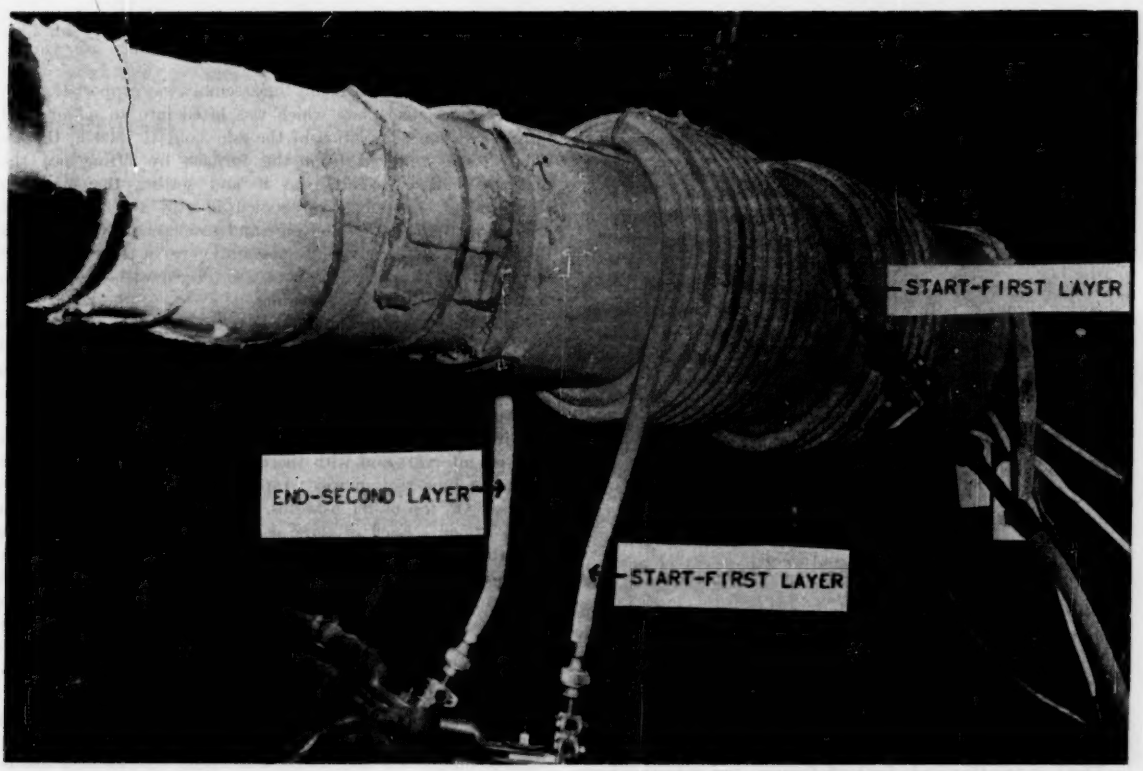

Fig. 28 Arrangement of induction-heating coils for postweld heat-treatment

penetrant-tested and then radiographed. If defects were revealed, repairs were made and the weld was reinspected. The same procedure was used at the $^{7}/_{8}$-in. level and upon completion of the weld. When the weld was radiographically acceptable, it was heat-treated by induction means or in a furnace. After heat-treatment, the weld and a 2-in-wide band on each side were polished, liquid-penetrant-inspected, and radiographed.

The arbitrary standard for liquid-penetrant inspection required the removal of all defects except obvious pinholes approximately $^{1}/_{32}$ in. in diameter. In the several inspections applied to each weld joint during the course of and on completion of welding, no cracking was observed at any time.

The radiographic standard which was established for this job was that listed in Paragraph UW-51 of Section VIII of the ASME Unfired Pressure Vessel Code, 1956, except that less than half the slag permitted in UW-51 was acceptable for satisfactory welds in this system. The standards of acceptable porosity shown in Section VIII were not satisfactory for this job; however, because of the virtual lack of porosity encountered in the welds, interpretation was no problem.

While no cracking was revealed by both the liquid-penetrant and radiographic inspections, at the outset some difficulty was encountered with trapped slag. The slag became entrapped in slight undercutting of the steep side wall or between adjacent beads in a split-weave layer. The welders from past experience with stainless steels had expected to "burn" this out during deposition of the next succeeding layer. However, the molten weld metal behaved more sluggishly and apparently penetrated less than other stainless steels such as Types 308 and 347. The institution of the shop requirement that all weld beads and layers must be ground smooth and all undercutting eliminated markedly diminished the incidence of trapped slag. A welding engineer

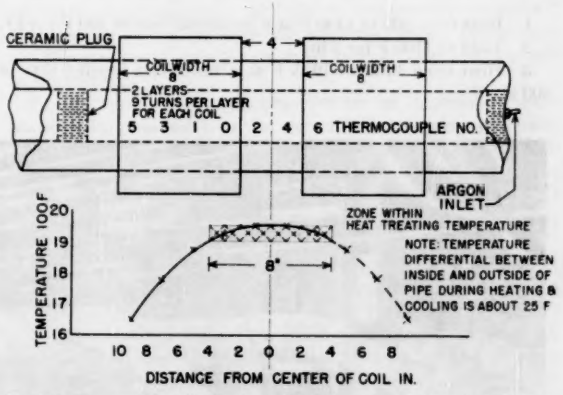
CERAMIC PLUG
4
COIL WIDTH 8"
COIL WIDTH 8"
2 LAYERS 9 TURNS PER LAYER FOR EACH COIL
5 3 1 0 2 4 6 THERMOCOUPLE NO.
ARGON INLET
ZONE WITHIN HEAT TREATING TEMPERATURE
NOTE: TEMPERATURE DIFFERENTIAL BETWEEN INSIDE AND OUTSIDE OF PIPE DURING HEATING & COOLING IS ABOUT 25 F
8"
TEMPERATURE 100F
20
19
18
17
16
10 8 6 4 2 0 2 4 6 8
DISTANCE FROM CENTER OF COIL IN.

Fig. 29 Temperature distribution—60-cycle induction heating of Type-316 stainless-steel pipe 10.8 in. OD × 2.6 in. wall

working with the welders evolved a technique which virtually eliminated undercutting of the side wall and required less grinding. (This permitted four welders whose shop instruction in the K-welding technique included the benefit of shop experience with the trapped slag to complete 76 joints on the job site with only one minor repair.)

Radiography. The radiographic inspections specified at the levels B, C, and D in Figs. 24 and 25 were affected in the shop using radium and a specially prepared high-activity cobalt-60 source. At level B ($^{5}/_{8}$ in. weld thickness) a panoramic exposure was made with the film on the outside of the pipe and with a 25-milligram source of radium located centrally in the bore of the pipe. At level C ($1^{7}/_{8}$ in.) a similar panoramic exposure was made

with a 50-milligram source of radium. The completed weld both before and after heat-treatment was inspected using a 645-millicurie cobalt-60 source. For this inspection, the source was located inside the pipe against the inner wall with the film opposite and on the outside so that slightly more than 120 deg of the weld was exposed. Three exposures were required to examine the entire weld. In all cases, previous evaluations of the techniques used indicated that the true sensitivity was 2 per cent or better. Since there were no radiographic access openings in the system, all of these welds were examined by locating the radiation source inside the pipe from an open end.

In the field, partial and complete welds were radiographed by "shooting through" both walls of the pipe. Two special isotope cameras, one containing 10 curies of iridium 192 and one containing 10 curies of cobalt 60, were used. The camera was mounted on the pipe such that the source was 1 in. from the outer surface of the pipe with the film cassette mounted on the opposite outer surface. For Level B ($^5/_8$ in. weld thickness) five overlapping exposures were required using iridium 192. For Levels C and D, six exposures were required using the cobalt-60 source. Fig. 27 shows the camera containing the iridium source in place.

As with the shop-inspection technique, the field technique was developed and evaluated prior to use in the field. The sensitivity of inspection was evaluated at 2 per cent of one wall thickness or better.

Postweld-Heat-Treatment. Shop butt welds in assemblies containing bends were heat-treated by placing the entire assembly in a furnace so that both bend and weld would benefit from the heat-treatment. Those shop welds joining straight lengths to heat-treated bend-assemblies were heat-treated individually by electrical induction means applied locally. All field butt welds were heat-treated by the latter method.

The heat-treating cycle for both furnace and induction heats established from previous investigations [13, 14, 15] and recommended by the metallurgical department is as follows:

1 Heat from 600 to 1100 F at a maximum rate of 300 F per hr.
2 Hold at 1100 F for 2 hr.
3 Heat from 1100 to 1925 F at a maximum heating rate of 600 F.
4 Hold within the temperature range 1900 to 1950 F for 2 hr.
5 Air cool.

For furnace heat-treatment, the assembly was supported on refractory on a steel plate which was lifted into an oil-air fired furnace. Upon completion of the 2-hr hold at 1900 F, the assembly was removed from the furnace by lifting out the plate with the assembly on it and setting the plate on stools. The assembly then cooled in still air. To prevent scaling on the inside of the pipe and to eliminate the need for its removal, all the time the assembly was in the furnace and cooling down to 600 F, the bore was purged with argon gas in the same manner as during bending.

Since the electrical induction heat-treatment of such a relatively small diameter, thick-walled stainless-steel butt-joint had not been attempted before, an investigation was undertaken to establish the heat distribution across a weld joint and the temperature differential between the inside and outside surfaces.

With thermocouples mounted on the outside of the pipe at 2-in. intervals and with thermocouples on the inside of the pipe, the pipe section was wrapped with a $^3/_4$-in. layer of asbestos. On top of the asbestos, two flexible water-cooled coils were formed. Each of these comprised two layers containing nine turns each as shown in Figs. 28 and 29. The distance between the two coils was 4 in. Each coil was connected to a separate water supply and to a separate induction unit. The power was supplied and controlled by two Smith-Dolan 60-cps, single-phase, 75-kva units. The results of temperature surveys show that an 8-in. width was heated within the range of 1900 to 1950 F and the temperature differential between inside and outside walls was 25 deg F, Fig. 29. During heating and cooling the inside of the pipe was purged with argon to prevent scaling. This technique was used for those welds not furnace heat-treated in the shop and for all field welds. (In the field the power was supplied by a combination of four 40-kva units, two connected in series to each coil.)

Upon completion of final inspection, wood covers were placed over the field-weld end preparation and held in place and protected by thick steel clamps. For further protection against damage during shipment and erection, each assembly was en-

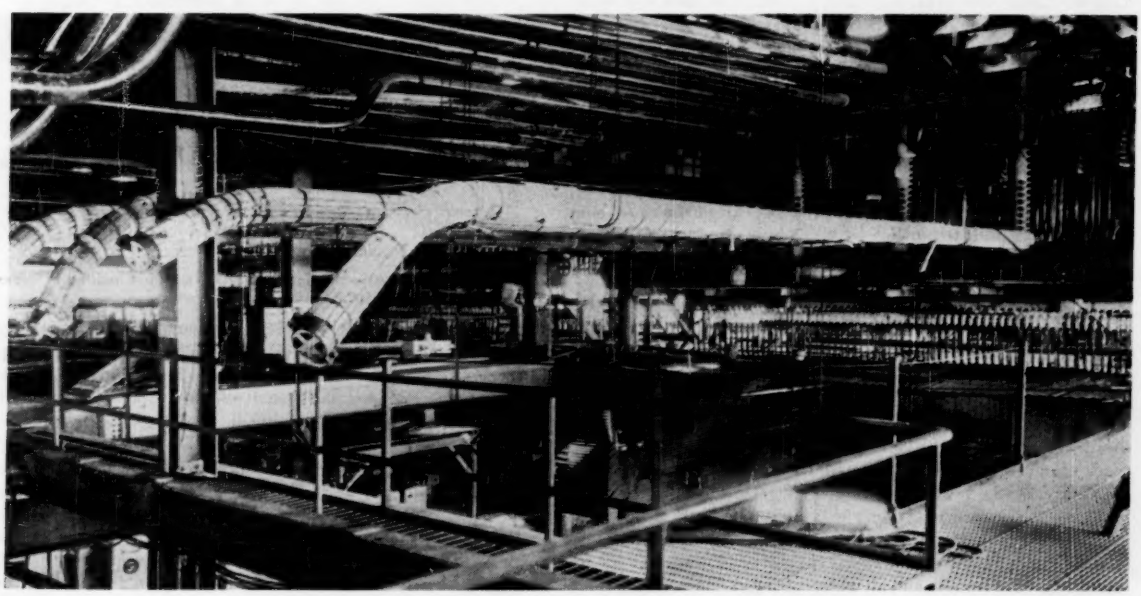

Fig. 30 Piping assembly in place showing protective wood lagging

cased in a thick wood-lath covering which remained in place throughout installation, Fig. 30. This lagging was not removed until the assembly was insulated.

Acknowledgment

The authors are indebted to the Philadelphia Electric Company for permission to publish this paper. They are especially appreciative of the guidance and co-operation of Mr. J. H. Harlow, Chief Mechanical Engineer of the Philadelphia Electric Company, and the Members of the Eddystone Metallurgical Committee. It is with deep respect that they acknowledge the untimely passing of Mr. G. E. Klapper and his contribution as chairman of this committee for Philadelphia Electric Company.

The contributions of the authors' colleagues at The M. W. Kellogg Company is acknowledged, in particular those of Mr. C. Diehl for the supervision of all welding, and Mr. H. E. Richards for capable assistance in the performance of the metallurgical program.

References

1 H. S. Blumberg, "Metallurgical Considerations of Main Steam Piping for High-Temperature, High-Pressure Service," TRANS. ASME, vol. 79, 1957, pp. 1377–1397.

2 O. R. Carpenter and R. D. Wylie, "Weldability of Chromium-Nickel-Moly Stainless Steels," Report No. 395, The Babcock & Wilcox Company.

3 F. P. Fairchild, "Eight Years of Experience With Austenitic Steel Piping Materials at Elevated Steam Conditions," TRANS. ASME, vol. 79, 1957, pp. 1371–1376.

4 R. M. Curran and A. W. Rankin, "Austenitic Steels in High Temperature Steam Piping," TRANS. ASME, vol. 79, 1957, p. 1398.

5 E. F. Nippes, W. F. Savage, et al., "An Investigation of the Hot Ductility of High Temperature Alloys," *Welding Journal*, Welding Research Supplement, vol. 34, April, 1955, pp. 183s–196s.

6 E. F. Nippes, W. F. Savage, and G. Grotke, "Further Studies of the Hot Ductility of High Temperature Alloys," Research Division, Rensselaer Polytechnic Institute, June, 1956.

7 H. M. Soldan and C. R. Mayne, "Role of Hot Ductility as Related to Service Performance of Heavy Wall Austenitic Steel Pipe Welds," presented at Sixth Annual Meeting, AEC Welding Committee, September, 1956.

8 R. J. Christoffel, "Elevated Temperature Properties of Welded Joints in Type 347 and Type 316," General Electric Materials and Process Laboratory Report DF59SL507, May 27, 1959.

9 W. F. Simmons and H. C. Cross, "Report on the Elevated Temperature Properties of Stainless Steels," ASTM Special Technical Publication No. 124.

10 "The Elevated Temperature Properties of Weld Deposited Metal and Weldments," ASTM Special Technical Publication No. 226.

11 O. R. Carpenter and N. C. Jessen, "Some Factors Controlling the Ductility of 25% Cr 20% Ni Weld Deposits," *Welding Journal*, vol. 26, no. 12, Research Supplement 727S–720S, 1947.

12 C. Diehl, H. S. Blumberg, and W. G. Benz, Jr., "Controlled Internal-Contour Shielded-Root Welds Without Backing Rings," TRANS. ASME, vol. 75, 1953, pp. 1103–1115.

13 W. G. Benz and R. H. Caughey, "Fabrication of Austenitic Stainless Steam Piping for Operation at 1100 F," ASME Paper No. 53—SA-58.

14 R. M. Curran and A. W. Rankin, "Welding Type 347 Stainless Steel for 1100 F Turbine Operation," *Welding Journal*, vol. 34, 1955, pp. 205–213.

15 R. M. Curran and A. W. Rankin, "Preventing Weld Cracks in 1100 F Stainless Piping," *Heating, Piping, and Air Conditioning*, vol. 27, 1955, pp. 116–119.

DISCUSSION

Harry S. Blumberg[2]

The authors are to be complimented on a well-written paper, which summarizes a wealth of experimental data. Together with a preceding paper on this subject (Reference [1] in their bibliography), there is disclosed the background of the problem and the results to date of five years of an extensive, continuous metallurgical investigation by the piping fabricator in an effort to fill certain gaps in knowledge. Such background is required for the sound, practical selection of materials, their properties, and their satisfactory behavior in service, which culminates in the recognition of important requirements for specifications. The data presented extend knowledge in this field to a considerable degree. The paper furnishes much added assurance regarding the original selection four years ago of the Type-316 composition for main steam piping at Eddystone No. 1 Unit. Further, it will provide a deeper technical basis for materials selection for newly contemplated units than was available when the Eddystone Unit was first engineered. The Utilities Industry will welcome the publication and application of these findings.

These authors have summarized their findings excellently. A full treatment of the subject would require textbook handling, with descriptions of details of test techniques, their general significance, and specific interpretation as related to Eddystone No. 1 Unit. Such treatment, although of value to some, would have been too detailed for engineering application. Accordingly the summary method employed by the authors is well suited for the needs of utility engineers. The conclusions drawn are direct and it is reassuring to learn that the program results show that after long exposure at the accelerating test temperature of 1300 F, Type-316 base metal joints welded with 16-8-2 electrode possess satisfactory high temperature strength, ductility, hardness, and stability, as well as metallurgical structure.

The direct comments which I offer are as follows:

1 The authors did not report on the surface condition of the test pieces exposed for 1000 and 10,000 hours at 1300 F, which is considered equivalent to a time acceleration factor of about 15 times beyond that at 1200 F. There are still those in the metallurgical engineering field who are concerned with the possibility of surface deterioration in the form of "catastrophic oxidation" of molybdenum bearing austenitic stainless steels. The authors are in a position to state the results of their findings and thus add to experience.

2 The rupture test data reported are an important contribution. Information is given for 1000-hour-aged specimens. These data and those for specimens aged 10,000 hours at 1300 F (considered equivalent to about 150,000 hours at 1200 F) are of value in assessing the high temperature strength of the welded joints in the program. This information will furnish added bases for the Subcommittee on Allowable Stresses.

3 It would be interesting if the authors would advise what part of their program is still to be completed and whether these findings will soon be available.

4 The paper emphasizes the many planned precautions which were exercised during three of the four main phases of "The Useful Cycle of Steam Piping Materials," which this discusser summarized in Table 1, Reference [1] of the bibliography. These three phases are steel manufacture, conversion to piping, and fabrication. The eleven summary points in the Caughey-Benz paper crystallize the care taken in materials procurement and show the extensive quality controls utilized, which extend considerably beyond the requirements of conventional ASTM Specifications. These procedures have undoubtedly played an important part in the procurement of material which has behaved so satisfactorily in fabrication, as reported. The procedures described will undoubtedly be used in the future in specifications for materials to be used in high temperature high pressure units.

5 The practical value of the paper is enhanced by the description of the fabrication procedure.

[2] Consulting Metallurgist, New York, N. Y. Mem. ASME.

A. B. Wilder[3]

The authors have emphasized the importance of the proper selection of material and their fabrication for high pressure steam service. In selecting AISI Type-316 austenitic stainless steel they have chosen material which has been used for a number of years both in chemical processing and petroleum refining industries. Comments by the authors regarding the following items will be appreciated.

1 What metallurgical factors were responsible for the superior properties of 16-8-2 weld metal in comparison with AISI Types-316 and 347 weld metal?

2 What effect has grain size of AISI Type-316 steel in the cast and forged conditions on the results obtained with the RPI hot ductility test?

3 The completed welds were treated at 1950 F. What is the nature and significance of the transition zone in the piping material due to this localized heat-treatment?

Authors' Closure

The authors appreciate very much the comments of both Mr. H. S. Blumberg and Mr. A. B. Wilder and the opportunity to reply to the interesting and significant questions which they have posed.

On the question of the resulting surface condition of the specimens which were subjected to 1000 and 10,000 hours at 1300 F in the air atmosphere of the laboratory furnaces, no evidence of excessive or "catastrophic oxidation" was observed. The thickness of the scale formation was not specifically measured. It was a uniform, tightly adherent scale. It was noted not to be abnormally heavy in any case.

Still to be reported are the results of the stress rupture tests on those specimens of Type 347 and 316 which previously were subjected to the 10,000-hour aging treatment. These will be made available as soon as they are completed. In addition to this, it should be noted here that the test program is being continued to include similar tests on three additional alloy steel compositions, namely: Babcock & Wilcox 15-15N, Armco 17-14 Cu/Mo, and Jessop Gl8B. It may be expected that this work will be made the subject of an additional paper.

[3] Chief Metallurgist, National Tube Division, United States Steel Corporation, Pittsburgh, Pa.

It is believed that the metallurgical factor responsible for the superior properties of the 16-8-2 weld metal, compared with the Type 316 and Type 347, is its chemical-physical stability when subjected to long-time aging at elevated temperature both with and without stress. The higher ductility values of the 16-8-2 and the lack of evidence for any marked embrittlement are the significant features of this material.

The separate effect of grain size in the RPI hot ductility experiments which compared the as-cast and forged properties of the Type-316 composition was not made a part of this investigation. Although it would be possible to distinguish the as-cast from the forged material on the basis of grain size comparing only ASTM numbers, the forged material being slightly finer, it is doubtful that this effect alone was responsible for the improved ductility observed. It is certain that the additional and proved effects of hot forging or the improvement in the chemical and physical homogeneity of the metal were equally important.

On the question of the nature and significance of the transition zone in the austenitic stainless steel weld joint due to the localized induction heat-treatment at 1950 F, it should be emphasized that this practice is used only where it is not possible, due to available shop furnace size, to heat-treat the welded pipe assembly as a unit and in the field on field-made butt welds.

A study was not made to determine the exact nature or physical structure existing in the transition zone of the Type-316 fabricated pipe assemblies represented in this program. Past experience, however, on Type-347 piping similarly heat-treated has shown it to be made up of the austenite matrix in which carbide precipitation in varying degrees and form has taken place. At the low temperature end of this zone, the typical "dot-like" intergranular carbides are evident, at the upper temperature levels certain coalescence of the carbides may be seen.

This has been a practice of long standing or since about 1953 on Type-347 piping. Accordingly, there are many weld joints which have been in continuous service at temperatures of 1050 and 1100 F which have been heat-treated in this manner in addition to those which were subjected to a complete furnace heat-treatment in the shop. No difficulty has been experienced in service from any of the welded joints heat-treated in either manner. It does not appear, therefore, that the transition zone resulting in the pipe from the localized heat-treatment has had any significant effect on the critical properties of the material in this particular service.

D. B. MACKAY
Research Specialist,
Advanced Systems.

E. L. LEVENTHAL
Senior Research
Engineer, Technical Staff.

Missile Division, North American
Aviation, Inc., Downey, Calif.

Solar Turbo Power Plant Design

This paper discusses the design of a lunar-based power plant powered entirely by solar radiation. Factors affecting power plant design and a discussion of a performance basis for a working fluid are also presented. Graphs and equations which illustrate theory, optimize results, and demonstrate inter-component relationships are included. Also, a design for a novel, compact power plant is introduced.

Introduction

It is this paper's purpose to discuss the design and performance characteristics of a lunar-based turbo power plant actuated entirely by solar radiation.

Power generated by chemical energy suffers an important drawback: The shaft power output available per pound of chemical propellant is limited because even the most efficient heat engine known requires about four pounds of propellant per kilowatt hour of shaft power. Power derived from a nuclear source has also been analyzed and evaluated (Reference [1]).[1] This mode of power supply has a distinct weight advantage over a chemical power plant for long term operation. However, a nuclear power plant has the following inherent disadvantages: production of a radiation environment, cost, and hazards associated with transport.

The obvious limitation of solar power on the lunar surface is the long shutdown period caused by the lunar night—14 earth days in duration. However, investigation of power needs has shown, for example, an important refrigeration requirement existent during the lunar day—offering an interesting match of power needs with solar power capability. Use of solar radiation for the generation of power is most attractive when power requirements are moderate.

The generation of power from solar radiation on the moon, as in space, is aided by the absence of an atmosphere. Solar radiation on the moon is estimated at 430 Btu/hr sq ft (Reference [2]), about one and one half times greater than radiation recorded on earth.

This paper proposes a method whereby this power can be converted into usable energy: A two-dimensional parabolic reflector that directs solar radiation into a boiler tube located at, or near, the focal point of the reflector. Through this means, high temperatures can be obtained in a working fluid.

Lunar Power Plant

Fig. 1 is a schematic representation of a compact lunar power plant. It will produce power in the following manner: the working fluid is evaporated in the vapor generator—consisting of mirror and boiler tubes—then introduced into the turbine at a controlled temperature and pressure T_1 and P_1. The vapor then

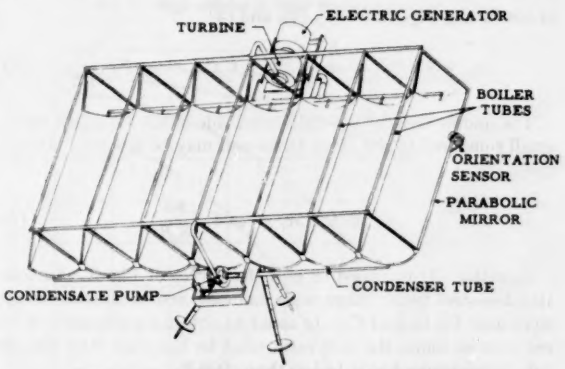

Fig. 1 Compact solar turbo power-plant schematic

[1] Numbers in brackets designate References at end of paper.

Contributed by the Solar Energy Applications Committee and presented at the Annual Meeting, Atlantic City, N. J., November 29–December 4, 1959, of The American Society of Mechanical Engineers.

Note: Statements and opinions advanced in papers are to be understood as individual expressions of their authors and not those of the Society. Manuscript received at ASME Headquarters, July 24, 1959. Paper No. 59—A-74.

Nomenclature

c_1 = plate properties constant defined by Equation (20)
c_2 = environment constant defined by Equation (21)
c_3 = integration constant Equation (25)
d = boiler tube outside diameter
f = fluid work factor, defined by Equations (7)
h_{fg_1} = latent heat of evaporation at temperature T_1
k = thermal conductivity of plate material
r_m = reflectivity of the environment's surface
A_e = effective radiator area defined by Equation (16)
A_r = actual radiator area (includes both sides)
B = width of one reflector
C = average specific heat of saturated liquid (working fluid)
C_f = geometric perfection factor of parabolic mirror
C_s = reflectivity of the mirror surface
F_a = radiation form factor for the boiler side facing the sun
F_b = radiation factor of the radiator side away from the sun
L = length of vapor generator
L_t = total plate length
L_w = width of plate parallel to heat flow
N = number of parallel reflector units
Q_a = heat absorbed by the working fluid
Q_m = total solar energy striking mirror
Q_p = internal heat transferred into plate, variable
Q_r = waste heat radiated from power plant

(Continued on next page)

expands through the turbine, producing the shaft power necessary to drive an electric generator or some other power-consuming device. Next, the fluid passes through the radiator wherein the vapor is completely condensed. This liquid enters the condensate pump which, in turn, increases liquid pressure. In this state, the liquid again enters the boiler tube and the process is repeated.

Boiler Design. The development of a satisfactory power plant is dependent largely upon the design of a suitable vapor generator which includes boiler tubes designed to absorb heat and a lightweight reflector. A parabolic mirror was selected to concentrate the sun's rays on the boiler tube located on the focal point (Fig. 2).

The solar energy Q_m reaching the vapor generator of length L is

$$Q_m = S_c BLN \tag{1}$$

However, only a fraction of the solar energy Q_m reaches the working fluid. This is attributable to four factors: (*a*) Imperfect reflectivity of the mirror surface, (*b*) geometric imperfection of the mirror, (*c*) reradiation of boiler tube heat, and (*d*) the reflection of direct solar heat from the boiler tube surface.

In a simplified case, where the entire boiler tube surface absorptivity and emissivity are constant, the net heat absorbed by the fluid can be expressed mathematically.

$$Q_a = S_c(B - d)LNC_s C_f \alpha_t + S_c dLN\alpha_t - \epsilon_t \sigma T_t^4 \pi dLN \tag{2}$$

The efficiency of the vapor generator can be expressed as a ratio of the net heat absorbed by the fluid, Q_a, divided by the solar heat reaching the generator, Q_m, or

$$\eta_m = \frac{Q_a}{Q_m} \tag{3}$$

or combining Equations (1), (2), and (3)

$$\eta_m = C_s C_f \alpha_t + \alpha_t \frac{d}{B}(1 - C_s C_f) - \epsilon_t \sigma T_t^4 \frac{\pi d}{S_c B} \tag{4}$$

The middle term of the right-hand side of the Equation (4) is small compared to the other terms and may be ignored. Therefore

$$\eta_m \cong C_s C_f \alpha_t - \epsilon_t \sigma T_t^4 \frac{\pi d}{S_c B} \tag{5}$$

Equation (5) was used to plot the curves of Fig. 3. Smooth stainless-steel boiler tubes were assumed and estimated values were used for C_s and C_f. In order to obtain an efficiency of 70 per cent or more, the d/B ratio must be less than 0.01 and/or tube temperature has to be less than 1000 R.

The properties of various surface finishes were investigated.

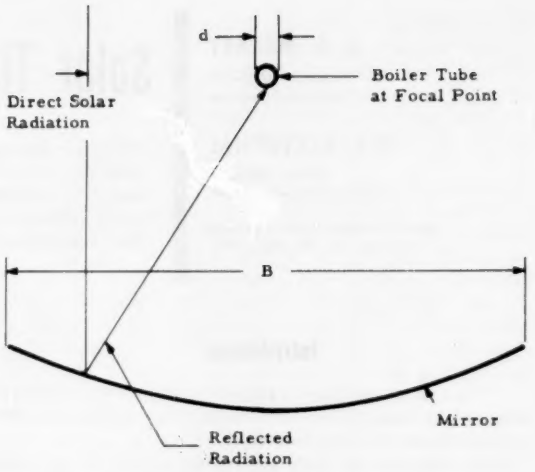

Fig. 2 Solar energy converter

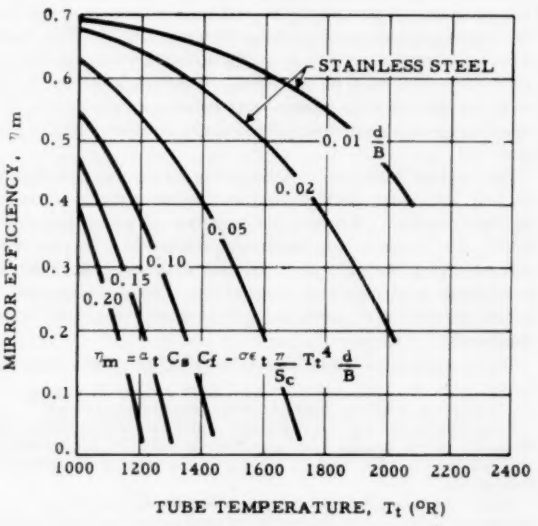

Fig. 3 Mirror efficiency

Nomenclature

S = entropy of working fluid
S_c = solar constant
T = absolute temperature
T_1 = upper temperature of working fluid
T_2 = lower temperature of working fluid
$T_{2'}$ = temperature of working fluid at turbine exhaust for a type (*b*) fluid
T_m = surface temperature of the environment
T_p = plate temperature, variable
T_t = temperature of tube surface
W_a = shaft work from power plant
α_a = absorptivity for surface facing the sun
α_b = absorptivity for surface away from the sun
α_m = absorptivity for solar radiation of upper part of tube (Fig. 5)
α_t = absorptivity for solar radiation of tube
ϵ_a = emissivity of surface facing the sun
ϵ_b = emissivity of radiator surface not facing the sun
ϵ_m = emissivity of upper part of boiler tube and mirror
ϵ_t = emissivity of boiler tube surface
η_c = cycle thermal efficiency
$\eta_{c_{ideal}}$ = ideal cycle thermal efficiency
η_m = vapor generator efficiency
η_t = turbine Rankine efficiency
θ_m = angle of incidence of the sun's rays and a normal to the environment surface
θ_p = angle of incidence of the sun's rays and a normal to the mirror surface
σ = Stefan-Boltzmann constant
Ω = efficiency of radiator surface

The more promising finishes considered for the power plant are presented in Table 1.

Table 1

Surface finish	Absorptivity to solar radiation	Emissivity	Reference
Deposited copper oxide	0.93	0.11	[2]
Stainless steel	0.76	0.124	[3]
Platinum black	0.97	0.92	[4]
Deposited silver optical reflector	0.07	0.01	[5]
Polished aluminum	0.26	0.04–0.05	[6]
White paint	0.12–0.18	0.95	[7]
Light blue paint	0.39	0.92–0.95	[7]
White porcelain enamel	0.34–0.43	0.90	[8]

Employing Equation (5) and the data derived from Table 1, vapor generator efficiencies are compared in Fig. 4. Deposited copper oxide on a highly polished surface was found to be the most efficient surface finish.

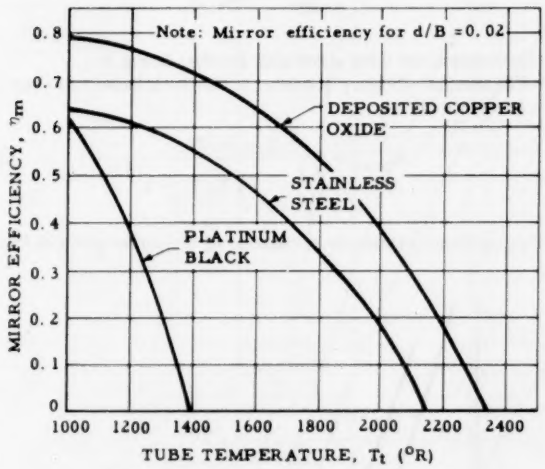

Fig. 4 Mirror efficiency (single over-all finish)

Further improvements in the vapor generator are possible through design modification. For example, the upper section of the boiler tube may be coated or shielded to reduce radiation heat loss. The tube area that does not receive concentrated solar radiation may be insulated or coated with a low-emissivity finish. Silver plating the upper three-quarters of the boiler tube as shown in Fig. 5 was analyzed. In this instance, Equation (4) can be modified as follows:

$$\eta_m = C_s C_f \alpha_t - \frac{d}{B}\left[C_s C_f \alpha_t - \alpha_m + \frac{\sigma T_t^4 \pi}{4 S_c}(3\epsilon_m + \epsilon_t)\right] \quad (6)$$

The data presented in Fig. 6 were obtained by employing Equation (6) and the copper oxide and silver plating finishes as indicated in Fig. 5. This design refinement improves considerably the vapor generator efficiency—an efficiency of 75 per cent is obtained over a wide range of temperatures and d/B ratios.

Fluid Analysis

Knowledge of cycle efficiency is necessary before optimum upper and lower working fluid temperatures can be established. Unfortunately, however, cycle efficiency must be determined indirectly by trial and error. To expedite this process, it is important to express cycle efficiency in terms of convenient parameters; in this case, ratio T_2/T_1 was chosen. T_2 indicated condenser fluid temperature and T_1 boiler outlet temperature.

A method to determine thermal efficiencies for several fluids was derived (Reference [1]). The use of this method, however, depends upon the slope of the saturated vapor line in a temperature-entropy diagram for the particular fluid. The applicability can be explained by referring to Fig. 7 in which ideal Rankine cycles are shown for two types of working fluids.

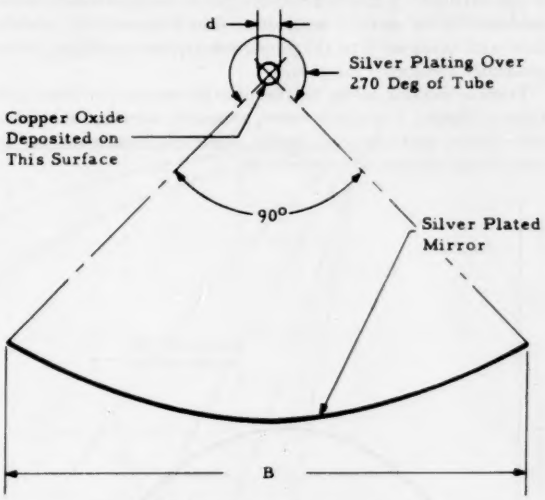

Fig. 5 High efficiency solar energy converter

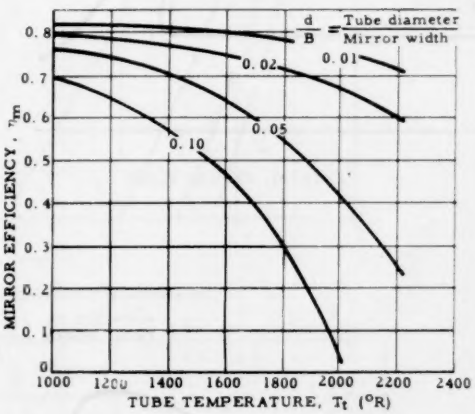

$$\eta_m = \alpha_t C_s C_f - \frac{d}{B}\left[\alpha_t C_s C_f - \alpha_m + \frac{\sigma T_t^4 \pi}{4 S_c}(3\epsilon_m + \epsilon_t)\right]$$

ASSUMED CONDITIONS

α_t = 0.93, solar absorptivity of tube } bottom one-quarter of tube
ϵ_t = 0.11, emissivity of tube }

ϵ_m = 0.01, emissivity of mirror and upper three-quarters of tube

C_s = 0.93, reflectivity of mirror surface

C_f = 0.95, geometric perfection of parabola

S_c = 430 Btu/(hr)(sq ft), solar constant

σ = 0.173(10^{-8}) Btu/(hr)(sq ft)($°R^4$), Stefan Boltzmann constant

α_m = 0.07, solar absorptivity of upper three-quarters of tube

Fig. 6 Mirror efficiency (top three quarters of tube silver plated)

In Fig. 7, the conditions of the expanding vapor in an ideal prime mover are shown by the portion of the cycle between Points 1 and 2′. In type (*a*), point 2′ is in the "wet" region, and the temperature at 2′ is equal to the saturated liquid temperature at point 2. In type (*b*), the vapor expands in the superheat region—and the vapor temperature, upon leaving the ideal prime mover, exceeds saturation temperature. Also, the rejection of heat from the cycle from points 2′ to 2 is at constant temperature for a type (*a*) fluid, but only partially at varying temperatures in a type (*b*) fluid. A fluid exhibiting type (*a*) characteristics can be analyzed by the method demonstrated in Reference [1], while a fluid with inherent type (*b*) properties requires a lengthy, independently conducted analysis.

Possible working media for the lunar power plant includes both types of fluids: Type (*a*)—water, ammonia, mercury, rubidium, and others; and type (*b*)—freons, diphenyl, Dowtherm, sulfur, and a large number of hydrocarbons.

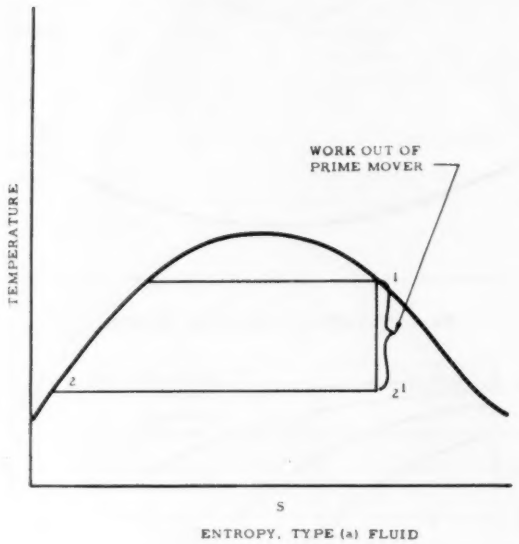

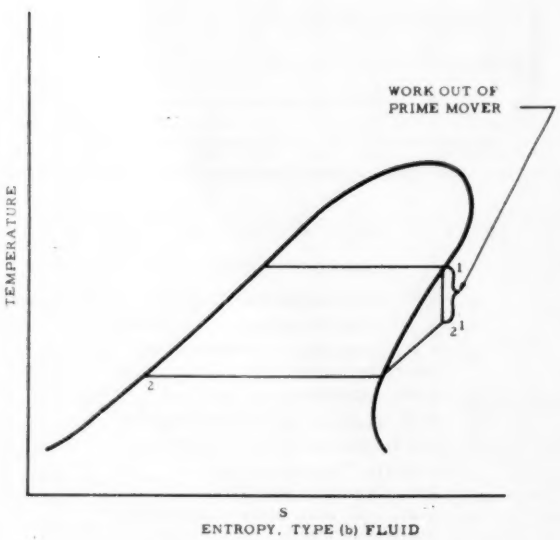

Fig. 7 Theoretical fluid cycles

The thermal efficiency of the cycle using a type (*a*) fluid can be determined by the method employed in Reference [1] obtaining values for two dimensionless parameters, i.e., a fluid parameter h_{fg_1}/CT_1 and a work factor f. In the fluid parameter, h_{fg_1} is the latent heat of evaporation at temperature T_1, and C is the average specific heat of the fluid between the temperatures T_1 and T_2. Because liquid specific heat does not change radically over wide temperature ranges, an average value can be used in most cases. The values for the fluid parameters for mercury and rubidium are shown in Fig. 8.

The work factor f is a ratio of the ideal work obtainable from an actual fluid operating between the temperature limits T_1 and T_2; and, the work obtainable from a ideal Carnot cycle operating between the same temperature limits. The work factor f is a useful tool with which to measure a fluid's power-producing efficiency. The fluid parameter was shown in Reference [1] to be related to f by the following equation:

$$f = \frac{1 + \dfrac{h_{fg_1}}{CT_1} + \left(\dfrac{T_2/T_1}{1 - T_2/T_1}\right) \log_e \dfrac{T_2}{T_1}}{\dfrac{h_{fg_1}}{CT_1} - \log_e \dfrac{T_2}{T_1}} \tag{7}$$

This equation was used to compute the data of Fig. 9.

The thermal efficiency is related to the work factor f as shown in Reference [1] by

$$\eta_{c_{ideal}} = \frac{1 - T_2/T_1}{\left(\dfrac{1}{f} - 1\right) T_2/T_1 + 1} \tag{8}$$

This equation permits the calculation of the curves given in Fig.

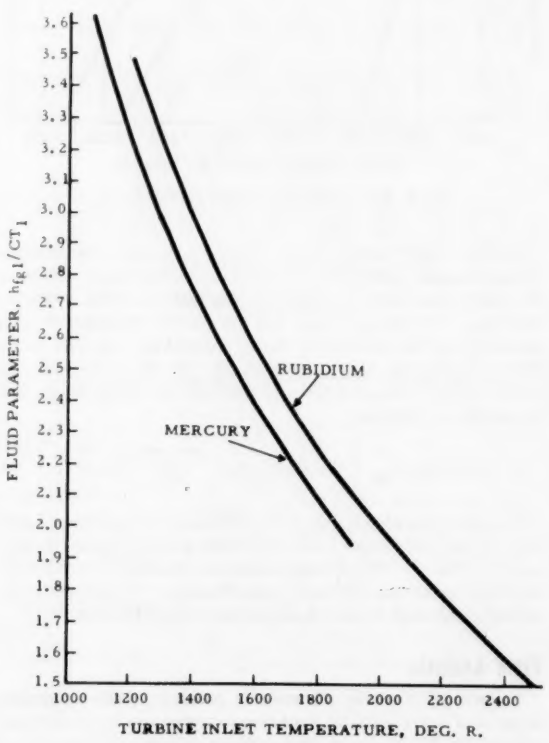

Fig. 8 Fluid parameters for mercury and rubidium

10. It is therefore possible to obtain the ideal power plant thermal efficiency for a required temperature ratio by the following process: (*a*) Obtain the fluid parameter, (*b*) use this parameter with Fig. 9 to obtain the work factor *f*, (*c*) use work factor *f* with Fig. 10 to obtain ideal thermal efficiency. This procedure can be shortened by substituting the value of *f* determined in Equation (7) into Equation (8) and solving for the thermal efficiency. This latter procedure was used to obtain the data of Fig. 11. With this figure, it is possible to obtain the thermal efficiency directly from a known fluid parameter.

Cycle thermal efficiency was determined for two type (*b*) fluids—diphenyl and Dowtherm A. The efficiency data for these fluids are shown in Figs. 12 and 13.

Cycle Analysis

In designing a lunar power plant it is desirable to come up with a compact and efficient *configuration*—especially since it will probably be transported to its site in a space vehicle. It is therefore necessary to establish a mathematical relationship between the power plant components. The following material discusses this relationship.

The heat energy added to the working fluid within the boiler tubes—when the mirror is facing the sun—can be expressed by combining Equations (1) and (3) or

$$Q_a = \eta_m S_c BLN \tag{9}$$

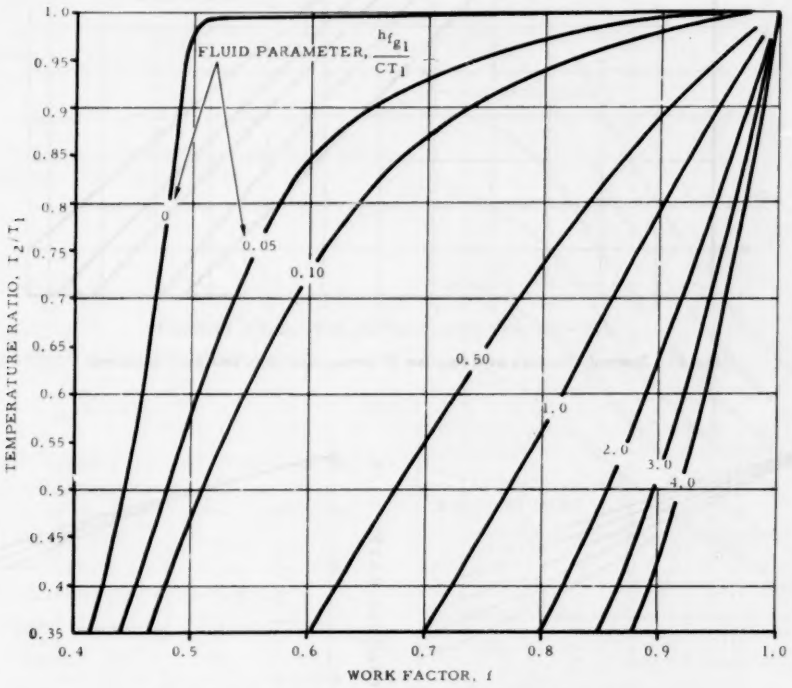

Fig. 9 Relationship between work factors and fluid parameters

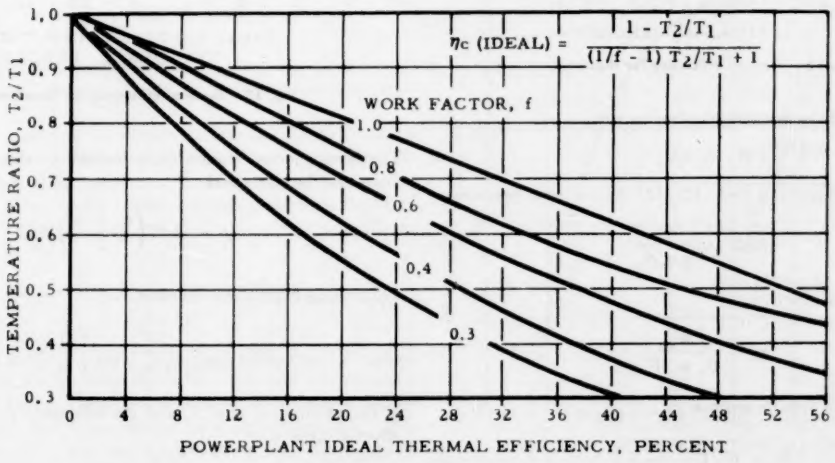

Fig. 10 Power plant thermal efficiency

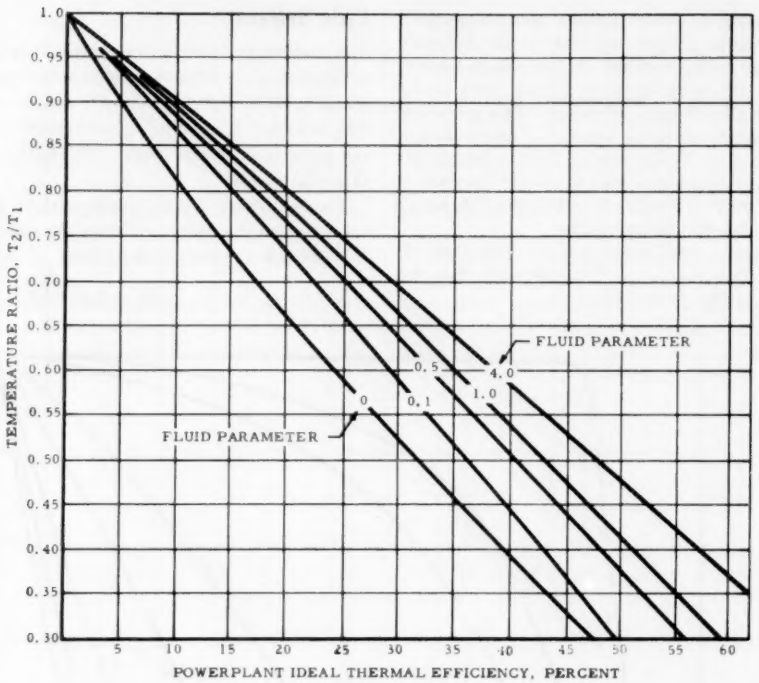

Fig. 11 Thermal efficiency as a function of temperature ratio and fluid parameter

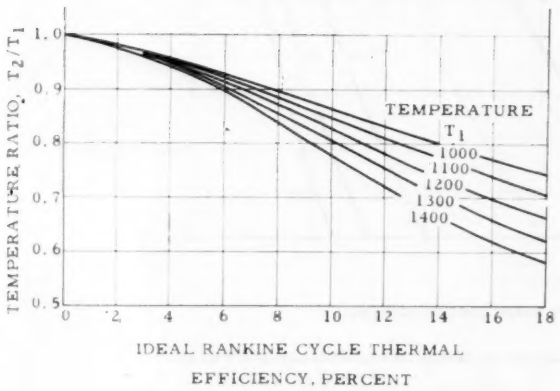

Fig. 12 Thermal efficiency for diphenyl

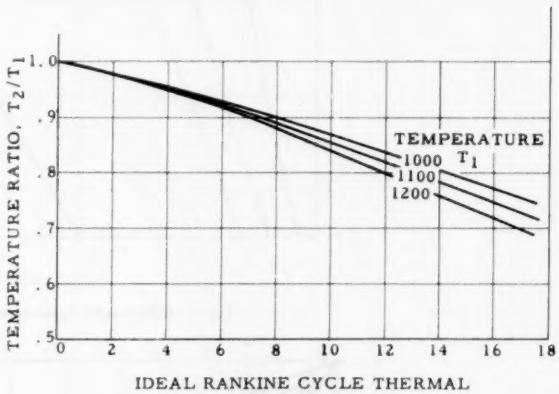

Fig. 13 Thermal efficiency for Dowtherm A

The shaft work of the power plant can be written as

$$W_a = \eta_c Q_a \tag{10}$$

Combining Equations (9) and (10), the mirror area becomes

$$BLN = \frac{W_a}{\eta_c \eta_m S_c} \tag{11}$$

The thermal efficiency is,

$$\eta_c = \frac{W_a}{Q_r + W_a} \tag{12}$$

Equation (12) can also be written

$$Q_r = W_a \left(\frac{1}{\eta_c} - 1 \right) \tag{13}$$

The heat rejected from a cycle featuring extended radiator surfaces may be expressed

$$Q_r = A_r \Omega \left(\frac{\epsilon_a + \epsilon_b}{2} \right) \sigma T_2^4 \tag{14}$$

Combining Equations (13) and (14)

$$\Omega A_r = \frac{2W_a}{(\epsilon_a + \epsilon_b)\sigma T_2^4} \left[\frac{1}{\eta_c} - 1 \right] \tag{15}$$

If the product of area A_r and the efficiency Ω are written as an effective area A_e or

$$A_e = \Omega A_r \tag{16}$$

then, Equation (15) becomes

$$A_r = \frac{2W_e}{(\epsilon_a + \epsilon_b)\sigma T_2^4}\left[\frac{1}{\eta_c} - 1\right] \tag{17}$$

Assuming the power plant is of the compact design indicated in Fig. 1, a balance has to exist between the receiving surface and the radiating area; the mirror surfaces must be capable of dissipating the waste heat produced. This condition is mathematically satisfied by combining Equations (15) and (11). The results, after simplification—and noting that A_r equals $2BLN$—can be written as

$$\frac{(\epsilon_a + \epsilon_b)\sigma T_2^4 \Omega}{S_c} = \eta_m(1 - \eta_c) \tag{18}$$

It then becomes necessary to determine the design conditions fulfilling these requirements. The heat transfer from both sides of a plate element is indicated

$$dQ_p = (c_1 T_p^4 - c_2) L dL_w \tag{19}$$

Where c_1 and c_2 are constants dependent upon the properties of the plate surface and the environment wherein,

$$c_1 = \sigma(\epsilon_a + \epsilon_b) \tag{20}$$

and

$$c_2 = S_c(\alpha_a \cos\theta_p + F_a\alpha_a r_m \cos\theta_m + F_b\alpha_b r_m \cos\theta_m) + T_m^4\sigma[F_a\epsilon_a + F_b\epsilon_b] \tag{21}$$

The internal heat passing a section of the plate equals

$$Q_p = -ktL\frac{dT_p}{dL_w} \tag{22}$$

Net heat loss from an element equals the difference of the heat entering the element and the heat leaving it, or

$$dQ_p = -ktL\frac{d^2T_p}{dL_w^2}dL_w \tag{23}$$

Equating Equations (23) and (19), and simplifying

$$\frac{d^2T_p}{dL_w^2} = -\frac{c_1}{kt}T_p^4 + \frac{c_2}{kt} \tag{24}$$

The first step in integrating Equation (23) can be written as

$$\frac{dT_p}{dL_w} = -\sqrt{\frac{2c_1}{5kt}T_p^5 - \frac{2c_2}{kt}T_p + c_3} \tag{25}$$

where c_3 is the integration constant.

Equation (25) can be graphically integrated by suitable substitution.

Following the graphical integration, the results can be arranged into convenient parametric groups to simplify the computations. It was found desirable, therefore, to obtain an expression for plate efficiency: The ratio of actual heat dissipated from the plate to the theoretical amount dissipated if the plate were at uniform temperature T_2, or

$$\Omega = \frac{Q_p}{L_t L c_1 T_2^4} \tag{26}$$

Fig. 14 is the result of such a procedure, indicating the values of plate efficiency for varying values of plate and environment parameters. If the power plant is located at a lunar subsolar point, waste heat dissipation would be greatly impaired. For these conditions $\cos\theta_p$ and $\cos\theta_m$ become unity. F_a equals 0 and F_b equals 1 and

$$c_1 = \sigma(\epsilon_a + \epsilon_b) \quad \text{and} \quad c_2 = S_c(\alpha_a + \alpha_b r_m) + T_m^4\sigma\epsilon_b$$

Using Fig. 14, and assuming a set of plate properties, the plate efficiency was computed for a series of values of T_2. Fig. 15 presents the results of this computation.

To use Equation (18), a configuration was established and the temperature was determined by a graphical solution. The left-hand side of Equation (18) was plotted as a function of the condensing vapor temperature—the latter is assumed to be equal to the outer wall temperature of the radiator tube. To evaluate the right-hand side of the Equation (18), a temperature T_1 was

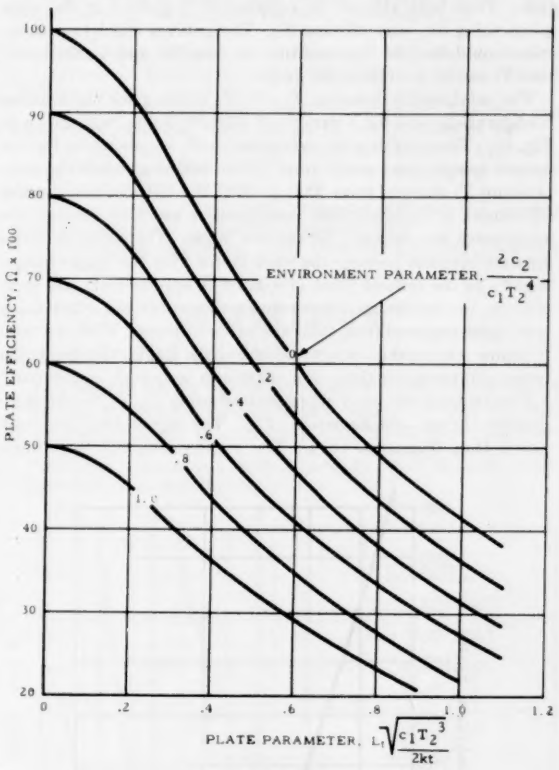

Fig. 14 Plate efficiency

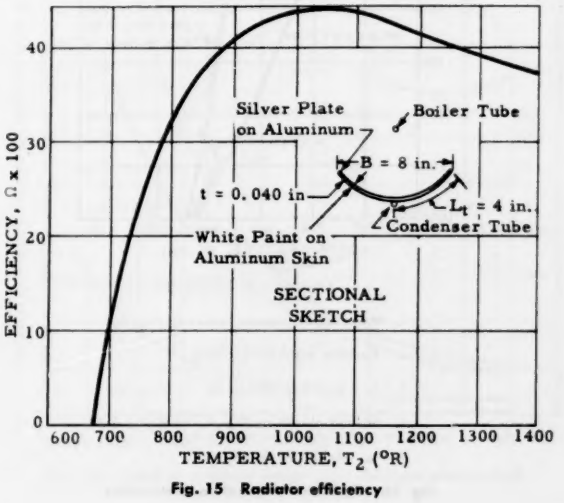

Fig. 15 Radiator efficiency

selected and a range of values were chosen for T_2. The values of η_m were taken for the appropriate mirror configuration and η_e ideal values were obtained from the efficiency data presented earlier for the desired fluid. The ideal thermal efficiency was then converted to actual efficiency by use of the following equation:

$$\eta_e = \eta_{e\text{ideal}} \times \eta_t \tag{27}$$

A series of values for the right-hand side of the Equation (18) were plotted on the same graph as the left-hand side of the equation. Thus both sides of the equation were plotted on the same graph using the same abscissa T_2. The point at which two curves cross would then be the condition for equality and the temperature T_2 can be read from the graph.

The relationship between T_1 and T_2 existing for the selected configuration, and for a variety of working fluids, was shown in Fig. 16. The resulting temperatures for T_2 are shown to be in a narrow temperature range from 770 to 850 deg, while the temperature T_1 changes from 2000 to 1000 R. Because the thermal efficiencies of diphenyl and Dowtherm A are very similar, the same curve was obtained for the two fluids. The curve for water appears irregular because the work factor f for this fluid changes rapidly as the critical point of 1165 R is approached. By comparison, the maximum temperatures chosen for the other fluids were quite removed from their critical conditions. With the temperature relationship determined from the fluids, the remaining items of interest for the power plant can be quickly computed.

The thermal efficiency was obtained using T_1, T_2, the ideal efficiency curves, and Equation (27). The mirror area was computed from Equation (11). The results obtained for several fluids are shown in Fig. 17, with mercury requiring the least area. The attainment of the lowest mirror areas requires careful consideration of the vapor pressure, specific volume, and moisture content of the vapor at the turbine exhaust. If the temperature is too low, large volumes may have to be handled. By increasing T_2 and using only a portion of the mirror area as a radiator, the condition can be remedied.

However, this alteration reduces cycle efficiency and increases mirror area. In Fig. 17, the dotted curve for mercury—where T_2 equals 900 deg R—exemplifies this type of cycle efficiency reduction.

When T_1 equals 1300 R, the mirror area is shown to increase from approximately 36.7 sq ft to 44 sq ft per kw of power produced. For this condition, the radiator area A_r has been computed by Equation (15) and found to be 51.6 sq ft/kw. However, the radiator area includes both sides of the mirror surface; consequently, this number must be divided by two to obtain the mirror area to be used. In other words, in this case 25.8 sq ft of mirror would be used as a radiator. The curve for T_2 equals 900 R probably demonstrates more clearly the capabilities of a mercury power plant.

The mirror area for water is also worthy of note. The mini-

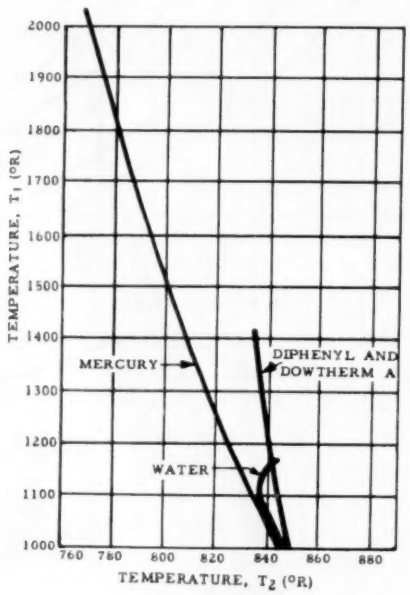

ASSUMED CONDITIONS

1. Radiator efficiency shown in Fig. 15
2. Turbine efficiency = 80%
3. S_c = 430 Btu/(hr)(sq ft)
4. Mirror shown in Fig. 6 and d/B = 0.02
5. ϵ_a = 0.01 and ϵ_b = 0.95

Fig. 16 Optimum temperature relationship

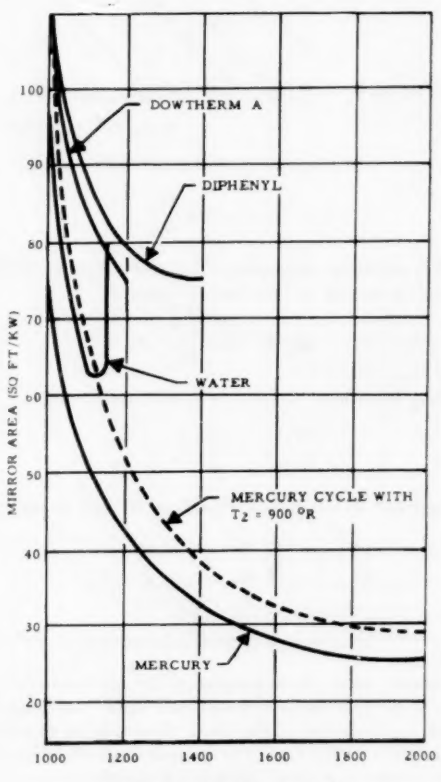

ASSUMED CONDITIONS

1. Mirror efficiency for d/B = 0.02 and configuration shown in Fig. 6
2. Turbine Rankine efficiency = 80%
3. Radiator efficiency shown in Fig. 15
4. Temperature T_2 taken from Fig. 16 unless noted

Fig. 17 Minimum mirror area

mum area occurs when T_1 equals 1130 deg and T_2 equals 836 F. For T_1 greater than 1130 R the area increases rapidly to approximately 80 sq ft/kw at 1165 R, the critical temperature of water. There are other disadvantages to water, too; the turbine inlet pressure corresponding to 1130 R is approximately 2530 psia and would therefore require high-pressure components of rugged construction. When operating at the temperature limits indicated, however, the available energy per pound of water exceeds that of other working fluids. This high available energy will require a turbine with multiple pressure stages to be effectively absorbed. For these reasons, water is not as attractive as mercury as a working fluid.

The two other fluids, diphenyl and Dowtherm A, were also disappointing. Chemically stable at temperatures approaching 1300 F, these fluids, unfortunately, exhibited poor cycle efficiencies and require large mirror areas. The areas shown in Fig. 16 can probably be reduced to some degree by altering mirror configuration. The pressures associated with the T_2 values in obtaining these curves are relatively high, and the vapor is in the superheat region. Because of these conditions, the high moisture problem does not exist and lower temperatures and pressures are permissible. Therefore a configuration with a higher radiator efficiency Ω should be investigated if these fluids are to be given further serious consideration.

Conclusions and Recommendations

This investigation has demonstrated the feasibility of a solar turbo power plant. A rugged, compact unit requiring an approximate 35 sq ft of mirror area per kilowatt was predicted with 1350 R (890 F) mercury inlet temperature, to the turbine. Lower areas are possible at higher inlet temperatures, but these, however, are only modest reductions. The design of an efficient vapor generator was found to be extremely important in obtaining an optimum power plant. A gain in efficiency in transferring solar energy to heat energy in the working fluid creates a change of effects which result in a more efficient power plant. It permits the use of higher temperatures in the working fluid. These higher temperatures result in increases in cycle efficiency—reducing radiator area and/or the temperature T_2.

For these reasons special attention should be given the surface finishes of the mirror and boiler tubes.

Few satisfactory working fluids were found during the course of this study—due, in all probability, to the small amount of time invested in this area. More effort could be profitably spent in this area of research. Further efforts should be expended also in the analysis and development of power-plant systems to permit plant operation during off-design conditions. Probably, the greatest departure from the design conditions is represented during the time interval when the sun has just appeared over the horizon. In this instance, the radiator heat rejection rate would be much greater than it would be at noon. This possible increased heat rejection rate will cause the uncontrolled temperature to fall, necessitating the development of some form of back pressure regulation. A bypass vapor system, orifices in the condenser section, regulation of liquid removal from the condenser tubes, thermostatic valves, or other types of automatic devices, are possible control devices.

The performance of this power plant should be compared to other electrical generator systems, such as the static electrical generators of the solar series—thermo-ionics, Peltier effect.

The operation of a prototype unit of a solar turbo power plant will be very profitable because it can provide engineering data applicable in the improvement and refinement of later designs.

References

1 D. B. Mackay, "Powerplant Heat Cycles for Space Vehicles," presented at the IAS National Summer Meeting, Los Angeles, Calif., June 16–19, 1959.

2 A. R. Hibbs, "The Temperature of an Orbiting Missile,' Progress Report No. 20-294, Jet Propulsion Laboratory, California Institute of Technology, Pasadena, Calif., March 24, 1956.

3 P. A. Unger, "Preparation of a Selectively Black Surface for Use in the Collection of Solar Energy," Department of Chemical Engineering, Massachusetts Institute of Technology, Cambridge, Mass.

4 W. S. Shipley, Progress Report No. 20-319, Jet Propulsion Laboratory, California Institute of Technology, Pasadena, Calif., 11 April, 1957.

5 W. H. Coblenz, "The Diffuse Reflecting Power of Various Substances," *Bulletin U.S. Bureau of Standards*, vol. 9, pp. 283–324.

6 Frederick E. Fowle, "Smithsonian Physical Tables," eighth revised edition, Smithsonian Institute, Washington, D. C., 1934, pp. 378–381.

7 M. Fishenden and O. A. Saunders, "Calculation of Heat Transmission," His Majesty's Stationery Office, London, England, 1933, pp. 17–22.

8 "Increased Light Values With White Paint," *Industrial and Engineering Chemistry*, News Edition 13, vol. 19, 1935, p. 397.

9 I. G. Priest, "The Priest-Lange Reflectometer Applied to Nearly White Porcelain Enamel," *U.S. Bureau of Standards Research Journal*, vol. 15, 1935, p. 544.

10 K. Anderson, "Engineering Properties of Diphenyl," Argonne National Laboratory, ANL-5121, August 11, 1953.

11 Dowtherm Handbook, Dow Chemical Company, Midland, Mich., 1954.

DISCUSSION

C. L. Walker[2] and Y. S. Tang[2]

The authors are to be congratulated on the comprehensive work they presented. As an evidence that the subject is indeed of common interest, the company with which these discussers

[2] Research Department 7897, Allison Division, General Motor Corporation, Indianapolis, Ind.

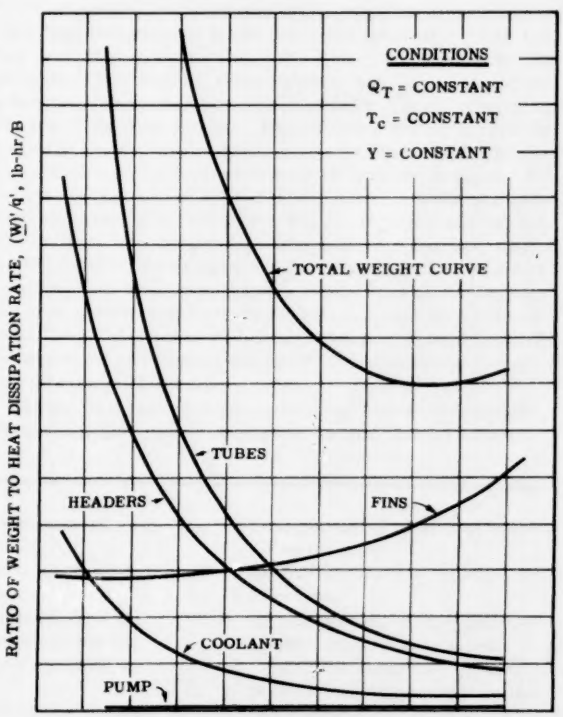

Fig. 18 Sketch of optimum design point determination method

are associated has also been actively investigating similar power plants for some time. The problem of optimizing the design involves study of quite a number of alternative systems.

It probably is worth while to mention in the paper the basis of selection of such a configuration of collector as described. For instance, a comparison between the performance of three-dimensional parabolic dish type and that of two-dimensional parabolic trough-type collectors will shed additional light on the area of development required. The idea of combining collector surface with radiator surface was well taken in the system described. It might be added, however, according to our analysis of weight optimization of a space radiator, the fin surface does not usually constitute the major part of the total weight.

Fig. 18 illustrates a typical set of curves in weight analysis, where

W' = weight per foot of tubing
q' = heat dissipation per foot of tubing
Q_t = total heat load to be dissipated
T_c = average temperature of radiator coolant
Y = length of one coolant tube

The saving in weight as a result of eliminating radiator fin surface may not be as appreciable as it first appears. The attendant mechanical considerations necessary to prevent distortion of the collector, due to temperature variations in the condenser tubes, may also be worth noting.

Analysis of Solar-Furnace Performance in Mechanical Testing at Extremely High Temperatures[1]

G. S. LEON
Research Assistant

M. E. SHANK
Associate Professor of Mechanical Engineering, Massachusetts Institute of Technology, Cambridge, Mass. Mem. ASME

The use of the solar furnace for investigating properties of materials has received increased attention. However, such work has been limited to determining physical properties of refractory materials. Analyses of performance, related to such work, have been confined to investigations of flux distribution and temperature on flat-plate, hemispherical, and cavity receivers at the focal spot. Heat conduction away from the focal spot usually has not been considered. The present investigation is concerned with the analysis of fluxes and temperatures that can be attained in tensile specimens undergoing mechanical tests. Account is taken of heat loss by conduction and reradiation. It is shown that, (a) attainable temperatures are considerably lower than those reached in flat-plate receivers, (b) with normal low-aperture furnaces (i. e., 60 deg) a large furnace is necessary to reach high temperatures with adequately large specimens, and (c) furnaces best-adapted to mechanical testing would have larger apertures (120 deg) than are now commonly conceived.

THE USE OF THE SOLAR FURNACE for investigating the properties of materials at very high temperatures has received increased attention recently because of the growing demand for information on materials properties and the apparent advantages of the solar furnace for this type of work [1 to 6][2]. Among the advantages cited are the extremely high temperatures that can be attained by concentrating the rays of the sun and the ease of avoiding contamination [1, 3].

Materials research with solar furnaces has been limited to finding such physical properties of refractory material as melting points and transition temperatures [7, 8]. The test material, usually in the shape of a block, is placed directly in the focus of the furnace. Some of the analyses which have appeared in the literature are limited to an investigation of the flux distribution and temperature of the flux at the focus [12, 13]. In others, where the physical conditions of the material are taken into account, heat conduction away from the focal spot is not considered in determining the equilibrium temperatures [9, 10, 11].

The determination of the mechanical properties of materials at very high temperatures is one important application which has not been thoroughly investigated. This would include tensile strengths, deformation characteristics, and other short-time properties. Such work presents an entirely different concept in the use of the solar furnace. First, a tensile specimen must be heated uniformly. If the specimen is perpendicular to the mirror axis, rotation of the specimen is required as shown in Fig. 1. To heat the specimen on all sides at the same time, it is placed coincident with the axis of the furnace, Fig. 2. In either case the flux distribution and temperature determination requires major modifications of the analyses mentioned before. The use of an axial specimen would permit much simpler loading devices than would be necessary with rotating specimens perpendicular to the axis. The axial orientation also suggests that a different shape of furnace might be better for this application than the usual small-aperture parabolic furnaces.

The results presented in this paper are an attempt to determine the most suitable manner of adapting the solar furnace for testing

[1] This research was supported by the United States Air Force through the Air Force Missile Development Center, Holloman Air Force Base, New Mexico, under Contract AF 29(600)-1705.

[2] Numbers in brackets designate References at end of paper.

Contributed by the Solar Energy Applications Committee and presented at the Annual Meeting, Atlantic City, N. J., November 29–December 4, 1959, of THE AMERICAN SOCIETY OF MECHANICAL ENGINEERS.

NOTE: Statements and opinions advanced in papers are to be understood as individual expressions of their authors and not those of the Society. Manuscript received at ASME Headquarters, August 11, 1959. Paper No. 59—A-79.

Nomenclature

P_0 = solar radiation constant, 2 cal/cm² min
ψ = radiation flux density absorbed on specimen surface in the focal spot, Btu/in.² hr
ψ^* = ideal flux density absorbed with no losses, Btu/in.² hr
T = temperature, deg R
σ = Stefan-Boltzmann constant, 1.19 10^{-11}, Btu/in.² hr (deg R)⁴
η_a = fraction of solar radiation transmitted through atmosphere
η_r = fraction of solar radiation reflected by mirror
η_g = index of geometric perfection—fraction of radiant energy actually concentrated in focal spot relative to theoretical amount
α = total absorptivity of specimen material
α_0 = total normal absorptivity of specimen material
ϵ = total emissivity of specimen material
ϵ_0 = total normal emissivity of specimen material
β = angle of incidence of radiation on specimen
θ = angle formed by mirror axis and vector from focus to a point on the mirror surface
θ_m = aperture—maximum angle to rim of mirror
f = focal length from vertex of mirror to focus

(Continued on next page)

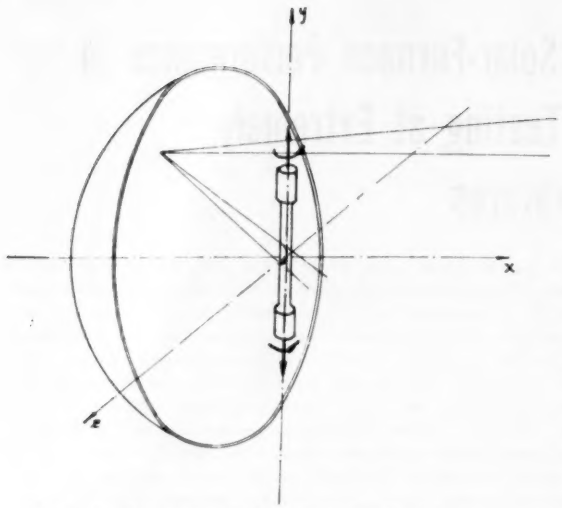

Fig. 1 Specimen perpendicular to the axis and rotating

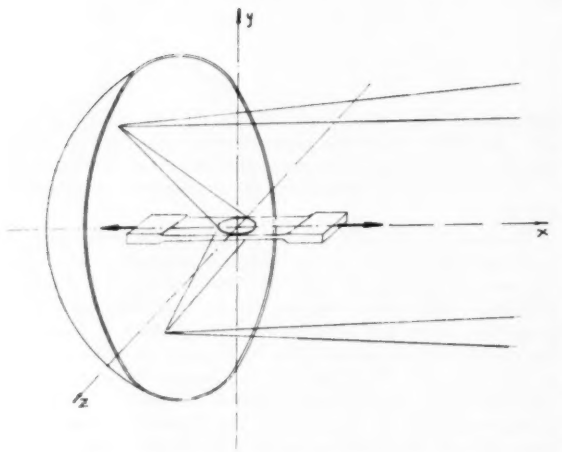

Fig. 2 Axially oriented specimen heated uniformly

mechanical properties. The analysis is concerned first with heat absorbed by specimens in the two orientations described and secondly with the temperatures that can be reached by specimens of different sizes, shapes, and physical properties, assuming the temperatures reached are below the melting point. These factors are important since they give information on the shape and size of furnace best suited for this application. In adapting the solar furnace for mechanical testing we are interested in reaching the highest possible temperatures. The analysis was performed on the basis of a parabolic condensing mirror since this is by far the most common furnace shape [14]. Details of the analysis appear in the Appendix.

Results and Discussion

Comparison of Flux Densities. The heat absorbed per unit area and unit time establishes an upper limit to the temperature that can be reached. This quantity can be determined independently of the absolute size of the furnace. The size of the furnace is also important, however, since it establishes the total amount of heat absorbed. When conduction of heat is considered in determining the maximum temperature, the size of the furnace must therefore be considered also.

The method of determining the radiation absorbed per unit surface area of the specimen is straightforward. It is only necessary to find the contribution of radiation from each point on the mirror whose reflection falls on the surface of the specimen. The part of this radiation that is absorbed will then depend on the absorptivity of the material. Finally all the contributions are added to give the total flux absorbed per unit surface area. This process is described in References [9] and [10] for focusing on a plane perpendicular to the mirror axis. A much more general approach was necessary in this analysis because the flux is being absorbed in many different orientations over the surface of the specimens. (See Appendix.)

The flux absorbed will therefore depend on the intensity of the radiation reaching the condensing mirror. This can be expressed in terms of the solar constant and the fraction of radiation transmitted through the atmosphere as $\eta_a P_0$. It will also depend on the aperture of the condenser θ_m and the reflectivity of the mirror η_r. The geometric perfection of the mirror η_g is a measure of how effectively the radiation is actually concentrated and must also be included, as shown in the Appendix. Finally, in considering the absorptivity of the material, the angle of incidence of the radiation must be taken into account. This is extremely important since the absorptivity of most materials tends to decrease as the incidence angle increases. In this analysis the variation of absorptivity with angle of incidence is assumed to be,

$$\alpha = \alpha_0 \cos \beta \tag{1}$$

where α_0 is the total normal absorptivity and β is the angle of incidence. This is a good approximation for most materials [10, 15]. All these considerations are limited to materials that are opaque to the radiation.

Fig. 3 gives the results of the analysis, showing the ideal flux density absorbed by the specimen in the two orientations mentioned previously as it varies with the aperture of the mirror. The aperture is the angle formed by the axis of the mirror and a line connecting the focus with the rim of the mirror. The actual flux density absorbed can then be expressed as

$$\psi = \eta_a \eta_r \eta_g \alpha_0 \psi^* \tag{2}$$

These coefficients will vary for each particular case, but, normally, atmospheric transmission may be 0.8 in a good locality and the reflectivity may be as high as 0.9. The coefficient of geometric perfection is difficult to evaluate and must be determined experimentally for each furnace. Values have been quoted of 0.35 and 0.76 [9, 16]. The wide difference of these two values and the scarcity of this type of information is indicative of how little quantitative data have been published on the actual performance

Nomenclature

ρ = distance from focus to point on mirror surface
γ = angle subtended by sun's image, 0.00932 radians
r = radius from mirror axis to point on mirror surface
ϕ = angle between radius r and vertical axis of mirror
ν = orientation of plane passing through focus relative to vertical axis of mirror (see Fig. 8)
s = periphery of specimen
A = cross-sectional area of specimen
k = thermal conductivity of specimen material, $\frac{\text{Btu in.}}{\text{in.}^2 \text{ hr deg F}}$
L = length of specimen absorbing radiation
R = parameter in heat-conduction equation, see Equation (10a), $\frac{\text{hr deg F in.}^2}{\text{Btu}}$

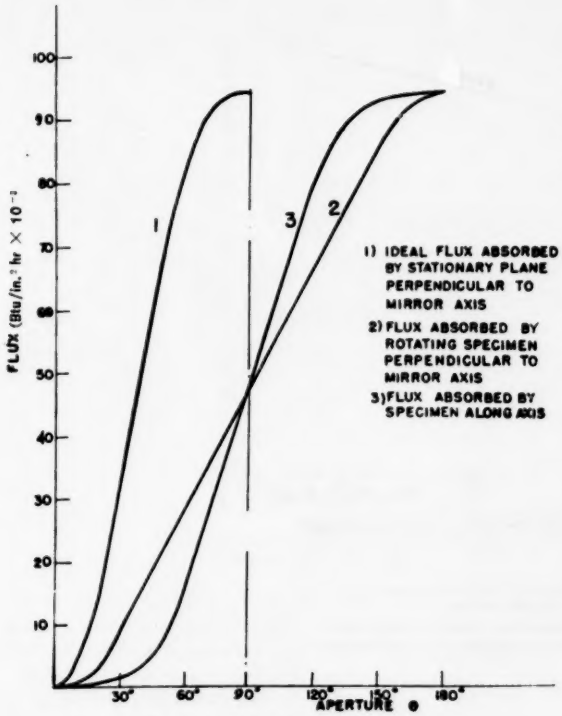

Fig. 3 Ideal flux density absorbed

of solar furnaces. If blockages of the mirror from instruments or cutouts exist, these must be taken into account.

Referring to Fig. 3, it can be seen that, for usual apertures of 60 deg or less, the rotating specimen absorbs more heat per unit area of surface than the axial specimen. This is due to the unfavorable angle of incidence of the radiation on the axial specimen for apertures below 45 deg. For apertures greater than this the flux absorbed by the axial specimen increases rapidly, becoming greater than on the rotating specimen after a 90-deg aperture is reached. The advantage of not having to rotate a specimen is very real. From these curves it can therefore be argued that small aperture furnaces do not lend themselves well to mechanical testing and that the best furnace shape would have an aperture of over 90 deg with a cutout below 45 deg.

Although an aperture of 180 deg has no physical significance, apertures slightly over 90 deg are perfectly reasonable. The aperture would be limited by practical considerations, since the size of the mirror increases rapidly as the aperture goes beyond 90 deg. As explained in the Appendix, reflections from large angles give a large image at the focus. This means that the flux density per unit of mirror area is small. However, the area of the mirror increases very rapidly as a function of the angle, which offsets the decreasing density and results in a continued rise in the flux curves. The concentration efficiency of the mirror tends to be low as a consequence.

Most furnaces in operation have apertures of 60 deg or less [14] because the heat is usually wanted on a surface perpendicular to the axis of the mirror. The flux densities absorbed in that case are very much greater than would be the case with tensile specimens. This is shown by the third curve in Fig. 3 giving the flux density for a flat-plate receiver. The reasons for this difference can be explained in general terms. First, the total surface absorbing radiation on the tensile specimen is greater than the spot on the flat-plate receiver. Secondly, the angle of incidence is less favorable on the tensile specimen than on the flat plate.

The flux absorbed by the rotating specimen is less than half the amount absorbed by the flat plate because it rotates at a uniform rate. If the plate could be rotated instantaneously, letting one side face the mirror for half the time, then the average flux absorbed by each side would be half as much as that absorbed by one side if the plate were stationary. When the plate is rotated at a uniform rate, however, there will be periods when neither side of the plate is facing the mirror very favorably and the average flux will therefore be less than half. This is exactly what happens to the specimen.

Specimen Temperatures. The steady-state temperatures were determined assuming that the flux density described in the previous section was absorbed over some length L of the specimen. Some of this heat is lost by radiation over the same area that is absorbing and some of it is conducted along the specimen and lost by radiation over its length. The specimen was considered to have a constant cross section and to be long enough for the temperature at the ends to approach the ambient temperature asymptotically.

In solving this problem, as described in the Appendix, the emissivity of the material was taken equal to the absorptivity and both were assumed to vary as the cosine of the incidence angle. It was also assumed that the emissivity and the thermal conductivity were constant with temperature. In this manner the problem was partially nondimensionalized and a solution was made in terms of a parameter R involving the physical properties and dimensions of the specimen such that

$$R = \frac{\epsilon_0 L^2 s}{Ak} \tag{3}$$

ϵ_0 is the total normal emissivity (or absorptivity), s is the circumference, A is the cross-sectional area, and k the thermal conductivity. The length L can be taken as the diameter of the spot and therefore this relation also depends on the absolute size of the furnace. If there is a considerable amount of heat being supplied outside the spot, some correction can be applied to this length. Generally the correction is not great and in the case of the rotating specimen it is difficult to evaluate.

The results of these calculations are shown in Fig. 4. They give the maximum specimen temperature as a function of the flux density absorbed. The upper bound, for an infinite value of R, occurs when no heat is conducted away. By comparing these curves with Fig. 3, some idea can be formed of the maximum temperatures that can be expected using the solar furnace for this application.

For these curves to apply, the specimen cannot be large compared to the size of the spot. Otherwise, some deviation from true focusing will exist which tends to reduce the flux density given in Fig. 3. This effect is analyzed by De La Rue, Loh, Brenner, and Hiester [17]. By making the limitation that the size of the spot must be at least as large as the diameter or width of the specimen the deviation is not serious and decreases as the relative size of the spot increases. If the spot is much larger than the specimen thickness this results in a higher temperature, but only part of the concentrated energy falls on the specimen and therefore the efficiency of the furnace is reduced.

If the specimen is short compared to the region being heated and its ends are held at the ambient temperature, the maximum temperature at the center will be lower than given in Fig. 4. This effect is demonstrated in Fig. 5, which gives the typical variation of temperature along the length of a specimen approaching ambient conditions asymptotically and also abruptly. The difference in the maximum temperature is not very great in this case, but if a shorter specimen were used the effect would become considerable. In an actual test setup it would therefore be advantageous to use long grips in pulling the specimens.

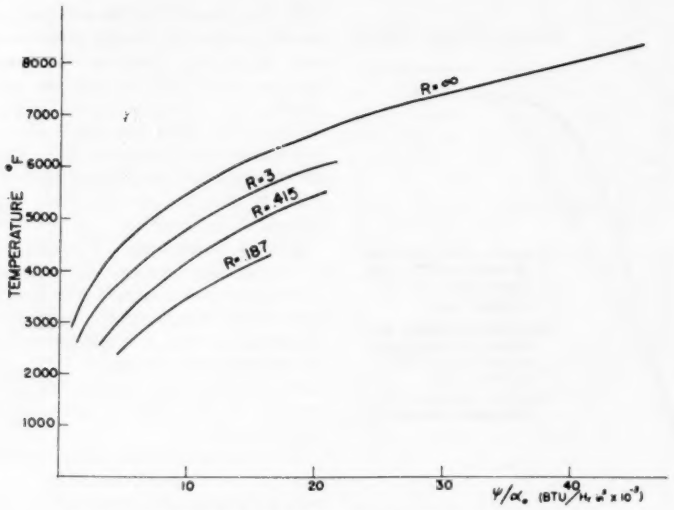

Fig. 4 Maximum calculated specimen temperature versus flux absorbed

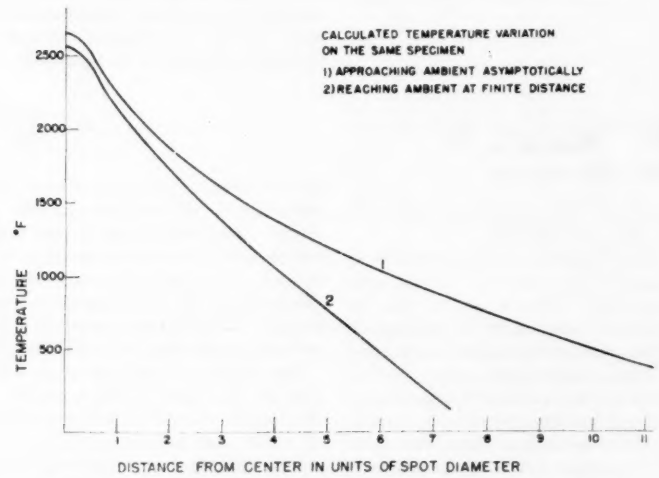

Fig. 5 Typical calculated temperature variation over length of specimen

Table 1 Maximum specimen temperature and mirror size for typical conditions

Mirror aperture of 60 deg, $\eta_a = 0.80$, $\eta_r = 0.80$, $\eta_\sigma = 0.50$
Specimen, rectangular cross section, 0.25 × 0.050 in., $k = 5$ Btu in/in.² hr deg F, $\dot{\epsilon}_0 = \alpha_0 = 0.5$
For axial specimen $\psi^* = 15{,}000$ Btu/in.² hr, rotating specimen $\psi^* = 28{,}000$ Btu/in.² hr

L, in.	R, hr deg F in²/Btu	Axial T, deg F	Rotating T, deg F	Mirror diam, ft
0.25	0.276	2850	3750	5
0.32	0.50	3250	4150	6.7
0.46	1.0	3600	4500	9.5
1.00	5	4050	5000	21
5.00	120	4500	5400	103

Table 1 gives some representative values of temperature as it is affected by size of the furnace. This is based on a 60-deg aperture and assumes 20 per cent loss of the sun's radiation from atmospheric absorption, 20 per cent from imperfect reflection of the mirrors, and a 50 per cent loss from geometric imperfections. The specimen dimensions and properties are given in the table. The length along the specimen receiving radiation is assumed equal to the focal-spot diameter and from this the size of the furnace is computed. Note that a smaller mirror of the same aperture could not be used with this size specimen since its spot would not cover the specimen width. Similarly, a much larger specimen could be used with the largest mirror with very little decrease in temperature. Fig. 6 gives similar data graphically and shows a distinct limit to what the furnace size alone can do if the flux density is fixed.

Table 2 Maximum specimen temperature and mirror size for large aperture furnace

Mirror aperture of 120 deg—cutout below 30 deg
For axial specimen $\psi^* = 78{,}000$
All other conditions as for Table 1.

L, in.	R, hr deg F in²/Btu	Axial T, deg F	Mirror diam, ft
0.25	0.276	5500	15
1.60	11.3	7100	100

For comparison, Table 2 gives similar information for a furnace with an aperture of 120 deg and a cutout below 30 deg. The specimen size and physical properties, and the efficiencies, are

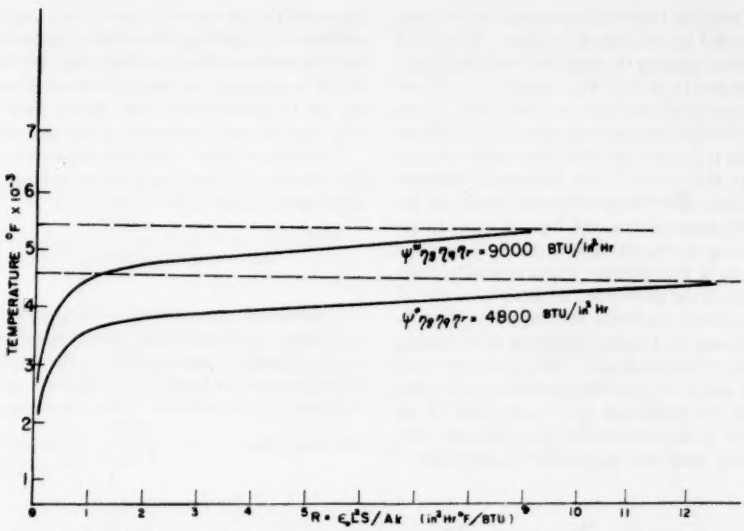

Fig. 6 Calculated maximum specimen temperature for constant flux absorbed as it varies with parameter *R* (see Table 1)

kept the same as in Table 1. Figures are only given for an axial specimen since for large apertures the axial specimen absorbs more flux (see Fig. 3) and has other practical advantages in testing.

The diameter of such a furnace is three times as great as for a 60-deg furnace giving the same size spot. But the temperature that can be reached in such a furnace with a 15-ft diam (0.25-in-diam spot) is as high as can be reached with the largest 60-deg-aperture furnace. As the size is increased to, say, 100-ft diam (1.6-in-diam spot), temperatures over 7000 F are possible.

One very important point which is not shown by these figures is the temperature gradients that exist in the specimen. These gradients are very severe in small furnaces since they amount to hundreds of degrees from the center to the edge of the spot. This effect can be seen in the temperature curves in Fig. 5. The gradients would have effects that would be difficult to evaluate when trying to obtain mechanical data and the difficulties in trying to obtain true temperature and elongation would have additional complications. Variation of temperature through the thickness is also very likely, although in the analysis the temperature was assumed constant at each cross section. As the size of the spot becomes larger this effect is not as serious since the temperature drop takes place over a greater physical length.

Conclusions

From the results obtained some conclusions can be reached as to the performance of solar furnaces for the mechanical testing of materials:

1 The temperatures that can be reached are considerably lower than have been obtained by simply putting an object in the focal spot of a furnace. This difference has been explained in terms of the reduced flux densities absorbed by the tensile specimens. These reductions were due to the larger areas over which the flux is absorbed and the unfavorable incidence angles of much of the radiation.

2 With normal low-aperture furnaces, a large furnace is necessary to reach high temperatures with adequately large specimens. In the 60-deg, 5-in-diam-focal-spot furnace that is to be built by the Air Force in New Mexico [18], a temperature of 5400 F can be reached with a rotating specimen. This figure may be higher if the efficiencies obtained with this furnace are higher than those assumed for Table 1. The temperatures would also be higher if ceramic materials with low conductivities and high absorptivities were tested.

3 The furnace shape best adapted to mechanical testing would have larger apertures than those commonly used. As shown previously (see Fig. 3) the large-aperture furnace gives much higher flux densities and therefore much higher temperatures can be reached. Also, the axially oriented specimen absorbs more heat than the rotating specimen and the axial orientation is preferable because it permits a much simpler mechanical loading mechanism. This shape furnace would not lend itself to the type of materials work now commonly done in solar furnaces, but might have other applications not yet investigated.

Two points which were not investigated in detail should be mentioned here since they bear on the performance of solar furnaces for mechanical testing. First, special-shape furnaces other than parabolic might be devised [19] which may operate more efficiently since, as was pointed out, much of the concentrated flux is lost when the spot is larger than the specimen diameter. Second, insulation or special chamber designs can also be devised which would give higher ambient temperatures and therefore also result in higher specimen temperatures. This last point must be considered in conjunction with a specific furnace and incorporated into the design of the test setup and for this reason could not be included in the general type of investigation presented here.

APPENDIX
Discussion of Analysis

The many analyses and performance studies of solar furnaces which have appeared in recent years are limited to the flux on surfaces perpendicular to the mirror axis and neglect all heat loss due to conduction away from the spot [9, 10, 11, 12, 13]. In the present paper, the different orientations of the specimen surface were considered in obtaining the flux densities absorbed. The loss of heat by conduction was also considered to find the temperatures under thermal equilibrium. The results, therefore, represent a more realistic evaluation of solar furnace performance in the particular application of mechanical testing. The method of analysis will be presented to give a better understanding of the theory involved.

Flux Density. The reflection from any point on the parabolic mirror forms a cone whose diameter at the focus is given by $\rho\gamma$,

where ρ is the distance from the point on the mirror to the focus and γ is the angle subtended by the disk of the sun. When this cone is intersected by a plane passing through the focus, the image on the plane is an ellipse except at very high angles of incidence where the error has no practical effect on the total flux. If the focal spot is defined as a circle of diameter equal to the least minor axis of these ellipses, then it is seen that the image reflected from all points must include this circle. The minimum diameter usually results when a reflection comes from the center of the mirror at which point the distance from the focus is equal to the focal length f. The overlap of ellipses outside the focal spot will give a decreasing amount of flux density which generally drops quite fast [20]. Similarly, if the mirror has imperfections and all the rays are not centered about the focus, the ellipses may be distorted and their overlap may be random, resulting in a decrease of the average flux density in the focal spot. This loss is generally treated in terms of the index of geometric perfection η_g which is applied to the flux in the focal spot and which must be determined experimentally. If the sun's radiation is assumed to be uniform over its surface and the geometric imperfection is neglected the flux density in the focal spot can be expected to be uniform. In applying the index of geometric perfection the fact must be accepted that the flux may not be uniform on the spot and it is necessary to think in terms of an average flux density. As will be pointed out later, this is further complicated by the fact that the sun's radiation is not uniform (limb darkening).

Referring to Figs. 7 and 8 an expression can be derived for the flux density absorbed by a plane passing through the focus but tilted with respect to the z-axis.

$$d\psi = (\eta_a P_0)(r d\phi dr)(\eta_r)(\alpha_0 \cos \beta) \Big/ \frac{\pi \rho^2 \gamma^2}{4 \cos \beta} \qquad (4)$$

To understand this expression the groups of terms can be defined as follows: $\eta_a P_0$ is the flux density incident on the mirror, $r d\phi dr$ is the element of area normal to the incident rays, η_r is the attenuation due to incomplete reflection, and $\alpha_0 \cos \beta$ is the absorptivity of the surface. This represents the total energy in the elliptical image of area $\frac{\pi \rho^2 \gamma^2}{4 \cos \beta}$ and therefore the total expression

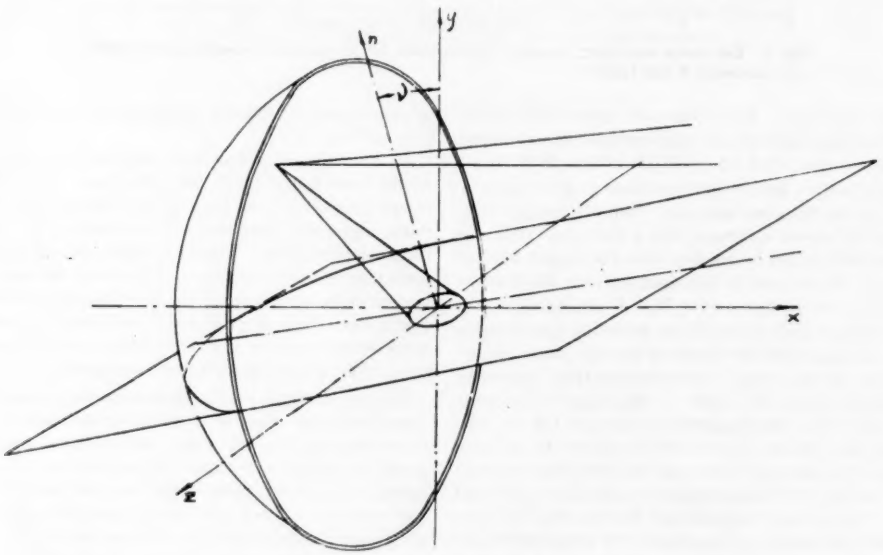

Fig. 7

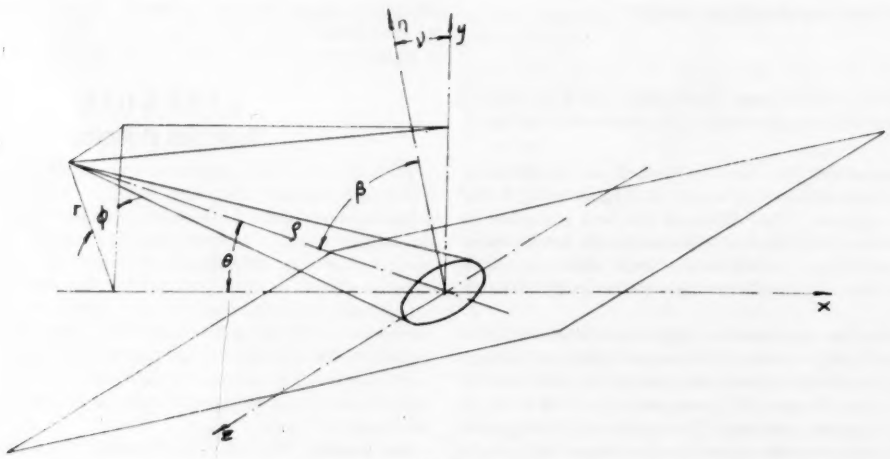

Fig. 8

gives the flux density absorbed in terms of the point on the mirror that is reflecting. Reducing this relation by use of the equation for the parabolic mirror which gives,

$$\rho = \frac{2f}{1 + \cos\theta} \tag{5}$$

and introducing geometric relations from Fig. 8, then

$$d\psi = \frac{4\eta_r\eta_a P_0\alpha_0}{\pi\gamma^2}\{\sin\theta[\sin\nu\cos\theta + \cos\nu\sin\theta\cos\phi]^2\}d\theta d\phi \tag{6}$$

This expression can be integrated over the surface of the mirror to give the total flux density absorbed, noting that ϕ is a function of θ and ν. Since this integration is a sum of the contributions from every spot on the mirror the index of geometric perfection is introduced at this point.

$$\psi = \eta_g\left\{\int_{\theta=0}^{\theta=(\theta\leq\nu)} 2\int_{\phi=0}^{\phi=\pi} d\psi + \int_{\theta=\nu}^{\theta=(\theta\leq\pi-\nu)} 2\int_{\phi=0}^{\phi=\cos^{-1}\left(-\frac{\tan\nu}{\tan\theta}\right)} d\psi\right\} \tag{7}$$

Depending on the aperture of the mirror θ_m and the value of ν, either one or both integrals must be used.

For the particular case where $\nu = 0$ the expression can be integrated directly

$$\psi_{\nu=0} = \frac{2\eta_r\eta_g\eta_a\alpha_0 P_0}{3\gamma^2}\{2 - 3\cos\theta_m + \cos^3\theta_m\} \tag{8}$$

If a thin flat specimen is considered or a specimen of small diameter (see Fig. 1) oriented along the axis of the mirror, this expression gives the flux absorbed by such a specimen per unit area within the focal spot. The restriction on the size comes from the fact that the spot must cover the section of the specimen. Otherwise the overlap of images that results as the focusing surface is moved away from the focal spot can reduce the flux density considerably [17]. The function given by Equation (8) is shown plotted in Fig. 3.

To get the flux on a tilted plane a numerical integration was necessary and was performed for different orientations and apertures as shown in Fig. 9. Again, if a cylinder of small diameter or a thin flat specimen lying along the z-axis is considered, these curves give the flux absorbed per unit area by an element of the cylinder at each orientation as it is rotated about the z-axis. To get the average flux density on such a specimen rotating at a uniform rate, the flux given for a particular aperture by one of these curves can be integrated and averaged for a complete revolution. The results of these integrations are also shown in Fig. 3.

Temperature. The expression for conduction in a bar of uniform cross section, absorbing and emitting radiant energy, is given by

$$Ak\frac{d^2T}{dx^2} + s\eta_a\eta_r\eta_g\alpha_0\psi^* - s(^2/_3\epsilon_0)\sigma T^4 = 0 \tag{9}$$

The $(^2/_3\epsilon_0)$ term is the total emissivity in terms of the normal total emissivity. This expression assumes that heat is absorbed and lost uniformly through the interior and that the temperature is therefore uniform at a cross section. Rearranging and expressing the length in units of the length over which radiation is absorbed, and taking the absorptivity equal to the emissivity, the relation can be written as

$$-\frac{d^2T}{d(x/L)^2} = \left(\frac{\epsilon_0 sL^2}{Ak}\right)[\eta_a\eta_r\eta_g\psi^* - {}^2/_3\sigma T^4] \tag{10}$$

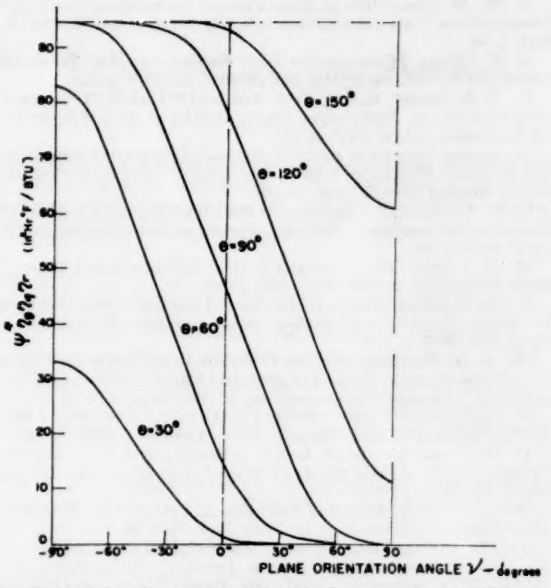

Fig. 9 Ideal flux density absorbed at the focus on planes at different orientation and for different mirror aperture θ_0

$$-\frac{d^2T}{d(x/L)^2} = R[\eta_a\eta_r\eta_g\psi^* - {}^2/_3\sigma T^4] \tag{10a}$$

This expression can be integrated by finite-difference methods with the boundary conditions that at $x/L = 0$, $dT/d(x/L) = 0$, and that as x/L becomes large the temperature approaches the ambient temperature asymptotically. The solution requires iteration starting with $T = T_m$ at $x/L = 0$ until the second boundary condition is satisfied. An iterated solution is shown in Fig. 5.

As previously mentioned, the radiation from the sun is not uniform but actually peaks at the center [12, 13]. Therefore the flux in the focal spot also tends to peak at the center. This fact produces an increase in the average flux in the focal spot because the center of the image is hottest and is the part of the ellipse that contributes to the flux in the spot. This nonuniformity of the flux, though it may not alter the total flux very greatly, will tend to increase the tensile-specimen gradients mentioned previously. The magnitude of these gradients would indicate strongly that the temperature is not uniform at a cross section of the specimen as was assumed for this solution.

References

1 T. S. Laszlo, "Solar Furnace in High-Temperature Research," *Science*, vol. 124, October, 1956, p. 797.

2 P. Duwez, "Solar Furnace in Ceramic Research," *American Ceramics Society Bulletin*, vol. 36, November, 1957, p. 410.

3 W. M. Conn, "Recent Progress in Solar Furnaces for High Temperature Research and Development Work," *Journal of the Franklin Institute*, vol. 257, January, 1954, p. 1.

4 W. M. Conn, "Solar Furnaces of 120-In. Diam for Studying Highly Refractory Substances," *Review of Scientific Instruments*, vol. 22, 1951, p. 945.

5 E. T. Burda, "Applied Solar Energy Research," Stanford Research Institute, 1955.

6 P. E. Glazer, "Engineering Research With a Solar Furnace," *Journal of Solar Energy*, vol. 2, April, 1957, p. 7.

7 P. Duwez and E. Loh, "Phase Relationships in the System Zirconia-Thoria," *American Ceramics Society Journal*, vol. 40, September, 1957, p. 321.

8 W. M. Conn, "Use of Solar Furnace for Studying Systems of Alumina-Silica," *American Ceramics Society Bulletin*, vol. 33, March, 1954, p. 69.

9 P. Duwez, "Utilization of Solar Furnaces in High-Temperature Research," TRANS. ASME, vol. 79, 1957, pp. 1019–1023.

10 N. K. Hiester, T. H. Tietz, E. Loh, and P. Duwez, "Theoretical Considerations on Performance Characteristics of Solar Furnaces," *Jet Propulsion*, vol. 27, 1957, p. 507.

11 Joseph Farber and Burton I. Davis, "Analysis of Large Aperture Parabolic Mirrors for Solar Furnaces," *Journal of the Optical Society of America*, vol. 47, 1957, p. 216.

12 A. W. Simon, "Calculation of the Concentration of the Solar Radiation Through the Focal Spot," *Journal of Solar Energy*, vol. 2, April, 1958, p. 25.

13 P. D. Jose, "Flux Through the Focal Spot of a Solar Furnace," *Solar Energy*, vol. 1, April-July, 1957, p. 19.

14 R. K. Cohen and N. K. Hiester, "A Survey of Solar Furnace Installation in the United States," *Journal of Solar Energy*, vol. 1, April-July, 1957, p. 115.

15 A. G. Worthing, "On the Deviation From Lambert's Cosine Law of the Emission From Tungsten and Carbon at Glowing Temperatures," *Astrophysical Journal*, vol. 36, December, 1912, p. 345.

16 T. Laszlo, "Temperature and Flux Versus Geometrical Perfection," *Journal of Solar Energy*, vol. 1, April-July, 1957, p. 78.

17 R. De La Rue, Jr., E. Loh, J. I. Brenner, and N. K. Hiester, "Flux Distribution Near the Focal Plane," *Journal of Solar Energy*, vol. 1, April-July, 1957, p. 94.

18 Cover story, *Journal of Solar Energy*, vol. 2, April, 1957, p. 1, (Solar Furnace at Holloman Air Force Base, New Mex.).

19 W. A. Baum and J. Strong, "Basic Optical Considerations in the Choice of a Design for a Solar Furnace," Tech. Memo. No. HDGR-57-14, September, 1957, Air Force Missile Development Center, Holloman Air Force Base.

20 A. W. Simon, "Calculation of the Concentration of Solar Energy at Points Outside the Focal Spot," *Journal of Solar Energy*, vol. 2, April, 1958, p. 22.

DISCUSSION

Eugene S. Cotton[3]

The essential point of this paper, to show the value of utilizing 90 deg or larger rim angles for heating axial specimens, has been generally neglected in the literature of solar concentrators. As the authors have pointed out, such specimens would have large temperature gradients from edge to center and in depth unless special precautions are taken to insure uniform heating.

However, I believe that the use of very large aperture furnaces would tend to become prohibitive in cost. The alternative mentioned by the authors of seeking special-shape two-mirror configurations would probably be more practical in the end. Although more precision would have to be incorporated into the surfaces in order to correct for aberrations, the distribution of flux could be made to conform much more closely to the sample configuration. It becomes increasingly evident that each solar concentrating surface must be designed for its principal use, and that no single device will satisfy all users.

Our own experience with a large furnace has demonstrated that a departure from the paraboloidal shape is not only economical but also very useful. Using preformed spherical segments of plate glass on an anastigmatic mounting, we have been able to attain a coefficient of geometrical perfection slightly larger than 0.5. Unlike the authors, we are interested in plane targets, so that the formation of a good solar image is our goal. In the case of axial specimens a strongly astigmatic image using thin radial segments might be quite feasible, and large angles could be attained without the large increase in aperture necessary with a paraboloid. Lost radiation could be refocused by a secondary mirror surrounding the rear section of the sample.

The paper under discussion presents an important and necessary view on the design of future solar concentrating devices for research. The error of creating several large instruments with similar characteristics can be avoided by designing each one for its principal field of research.

[3] Radiation Physics Laboratory, Pioneering Research Division, QM Research and Engineering Command, Natick, Mass.

Journal of ENGINEERING FOR POWER

Information for Authors

• Manuscripts should be submitted in final form to the Editor. Each manuscript must be accompanied by a statement that it has not been published elsewhere nor has it been submitted for publication elsewhere. A paper which would occupy more than 8 pages of the Journal may be returned to the author for abridgment.

• The author should state his business connection, the title of his position, and his mailing address. A short abstract (50 to 100 words) should be included on the first page immediately preceding the introductory paragraph of the paper.

Three copies of the manuscript are required. One of these must be a carefully prepared printer's copy, typed in double spacing, on one side of the page only, with wide margins, on $8^1/_2$ by 11-in. opaque white paper. Mimeographed manuscripts, if prepared with exceptional care, can be accepted provided they are completely edited.

• As far as possible, all mathematical expressions should be typewritten. Greek letters and other symbols not available on the typewriter should be carefully inserted in ink. Care should be taken to distinguish between capital and lowercase letter, between zero (0) and the letter (*O*), between the numeral (1) and the letter (*l*), etc. A letter representing a vector cannot be printed with an arrow above or below it. The letter should be underscored with a single wavy line, wherever it appears in the text, to designate boldface type.

• A list of symbols carefully marked for the use of the editor (thus: κ, Greek l.c. kappa), if it has not been included in the body of the paper, should accompany the manuscript on a separate page.

• Before preparing a manuscript the author should study printed articles in the Journal, with special attention to the form and style of mathematical expressions, tables, footnotes, references, and abstract. Numbers that identify mathematical expressions should be enclosed in parentheses. Numbers that identify references at the end of the paper should be enclosed in brackets. Care should be taken to arrange all tables and mathematical expressions in such a way that they will fit into a single column when set in type. Equations that might extend beyond the width of one column (fractions that should not be broken or long expressions enclosed in parentheses) should be rephrased to go on two or more lines within column width. Fractional powers are preferred to root signs and should always be used in more elaborate formulas. The solidus should be used instead of the horizontal line for fractions wherever possible.

• A normal paper should not exceed 8 pages in the Journal. It is about 8000 words or 20 double-spaced typewritten pages exclusive of drawings. A Technical Brief should not exceed 750 words or about one page in the Journal inclusive of drawings.

• Originals and two copies of figures must accompany the manuscript. Line drawings should not be larger than $8^1/_2 \times 11$ in. and should be planned for reduction to column width. Lettering should be large enough to be clearly legible when the illustration is reduced. The originals of line drawings must be in India ink on white or pale blue tracing paper or tracing cloth. Photographs of equipment or test specimens must be glossy prints and should be used sparingly. Captions for figures should be typed double-spaced and included as the last page of the manuscript. The figure number and author's name should be written in the margin or on the back of each illustration.

• Titles of papers should be brief.

• Authors can obtain copies of the ASME Manual MS-4, "An ASME Paper," from the Editor and are urged to do so before drafting their papers in final form.

• Papers published in Journals of the Transactions of the ASME must be presented at a Meeting, either in person or by title.

• An author is entitled to 25 preprints free of charge (in the case of two authors, 15 each; three or more authors, 10 each). Larger quantities of preprints or reprints can be ordered from Editorial Department, The American Society of Mechanical Engineers, 29 West 39th Street, New York 18, N. Y. Quotations will be sent on request.

Please address all communications to:

Editor, ASME,

29 West 39th Street,

New York 18, N. Y.

ASME Publications Committee

NOW

IN ONE VOLUME

The technical papers listed at the right

Originally published in the 1959 issues of the

Journals of Engineering for Power and Industry

they have been brought together in

SECTION 1 *of the* 1959 ASME TRANSACTIONS

PUBLISHED

IN SECTION 2 are the one-hundred and twelve papers and discussions contained in the 1959 Journals of Basic Engineering and Heat Transfer.

IN SECTION 3, the technical papers, discussions, design data, brief notes on technical matters in mechanics, and book reviews contained in the 1959 issues of the Journal of Applied Mechanics—a total of 145 contributions.

Studies of Air Pollution Control.
Characteristics of Airborne Particles.
Stage Performance and Radial Matching of Axial Compressor Blade Rows.
The Measured and Visualized Behavior of Rotating Stall in an Axial-Flow Compressor and in a Two-Dimensional Cascade.
Availability Balance of Steam Power Plants.
Pulverized-Coal Transport Through Pipes.
Operating Results of an Experimental Supercritical Steam Generator.
Some Notes on the Strength of the Enrico Fermi Reactor Vessel Structure.
Some Thoughts About the Development of Automotive Gas-Turbine Units.
Electrostatic Shaft Voltage on Steam-Turbine Rotors.
The Control System of a 225,000-Kw Double-Automatic Extraction Steam Turbine and Related Reducing Stations
Design of 321-Mw Cross-Compound Steam Turbine—River Rouge Unit No. 3.
Five Years' Experience on the Consolidated Edison System With Protection of Turbine Generators and Boilers by Automatic Tripping.
A Simplified Regenerator Theory.
Development of a Smooth Running, Double-Spool, Gas-Turbine Rotor System.
M-252 Alloy for Heavy-Duty Gas-Turbine Buckets.
The Calibration of Thermocouples by Freezing Point Baths and Empirical Equations.
Theoretical Stresses Near a Circular Opening in a Flat Plate, Reinforced With a Cylindrical Outlet.
Effect of Steam-Turbine Reheat on Speed-Governor Performance.
Load Capacity Tests on Tapered-Land and Pivoted-Shoe Thrust Bearings for Large Steam-Turbine Application.
Gas Turbine Progress Report Covering: Materials. Turbine Cooling. Fuels. Cycle Components. Compound Piston-and-Turbine Engines. Aviation. Rocket Turbines. Automotive. Railroad. Marine. Industrial and Central Station. Nuclear.
The Aerodynamic Approach to Furnace Design.
Use of Flow Models for Boiler-Furnace Design
Use of Models for Studying Pulverized-Coal Burner Performance.
Basic Principles of Combustion-Model Research.
A New Performance Criterion for Steam-Turbine Regenerative Cycles.
Power Test Code Thermometer Wells.
Flow-Induced Noise in Heat Exchangers.
The Effect of Fuel Types and Admission Method Upon Combustion Efficiency.
Torsion of a Prismatical Bar Whose Section Is a Crescent.
The Transient Response of Gas-Turbine-Plant Heat Exchangers—Regenerators, Intercoolers, Precoolers, and Ducting.
Stresses in Hollow Cylinders Due to Asymmetrical Heat Generation.
Dynamic Loading of Spur Gear Teeth.
Analytical Design of an Ackermann Steering Linkage.
Structural Error Analysis in Plane Kinematic Synthesis.
The Design of Linkages to Generate Functions of Two Variables.
Helical Springs of Hollow Circular Cross Section.
Design of Helical Springs for Minimum Weight, Volume, and Length.
Stress and Strain in Spinning Paraboloid Dishes.
Torispherical Shells—A Caution to Designers.
Drilling by Vibration.
Vibrations of Vertical Pressure Vessels.
The Strength of Thick-Walled Cylinders.
Steady-State Creep Analysis of the Weight Loadings of Furnace Tubes on Multiple Supports.
How to Replace Gears by Mechanisms (Linkages).
The Effect of a Lead Additive on the Machinability of Alloy Steels.
Controlled Contact Cutting Tools.
A Study of the Effects of Tool Flank Wear on Tool Chip Interface Temperature.
Synthesis of Path-Generating Mechanisms by Means of a Programmed Digital Computer.
Synthesis of the Four-Bar Linkage to Match Prescribed Velocity Ratios.
High-Range Plasticity of Metals Beyond Normal Work-Hardening.
Self-Excited Vibrations in Metal Cutting.
Factors Influencing the Performance of Grinding Wheels.
Vibrations of Flexible Precision Grinding Spindles.
The Effect of Process Variables on Extrusion Pressures of Lead.
Approximate Solutions to a Problem of Press Forging.
Theory and Experiment of Press Forging Axisymmetric Parts of Aluminum and Lead.
A Three-Dimensional, Tool-Life Equation—Machining Economics.
Observations on the Shearing Process in Metal Cutting and on the Angle Relationships in Metal Cutting.
Dynamic Problems Associated With Satellite Orbit Control.
Study of Machinability of Metals.
Four-Bar Linkages—Approximate Synthesis.
A Theory for the Effect of Mean Stress on Fatigue of Metals Under Combined Torsion and Axial Load or Bending.
An Analysis of Critical Stresses and Mode of Failure of a Wire Rope.
An Application of Statistics to the Dimensioning of Machine Parts.
The Dynamic Analysis and Design of Relatively Flexible Cam Mechanisms Having More Than One Degree of Freedom.
Power Heat Balance Considerations in Design and Operation of Industrial Plants.
Influence of Hot and Cold Storage-Loads on the Refrigerated-Space Temperature of a Cooling Complex.
Development and Uses of a New Line of Vibratory Feeders and Unit Vibrators.
A Mechanical Time-Delay Device Sensitive to Centrifugal Fields.

PRICES: **For each section $16.00** **($8.00 to ASME members)**
For all three sections $38.00 **($19.00 to ASME members)**

Public and engineering college libraries may purchase these sections at members' prices

THE AMERICAN SOCIETY OF MECHANICAL ENGINEERS

29 W. 39th Street **New York 18, N. Y.**